MATERIALS FOR ADAPTIVE STRUCTURAL ACOUSTIC CONTROLS

Period February 1, 1993 to January 31, 1994

Annual Report

VOLUME II

OFFICE OF NAVAL RESEARCH
Contract No. N00014-92-J-1510

APPROVED FOR PUBLIC RELEASE -- DISTRIBUTION UNLIMITED

L. E. Cross

PENNSTATE

THE MATERIALS RESEARCH LABORATORY
UNIVERSITY PARK, PA

REPORT DOCUMENTATION PAGE

Form Approved
OMB No 0704-0188

1. AGENCY USE ONLY (Leave blank)	2. REPORT DATE	3. REPORT TYPE AND DATES COVERED
	4/11/94	ANNUAL REPORT 02/01/93 TO 01/31/94

4. TITLE AND SUBTITLE

MATERIALS FOR ADAPTIVE STRUCTURAL ACOUSTIC CONTROL

5. FUNDING NUMBERS

6. AUTHOR(S)

L. ERIC CROSS

7. PERFORMING ORGANIZATION NAME(S) AND ADDRESS(ES)

MATERIALS RESEARCH LABORATORY
THE PENNSYLVANIA STATE UNIVERSITY
UNIVERSITY PARK, PA 16802

8. PERFORMING ORGANIZATION REPORT NUMBER

9. SPONSORING / MONITORING AGENCY NAME(S) AND ADDRESS(ES)

OFFICE OF NAVAL RESEARCH
CODE 1513:NRJ
800 NORTH QUINCY STREET
ARLINGTON, VA 22217

GERALD T. SMITH
OFFICE NAVAL RESEARCH RES. REP
536 SOUTH CLARK STREET, RM 286
CHICAGO, ILLINOIS 60606-1588

10. SPONSORING / MONITORING AGENCY REPORT NUMBER

11. SUPPLEMENTARY NOTES

12a. DISTRIBUTION / AVAILABILITY STATEMENT

12b. DISTRIBUTION CODE

13. ABSTRACT *(Maximum 200 words)*

SEE FOLLOWING PAGE

Accesion For	
NTIS CRA&I	☒
DTIC TAB	☐
Unannounced	☐
Justification	
By	
Distribution /	
Availability Codes	
Dist	Avail and / or Special
A-1	

14. SUBJECT TERMS

15. NUMBER OF PAGES

16. PRICE CODE

17. SECURITY CLASSIFICATION OF REPORT	18. SECURITY CLASSIFICATION OF THIS PAGE	19. SECURITY CLASSIFICATION OF ABSTRACT	20. LIMITATION OF ABSTRACT

NSN 7540-01-280-5500

Standard Form 298 (Rev 2-89)
Prescribed by ANSI Std 239-18
298-102

ABSTRACT

The research goals of this ONR sponsored University Research Initiative entitled "Materials for Adaptive Structural Acoustics Control" relate directly to the sensing and actuating material which must be integrated to function in adaptive control of acoustic structures. This report documents work in the second year of the program and for convenience the activities are grouped under the headings General Summary Papers, Materials Studies, Composite Sensors, Actuator Studies, Integration Issues, Processing Studies, and Thin Film Ferroelectrics.

The general papers cover a new comprehensive description of ferroelectric ceramics and their applications, analysis of high temperature piezoelectric sensors and the possible application of nonlinearity in enhancing the "smartness" of ceramics and composites. Scale effects on ferroics are of increasing interest and the manner in which nano-scale polar regions control the properties of relaxor ferroelectrics is again emphasized.

For material studies the detailed examination of the evolution of diffuse, then relaxor behavior in lanthanum modified lead titanate has been completed. Interest in the soft PZTs, relaxor and phase switching materials continues, with a new thrust developing towards a more complete description of domain walls and morphotropic phase boundaries in perovskites. Materials issues in the wear out and fatigue effects in polarization switching systems have been subjected to detailed evaluation and the precautions necessary to fabricate long lasting materials which will stand 10^9 switches without any fatigue are delineated.

Sensor studies have continued to focus on flextensional composites and have demonstrated both the very high hydrostatic sensitivity and the amplified actuation response of this configuration. Integration of sensors with the "moonie" actuators has been accomplished in individual cells. Actuator studies cover the gamut from highly reproducible micro positioning using electrostrictive compositions to high strain polarization switching shape memory ceramics capable of driving a latching relay device. Studies of the destruct mechanisms in practical MLA systems complement the earlier materials work and show the importance of internal electrodes and consequent stress concentrations for crack initiation. Integration studies have focused upon more detailed evaluation of 1:3, 2:2 and tubular 1:3 composites and upon the influence of the polymer characteristic and of face plates and edge guards upon sensing and actuation capabilities. In processing, the interest in dielectrophoretic forming of composites is continuing and assembly of interesting 1:3 composites is demonstrated. Guidelines for the transducer application of electrostrictive materials have been formulated and a useful classification scheme proposed. In fiber PZTs techniques for fabricating thin (30 μ) fibers are demonstrated, the first successful technique for poling fibers is described and it is shown that properly poled fibers have electro-elastic characteristics similar to bulk material. Film papers are selected to reflect the transducer capabilities of lead titanate and of phase switching lead zirconate titanate stannate antiferroelectric compositions.

MATERIALS FOR ADAPTIVE STRUCTURAL ACOUSTIC CONTROLS

Period February 1, 1993 to January 31, 1994

Annual Report

VOLUME II

OFFICE OF NAVAL RESEARCH
Contract No. N00014-92-J-1510

APPROVED FOR PUBLIC RELEASE -- DISTRIBUTION UNLIMITED

L. E. Cross

PENNSTATE

1855

THE MATERIALS RESEARCH LABORATORY
UNIVERSITY PARK, PA

TABLE OF CONTENTS

APPENDICES

General Summary of Papers (continued)

4. Newnham, R. E. Size Effects and Nonlinear Phenomena in Ferroic Ceramics. 3rd European Ceramic Society Conference, Madrid (1993).

5. Cross, L. E. Relaxor Ferroelectrics: Useful Electron Nanocomposite Structures, Proc. IUMRS, Ikabakura, Tokyo (September 1993).

Materials Studies

6. Rossetti, G. A., Jr., W. Cao, and C. A. Randall. Microstructural Characterization and Diffuse Phase Transition Behavior of Lanthanum Modified Lead Titanate. Ferroelectrics: Proceedings of IMF8, Gaithersburg, Maryland (August 1993).

7. Cao, W. and L. E. Cross. Distribution Function of Coexisting Phases in a Complete Solid Solution System. J. Appl. Phys. 73(7), 3250 (1993).

8. Cao, W. Polarization Gradient Coefficients and the Dispersion Surface of the Soft Mode in Perovskite Ferroelectrics. J. Phys. Soc. Jpn. **63**, 827 (1994).

9. Cao, W. and L. E. Cross. Nonlinear and Nonlocal Continuum Theory on Domain Walls in Ferroelectrics. Ferroelectrics: Proceedings of IMF8, Gaithersburg, Maryland (August 1993).

10. Cao, W. and C. Randall. Theory on the Fringe Patterns in the Study of Ferroelectric Domain Walls Using Electron Holograpy. Solid State Comm. **86**, 435-439 (1993).

11. Zhang, Q. M., H. Wang, N. Kim, and L. E. Cross. Direct Evaluation of Domain Walls and Intrinsic Contributions to the Dielectric and Piezoelectric Constants and Their Temperature Dependence in Lead Zirconate Titanate Ceramics. J. Appl. Phys. **75** (1), 454 (1994).

12. Subbarao, E. C., V. Srikanth, W. Cao, and L. E. Cross. Domain Switching and Microcracking during Poling of Lead Zirconate Titanate Ceramics. Ferroelectrics **145**, 271-281 (1993).

13. Li, S., W. Cao, R. E. Newnham, and L. E. Cross. Electromechanical Nonlinearity of Ferroelectric Ceramic and Related non 180° Domain Wall Motion. Ferroelectrics **139**, 25-49 (1993).

14. Jiang, Q., W. Cao, and L. E. Cross. Electrical Fatigue in Lead Zirconate Titanate Ceramics. J. Am. Ceram. Soc. **77**(1), 211-215 (1994).

15. Jiang, Q., E. C. Subbarao, and L. E. Cross. Grain Size Dependence of Electrical Fatigue Behavior in Hot Pressed PLZT Ferroelectric Ceramics. (Submitted to Acta. Met.)

16. Jiang, Q., E. C. Subbarao, and L. E. Cross. Effects of Composition and Temperature on electrical Fatigue of La Doped Lead Zirconate Titanate Ceramics. J. Appl. Phys. (in press).

17. Jiang, Q. and L. E. Cross. Effect of Porosity on Electrical Fatigue Behavior in PLZT and PZT Ceramics. J. Mat. Sci. **28**, 4536-4543 (1993).

Materials Studies (continued)

18. Jiang, Q., E. C. Subbarao, and L. E. Cross. Effects of Electrodes and Electroding Methods on Fatigue Behavior in Ferroelectric Materials. Ferroelectrics: Proceedings of IMF8, Gaithersburg, Maryland (August 1993).

19. Jiang, Q., E. C. Subbarao, and L. E. Cross. Fatigue in PLZT: Acoustic Emission as a Discriminator Between Microcracking and Domain Switching. Ferroelectrics: Proceedings of IMF8, Gaithersburg, Maryland (August 1993).

20. Jiang, Q., E. C. Subbarao, and L. E. Cross. Field Induced Stress Concentration and Electrical Fatigue in Ferroelectric Ceramics. IEEE Trans. on Ultrasonic Ferroelectrics and Frequency Control (submitted).

21. Jiang, Q., E. C. Subbarao, and L. E. Cross. Dielectric Properties of Single Grain in PLZT Ferroelectric Ceramics. Ferroelectric Letters (in press).

22. Li, S., A. S. Bhalla, R. E. Newnham, and L. E. Cross. Quantitative Evaluation of Extrinsic Contribution to Piezoelectric Constant d33 in Ferroelectric PZT Ceramics. Materials Letters 17, 21-26 (1993).

23. Wang, H., Q. Zhang, and L. E. Cross. A High Sensitivity Phase Sensitive d33 Meter for Complex Piezoelectric Constant Measurement. Jpn. J. Appl. Phys. 32(Pt. 2; No. 9A), L1281-83 (1993).

Composite Sensors

24. Newnham, R. E., Q. C. Xu, and S. Yoshikawa. Metal-Electroactive Ceramic Composite Actuator. U.S. Patent# 5,276, 657.

25. Onitsuka, K., A. Dogan, J. A. Tressler, Q. C. Xu, S. Yoshikawa, and R. E. Newnham. Metal-Ceramic Composite Transducer–The Moonie. Ferroelectrics: IMF8, Gaithersburg, Maryland (August 1993).

26. Tressler, J. F., Q. C. Xu, S. Yoshikawa, K. Uchino, and R. E. Newnham. Composite Flextensional Transducer for Sensing and Actuating. Ferroelectrics: IMF8, Gaithersburg, Maryland (August 1993).

27. Newnham, R. E., A. Dogan, Q. C. Xu, K. Onitsuka, J. Tressler, and S. Yoshikawa. Flextensional "Moonie" Actuators. IEEE 1993 Ultrasonics Symp. Proc., Baltimore, Maryalnd; Vol. 2, pp. 509-514 (1993).

28. Harshe, G., J. P. Dougherty, and R. E. Newnham. Theoretical Modeling of Multilayer Magnetoelectric Composites. Int. J. of Appl. Mag. in Mtls. 4, 145-159 (1993).

29. Newnham, R. E. and G. R. Ruschau. Electromechanical Properties of Smart Materials. J. Intelligent Mtls. Systems and Structures 4, 289 (1993).

30. Onitsuka, K., A. Dogan, Q. Xu, S. Yoskikawa, and R. E. Newnham. Design Optimization for Metal-Ceramic Composite Actuator, "Moonie." Ferroelectrics: IMF8, Gaithersburg, Maryland (August 1993).

Actuator Studies

31. Uchino, K. Relaxor Ferroelectric Devices. Ferroelectrics: Proceedings IMF8, Gaithersburg, Maryland (August 1993).

32. Uchino, K. Recent Development of Piezoelectric Actuators for Adaptive Structures. 3rd International Conference on Adaptive Structures (1991).

33. Furuta, A. and K. Uchino. Dynamic Observation of Crack Propagation in Piezoelectric Multilayer Actuators. J. Am. Ceram. Soc. **76**(6), 1615 (1993).

34. Uchino, K. Ceramic Actuators Principles and Applications. MRS Bull. (April 1993).

35. Uchino, K. Applications of Piezoelectric Ceramics in Smart Actuator Systems. ADPA/AIAA/ASME/SPIE Cont. on Active Mtls. (1992).

36. Uchino, K. and A. Furuta. Destruction Mechanism of Multilayer Ceramic Actuators. ISAF92, South Carlonia (1992).

37. Furuta, A. , K. Y. Oh, and K. Uchino. Shape Memory Ceramics and Their Application to Latching Relays. Sensors and Materials **3**, 205 (1992).

38. Uchino, K. Piezoelectric Ceramics in Smart Actuators Systems. 1st European Conference on Smart Structures and Materials, Glasgow (1992).

39. Zhang, Q. M., J. Chen, and L. E. Cross. Electric Field Induced Piezoelectric Response in Ferroelectric Materials Near the Paraelectric-Ferroelectric Transition. Proceedings Ultrasonics Symposium, pp. 525 (1993).

Integration Issues

40. Zhang, Q. M., W. Cao, J. Zhao, and L. E. Cross. Piezoelectric Performance of Piezoelectric Polymer Composites with 2-2 Connectivity–A Combined Theoretical and Experimental Study. IEEE Transactions UFFC (accepted) (1993).

41. Chen, J., Q. M. Zhang, L. E. Cross, and C. M. Trottier. Modeling and Design of 1-3 Tubular Composites for Smart Transducer Applications. 1994 Proceedings International Conference on Intelligent Materials (submitted) (1994).

42. Wang, H., Zhang, and L. E. Cross. Piezoelectric Relaxation of P(VDF-TrFE) Copolymers. Ferroelectrics: IMF8, Gaithersburg, Maryland (August 1993).

43. Zhao, J., Q. M. Zhang, and W. Cao. Effects of Face Plates and Edge Strips on Hydrostatic Piezoelectric in 1-3 Composites. J. Mat. Sci. (submitted).

Processing Studies

44. Yoshikawa, S. and T. R. Shrout. Multilayer Piezoelectric Actuator Structures and Reliability. Proceedings Structural Dynamics, Materials Conference AIAA/ASM Adaptive Structures Forum, Pt. 6, 3581-3586 (1993).

Processing Studies (continued)

45. Bowen, C. P., T. R. Shrout, R. E. Newnham, and C. Randall. Intelligent Processing of Composite Materials. J. Intelligent and Smart Materials (submitted) (1993).

46. Shrout, T. R., C. A. Randall, B. P. Brodeur, and S. J. Jang. Classification of Electrostrictive Based Materials for Transducers. U.S. Japan Meeting on Dielectrics, Lahaina, Hawaii (November 1994).

47. Yoshikawa, S., U. Selvaraj, P. Moses, Q. Jiang, and T. R. Shrout. $Pb(ZrTi)O_3$ [PZT] Fibers–Fabrication and Properties. J. of Intelligent Material Systems and Structures (submitted) (1994).

48. Miller, D., C. A. Randall, A. S. Bhalla, R. E. Newnham, and J. Adair. Electrorheological Properties of $BaTiO_3$ Suspensions. Ferroelectric Letters **15**, 141-151 (1993).

49. Randall, C. A., C. P. Bowen, T. R. Shrout, A. S. Bhalla, and R. E. Newnham. Dielectrophoresis: A Means to Assemble Novel Electroceramic Composite Materials. Proceedings of Electrorheological Fluids. Feldrick, Austria (1993).

Thin Film Ferroelectrics

50. Udayakumar, K. R., S. B. Krupanidhi, K. Kushida, and L. E. Cross. Origina of Orientation in Sol-Gel-Derived Lead Titanate Films. J. Am. Ceram. Soc. **76**, 1345 (1993).

51. Brooks, K. G., J. Chen, K. R. Udayakumar, and L. E. Cross. Electric Field Forced Phase Switching in La Modified Lead Zirconate Titanate Stannate Films. J. Appl. Phys. **75**, 1399 (1994).

52. Sheen, J., R. Guo, A. S. Bhalla, and L. E. Cross. Measurements of Dielectric Constant and Quality Factor of $Ba(Mg_{1/3}Ta_{2/3})O_3$ at X Band Frequencies. Ferroelectric Letters **16**, 33 (1993).

Graduating Students in the Program

53. Rossetti, George A., Jr. PhD Thesis (Abstract), Solid State Science. Structural and Thermodynamic Investigation of the Ferroelectric Phase Transition in Lanthona-Substitued Lead Titanate. May 1993.

54. Chen, Jaiyu. PhD Thesis (Abstract), Electrical Engineering. Electrical and Electromechanical Properties of Ferroelectric Thin Films for Microelectromechanical Applications. August 1993.

55. Alberta, Edward. MS Thesis (Abstract), Solid State Science. The Dielectric, Piezoelectric and Pyroelectric Properties of Lead Zirconate-Lead Zinc Niobate-Lead Titanate Ceramics. October 1993.

MATERIALS STUDIES
(continued)

APPENDIX 13

Ferroelectrics, 1993, Vol. 139, pp. 25–49
Reprints available directly from the publisher
Photocopying permitted by license only

ELECTROMECHANICAL NONLINEARITY OF FERROELECTRIC CERAMICS AND RELATED NON-180° DOMAIN WALL MOTIONS

SHAOPING LI, WENWU CAO, R. E. NEWNHAM and L. E. CROSS
Materials Research Laboratory, The Pennsylvania State University, University Park, PA 16802 USA

(Received June 13, 1992; in final form August 26, 1992)

Using an optical interferometer and other experimental techniques, the mechanical and dielectric response of lead zirconate titanate $Pb(Zr_xTi_{1-x})O_3$ ceramics to an a.c. electric field have been investigated directly. The experimental results demonstrate the importance of the domain wall motion in generating the electromechanical nonlinearities in ferroelectric ceramics. It has been verified that the couplings between the acoustic vibrations and the movement of domain walls is an important factor in terms of extrinsic properties of ferroelectric polycrystalline materials. A phenomenological theory has been extended to describe the extrinsic contributions to the piezoelectric, elastic and dielectric properties. These effects can be attributed to both the linear and nonlinear vibrations of non-180° domain walls in ferroelectric ceramics. The proposed theory shows qualitative agreement with the experimental results.

Keywords: ferroelectric ceramic, PZT, nonlinearity, domain walls, piezoelectricity

I. INTRODUCTION

Electromechanical nonlinearity in ferroelectric polycrystalline materials is an important problem in modern ultrasonic engineering. Ferroelectric ceramics are widely used as transducers, resonators, actuators, motors, and capacitors which represent a very large segment of the electroceramics market. One of the limitations of ferroelectric transducers for practical use are the nonlinear effects which occur at high drive level,[1–6] because ferroelectric ceramics are the strongest known nonlinear piezoelectric materials.[7] Moreover, techniques for fabricating ferroelectric thin films have made great progress during recent years leading to the possibility of utilizing nonlinear phenomena of ferroelectric polycrystalline thin film devices in conjunction with integrated circuits. Significant nonlinear phenomena in thin films can be observed under voltages of less than a volt. In practical applications, the nonlinearity of ferroelectric polycrystalline materials directly influences the performance of microwave acoustic devices such as convolvers and correlators.[7–9] The so-called "smart ceramic systems"[10] incorporating sensors and actuators also need to exploit the nonlinear properties of ferroelectric ceramics. In short, on certain occasions, one wants to avoid the nonlinearities, while on other occasions one wants to benefit from them. Therefore, from a technological point of view, it is important to study the nonlinear electromechanical properties in ferroelectric ceramics so as to optimize the choice of piezoceramics most suitable for transducers, actuators, resonators, ultrasonic motors and other acoustic devices, as well as to

develop new types of nonlinear electronic devices such as frequency mixers and doublers, and piezoelectric thin film devices.

The piezoelectric effects in ferroelectric ceramics are caused by two mechanisms: (1) the intrinsic piezoelectric effect[11-12] connected with the deformation of each unit cell of the ferroelectric material by an electric field and (2) the extrinsic piezoelectric effect[13-15] that, for example in lead zirconate titanate (PZT) system, refers to the motion of non-180° domain walls and the movement of the interphase phase boundary between the tetragonal and rhombohedral phase regions.[16] It is believed that the piezoelectric effect in polycrystalline ferroelectrics is caused not only by the ionic displacement in connection with the change of the polarization magnitude, but also by the movements of domain walls and interphase boundaries. Studies on materials such as $BaTiO_3$ and PZT[17] have shown that as much as 60%–70% of the piezoelectric moduli values may originate from the extrinsic contributions. In fact, the performance of many transducers, actuators and capacitors are based on the control of domain structures under applied electric field. Microstructure investigations[18-20] showed that the poled ferroelectric ceramics contain a large number of non-180° domain boundaries which strongly affect their electromechanical behavior.[21-27] In general, these domain structures give rise to complex linear and nonlinear behavior which is very sensitive to the quality of the sample and its defect concentration, as well as the external boundary conditions.

Even though the investigation of the electromechanical nonlinearity in ferroelectrics has been carried on for the last three decades, most of the studies[28-30] are based on thermodynamic theory only, without considering the dynamics of domain walls. Very little work[31,32] has been done to describe the behavior of electromechanical nonlinearity in terms of domain wall motion, even though the domain wall motion plays a dominant role over a wide range of external field levels, and also the frequency response of domain wall motions spans a range from almost zero hertz to the microwave regime. Moreover, a number of ambiguities still remain in this area due to the lack of sufficient information about the relationship between electromechanical coefficients and the motions of non-180° domain walls and the movement of interphase boundaries.

Here, it should be mentioned that one of the challenges facing materials scientists is to develop a scientific foundation for the understanding and the rational design of sophisticated material systems with novel microstructures as well as multiple functional characteristics. At present, the major shift in ferroelectric research and development is underway from single-crystal devices to fully integrated polycrystalline thin film devices in which the ferroelectric elements are an integral part of the silicon or GaAs integrated circuit, or very elegant micro-transducers with multiple functions for various applications. The key issue for this development is from general qualitative investigation of physical properties of polycrystalline materials towards more quantitative examination of the relationship between the microstructures and macroscopic properties. Basically, it has been known that one of the simplest types of composite with piezoelectric constituents is a single phase polycrystalline aggregate, with grains made of the same piezoelectric substance but with mismatched orientations of the crystallographic axes at the grain boundaries. Since the micro-piezoelectricity combining micromechanics and microelectronics is of great significance in microferroelectricity, the quantitative study of the rela-

tionship between the microstructure and related properties in polycrystalline materials is the basis for further development in microferroelectricity.

It is the objective of this work to evaluate the linear and nonlinear elastic, dielectric, and piezoelectric coefficients arising from the domain wall motions, and to form a tentative model based on the observed linear and nonlinear effects in an attempt to gain some physical insight into the relationship between domain wall motions and nonlinear electromechanical properties in ferroelectric ceramics. This paper is structured as follows: in sections II and III, we present a general description of the electromechanical properties arising from the non-180° domain wall motions in the ferroelectric ceramic. Through considering the macroscopic nonlocal motion of domain walls in the presence of external fields, we obtain expressions for a number of experimentally accessible quantities. In section IV, we show some experimental results which characterize the dynamic electromechanical response of the PZT ferroelectric ceramics. Some of the experimental results strongly support our approach to the problem.

II. THEORETICAL

2.1. *Domain and Interphase Structures*

In a $Pb(Zr_xTi_{1-x})O_3$ system with composition near the morphotrophic phase boundary, the tetragonal and rhombohedral phases coexist. Therefore, besides the 180° domain wall, there are 71°, 110° and 90° domain walls. Also interphase boundaries between the two phases exist. Here, we do not discuss the case for 180° domain walls. The 180° domain wall motion does not significantly affect the piezoelectric and electromechanical properties because the spontaneous deformations of the antiparallel domains are the same.[61,62] In order to investigate systematically the relationship between linear piezoelectric effect and the non-180° domain wall motions in ferroelectric ceramics, Arlt *et al.*[13,14] first presented a phenomenological model for the vibrating 90°-domain wall under electric field and mechanical stress to describe the linear piezoelectric behavior of ferroelectric ceramics. We have generalized this model to describe the nonlinear effects resulting from the vibrating 90°-domain walls.[33]

Here, we will try to model non-180° domain wall motions for the cases of rhombohedral phase and interphase conversion between the tetragonal and rhombohedral regions, respectively. As we know, the symmetry of the ferroelectric phase is fully determined by the symmetry of the parent phase. The spontaneous polarization has equal probability to lie in all the equivalent directions prescribed by the prototypic form from which the ferroelectric phase is derived. From phenomenological theory,[12] we can find eight energetically equivalent variants in the rhombohedral ferroelectric stable states of PZT system as following:

$$\begin{aligned} &\text{I. } (P_1, P_2, P_3), \quad \text{II. } (P_1, P_2, -P_3), \quad \text{III. } (-P_1, P_2, P_3), \\ &\text{IV. } (P_1, -P_2, P_3), \quad \text{V. } (-P_1, P_2, -P_3), \quad \text{VI. } (P_1, -P_2, -P_3), \\ &\text{VII. } (-P_1, -P_2, P_3), \quad \text{VIII. } (-P_1, -P_2, -P_3) \end{aligned} \tag{1}$$

where $P_i (i = 1, 2, 3)$ are the components of the spontaneous polarization P_0 in

Cartesian coordinates, $P_1^2 = P_2^2 = P_3^2 = P_0^2/3$. Accordingly, the spontaneous strain under zero stress conditions can be written as:

$$S_{11} = S_{22} = S_{33} = (Q_{11} + 2Q_{12})P_0^2/3 \qquad (2)$$

$$S_{12} = Q_{44}P_1P_2, \quad S_{23} = Q_{44}P_2P_3, \quad S_{13} = Q_{44}P_1P_3$$

where, Q_{ij} are the electrostrictive coefficients. Obviously, the normal components of s_{ij} are the same for all of the orientation states, and the shear components of the spontaneous strain tensor in the corresponding Equation (1) have the following forms:

$$\text{I(VIII)}.\ S_{12} = S_{23} = S_{31} = \frac{Q_{44}}{3}P_0^2; \quad \text{II(VII)}.\ S_{12} = -S_{23} = -S_{31} = \frac{Q_{44}}{3}P_0^2;$$

$$\text{III(VI)}.\ S_{12} = -S_{23} = S_{31} = \frac{-Q_{44}}{3}P_0^2;$$

$$\text{IV(V)}.\ S_{12} = S_{23} = -S_{31} = \frac{-Q_{44}}{3}P_0^2 \qquad (3)$$

These eight low temperature variants will form 180°, 71° and 110° twin structures. For instance, the polarization vectors in a twin structure between states (I) and (VII) form a angle θ,

$$\theta = \cos^{-1}(\tilde{n}_{111}\cdot\tilde{n}_{\bar{1}\bar{1}1}) = \cos^{-1}\left(\frac{-1}{3}\right) \simeq 110°$$

where $\tilde{n}_{111}$ and $\tilde{n}_{\bar{1}\bar{1}1}$ are unit vectors in [111] and $[\bar{1}\bar{1}1]$, respectively. The twin boundary is then called 110° domain wall. We choose primed and unprimed coordinate systems for a basic piezoelectric element as shown in Figure 1, which contains a single 110° domain wall and separates the polarization states (I) and (VII). In the primed system, domain wall is located in $z' = 0$ plane.[24] A displacement Δl of the domain wall gives rise to a change in the electric dipole moment δP_i in volume ΔlA,[34,35]

$$\delta\vec{P}' = \frac{2}{\sqrt{3}}\Delta lAP_0\begin{bmatrix}1\\1\\0\end{bmatrix} \qquad (4)$$

Δl is the displacement of the domain wall and A is the area of the vibrating domain wall per unit volume. This movement of domain walls also induce a change in the elastic dipole moment, which in the primed coordinate can be written as

$$\delta\tilde{U}' = \Delta lAS_0\begin{bmatrix}0 & 0 & 1\\0 & 0 & 1\\1 & 1 & 0\end{bmatrix} \qquad (5)$$

where,

$$S_0 = \frac{2Q_{44}}{3}P_0^2$$

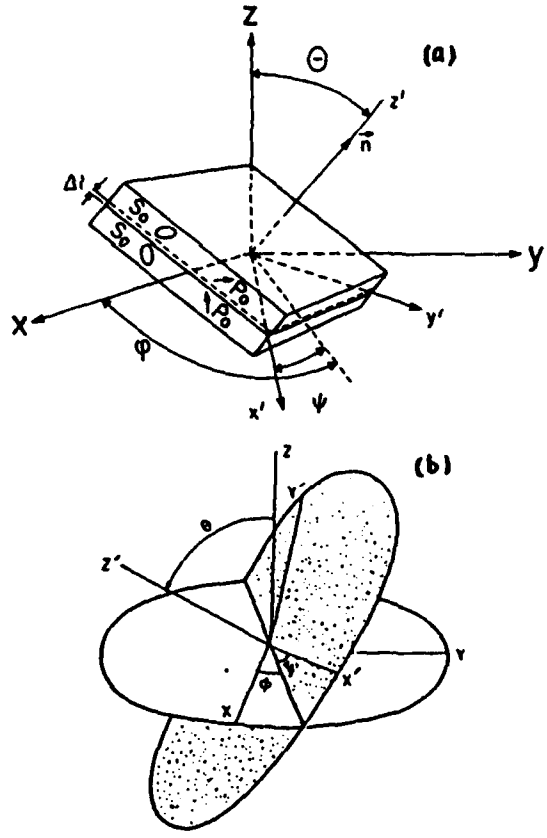

FIGURE 1 (a) A basic element of a twin structure in a rhombohedral ferroelectric ceramic. (b) The unprimed and primed coordinate systems. The relative orientation is characterized by the Eulerian angles (ϕ, ψ, θ).

where, P_0 and S_0 are the spontaneous polarization and strain, respectively, in the rhombohedral phase. Finally, in (x, y, z) coordinate system, the changes of induced electric and elastic dipoles can be obtained through a coordinate transformation:

$$\delta P_i = \Delta l A P_0 f_i(\Theta, \Phi, \Psi) \tag{6}$$

and,

$$\delta U_{ij} = \Delta l A S_0 F_{ij}(\Theta, \Phi, \Psi) \tag{7}$$

where

$f_1 = [\cos\Phi(\cos\Psi - \sin\Psi) - \cos\Theta\sin\Phi(\sin\Psi + \cos\Psi)]$, $f_2 = [\sin\Phi(\cos\Psi - \sin\Psi) + \cos\Theta\cos\Phi(\sin\Psi + \cos\Psi)]$, $f_3 = \sin\Theta(\cos\Psi + \sin\Psi)$; and

$F_{11} = 2\sin\Theta\sin\Phi[\cos\Psi\cos\Phi(\cos\Psi - \sin\Psi) - \sin\Phi\cos\Theta(\cos\Psi + \sin\Psi)]$,

$F_{22} = 2\sin\Theta\cos\Phi[\sin\Phi(\cos\Psi - \sin\Psi) + \cos\Theta\cos\Phi(\cos\Psi + \sin\Psi)]$,

$F_{33} = 2\cos\Theta\sin\Theta(\sin\Psi + \cos\Psi)$,

$$F_{13} = \sin\Phi(\cos\Psi + \sin\Psi)[\cos^2\Theta - \sin^2\Theta] + \cos\Theta\cos\Phi(\cos\Psi + \sin\Psi),$$
$$F_{23} = \cos\Theta[\sin\Phi(\cos\Psi - \sin\Psi) + \cos\Phi\cos\Theta(\cos\Psi + \sin\Psi)] - \sin^2\Theta\cos\Phi[\cos\Psi + \sin\Psi],$$
$$F_{12} = \sin\Theta(\cos\Psi - \sin\Psi).$$

Next, let us discuss the case of interphase conversion in the ferroelectric ceramic. It is known[15] that the tetragonal (T) and rhombohedral (R) ferroelectric phases coexist in the PZT system for compositions near the MPB. According to SEM, SAED and TEM results, the domain structure in PZT ceramics with compositions near the MPB consists of alternating T and R phase layers which resemble the 90° domain structure in tetragonal distorted ceramics. Based on experimental results, Lucuta proposed[19,20] a layered model of ferroelectric domains $T_1RT_2RT_1$, assuming the R domains are in between two different oriented T domains as shown in Figure 2. With a rhombohedral phase in between two 90° tetragonal domains, the polarization direction changes as follows: [001]---[111]---[010]---[111]---[001], corresponding to a repetitive domain sequence $T_1RT_2RT_1$ . . . The interphase boundary conversion will induce changes in the electric and elastic dipole moments. As an example, when the polarization along the [111] direction in a R domain is switched into the polarization along the [001] direction in a T domain, the induced electric and elastic dipole moments in the primed coordinate system are:

$$\delta\vec{P}' = \Delta l A \frac{P_0}{\sqrt{3}} \begin{bmatrix} 1 \\ 1 \\ -(\sqrt{3}-1) \end{bmatrix} \tag{8}$$

$$\delta\tilde{U}' = \Delta l A \begin{bmatrix} u_{11} & u_{12} & u_{13} \\ u_{21} & u_{22} & u_{23} \\ u_{31} & u_{32} & u_{33} \end{bmatrix} \tag{9}$$

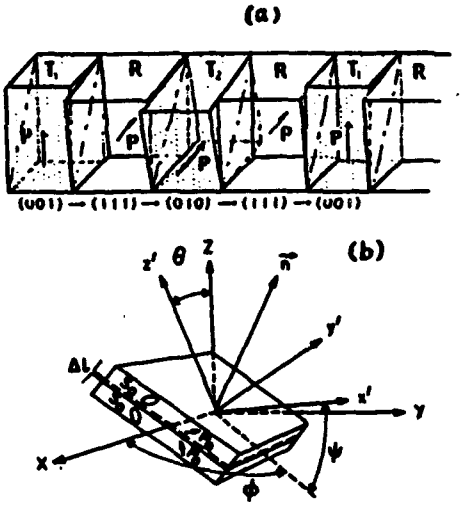

FIGURE 2 (a) Packing model of T-R twin-related domains along the (011) habit plane showing the coexistence of T and R ferroelectric phases in PZT at the MPB [After Lucuta Reference 20]. (b) A basic element of the interphase boundary in the PZT system at the MPB.

where,

$$u_{12} = u_{13}u_{21} = u_{23} = u_{31} = u_{32} = \frac{Q_{44}}{3} P_0^2;$$

$$u_{11} = u_{22} = \frac{(Q_{11} - Q_{12})}{3} P_0^2; \qquad u_{33} = \frac{-2(Q_{11} + Q_{12})}{3} P_0^2$$

Note: here we assume that the magnitude of the spontaneous polarization in the rhombohedral phase is equal to that in the tetragonal phase, and all coefficients Q_{11}, Q_{12}, and Q_{44} are the same in both phases. Finally, in the (x, y, z) coordinate system, the changes of electric and elastic dipole moments can be written as:

$$\delta P_i = [\tilde{R}_{ij}][\delta P_i']; \qquad [\delta U_{ij}] = [\tilde{R}_{ij}][\delta U_{ij}'][R_{ij}] \tag{10}$$

$$[R_{ij}] = \begin{bmatrix} \cos\Psi & \sin\Psi & 0 \\ -\sin\Psi & \cos\Psi & 0 \\ 0 & 0 & 1 \end{bmatrix} \begin{bmatrix} 1 & 0 & 0 \\ 0 & \cos\Theta & \sin\Theta \\ 0 & -\sin\Theta & \cos\Theta \end{bmatrix} \begin{bmatrix} \cos\Phi & \sin\Phi & 0 \\ -\sin\Phi & \cos\Phi & 0 \\ 0 & 0 & 1 \end{bmatrix}$$

2.2. *The Model*

Generally speaking, the domain wall motion is accomplished by a succession of steps beginning at initiating nuclei,[36,37] but in the sideways motion of the non-180°, this may not be exactly true.[38] The entire ceramic specimen is a complex electromechanical system with the domain walls in different grains having different orientations and different boundary conditions. The movements of the domain walls are not independent; there are strong interactions between them. The microscopic process for individual domain wall motion is rather complicated and not well understood. However, if we are only interested in the macroscopic effects resulting from the collective motion of domain walls, the microscopic details of each individual domain may be neglected.

In this analysis, we assume that the average displacement of a domain wall in a certain direction is quasi-one dimensional, i.e., the wall moves as a plane without bending. Figure 3 shows the variation of the wall energy as a function of position

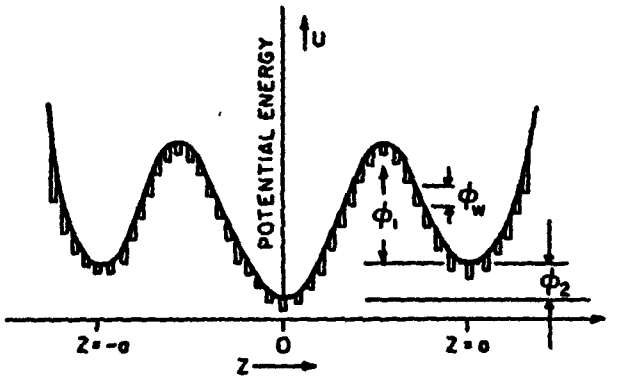

FIGURE 3 Schematic plot of the energy potential for non-180° domain wall motion in PZT ceramics.

in a ceramic sample. The height of the potential barrier ($\Phi_1 + \Phi_2$) is the minimum energy required for the wall to relocate from a depoling state to the poled state. Φ_w is the height of potential barrier for a non 180° domain wall going across one lattice distance.

In a depolarized ceramic sample, all domain walls are randomly oriented, and the distribution of domain walls possesses the symmetry of $\infty\infty m$. Obviously, domain walls are located at the minima of the potential energy ($z = 0$).

When an external ac field is applied, the domain walls oscillate. However, as long as the magnitude of the domain wall vibration is not very large, the macroscopic potential energy for domain wall motions is symmetric with respect to the z axis, i.e. $U(\Delta z) = U(-\Delta z)$. The situation is different for a poled ceramic. During the poling process, the domain walls overcome certain energy barriers, and move into new equilibrium positions. As shown in Figure 3, the new positions are metastable states ($z = a$, or $z = -a$). After the field is removed, the orientation distribution of the domain walls becomes conical in the poled samples. The potential for domain wall motion is no longer symmetric in the poled state, i.e. $U(a - \Delta z) \neq u(a + \Delta z)$.

It also has been shown[39,40] experimentally that the domain wall motion in a poled ceramic is highly nonlinear. Therefore, the potential energy for the domain wall motion may be expanded as a polynomial function of the domain wall displacement[33]:

$$u = U_0 + \frac{C_1}{2}\Delta l^2 + \frac{C_2}{3}\Delta l^3 + \frac{C_3}{4}\Delta l^4 + \text{higher-order terms} \tag{11}$$

where U_0 is the residual energy of a domain boundary, which is assumed to be independent of the domain wall motion. The presence of the third power term describes the asymmetric feature of the domain wall motion in a ferroelectric ceramic. The odd terms will be zero if domain wall vibrations take place around a potential energy minimum of the domain wall. Therefore, the differential equation of the forced vibration of a non-180° domain wall in a ferroelectric ceramic may be expressed as follows[13,14,38]:

$$Am\ddot{\Delta l} + Ab\dot{\Delta l} + \frac{\partial U}{\partial \Delta l} = -\left(\frac{\partial W_E}{\partial \Delta l} + \frac{\partial W_M}{\partial \Delta l}\right) \tag{12}$$

where m represents the effective mass of the domain wall, b is the damping constant, and the dots on top of Δl represent the derivatives with respect to time. The third term is the restoring force. W_E and W_M are the energies of the average electric and elastic dipoles $\langle \delta P_i \rangle$ and $\langle \delta U_{ij} \rangle$ induced by the electric field and stress, respectively, which may be written as

$$-(W_E + W_M) = \left(\sum \langle \delta P_i \rangle E_i e^{j\omega_1 t} + \sum \langle \delta U_j \rangle T_j e^{j\omega_2 t}\right) \tag{13}$$

In general, the electric and elastic driving frequencies are different, $\omega_1 \neq \omega_2$. The physical origins of the restoring force, damping effects and effective mass have

been discussed separately by several scientists.[36-45] If we consider only the first three terms of the restoring force, Equation (12) becomes

$$Am\Delta\ddot{l} + Ab\Delta\dot{l} + AC_1\Delta l + AC_2\Delta l^2 + AC_3\Delta l^3 = -\left(\frac{\partial W_E}{\partial \Delta l} + \frac{\partial W_M}{\partial \Delta l}\right) \quad (12')$$

This equation describes the interrelationship between the amplitude of the non-180° domain wall vibration and the stiffness of the materials. The condition

$$C_1\Delta l >> C_2\Delta l^2,\ C_3\Delta l^3$$

allows one to employ a perturbation method[46] in solving Equation (12'). Approximate values can be obtained for the induced polarization δP_i and strain δU_{ij} resulting from the motion of non-180° domain walls. The detailed solutions are presented in Reference 33. According to Fousek and Brezina,[38] the resonant frequency of domain walls is much higher than the frequencies used in our experiments, which are less than 1 MHz. Thus, the inertia term can be neglected. This means that the damping is sufficiently strong that Equation (12') can be simplified to a relaxation equation.

III. LINEAR AND NONLINEAR COEFFICIENTS

We now consider the linear and nonlinear dielectric, piezoelectric, and elastic properties associated wth the 110° domain wall motion in ferroelectric ceramics. The average induced polarization and strain can be calculated by averaging δU_{ij} and δP_i over all domain wall orientations in the sample.[13,14] $\Delta P_i = \langle \delta P_i \rangle$, and $\Delta U_{ij} = \langle \delta U_{ij} \rangle$ may be expressed as:

$$\begin{aligned}
\Delta P_i &= [\Delta\epsilon_{ik} + \Delta r_{ijk}E_j]E_k + [\Delta d_{im} + \Delta e_{ilm}T_l]T_m + 2\Delta Q_{ijl}E_jT_l \\
&\quad + \Delta H_{ijkp}E_jE_kE_p + \Delta G_{ijkl}E_jE_kT_l + \ldots \\
\Delta U_l &= [\Delta d'_{jl} + \Delta Q'_{ijl}E_i]E_j + [\Delta S_{ln} + \Delta S_{lmn}T_m]T_n + 2\Delta e'_{lkm}E_kT_m \qquad (14) \\
&\quad + \Delta G'_{ijkl}E_iE_jE_k + \Delta W_{ijnl}E_iE_jT_n + \ldots \\
&\quad (i, j, k, p = 1, 2, 3 \text{ and } l, n, m = 1, 2, 3, 4, 5, 6)
\end{aligned}$$

In these expressions, ΔP_i is the total induced average polarization, and ΔU_l is the average strain component in Voigt notation, T_n is the stress, and E_k is the electric field and the expansion coefficients are defined below. The coefficients $\Delta d_{kl} = \langle \delta d_{kl} \rangle$ are the extrinsic piezoelectric constants of a ceramic sample:

$$\Delta d_{kl} = \int_0^{2\pi} d\phi \int_0^{2\pi} d\psi \int_0^{\pi} \frac{1}{\sqrt{3}} S_0P_0K(\omega_i)f_kF_lZ(\Theta)\, d\Theta \qquad (15)$$

where

$F_1 = F_{11}$, $F_2 = F_{22}$, $F_3 = F_{33}$, $F_4 = F_{23}$, $F_5 = F_{13}$, $F_6 = F_{12}$, and,

$$K(\omega_i) = \int_0^{\infty} \frac{Ag(\tau)\, d\tau}{C_1(1 + j\omega_i\tau)}$$

Note: Δd_{kl} depends on ω_2, the frequency of the applied elastic field, and $\Delta d'_{kl}$ depends on ω_1, the frequency of the applied electric field. $g(\tau)$ is the relaxation time distribution[13,14] assuming there exists more than one relaxation time. $Z(\Theta)$ is the distribution function of domain wall orientations obtained during the poling process. All quantities having the Δ symbol are caused by 110° domain wall vibrations only. The values of $\Delta s_{ln} = \langle \delta s_{ln} \rangle$ and $\Delta \varepsilon_{ik} = \langle \delta \varepsilon_{ik} \rangle$ are the extrinsic elastic and dielectric parameters of the ceramic:

$$\begin{aligned} \Delta s_{ln} &= \int_0^{2\pi} d\phi \int_0^{2\pi} d\psi \int_0^{\pi} S_0^2 K(\omega_2) F_l F_n Z(\Theta)\, d\Theta \\ \Delta \varepsilon_{ik} &= \int_0^{2\pi} d\phi \int_0^{2\pi} d\psi \int_0^{\pi} \frac{1}{3} P_0^2 K(\omega_1) f_i f_k Z(\Theta)\, d\Theta \end{aligned} \tag{16}$$

where $\Delta Q_{ijl} = \langle \delta Q_{ijl} \rangle$ (electrostrictive coefficients) and $\Delta r_{ijk} = \langle \delta r_{ijk} \rangle$ (nonlinear dielectric coefficients) can be expressed as follows:

$$\begin{aligned} \Delta Q_{ijl} &= \int_0^{2\pi} d\phi \int_0^{2\pi} d\psi \int_0^{\pi} \frac{-2}{3} S_0 P_0^2 K'(\omega_1, \omega_2) f_i f_j F_l Z(\Theta)\, d\Theta \\ \Delta Q'_{ijl} &= \int_0^{2\pi} d\phi \int_0^{2\pi} d\psi \int_0^{\pi} \frac{-2}{3} S_0 P_0^2 K'(\omega_1) f_i f_j F_l Z(\Theta)\, d\Theta \end{aligned} \tag{17}$$

where

$$K'(\omega_1) = \int_0^{\infty} \frac{C_2 A g(\tau)\, d\tau}{4C_1(1 + 2j\omega_1\tau)(1 + j\omega_1\tau)^2};$$

$$K'(\omega_1, \omega_2) = \int_0^{\infty} \frac{C_2 A g(\tau)\, d\tau}{4C_1(1 + j[\omega_2 + \omega_1]\tau)(1 + j\omega_1\tau)(1 + j\omega_2\tau)}.$$

and

$$\Delta r_{ijk} = \int_0^{2\pi} d\phi \int_0^{2\pi} d\psi \int_0^{\pi} -2P_0^3 K'(\omega_1) f_i f_k f_k Z(\Theta)\, d\Theta \tag{18}$$

Here, we should point out that the contributions of domain wall motion to the electrostrictive coefficients ΔQ_{ijl} and the nonlinear dielectric coefficients Δr_{ijk} have the same physical origin as those of the electro-optical coefficients and elasto-optical coefficients. In fact, in hot pressed transparent PLZT ceramics the changes of the remnant polarization give rise to changes in the birefringence Δn[47–50] because of the non-180° domain reversal induced by an external field.

The electroacoustic coefficients $\Delta e_{klm} = \langle \delta e_{klm} \rangle$ (the coefficients of the nonlinear piezoelectric effect) describe the change in the velocity of elastic waves, and are given by:

$$\begin{aligned} \Delta e'_{klm} &= \int_0^{2\pi} d\phi \int_0^{2\pi} d\psi \int_0^{\pi} \frac{-2}{\sqrt{3}} P_0 S_0^2 Z(\theta) K'(\omega_2) f_k F_l F_m\, d\theta \\ \Delta e_{klm} &= \int_0^{2\pi} d\phi \int_0^{2\pi} d\psi \int_0^{\pi} \frac{-2}{\sqrt{3}} P_0 S_0^2 Z(\theta) K'(\omega_1, \omega_2) f_k F_l F_m\, d\theta \end{aligned} \tag{19}$$

In some materials,[7] the extrinsic contribution to the electroacoustic effect (change

in velocity of sound under an applied electric field) may be two orders of magnitude larger than the intrinsic contribution. The third order elastic coefficients $\Delta S_{lmn} = \langle \delta S_{lmn} \rangle$ are:

$$\Delta S_{lmn} = \int_0^{2\pi} d\phi \int_0^{2\pi} d\psi \int_0^{\pi} -S_0^3 Z(\Theta) K'(\omega_2) F_l F_m F_n \, d\Theta \tag{20}$$

There are twenty one non-vanishing coefficients. The expressions for the higher order nonlinear piezoelectric coefficients $\Delta G_{ijkl} = \langle \delta G_{ijkl} \rangle$ and dielectric coefficients $\Delta H_{ijkp} = \langle \delta H_{ijkp} \rangle$ are given by the following integrals:

$$\begin{aligned} \Delta G'_{ijkl} &= \int_0^{2\pi} d\phi \int_0^{2\pi} d\psi \int_0^{\pi} \frac{1}{3\sqrt{3}} S_0 P_0^3 K''(\omega_1) f_i f_j f_k F_l Z(\Theta) \, d\Theta \\ \Delta G''_{ijkl} &= \int_0^{2\pi} d\phi \int_0^{2\pi} d\psi \int_0^{\pi} \frac{1}{3\sqrt{3}} S_0 P_0^3 K''(\omega_1, \omega_2) f_i f_j f_k F_l Z(\Theta) \, d\Theta \end{aligned} \tag{21}$$

Where

$$K''(\omega_1) = \int_0^{\infty} \left\{ \frac{C_2^2 A g'(\tau)}{4C_1^5 (1 + 2j\omega_1\tau)(1 + 3j\omega_1\tau)(1 + j\omega_1\tau)^3} - \frac{C_3 A g'(\tau)}{4C_1^4 (1 + 3j\omega_1\tau)(1 + j\omega_1\tau)^3} \right\} d\tau$$

$$K''(\omega_1, \omega_2) = \int_0^{\infty} \left(\frac{C_2^2 A g'(\tau)(1 + j\omega_1\tau)^{-2}}{4C_1^5 (1 + 2j\omega_1\tau)(1 + j[2\omega_1 + \omega_2]\tau)(1 + j\omega_2\tau)} - \frac{C_3 A g'(\tau)(1 + j\omega_1\tau)^{-2}}{4C_1^5 (1 + j[2\omega_1 + \omega_2]\tau)(1 + j\omega_2\tau)} \right) d\tau$$

and

$$[\Delta H_{ijkp}] = \int_0^{2\pi} d\phi \int_0^{2\pi} d\psi \int_0^{\pi} \frac{1}{9} P_0^4 K''(\omega_1) f_i f_j f_k f_p Z(\Theta) \, d\Theta \tag{22}$$

Note that all the quantities are frequency dependent. When electric and elastic fields are applied simultaneously with different frequencies, one finds the direct and converse effects have different magnitude, for example, if $\omega_1 \neq \omega_2$, $\Delta d_{kl}(\omega_1) \neq \Delta d_{kl}(\omega_2)$, therefore, we have used a prime on some of the constants in ΔU_i to indicate their frequency dependence. In general, the contributions from 71°, 110° and 90° twin structures can be all written in the form of Equation (14)–Equation (22) except that the integration coefficients would be different in each case.

If $T_1 = 0$, Equation (14) becomes:

$$\begin{aligned} \Delta P_i &= \Delta \varepsilon_{ik} E_k + \Delta r_{ijk} E_j E_k + \Delta H_{ijkp} E_j E_k E_p \\ \Delta U_i &= \Delta d_{kl} E_k + \Delta Q_{ikl} E_l E_k + \Delta G_{ijkl} E_l E_j E_k \\ & \qquad i, j, k, l, p = 1, 2, 3 \end{aligned} \tag{23}$$

The electric field induced longitudinal strain and polarization arising from the domain wall motion are:

$$\begin{aligned} \Delta U_3 &= \Delta d_{33} E_0 + \Delta Q_{333} E_0^2 + \Delta G_{3333} E_0^3 \\ \Delta P_3 &= \Delta \varepsilon_{33} E_0 + \Delta r_{333} E_0^2 + \Delta H_{3333} E_0^3 \end{aligned} \tag{24}$$

Similarly, the shear strain and related polarization under the applied a.c. electric field are described by:

$$\begin{aligned} \Delta U_5 &= \Delta d_{15} E_0 + \Delta G_{1115} E_0^3 \\ \Delta P_1 &= \Delta \varepsilon_{11} E_0 + \Delta H_{1111} E_0^3 \end{aligned} \tag{25}$$

There are no second harmonic and higher even harmonic components in shear vibrations. Therefore, it is expected that the dependence of Δd_{15} and $\Delta \varepsilon_{11}$ on the alternating electric field strength should have different characteristics than those of Δd_{33}, Δd_{31}, and $\Delta \varepsilon_{33}$.

Strictly speaking, under external forces the difference in free energy for the two domains of a twin is[51]:

$$\Delta g = \Delta \varepsilon_{(s)ij} \sigma_{ij} + \Delta P_{(s)i} E_i + \frac{1}{2} \Delta s_{ijkl} \sigma_{ij} \sigma_{kl} + \frac{1}{2} \Delta \kappa_{ij} E_i E_j + \Delta d_{ijk} E_i \sigma_{jk} \tag{26}$$

where, the first two terms are the differences of the spontaneous strain and polarization of the two domains, which is primary ferroic effect. The remaining three terms in Δg arise from external force induced differences in elastic compliance, dielectric susceptibility, and piezoelectric coefficients, which represent the secondary ferroic behavior. In this paper, only the primary ferroic effect is discussed. Based on this viewpoint, it could be found that the extrinsic properties of a twin structure arise from the orientational differences in their intrinsic properties. External forces or fields induce the differences in free energy for the two domains, causing domain walls to move, and creating the extrinsic contributions.

IV. EXPERIMENTAL RESULTS AND DISCUSSIONS

4.1. Experimental Procedure

Several compositions of the PZT solid solution system were selected for this study. The ceramic $Pb(Zr_xTi_{1-x})O_3$ specimens with $x = 0.90, 0.70, 0.60, 0.54, 0.52, 0.50, 0.40, 0.30$, and 0.15 were prepared by a conventional mixed oxide technique. The starting materials of PZT material are also included, both the powders made by the sol-gel method and the $Pb(Zr_{0.52}Ti_{0.48})O_3 + (0.4 - 0.8\%$ wt. $Nb_2O_3)$ powders. Well sintered ceramic samples were poled at an electric field of 30–65 kV/cm in the temperature range of 100°C–130°C. These poled samples were first checked with a commercial Berlincourt d_{33} meter. Values of the piezoelectric coefficients are listed in Table I. In addition, some ceramic samples, PZT-501A and PZT-401 which were made by commercial powders form the Ultrasonic Powders Inc., South Plainfield, NJ. And also several of the hard and soft PZT specimens, PZT-5, PZT-

TABLE I

Piezoelectric coefficients for $Pb(Zr_xTi_{1-x})O_3$ ceramics. The measurements were made by the commercial Berlincourt meter

Zr/Ti.	90/10	70/30	60/40	54/46	52/48	50/50	40/60	30/70	15/85
Density (10^3 kg/m^3)	7.44	7.55	7.60	7.62	7.7	7.4	7.6	7.59	7.3
d_{33} (10^{-12} m/V)	?	85-100	100-120	170-200	250-270	100-120	90-100	50-60	?

8 and PZT-4 used in this study are commercial products from Vernitron piezoelectric division, Bedford, OH.

Permittivity-temperature runs were made in a computer-controlled environmental chamber (Delta Design Model 2300) using liquid nitrogen as a cooling agent. Both heating and cooling rates are about 5°C/min. Data were recorded with a digital multimeter controlled by a desk top computer system (Model 9816, Hewlett Packard Inc.). The dielectric response of the sample was measured by using a modified Sawyer-Tower circuit and a precision capacitance meter (HP 4275A Multi-Frequency LCR Meter). The piezoelectric coefficients were measured by both optical interferometry and iterative methods.[53,54] The resonance-antiresonance method is widely used for measuring piezoelectric coefficients in weak electric fields at which the vibrating system remains linear. However, when the amplitude of the applied field becomes very large, the resonance-antiresonance method is no longer suitable due to the nonlinearity. Therefore, an interferometry technique was used for measurements under large alternating electric fields. The advantages of the interferometry, apart from its directness, are the simplicity in computational expressions. In addition, the measurements can be carried out under both resonance and non-resonance conditions and are not limited by the amplitude of the external fields. Moreover, a wide range of sample shapes and sizes can be tolerated. The HP4192 A LF impedance analyzer was used when employing the resonance technique which has been standardized by IEEE.[53] In measuring the nonlinear parameters, a sinusoidal driving field was used for convenience of interpretation. Resistive tunable low-pass active-filters were used (Package Date 730/740 Series, Frequency Devices, Inc.) in the measurement system. Samples were made as thin as possible in order to achieve a high field with low voltage. For larger displacements, Equation (2) of Reference 54 is no longer valid, and the cosine term in Equation (3) of Reference 54 must be expanded using the Fourier-Bessel expansion. It is important to realize that the nonlinear output signals may be caused by either the nonlinearity of materials or by the distortion of the input signal in the detecting system. There are two ways to avoid the detecting system producing nonlinear output signals. (1) Using the quartz as the pre-calibration sample, we can retrieve the actual measured experimental data in order to remove the nonlinear contribution of the detecting system. (2) Through keeping the thickness of the samples down, we can get sufficiently large strains while restricting the maximum displacement of the sample to values less than 140 Å.

4.2. *Results and Discussions*

A. *Nonlinear piezoelectric and dielectric coefficients.* Figure 4 shows the piezoelectric constants d_{kl} and the dielectric constants ε_{ii} plotted as a function of applied a.c. field strength. When the magnitude of the applied electric field is below a certain limiting value E_t (called the threshold field), d_{kl} and ε_{ii} remain constant. But beyond the threshold field ($E > E_t$), d_{lk} and ε_{ij} increase with the amplitude of the a.c. electric field. E_t signifies the onset of measurable nonlinearity, which is not always clearly defined. We use $\Delta d/d$ ($\Delta\varepsilon/\varepsilon$) > 2.5%– 4% as the criteria according to different experimental conditions. Generally, E_t depends on frequency, temperature and material properties. For instance, for PZT-501A with F = 200 Hz and T = 25°C, the threshold field for the piezoelectric coefficient d_{33} is approximately 300 V/cm. Analogously, when the applied field exceeds a certain value, dielectric losses also increase drastically with the amplitude of a.c. electric field,[33] but the threshold fields for the loss seem to be smaller than those for the dielectric and piezoelectric coefficinets. By using an oscilloscope to follow the polarization (P) and strain (S) under a.c. electric field (E) at a given frequency, it was found that the P and S vs. E curves are straight lines for small oscillation amplitudes, but the average slope of the hysteresis increases rapidly when the amplitude of the a.c. field exceeds certain values, as shown in the insertion of Figure 4. Since the non-180° domain wall motion is inherently a lossy process,[55–57] the strong correlation between loss and nonlinearity suggests that electromechanical nonlinearity in ferroelectric ceramics originates mainly from the

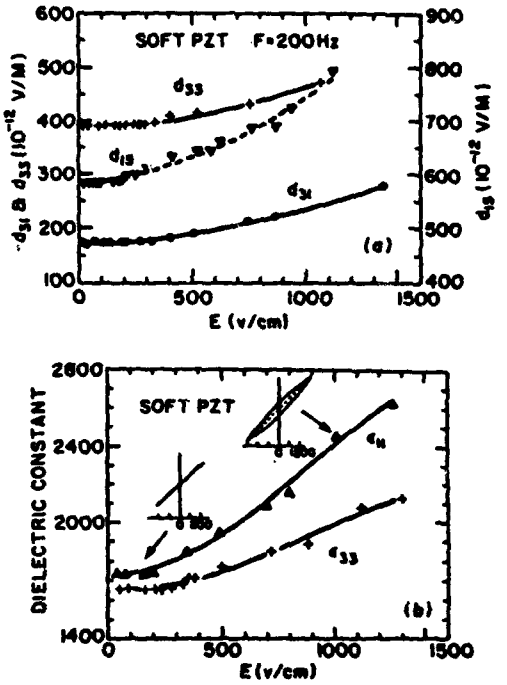

FIGURE 4 (a) a.c. electric field dependence of the piezoelectric coefficients d_{31}, d_{33}, and d_{15}. (b) a.c. electric field dependence of dielectric coefficients ε_{11}, and ε_{33}.

motion of non-180° domain walls. Spectrum analyses were made to identify the higher harmonic components in the responses of polarization and strain. It is found[33] that when the direction of a.c. field is perpendicular to the poling direction of the sample, only odd harmonics exist and the shape of the hysteresis loops (both for strain and polarization vs. a.c. electric field) is always symmetric. On the other hand, when an a.c. electric field E is parallel to the poling direction, both odd and even harmonics exist. They become obvious when external field is above the certain level. The shape of hysteresis loop is no longer symmetric. This may be understood from Equations (24) and (25). Assuming $E_{ac} = E_0 \cos \omega t$, from Equation (23), the longitudinal strain is:

$$\Delta U_3 = \Delta d_{33} E_{ac} + \Delta r_{333} E_{ac}^2 + \Delta G_{3333} E_{ac}^3 = Y_0 + Y_1 e^{j\omega t} + Y_{-1} e^{-j\omega t} + Y_2 e^{2j\omega t} + Y_{-2} e^{-2j\omega t} + Y_3 e^{3j\omega t} + Y_{-3} e^{-3j\omega t} + \ldots \quad (27)$$

where

$$Y_0 = \Delta r_{333} \frac{E_0^2}{2}; \qquad Y_1(\omega) = Y_{-1}(-\omega) = \left(\Delta d_{33} E_0 + \frac{3 \Delta G_{3333} E_0^3}{4} \right)$$

$$Y_2(\omega) = Y_{-2}(-\omega) = \Delta r_{333} \frac{E_0^2}{2}; \qquad Y_3(\omega) = Y_{-3}(-\omega) \frac{\Delta G_{3333} E_0^3}{4}$$

The term $(Y_n e^{jn\omega t} + Y_{-n} e^{-jn\omega t})$ represents the component of the nth harmonic oscillation. Based on Equation (27), we would like to elaborate a few points:

1. The third order term increases the amplitude of the fundamental frequency by an amount of $3\Delta G_{3333} E_0^3/4$.
2. The second order harmonic term creates an additional negative bias field which displaces the center of vibration of the domain wall.
3. Both the second and the third harmonic vibrations of non-180° domain walls contribute to the induced longitudinal strain. This implies that the hysteresis loops of both P vs. E, and S vs. E should be asymmetric when the a.c field is beyond the certain level. The situation is somewhat different for the shear strain. From Equation (23), we have

$$\Delta U_5 = \Delta d_{15} E_{ac} + \Delta G_{1115} E_{ac}^3 = Y_0 + Y_1 e^{j\omega t} + Y_{-1} e^{-j\omega t} + Y_3 e^{3j\omega t} + Y_{-3} e^{-3j\omega t} + \ldots \quad (28)$$

where

$$Y_0 = 0; \qquad Y_1(\omega) = Y_{-1}(-\omega) = \Delta d_{15} E_0 + \frac{3 \Delta G_{1115} E_0^3}{4}$$

$$Y_2(\omega) = Y_{-2}(-\omega) = 0; \qquad Y_3(\omega) = Y_{-3}(-\omega) = \frac{\Delta G_{1115} E_0^3}{4}$$

There is no second harmonic in the shear strain, which is in agreement with the experimental results. Measurements of the complex ε_{ij} have been carried out with doped PZT ceramics. Figure 5 shows the relative dielectric permittivity ε_{11} and ε_{33} of the PZT-5 ceramic as well as their loss tangents as a function of temperature from −200°C to 50°C at two different magnitudes of the applied a.c. electric field. Figure 6 shows the dielectric permittivity ε_{33} and its loss versus temperature at different a.c. electric field strengths. Clearly, the values of ε_{11} and ε_{33} as well as

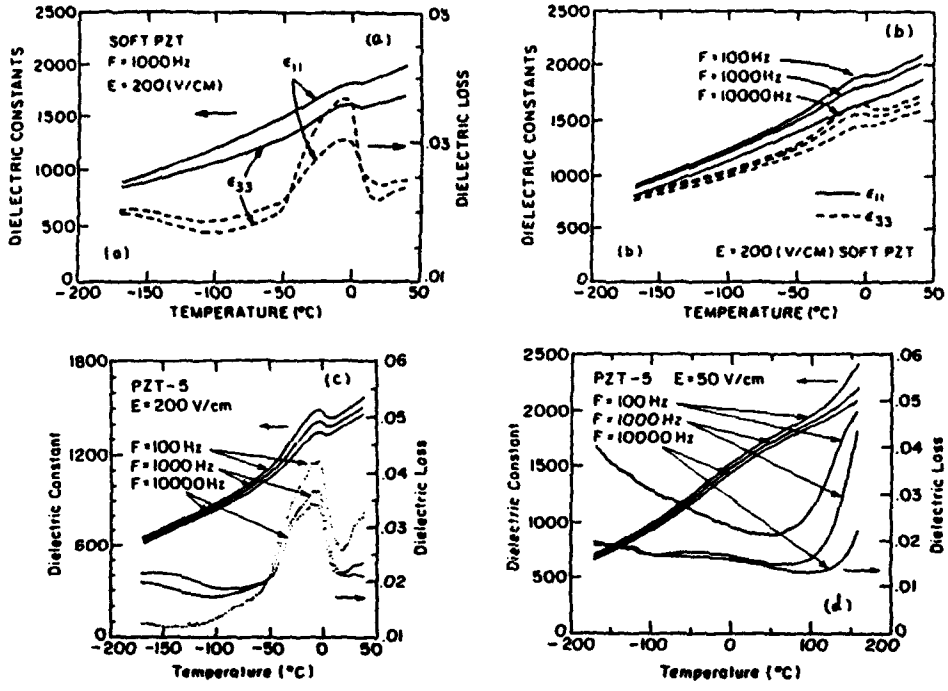

FIGURE 5 (a) ε_{11} and ε_{33} and their losses as a function of temperature for a PZT-501A sample. (b) The values of ε_{11} and ε_{33} as a function of temperature for PZT-501A at different frequencies. (c) and (d) are the temperature dependence of dielectric constant ε_{33} and its loss for a PZT-5 ceramic measured at the field levels of 200 V/cm and 50 V/cm, respectively, at three different frequencies.

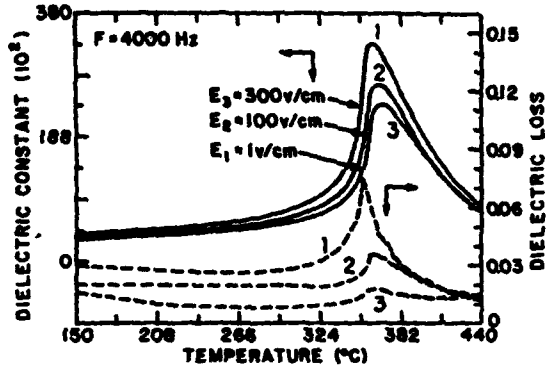

FIGURE 6 Temperature dependence of ε_{33} and its tan δ of a PZT-501A sample at different magnitudes of a.c. fields.

their losses are quite different at high temperatures, these differences become smaller as temperature decreases. This may reveal that part of the difference between ε_{11} and ε_{33} may come from the domain boundary vibrations which are frozen out at very low temperatures. It is found that PZT with composition near the morphotropic boundary has one relaxation region in the low temperature regime, which has been also observed by others.[13] The interesting thing is that under

a.c. external field, a pseudo relaxation peak can be observed (Figure 5(c)) in a very broad frequency range, which can be interpreted as the "clamping" of the large magnitude movement of domain walls. In Reference 33, it has been shown that the threshold fields of the piezoelectric coefficients increase with aging time, which is another strong implication that the threshold field is closely related to non-180° domain wall motion, because the reduction of the non-180° domain wall mobility is responsible for the aging phenomena in ferroelectric ceramics.[58] It is also found[33] that the threshold field strengths of the dielectric and piezoelectric coefficients decrease with increasing the magnitude of an applied positive d.c. bias field which provides the pinning to the wall motion. The nonlinearity also decreases with temperature due to the fact that the domain wall becomes less mobile at lower temperature. Figure 7 shows the distribution of threshold fields for the piezoelectric coefficients of the PZT system with different compositions and dopants. A pronounced minimum value for the threshold field is found for the composition near the morphotropic phase boundary (MPB), which reveals that the domain walls have the highest mobility for compositions at the MPB. In second order approximation, the extrinsic contributions to the piezoelectric coefficient is given in Equation (23):

$$d_{kl} = \Delta d_{kl} + \Delta Q_{ikl}E_i + \Delta G_{ijkl}E_iE_j \tag{29a}$$

Assuming the nonlinearity is purely extrinsic, one has:

$$\langle d_{kl}\rangle = d_{kl(in)} + \Delta d_{kl} + \Delta Q_{ikl}E_i + \Delta G_{ijkl}E_iE_j \tag{29b}$$

where $\langle d_{lk}\rangle$ is the measured piezoelectric coefficient, which include both the intrinsic contribution, $d_{lk(in)}$, and the extrinsic contribution, the contribution, Δd_{lk}. Based on the definition of threshold field strength of $\langle d_{lk}\rangle$ described earlier, we have:

$$\left|\frac{\langle d_{33}\rangle - (d_{33(in)} + \Delta d_{33})}{(d_{33(in)} + \Delta d_{33})}\right|_{E_t} = \frac{\Delta Q_{333}E_t}{d_{33(in)} + \Delta d_{33}} \geqslant 3\% \tag{29c}$$

This means that the threshold field is inversely proportional to the ratio between the electrorestrictive coefficient and the piezoelectric coefficient. From Equation (15) and Equation (17), it is found that $\Delta d_{33}/\Delta Q_{333}$ is proportional to $(C_1)^2/(P_0C_2)$.

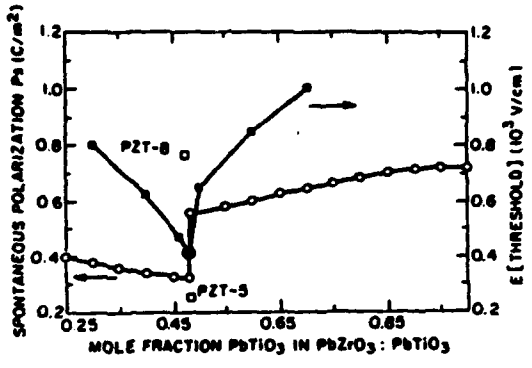

FIGURE 7 Dependence of the threshold field strength and the spontaneous polarization on the Ti/Zr ratio for PZT ceramics.

In Reference 41, the restoring force constant was estimated to be greater than the square of the spontaneous strain $C_1 > (S_0)^2$, and also $C_1 > C_2$. Therefore, $(\Delta d_{33}/\Delta Q_{333})$ can be estimated to be proportional to the spontaneous polarization. Thus from Equation (29c) one may conclude that the threshold field E_t should also increase with the spontaneous polarization. The experimental data in Figure 7 qualitatively shows this tendency. In addition, the threshold fields E_t for PZT-8 and PZT-4 are substantially higher than that of PZT-5 due to the influence of dopants on the domain wall mobility.

B. *Electromechanical nonlinearity under resonant frequency.* Many ultrasonic devices are operated at their resonance frequencies. When being driven at high field levels, the presence of nonlinearity alters the performance of these devices. In this section, we report some of the nonlinear effects under resonant conditions for a PZT-501A ceramic. Figure 8 shows the complex admittance circles at different drive levels. The outer circle (curve I) is measured at small-signal conditions, a field level of 1 V/cm. The system appears to be a typical linear piezoelectric resonator with very low loss. All the data points fall onto a perfect circle. The inner circle (curve II) was measured at a field level of 100 V/cm. One can see that the data points obviously deviate from the small circle showing the presence of nonlinearity.

This is expected from the measurements on piezoelectric effects because the relationship between d_{31} and field strength no longer remains linear under large field, invalidating the linear assumption made in the measurement technique. It is found that the magnitudes of $d_{31}[II](-190 \times 10^{-12}$ V/m) and the loss tangent $d'_{31}[II]/d_{31}[II]$ (0.085), which were measured at high drive levels but non-resonant frequencies using an interferometer, are larger than those values ($d_{31}[I] = -176 \times 10^{-12}$ V/m and $d'_{31}[I]/d_{31}[I] = 0.018$) measured at low driving levels. This strongly implies that the nonlinear effects at the resonance frequency are caused by the nonlinear increase in piezoelectric coefficients. We suggest that this nonlinear change in piezoelectric coefficients originates from the domain wall motion since the increase of the macroscopic-losses mainly arises from domain wall motions.[33] When the applied field exceeds a certain level, the nonlinear domain wall motions start to contribute to the piezoelectric effect, and the coupling between the vibrations

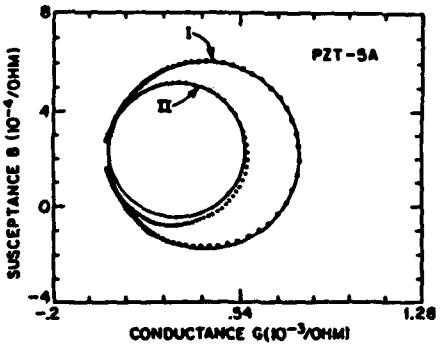

FIGURE 8 Complex admittance plot of PZT-501A bar measured with two different applied field strengths. Curve I: $E_1 = 1$ V/cm and curve II: $E_2 = 100$ V/cm.

of domain wall and extensional mode causes the nonlinear effects at the resonance frequency. The field dependence of the electromechanical properties causes the extremum frequencies of the admittance to shift as shown in Figure 9. Figure 9(a) is the amplitude of the admittance of a PZT-501A plate, which was measured with a spectrum analyzer. The resonant frequency f_m shifts towards lower frequencies with increasing applied a.c. voltage, but the anti-resonance frequencies f_n do not shift significantly as reported by Uchino *et al.*[6]

Interestingly, however, when measuring the absolute value of admittance $|Y|$ of a bar sample with an impedance analyzer, we found that both f_m and f_n shift noticeably to lower frequencies at higher driving level, as shown in Figure 9(b), which may imply that the nonlinearity affects certain vibration modes more severely than to the others. Meanwhile, the experimental results could be affected by the measurement techniques.

Figure 10 and Figure 11 show the dielectric losses and dielectric constants as a function of frequency, respectively, under different field levels near an isolated resonance. It can be seen that the resonance peaks of both the dielectric loss and the dielectric constant move toward lower frequencies at the high drive level. The

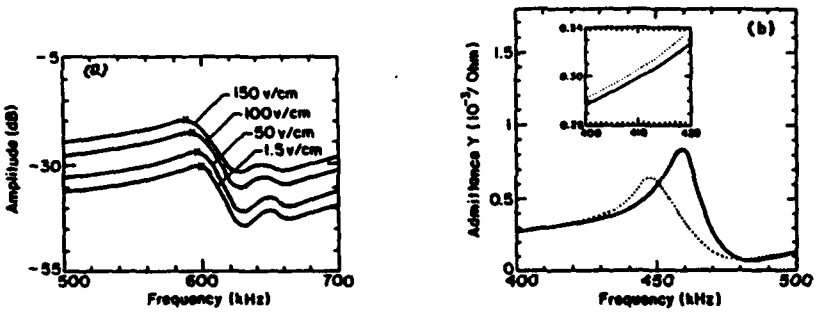

FIGURE 9 Typical admittance curves measured for the PZT-501A samples at different driving levels. (a) Measured electrical admittance of PZT-501A plate at four different driving levels. (b) Absolute value of admittance $|Y|$ for a PZT-501A bar at two driving levels. The solid line and the dash line represent results obtained at field levels of E_1 = 1 V/cm and E_2 = 100 V/cm respectively.

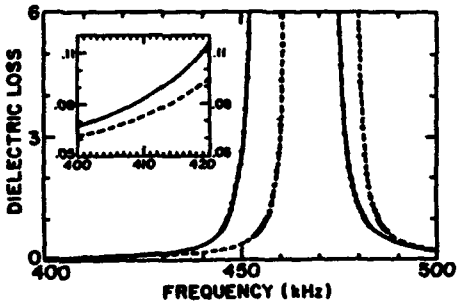

FIGURE 10 Dielectric losses vs frequency with respect to different driving levels for a PZT-501A bar in the vicinity of the resonance frequency. The dash line is for E_1 = 1 V/cm and the solid line is for E_2 = 100 V/cm.

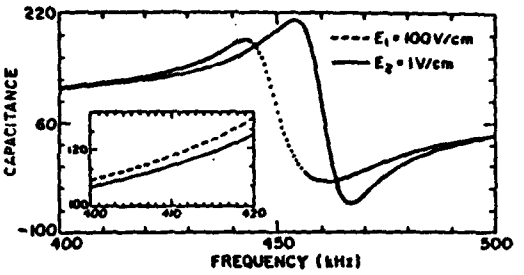

FIGURE 11 Capacitance of a PZT-501A bar vs. frequency in the vicinity of the resonance frequency at different driving levels.

dielectric loss in the vicinity of the resonant frequency also becomes larger for the case of higher drive level as shown in Figure 10. It should be noted that when large electric field is applied, nonlinear effects occur at all frequencies, hence, the dielectric loss, mechanical loss, dielectric constant, elastic constants, and piezoelectric coefficients become larger in all frequency ranges. Away from the resonance, the motions of non-180° domain walls are an important cause for the changes in the dielectric, elastic, and piezoelectric coefficients. At the resonant frequency, changes of these coefficients will profoundly lead to the shifts of the resonance and antiresonance frequencies, f_m and f_n. In addition, the mechanical quality factor Q_m and the electromechanical coupling factors K_t will also be affected. The factors controlling the shift of resonant frequency are important in ultrasonic engineering. From Reference 28, in second order approximation, the shift of the resonant frequency for extensional vibration of an electromechanically excited bar can be written as:

$$\delta\omega_r^D = -\left\{\frac{32[S_{111}^E]^2}{9\pi^2 S_{11}^E} + \frac{9S_{1111}^E}{32}\right\}\frac{\omega_r^D d_{31}^2 E^2 Q^2}{[S_{11}^E]^2 a^2} \tag{30}$$

where ω_r^D is the resonant frequency of the extensional mode for a linear system, s_{11}^E and s_{111}^E are the second and third order elastic compliance. The frequency of the P_3 maximum is also shifted by the electric field,

$$\delta\omega_r^P = -\left\{\frac{(\varepsilon_{333}^T)^2}{\varepsilon_{33}^T} + \frac{3\varepsilon_{333}^T}{4}\right\}\frac{\omega_r^P E^2 Q^2}{2\varepsilon_{333}^T a^2} \tag{31}$$

where ω_r^P is the small-signal resonance frequency, Q is the mechanical quality factor and a is the thickness of the sample. Equations (30) and (31) are for single domain and single crystal system. For ceramics, there exist additional shifts of the resonant frequencies by domain wall motion. From Equations (15)–(21) they can be expressed as:

$$\Delta\omega_r^D = -\left\{\frac{32[\Delta S_{111}]^2}{9\pi^2(S_{11(in)} + \Delta S_{11})} + \frac{9\Delta G_{1111}}{32}\right\}\frac{\omega_r^D(d_{31(in)} + \Delta d_{31})^2 E^2 Q^2}{(S_{11(in)} + \Delta S_{11})^3 a^2} \tag{32}$$

and

$$\Delta\omega_r^P = -\left\{\frac{[\Delta r_{333}]^2}{\varepsilon_{33(in)} + \Delta\varepsilon_{33}} + \frac{3\Delta H_{3333}}{4}\right\}\frac{\omega_r^P E^2 Q^2}{2(\varepsilon_{33(in)} + \Delta\varepsilon_{33})a^2} \tag{33}$$

Here $\varepsilon_{ij(in)}$, $d_{ik(in)}$, and $S_{nm(in)}$ are intrinsic properties. The total shift of these resonance frequencies are the sum of intrinsic and extrinsic contributions. The above analyses give rise to a relationship between the shifts of the maximum frequency and the damping constant (or losses), restoring force constants, as well as spontaneous polarization and strain. The results shown in Equations (30)–(33) may be used to qualitatively explain the experimental results.

The mechanical and electric responses of a piezoelectric material depends not only on its piezoelectric properties, but also on its elastic and dielectric parameters, according to the constitutive piezoelectric equations.[59] Therefore, a figure of merit of a piezoelectric material must include its elastic, dielectric and piezoelectric coefficients, which are defined as the electromechanical coupling factors (often called coupling coefficients). The coupling coefficient k is used as a characteristic index for the performance of a transducer. The value of k^2 is a measure of the magnitude of the transducer bandwidth. It is useful to clarify the extrinsic contribution to the electromechanical coupling coefficients and to understand how the domain wall movements influence the coupling coefficient. Figure 12 shows the measured field dependence of the coupling coefficient k_{31} and the mechanical quality factor Q_m. One can see that the coupling factor, and the mechanical losses increase with the increase of the magnitude of a.c. field. The correlation between the coupling factor and the loss factor indicates that the extrinsic contributions plays a very important role in terms of the electric-mechanical energy conversion in ferroelectric ceramic. It should noted that the coupling factor is dependent on the stress and strain level, which often show spatial variations.[60]

In the high temperature regime, for some PZT system, it is difficult to abstract information on domain wall contribution from the measurement of dielectric and piezoelectric coefficients for a PZT system.[3,59] The problem is that the conductivity of some PZT systems increases drastically at high temperatures just like in semiconductors. Thus, at high temperatures, the increase of conductivity which contribute to the lose factor could cover up the extrinsic contribution of domain wall motions. For this reason, we have to compare the measured results from both low and high field strength at the same temperatures in order to see the contribution

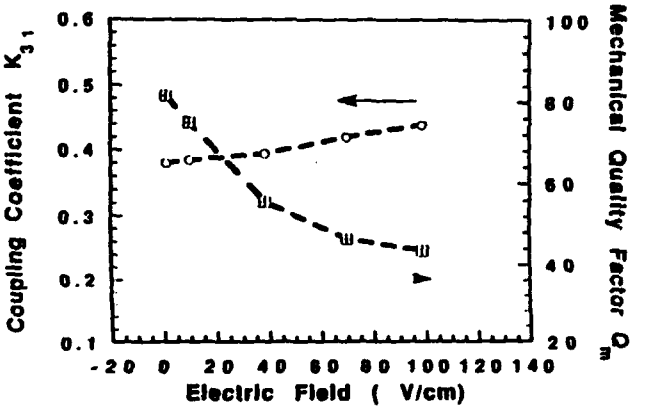

FIGURE 12 Variation of the electromechanical coupling factor k_{31} and the mechanical quality factor Q_m due to the increase of the applied a.c. electric field strength.

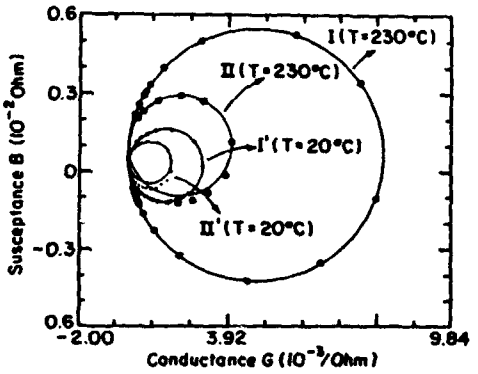

FIGURE 13 Susceptance (B) v.s. conductance (G) loops for a soft PZT ceramic at two different applied a.c. field strengths and two different temperatures.

TABLE II

Electromechanical coupling factors, piezoelectric coefficients and mechanical quality factors of PZT-5A ceramic at different temperatures and field levels

	T = 20°C			T = 230°C		
	k_{31}	Q_m	d_{31}	k_{31}	Q_m	d_{31}
E= 70 V/cm	0.418	47	-186	0.36	52.4	-218
E= 1 V/cm	0.387	80	-179	0.28	182	-195

of domain wall motions. Figure 13 presents the complex admittance circles of a PZT-5 ceramic resonator measured with two different applied field strengths at two different temperatures. The radii of these four circles are denoted by B_1, B_2, B_1', and B_2', respectively. Here B_1' (low drive level) and B_2' (high drive level) are for the room temperature measurements, B_1 (low drive level) and B_2 (high drive level) are for the measurements made at $T = 230$°C. It could be found that the ratio of (B_1/B_2) increases with temperature. The ratio of (B_1/B_2) is proportional to the nonlinear mechanical losses of the ceramic resonator in the vicinity of the resonance frequency, because the radii of these circles are proportional to the mechanical quality factor Q_m.[61] Table II lists the electromechanical coupling and piezoelectric coefficients as well as the mechanical quality factor for different temperatures and different drive levels. These results convincingly show that the increase of electromechanical coupling as the temperature increases arises from the increase of domain wall mobility.

V. SUMMARY

We have measured the dielectric and piezoelectric properties of PZT system in several compositions at both high and low field levels. The experimental results show that domain wall vibrations contribute significantly to the electromechanical nonlinearity in ferroelectric ceramics. The main results are summarized as follows:

1. A phenomenological model has been extended to evaluate the macroscopic nonlinear parameters associated with non-180° domain wall vibrations in ferroelectric ceramics. The theoretical description qualitatively agrees with some of the experimental results.
2. Dielectric and piezoelectric measurements have been carried out for PZT ceramic system at different field levels and temperatures, the results are compared with the theoretical model. It has been verified that the couplings between the acoustic vibrations and the movement of domain walls is an important factor in terms of extrinsic properties of ferroelectric ceramics. It is found that the nonlinear effects are extrinsic in nature and will easily occur at the resonant frequency because the coupling interaction between domain wall motions and the acoustic waves is maximum at the resonant frequency. The piezoelectric and dielectric coefficients and losses in the nonlinear regime are much larger than those in the linear regime. The threshold fields of the dielectric and piezoelectric coefficients are strongly affected by the bias field, temperature and compositions.
3. PZT ceramic with composition near the morphotropic phase boundary shows a pronounced maximum of the non-linear effect. The ratio of c/a axes is an important factor which affects the extrinsic properties in PZT ceramic system. Both shifts of f_m and f_n of the admittance at the high drive level due to the nonlinearity could be evaluated from non-180° domain wall motion. It has been suggested previously[31] that the nonlinear effects in the resonance frequency region originates from the collective resonance of domain walls. This opinion is questionable because the resonance frequency of ceramic samples depends on the sample size and is usually much lower than the domain wall resonance frequency. However, since the resonance frequency of domain walls is still a disputed topic, further investigation is required. We believe that the nonlinear effects contain both intrinsic and extrinsic contributions. In multidomain crystals, such as ferroelectric ceramics, the extrinsic contributions play the dominant role in generating these nonlinearities.

ACKNOWLEDGEMENTS

We thank Professor A. S. Bhalla for some stimulating discussions, Dr. D. Damjanovic for his assistance in the iterative method calculation and providing us with the computer program and Dr. U. Kumar for his assistance in preparing ceramic samples. This research was supported by the Office of Naval Research under grant No. N00014-89-J-1689.

REFERENCES

1. P. Gonnard, L. Eyraud, M. Troccaz and P. Eyraud, "Analysis of the Suitability of Piezoceramics for High Power Transducers," *Proc. IEEE. Ultrasonics Symposium*, 619–623 (1986).
2. Ralph S. Woollett and Charles L. Leblanc, "Ferroelectric Nonlinearities in Transducer Ceramics," *IEEE Transactions on Sonics and Ultrasonics*, SU-20(1), 24–31 (1973).
3. D. A. Berlincourt, D. R. Curran and H. Jaffe, "Piezoelectric and Piezomagnetic Materials and Their Function in Transducers," *Physical Acoustic*, 1(A), Chapter 3, Ed. by W. P. Mason, Academic Press, NY (1964).
4. J. M. Huckabay, Hollis C. Boehem and Elmer L. Hixson, "Admittance Measurement Accuracies Required to Determine Nonlinear Behavior in Sonar Transducers," *IEEE Transactions on Sonics and Ultrasonics*, SU-22(2), 101–104 (1975).

5. K. Lubitz and W. Wersing, "Automatic Performance Testing of Piezoelectric Ceramics for Power Transducers," *Ferroelectrics*, **40**, 237–244 (1982).
6. K. Uchino, Kiroyasu Negishi and Terukiyo Hirose, "Drive Voltage Dependence of Electromechanical Resonance in PLZT Piezoelectric Ceramics," *J. of Appl. Phys.*, Vol. **28**, Supplement **28-2**, 47–49 (1989).
7. R. Lec and J. F. Vetelino, "Influence of an External Electric Field on the Electroacoustic Properties of PZT-4," *Proc. IEEE. Ultrasonics Symposium*, 741–745 (1987).
8. E. A. Kraut, T. C. Lim and B. R. Tittmann, "Application of Nonlinear Interactions in Ferroelectric Ceramics to Microwave Signal Progressing," *Ferroelectrics*, **3**, 247–255 (1972).
9. A. Oliver, "Acoustic Surface Waves," Springer, New York (1978).
10. R. E. Newnham, Q. C. Xu, S. Kumar and L. E. Cross, "Smart Ceramics," *Ferroelectrics*, **102**, 1–8, (1990).
11. A. F. Devonshire, "Theory of Barium Titanate—Part I," *Phil. Mag.* **40**, 1040–1049 (1949).
12. M. J. Haun, E. Furman, S. J. Jang and L. E. Cross, "Thermodynamic Theory of the Lead Zirconate—Titanate Solid Solution System, Part I: Phenomenology," *Ferroelectrics*, **99**, 13–25 (1989).
13. G. Arlt, H. Dederichs and R. Herbiet, "90°-domain Wall Relaxation in Tetragonally Distorted Ferroelectric Ceramics," *Ferroelectrics*, **74**, 37–53 (1987).
14. G. Arlt and H. Dederichs, "Complex Elastic, Dielectric and Piezoelectric Constants by Domain Wall Damping in Ferroelectric Ceramics," *Ferroelectrics*, **29**, 47–50 (1980).
15. P. Gurk, "Contribution of Domain Wall Motion to the Permittivity of Rochelle Salt," *Phys. Stat. Sol.(a)*, **10**, 407–414 (1972).
16. V. A. Isupov, "Characteristics of Coexistence of Tetragonal and Rhombohedral Phases in Piezoelectric Ceramics Based on $PbTiO_3$ and $PbZrO_3$," *Sov. Phys. Solid State*, **18**(4), 529–534 (1976).
17. A. G. Luchaninov, A. V. Shil'Nikov, L. A. Shuvalov and I. JU. Shipkova, "The Domain Processes and Piezoeffects In Polycrystalline Ferroelectrics," *Ferroelectrics*, **98**, 123–126, (1989).
18. E. K. W. Goo, R. K. Mishra and G. Thomas, "Electron Microscopy Study of the Ferroelectric Domains and Domain Wall Structure in $PbZr_{0.52}Ti_{0.48}O_3$," *J. Appl. Phys.*, **52**(4), 2939–2943 (1981).
19. P. G. Lucuta, V. Teodoresu and F. Vasiliu, "SEM, SAED, and TEM Investigations of Domain Structure in PZT Ceramics at Morphotropic Phase Boundary," *Appl. Phys.*, **A37**, 237–242 (1985).
20. P. G. Lucuta, "Ferroelectric-Domain Structure in Piezoelectric Ceramics," *J. Am. Ceram. Soc.*, **72**(6), 933–937 (1989).
21. G. Arlt, "The Role of Domain Wall on the Dielectric, Elastic and Piezoelectric Properties of Ferroelectric Ceramics," *Ferroelectrics*, **76**, 451–458 (1987).
22. G. Arlt, "Microstructure and Domain Effects in Ferroelectric Ceramics," *Ferroelectrics*, **91**, 3–7 (1989).
23. R. Herbiet, U. Robels, H. Dederichs and G. Arlt, "Domain Wall and Volume Contributions to Materials Properties of PZT Ceramics," *Ferroelectrics*, **98**, 102–121 (1989).
24. E. I. Eknadiosiants, V. Z. Borodin, V. G. Smotrakov, V. V. Eremkin and A. N. Pinskaya, "Domain Structure of Rhombohedral $PbTi_xZr_{1-x}O_3$ Crystals," *Ferroelectrics*, **111**, 283–289 (1990).
25. L. Pardo, J. Mendiola, A. Gonzalez and J. De Frutos "Role of Domains on the Electromechanical Anisotropy of Ca-Modified $PbTiO_3$ Ceramics," *Ferroelectrics*, **94**, 189–194 (1989).
26. J. Von Cieminski, C. Kleint, H. Beige and R. Hoche, "Effects of Internal Mechanical Stress on the Electromechanical Properties of Ferroelectric Ceramics," *Ferroelectrics*, **109**, 95–100 (1990).
27. D. Berlincourt and H. A. Krueger, "Domain Processes in Lead Titanate Zirconate and Barium Titanate Ceramics," *J. of Appl. Phys.*, **30**, 1804–1810 (1959).
28. H. Beige and G. Schmidt, "Electromechanical Resonances for Investigating Linear and Nonlinear Properties of Dielectrics," *Ferroelectrics*, **41**, 39–49 (1982).
29. M. D. Bryant and R. F. Keltie, "A Characterization of the Linear and Non-linear Dynamic Performance of a Practical Piezoelectric Actuator, Part. 1: Measurements," *Sensors and Actuators*, **9**, 95–103 (1986).
30. M. D. Bryant and R. F. Keltie, "A Characterization of the Linear and Non-linear Dynamic Performance of a Practical Piezoelectric Actuator, Part. 2. Theory," *Sensors and Actuators*, **9**, 105–114 (1986).
31. A. F. Litvin, M. M. Pikalev, V. A. Doroshenko and V. Z. Borodin, "Electromechanical Nonlinearity of Polycrystalline Ferroelectrics Under Resonant Excitation," *Ferroelectrics*, **51**, 159–171 (1984).
32. H. J. Hagemann, "Loss Mechanisms and Domain Stabilization in Doped $BaTiO_3$," *J. Phys. C.*, **11**, 3333–3344 (1978).
33. Shaoping Li, Wenwu Cao and L. E. Cross, "The Extrinsic Nature of Nonlinear Behavior Observed in Lead Zirconate Titanate Ferroelectric Ceramics," *J. Appl. Phys.*, **69**, 7219–7224 (1991). Shaoping Li, "Extrinsic Contributions to the Response in Ferroelectric Ceramics," Ph.D. Thesis, The Pennsylvania State University (expected 1992).

34. A. S. Nowick and W. R. Heller, "Anelasticity and Stress-Induced Ordering of Point Defects in Crystals," *Adv. in Phys.*, **12**, 251–298 (1963).
35. A. S. Nowick and W. R. Heller, "Dielectric and Anelastic Relaxation of Crystals Containing Point Defects," *Adv. in Phys.*, **14**, 101–164 (1965).
36. R. E. Nettleton, "Effective Mass of 180° Domain Wall in Single Crystal Barium Titanate," *J. of Physical Society of Japan*, **22**(6), 1375–1386 (1967).
37. R. C. Miller and G. Weinreich, "Mechanism for the Sidewise Motion of 180° Domain Walls in Barium Titanate," *Phys. Rev.*, **117**, 117 (1960).
38. J. Fousek and B. Brezina, "Relaxation of 90°-Domain Walls of $BaTiO_3$ and Their Equation of Motion," *J. Phys. Soc. of Japan*, **19**(6), 830–838 (1964); and "Frequency Dependence of the Motion of 90° Domain Walls in Barium Titanate," *Bulletin of the Academy of Science of the USSR*, **28**, 624–628 (1964).
39. J. Fousek and B. Brezina, "The Movement of Single 90° Domain Walls of $BaTiO_3$ in an Alternating Electric Field," *Czech. J. Phys.*, **B10**, 511–528 (1960), and "The Motion of 90° Wedge Domains in $BaTiO_3$ in an Alternating Electric Field," *Czech. J. Phys.*, **B11**, 344–359 (1961).
40. G. Arlt and N. A. Pertsev, "Force Constant and Effective Mass of 90° Domain Walls in Ferroelectric Ceramics," *J. Appl. Phys.*, **70**(4), 2283–2289 (1991).
41. V. S. Postnikov, V. S. Pavlov, and S. K. Turkov, "Internal Friction in Ferroelectrics Due to Interaction of Domain Boundaries and Point Defects," *Phys. Chem. Solids*, **31**, 1785–1791 (1970).
42. V. S. Postnikov, V. S. Pavlov, and S. K. Turkov, "Internal Friction in $Pb_{0.95}Sr_{0.05}(Zr_{0.53}Ti_{0.47})O_3$ + 3% PbO Ferroelectric Ceramics," *Izu. Akad. Nauk.*, **31**, 1845–1850 (1967).
43. V. S. Postnikov, V. S. Pavlov, S. A. Gridnev, and S. K. Turkov, "Interaction Between 90° Domain Walls and Point Defects on the Crystal Lattice in Ferroelectric Ceramics," *Soviet Physics—Solid State*, **10**(6), 1267–1271 (1968).
44. Jan G. Smits, "Influence of Moving Domain Walls and Jumping Lattice Defects on Complex Material Coefficients of Piezoelectrics," *IEEE Transactions on Sonics and Ultrasonics*, **SU-23**(3), 168–174 (1976).
45. J. O. Gentner, P. Gerthsen, A. Schmidt, and R. E. Send, "Dielectric Losses in Ferroelectric Ceramics Produced by Domain Wall Motion," *J. Appl. Phys.*, **49**(8), 4485–4489 (1978).
46. A. H. Nayfeh, "Perturbation Methods," John Wiley & Sons Inc. (1973).
47. C. E. Land and W. D. Smith, *Appl. Phys. Lett.*, **23**, 57–60 (1973).
48. I. P. Kaminow, "An Introduction to Electric-optic Devices," Academic Press, New York (1974).
49. J. R. Maldonado and A. H. Meitzler, "Ferroelectric Domain Switching in Rhombohedral-Phase PLZT Ceramics," *Ferroelectrics*, **3**, 169–175 (1972).
50. C. J. Burfoot, and G. W. Taylor, "Polar Dielectrics and Their Applications," 304, The Macmillan Press Ltd. (1979).
51. R. E. Newnham, "Domains in Minerals," *Amer. Miner.*, **59**, 906–918 (1974).
52. G. Arlt, "Domain Contributions to Piezoelectricity in Ceramics," *IEEE, 1990 Ultrasonic Symposium*, 733–738 (1990).
53. Jan G. Smits, "Iterative Method for Accurate Determination of the Real and Imaginary Parts of the Materials Coefficients of Piezoelectric Ceramics," *IEEE Transactions on Sonic and Ultrasonics*, **SU-23**(6), 393–402 (1976).
54. Q. M. Zhang, W. Y. Pan and L. E. Cross, "Laser Interferometer for the Study of Piezoelectric and Electrostrictive Strains," *J. Appl. Phys.*, **68**(8), 2492–2496 (1988).
55. L. Benguigui, "Ferroelectric Losses in $BaTiO_3$ Produced by the 90° Domain Walls," *Ferroelectrics*, **7**, 315–317 (1974).
56. D. G. Sannikov, "Dispersion in Ferroelectrics," *Soviet Physics JETP*, **14**, 98–101 (1962).
57. P. Gerthsen, K. H. Hardtl, and N. A. Schmidt, "Correlation of Mechanical and Electrical Losses in Ferroelectric Ceramics," *J. Appl. Phys.*, **51**(2), 1131–1134 (1980).
58. Seiji Ikegami, and Ichiro Ueda, "Mechanism of Aging in Polycrystalline $BaTiO_3$," *J. of the Physical Society of Japan*, **22**(3), 725–734 (1967).
59. D. Berlincourt, B. Jaffe, H. Jaffe and H. H. A. Krueger, "Transducer Properties of Lead Titanate Zirconate," *IRE Trans. Ultrasonics Eng.*, 1–7 (1960).
60. J. G. Smits, "Eigenstates of Coupling Factors and Loss Factor of Piezoelectric Ceramics," Ph.D. Thesis Twente University of Technology, Netherlands (1978).
61. Takuro Ikeda, "Fundamentals of Piezoelectricity," Oxford University Press (1990).

APPENDIX 14

Journal

J. Am. Ceram. Soc., 77 [1] 211–15 (1994)

Electric Fatigue in Lead Zirconate Titanate Ceramics

Qiyue Jiang,* Wenwu Cao,* and L. Eric Cross*

Materials Research Laboratory, The Pennsylvania State University, University Park, Pennsylvania 16802–1801

Electric fatigue is a major obstacle for some potential applications of ferroelectric materials based on reversals of spontaneous polarization, such as memory devices and high strain actuators. Our studies of fine-grained hot-pressed lead zirconate titanate with lanthanum dopant (PLZT 7/68/32) show that fast fatigue is actually caused by contaminated surfaces instead of intrinsic structure deterioration or the change of domain states. All of the specimens with conventionally cleaned surfaces showed significant fatigue after 10^5 switching cycles, but specimens cleaned with a new cleaning procedure did not fatigue even after more than 10^8 switching cycles. This type of fatigue is found to be due to generated microcracking at the ceramic–electrode interface.

I. Introduction

MANY applications of ferroelectric materials, such as some piezoelectric, electrooptical, and electrostrictive devices, involve repeated reversals of polarization. One critical limitation on the performance of these devices is fatigue associated with repeated electrical cycling. Fatigue in ferroelectrics mainly refers to the degradation of ferroelectric properties upon repeated reversals of polarization, which appears in the hysteresis loop in the form of a decrease in remnant polarization (P_r) or saturated polarization (P_m) and is often accompanied by an increase of the coercive field (E_c).

In 1953, McQuarrie[1] first reported the time dependence of the P–E hysteresis loop in a $BaTiO_3$ ceramic. He found that after several weeks of switching at 60 Hz, the square-shaped hysteresis loop was changed to a distinct propeller shape with a noticeable decrease in both the maximum polarization and the remnant polarization. Merz and Anderson[2] studied fatigue behavior in a $BaTiO_3$ single crystal. A gradual reduction of the polarization after a few million switching cycles was observed and the fatigue behavior was related to the wave patterns of the electric field (sine wave or pulse train wave). The ambient atmosphere was also reported to have an effect on the switching stability of $BaTiO_3$ single crystal.[3] A loss of squareness of the hysteresis loop was observed when the crystal was switched under vacuum, N_2, H_2, or He gases. However, the deteriorated hysteresis loop could restore its original shape under ac cycling in O_2, or in dry air.

Fatigue experiments were also carried out on other ferroelectrics in the 1960s. Taylor[4] studied fatigue phenomena in 24 compositions of niobium-doped $Pb(Zr,Sn,Ti)O_3$ ceramics and discovered that the fatigue rate depended on the composition. Contrary to Ref. 2, he found little difference in fatigue behavior when the ac electric field pattern was changed from a sine wave to a pulse train wave. A more detailed study of fatigue in La- or Bi-doped PZT ceramics was carried out by Stewart and Cosentino.[5] They showed that the polarization decreased rapidly, and the remnant polarization was reduced to half of its original value after 5×10^6 switching cycles. They concluded that the patterns of the electric field, the types of electrodes, and the ambient conditions had no significant effects on the fatigue behavior. Stewart and Cosentino[5] also reported an interesting result: when a fatigued sample was heated above the paraelectric–ferroelectric phase transition temperature T_c, the properties could be restored. Contrary to Stewart and Cosentino, Fraser and Maldonado[6] also studied the same La-doped PZT ceramics and reported significant effects of electrodes. They found that when indium was used as the electrode material instead of gold or silver, there was still 85% of the original remnant polarization left after 10^9 switching cycles, but fatigue occurred much faster when using lead, aluminum, gallium, silver, and gold as electrode materials. Carl[7] observed significant degradation in the La- or Mn-doped $PbTiO_3$ ceramics; after only a few thousand switching cycles the polarization dropped to 30% of its original value together with some increase of the coercive field, and some cracks were also observed under SEM on surfaces of the samples.

Although the fatigue phenomena in ferroelectrics have been studied for over 30 years, their origin is still not clear. Some possible causes of fatigue under high ac field are (1) the gradual reorientation of domains into a more stable, i.e., minimum-energy, configuration;[1,8] (2) injection of charge carriers into the ferroelectrics which provide pinning for domain wall movement;[9] (3) structural inhomogeneity which produces traps for domain walls, reducing domain wall mobility;[10] (4) the appearance of microcracking caused by the large change of strain during switching.[7,11]

Despite the fact that the fatigue effect is the key factor which prevents some potential applications of ferroelectrics, very few conclusive results have been published. In addition, those published results by different investigators are often in contradiction, and there are no explanations for these discrepancies. Therefore, a systematic study of this subject is needed in order to understand the origin and mechanism of fatigue behavior. We report here an extensive study of the fatigue behavior of a La-doped lead zirconate titanate (PLZT) ceramic system. The reason for choosing a PLZT ceramic system is because of its relatively low coercive field, large polarization, and square-shaped hysteresis loop. Moreover, hot-pressed PLZT ceramics are transparent and are almost pore free, which can eliminate the structural complications in a regular ceramic, leading to some understanding of the fundamental aspects of fatigue. In this paper, the focus will be on the effect of surface contamination on the fatigue behavior. Inconsistencies reported in some previously experimental studies can be explained in terms of different surface conditions.

II. Experimental Procedure

Lanthanum-doped lead zirconate titanate ceramic specimens were fabricated from mixed oxides by hot pressing. The composition used in this study was $Pb_{0.93}La_{0.07}(Zr_{0.68}Ti_{0.32})_{0.9825}O_3$. Conventionally, this formula is simplified to the form 7/68/32 according to the mole ratio of La/Zr/Ti. The average grain size was about 5 μm. At room temperature 7/68/32 is in a rhombohedral phase. Samples were first cut into platelets with areas of

A. V. Virkar—contributing editor

Manuscript No. 195705. Received May 11, 1992; approved March 12, 1993. Supported by the Office of Naval Research under Grant No. N00014-89-J-1689.
*Member, American Ceramic Society.

about 10 mm² and thicknesses in the range of 150–300 μm, and then annealed at 600°C for 2 h to release the mechanical stress generated during the cutting, grinding, and polishing processes.

Three different surfaces were prepared: (a) ground by 3-μm abrasive, (b) polished by 1-μm diamond paste, (c) etched in H_3PO_4 acid for 2 min at 140°C. In the conventional cleaning procedure, organic solvents (alcohol or acetone) were used to rinse the samples and then the samples were dried in air at room temperature. An improved cleaning method used in our experiments is described as follows: first the samples were cleaned by conventional procedure, then they were further cleaned ultrasonically in alcohol solvent, and finally the samples were heated in a furnace for 1 h at 500–600°C to burn off the organic solvent. Gold electrodes were sputtered onto the sample surfaces.

The properties studied here are the remnant polarization P_r, the maximum polarization P_m, the coercive field E_c, and the dielectric constant ε of the depoled state. A high-voltage sine wave ac field was used to switch the polarization, and the hysteresis loops were measured through a conventional Sawyer-Tower circuit and a Nicolet 214 digital oscilloscope. The temperature dependence of the dielectric constant was measured with a Hewlett-Packard 4274A LRC meter, and the temperature was measured using a Fluke 8502A digital multimeter. The heating rate was set at 3°C/min.

III. Results and Discussion

(1) Fatigue in PLZT Specimens Cleaned by Conventional Procedure

In order to compare the results from different specimens and to emphasize the changes of the measured properties, the relative polarization and the coercive field are used in this paper; they represent the percentages of the polarization and coercive field with respect to the initial polarization and the coercive field obtained at 10^2 or 10^3 switching cycles. Figure 1 shows the typical results obtained from specimens cleaned by conventional procedure. One can see that fatigue started at about 10^3 switching cycles, and proceeded very rapidly between 10^5 and 10^6 cycles. The remnant polarization P_r dropped to 30% of the initial values after 10^6 switching cycles. The changes of the maximum polarizations, which are not shown here, exhibit a similar behavior as the remnant polarization P_r. Figure 2 shows typical hysteresis loops before and after the fatigue test, observed from a sample with ground surfaces. The coercive fields E_c also increased with switching cycles. There is a direct correlation between the changes of E_c and P_r; i.e., while the polarization decreases, the coercive field E_c increases, which is consistent with the results obtained by other researchers.[4,6,11] We found that the ground sample fatigued earlier and faster than the samples with polished and etched surfaces. The same experiments were also carried out using a sine wave field at other frequencies. No apparent changes were observed for frequencies less than 600 Hz. Curves (a) and (e) in Fig. 3 show the weak field dielectric constant as a function of temperature for a sample with polished surfaces before and after the fatigue test, respectively. One can see a substantial decrease of the dielectric constant in the fatigued sample. Samples with the other two types of surfaces exhibit similar results which are not shown here.

(2) Fatigue in PLZT Specimens Cleaned by Improved Procedure

Figure 4 shows the changes in the polarization and the coercive field with switching cycles for samples cleaned by an improved procedure described in Section II. The experiments were carried out at a frequency of 100 Hz. Samples with all three types of surfaces did not show fatigue even after 10^8 switching cycles. We found that the hysteresis loops recorded at 10^3 and 2×10^8 switching cycles are almost identical. These

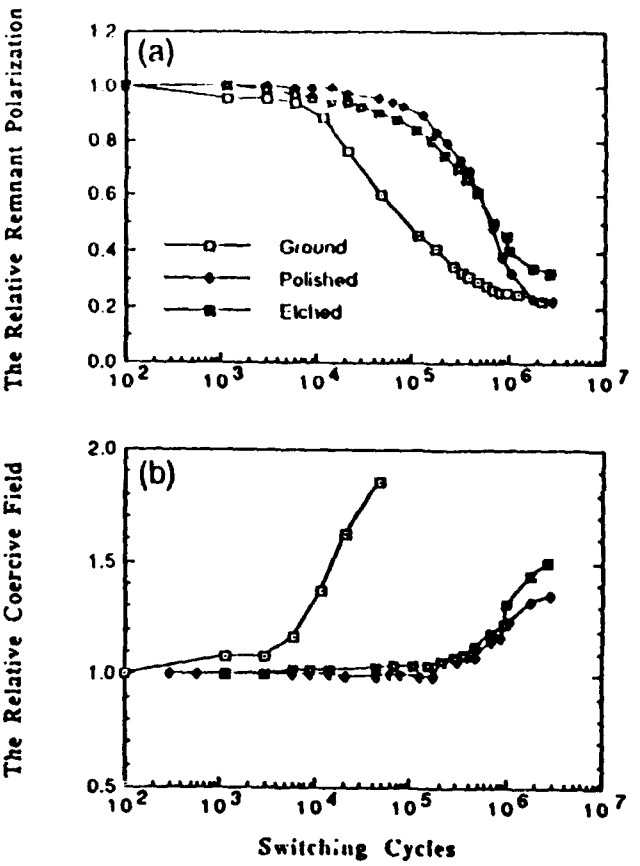

Fig. 1. Changes of the relative remnant polarization P_r (a) and the relative coercive field E_c (b) with switching cycles for a conventionally cleaned PLZT 7/68/32 specimen. Test frequency is 10 Hz.

experimental results tell us that the fatigue shown in Fig. 1 is purely extrinsic, i.e., resulted from an improper cleaning method. The actual lifetimes of PLZT 7/68/32 ceramics with grain size of 5 μm are much longer than those shown in Fig. 1 and are not affected by the surface roughness.

(3) Fatigue Originating from Surface Contamination

(A) Deterioration of the Ferroelectric–Electrode Interface under High ac Field: In fatigue experiments the possible sources of contaminants are abrasive residue from the grinding process, residue of solvents (water, alcohol, or acetone), water in the air, residue of the bonding glue, and skin grease from finger touch. Without further cleaning these residues are left on the surfaces of specimens, being sandwiched between the sample surface and the electrode, producing a poor interface contact. The effects of solvents and skin grease were further

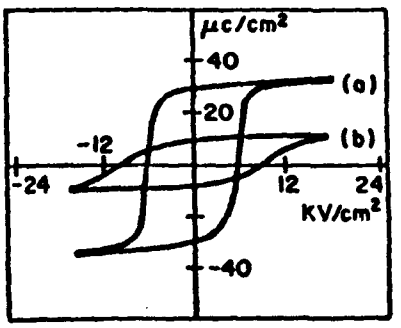

Fig. 2. Typical hysteresis loops after 10^3 (a) and 3×10^6 (b) switching cycles for a conventionally cleaned PLZT 7/68/32 sample with ground surfaces. Test frequency is 10 Hz.

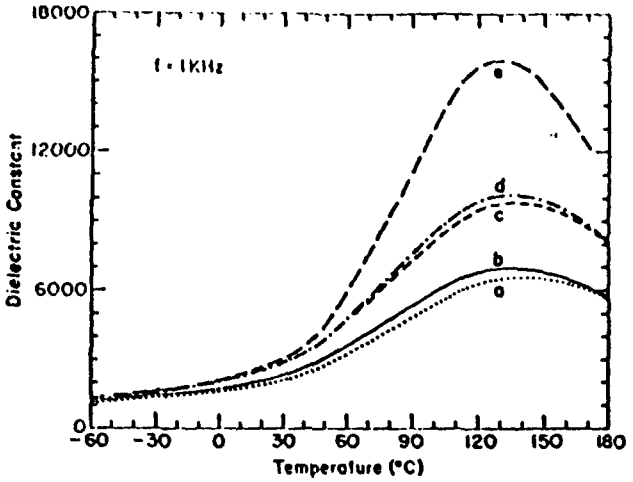

Fig. 3. Temperature dependence of the dielectric constant in depoled state for a conventionally cleaned sample with polished surfaces: (a) fatigued sample; (b) fatigued sample after heat treatment at 300°C for 3 h; (c) fatigued sample after heat treatment at 600°C for 1 h; (d) a 15-μm-thick layer was ground off from each side of the sample; (e) results from a virgin nonfatigued sample.

examined in the following experiments. First, the samples were etched by H_3PO_4 acid to remove a thin layer from the surface which might contain abrasive residue and skin grease. Then the following surface treatments were given to three different samples: (a) sample 1 was washed in water and acetone, and then both surfaces were rubbed with fingers; (b) sample 2 was washed in water and acetone, then dried in air at room temperature; (c) sample 3 was washed in water and acetone, then heat-treated in a furnace at 500°C for 1 h.

Figure 5 shows the results from fatigue tests on these three samples using a 100-Hz sine wave ac field. The remnant polarization of sample 3 did not decrease at all after 10^8 switching cycles; only E_c increased slightly (we note that in all etched samples, E_c shows a slight increase at the beginning and then becomes stable). P_r of sample 2 fatigued to 85% of its initial value after 10^7 switching cycles and E_c increased about 18%. Sample 1 was the worst among the three samples; its P_r reduced to 30% of the initial value and E_c increased 50% after only 2×10^6 cycles. Heating PLZT ceramic samples to 500°C after washing had two effects: (1) burning off the organic residues on the surface, and (2) releasing bulk and surface stresses. Since these three samples were already heat-treated at 600°C for 2 h to release stresses before the surface preparation described above, heating sample 3 to 500°C for 1 h after washing should not have changed its properties except to burn off solvent residues on the sample surfaces. Since the three samples with the same etched surfaces differed only in surface treatments, the discrepancies in the fatigue results can be explained only in terms of the different degrees of surface contamination.

Experiments also indicate that fatigue is initiated at the *ceramic–electrode interface*. Possible explanations for what might have happened at the interface are the following:[12,13] (1) electrochemical reaction, such as ionization of contaminants and field-induced chemical decomposition near the sample surface; (2) corona—high voltage can ionize water and organics, causing partial discharge which leads to a time related continuous degradation of the dielectric property; (3) a contact deterioration effect—residue of solvents and skin grease prohibit direct contact of the metal electrode with the sample surface, resulting in poor contact. Partial failure of the electrode was

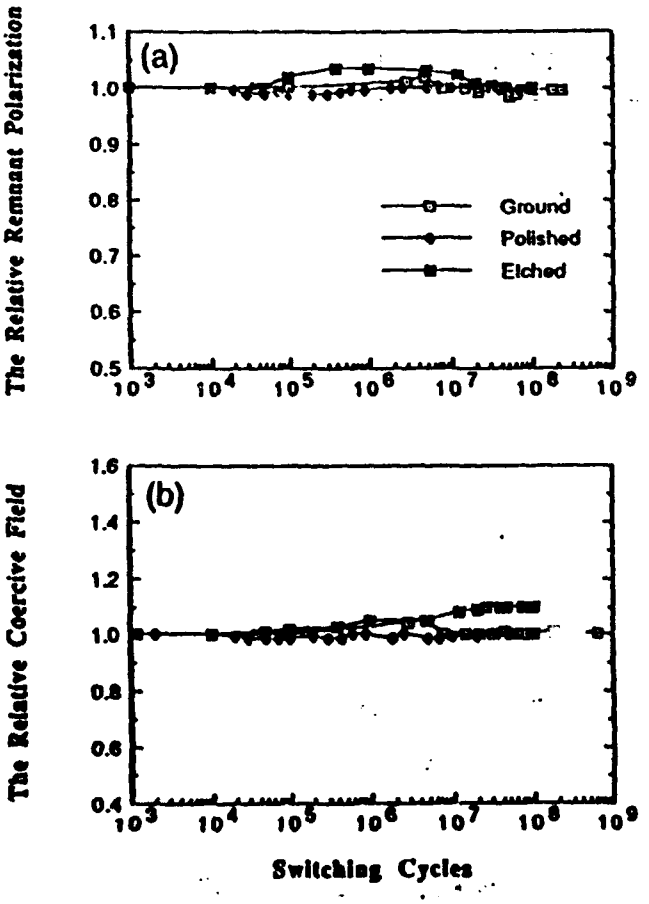

Fig. 4. Relative polarization (a) and the relative coercive field (b) versus switching cycles, respectively, for a specimen cleaned by an improved procedure. Test frequency is 100 Hz.

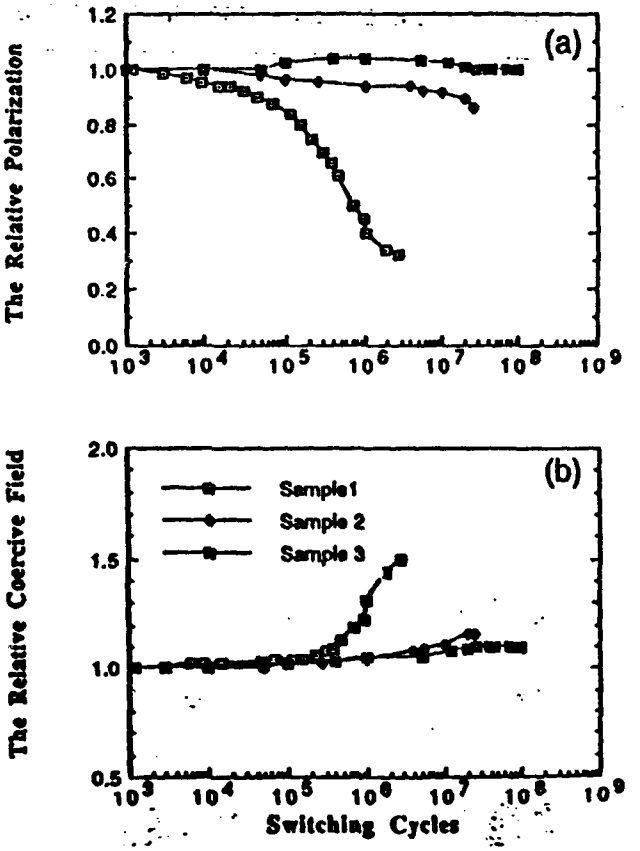

Fig. 5. *Effects of contaminations on the fatigue behavior.* Sample 1 was contaminated by solvent and skin grease; sample 2 was contaminated by solvent; sample 3 was cleaned by an improved procedure.

Fig. 6. SEM photograph taken from the electroded surface of a fatigued sample. Part of the electrode was peeled off from the sample surface during the switching process.

directly observed under SEM on the electroded surface of fatigued samples as shown in Fig. 6.

(B) Nature of the Fatigue: Fatigue caused by surface contamination started at the sample surfaces where high field concentrations occurred. In order to see if the fatigue damage extended into the interior of the ceramic with a prolonged switching time, we measured the bulk dielectric constant as a function of temperature. The sample thickness was 200 μm and the measurements were done at 1-kHz frequency. The maximum temperature in the measurement was 190°C, which was above the Curie temperature (130°C for PLZT 7/68/32). The results are given in Fig. 3. One can see a drastic decrease of the dielectric constant in the fatigued sample (after 2×10^6 cycles), especially close to the Curie temperature region (curve (a) in Fig. 3).

Different heat treatments were applied to this fatigued sample to see if the fatigued physical properties could be recovered. Curve (b) in Fig. 3 is the temperature dependence of the dielectric constant measured after the fatigued sample went through a heat treatment at 300°C for 3 h. Only partial recovery was achieved. The sample then experienced further heat treatment at 600°C for 1 h and further improvement was observed as shown in curve (c) of Fig. 3. However, the dielectric constant still did not recover to its initial value, which means that part of the damage is permanent. In order to investigate the depth of the damage from the surface initiated fatigue, 15 μm at the sample surfaces was ground off and the sample was re-electroded using the sputtering technique. The measured results are shown in Fig. 3, curve (d). No further improvement was achieved. The high field properties, i.e, the remnant polarization P_r and the coercive field E_c, were also measured after each heating, re-electroding, and thinning (Table I). One can reach the same conclusion from the results in Table I as from the results of weak field dielectric measurements. The dielectric and polarization measurements were also performed in a sample with a thickness of 700 μm; fatigue was observed after 2×10^6 cycles. However, it was found that the dielectric constant and the polarization could almost be restored to their initial values after a 150-μm layer was ground off from the sample surfaces. The experimental results indicate that fatigue damage propagated fairly deeply into the interior of the sample after more than 10^6 switching cycles (note the damage was only near the surface within 10^5 cycles).

Previously, fatigue in ferroelectrics was explained as due to the stabilization of domain walls,[1,5,8] which can be recovered by heating the fatigued sample into the paraelectric phase.[5,8] In our experiments, total recovery did not occur even after the fatigued sample was heated to as high as 600°C, 470°C higher than the Curie temperature. Hence, the fatigue that we have observed cannot be due to domain wall pinning; instead, we believe that intergranular microcracking is responsible for the nonrecoverable fatigue initiated by surface contamination. Scanning electron microscopy was performed on a fatigued sample (Fig. 7(a)) and a nonfatigued sample (Fig. 7(b)) with ground surfaces (the samples were etched using H_3PO_4 acid to remove gold electrodes). On the micrographs in Fig. 7(b), we can see some grinding damage and etch-pits for the nonfatigued sample, while for the fatigued sample (Fig. 7(a)) the majority of the grains do not have grinding damage or etch-pits. This means that a whole layer over these grains was pulled off during etching, which indicates that the bonding between grains was weakened in the fatigued sample near the surface. In addition, some

Table I. Comparison of the Remnant Polarization and the Coercive Field for a PLZT 7/68/32 Sample under Different Treatments

	Remnant polarization ($\mu c/cm^2$)	Coercive field (kV/cm)
Before fatigue	27.0	5.0
After fatigue	6.0	6.8
After 190°C heating	11.5	8.0
After 300°C heating	19.2	10.4
After 600°C heating	22.4	7.3
After removal of 15 μm from each side	22.5	7.2

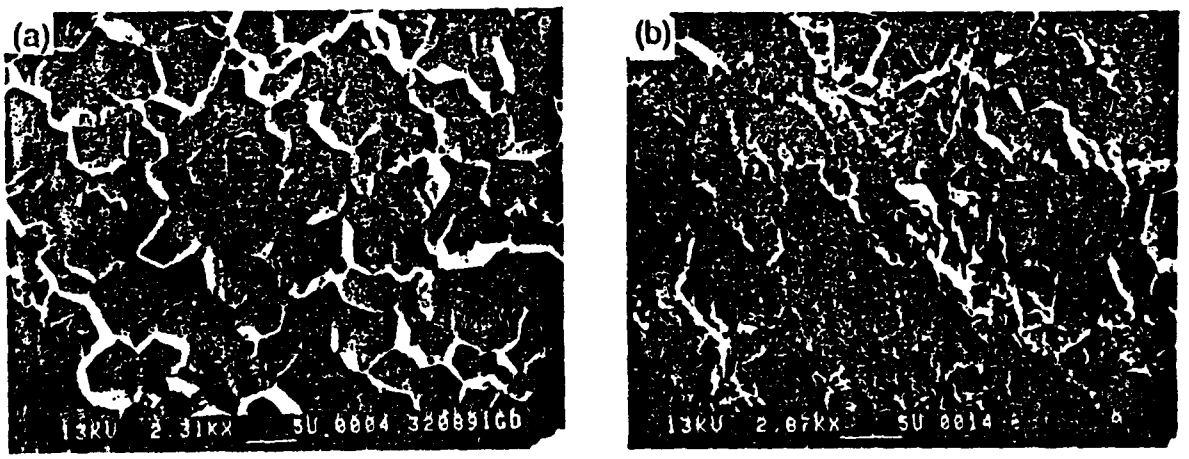

Fig. 7. SEM micrograph taken from a fatigued sample (a) and a nonfatigued sample (b) after chemical etching. Etch-pits were not found on the surface of the fatigued sample because a loosened layer was etched off.

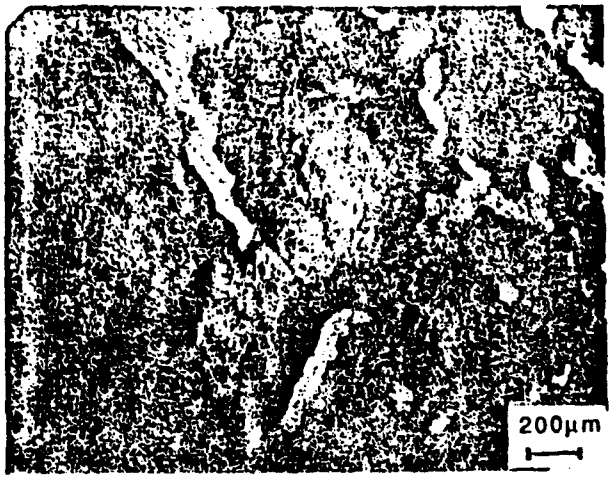

Fig. 8. Optical micrograph taken from a fatigued sample with transmission light. The opacity indicates the degree of mechanical damage or stress concentrations. The transparent regions are nonfatigued portions left in the sample.

minor cracks around grain boundaries are visible in Fig. 7(a), but large cracks were observed neither on the surfaces nor on the cross section of the fatigued sample.

Because ferroelectrics are both piezoelectric and electrostrictive, large strain can be generated during switching. In PLZT ceramics the field-induced strain can be as large as 0.1% or more.[14] When the deterioration of the interface occurs during the fatigue experiment, the regions under a good contact electrode are under a higher field, while the regions under a deteriorated interface effectively experience a much lower field. Hence, these two regions cannot be switched simultaneously under a constant voltage across the two electrodes. This generates stress concentrations at the boundaries between the switched regions and the nonswitched regions. If the grain boundaries have weaker mechanical strength than that of the grains, intergranular microcracking could be produced by these stress concentrations. An optical micrograph of a fatigued sample shows that this is indeed the case (see Fig. 8). The micrograph was taken from a fatigued sample under a transmitted light after the electrodes were carefully removed. It was found that some of the regions were changed from transparent to opaque, but some regions still remain transparent. The degree of opacity represents the degree of mechanical damage in the sample. In general, the worse the fatigue, the less the total area of the transparent regions.

IV. Summary and Conclusions

A systematic study has been carried out to determine the influence of surface conditions on the fatigue behavior of hot-pressed PLZT 7/68/32 ceramics with a grain size of 5 μm. It was found that the observed fatigue occurred within 10^5 switching cycles and was caused by surface contamination. We suggest that the fatigue initiated by surface contamination in hot-pressed PLZT 7/68/32 ceramics is through microcracking at the boundaries of the switched and nonswitched regions near the ceramic–electrode interface, which progressively extends into the interior of the ceramic with prolonged switching.

The conventional cleaning method has proved to be inappropriate for specimens used under high ac field. An improved cleaning procedure described here can eliminate fatigue for at least 10^8 switching cycles, which is a very encouraging result for some potential applications based on polarization reversals.

Contrary to some reported results,[3,6] we found that fatigue damage is permanent, although it is only limited at the surface region at the beginning. Some physical properties of the fatigued sample can be partially recovered through thermal treatment; however, complete recovery is not possible.

Acknowledgment: We wish to thank the Shanghai Institute of Ceramics, China, for providing the PLZT samples.

References

[1]M. McQuarrie, "Time Effects in the Hysteresis Loop of Polycrystalline Barium Titanate," *J. Appl. Phys.*, **24**, 1334–35 (1953).

[2]W. J. Merz and J. R. Anderson, "Ferroelectric Storage Device," *Bell Lab. Rec.*, **33**, 335–42 (1955).

[3]J. R. Anderson, G. W. Brady, W. J. Merz, and J. P. Remeika, "Effects of Ambient Atmosphere on the Stability of Barium Titanate," *J. Appl. Phys.*, **26**, 1387–88 (1955).

[4]G. W. Taylor, "Electric Properties of Niobium-Doped Ferroelectric Pb(Zr,Sn,Ti)O_3 Ceramics," *J. Appl. Phys.*, **38**, 4697–706 (1967).

[5]W. C. Stewart and L. S. Cosentino, "Some Optical and Electrical Switching Characteristics of a Lead Zirconate Titanate Ferroelectric Ceramics," *Ferroelectrics*, **1**, 149–67 (1970).

[6]D. B. Fraser and J. R. Maldonado, "Improved Aging and Switching of Lead Zircanate–Lead Titanate Ceramics with Indium Electrodes," *J. Appl. Phys.*, **41**, 2172–76 (1970).

[7]K. Carl, "Ferroelectric Properties and Fatigue Effects of Modified PbTiO$_3$ Ceramics," *Ferroelectrics*, **9**, 23–32 (1975).

[8]E. Fatuzzio and W. J. Merz, *Ferroelectricity*; pp. 102–104. North-Holland Publishing Co., New York, 1967.

[9]R. Williams, "Surface Layer and Decay of the Switching Properties of Barium Titanate," *J. Phys. Chem. Solids*, **26**, 399–405 (1965).

[10]A. Yu. Kudzin and T. V. Panchenko, "Stabilization of Spontaneous Polarization of $BaTiO_3$ Single Crystals," *Sov. Phys.—Solid State (Engl. Transl.)*, **14**, 1599–600 (1972).

[11]W. R. Salaneck, "Some Fatigue Effects in 8/65/35 PLZT Fine Grained Ferroelectric Ceramics," *Ferroelectrics*, **4**, 97–101 (1972).

[12]C. J. Tautscher, *Contamination Effects on Electronic Products*; pp. 4–5. Marcel Dekker, New York, 1991.

[13]K. L. Mittal and M. Antler, "Effect of Surface Contamination on Electric Contact Performance"; pp. 179–82 in *Treatise on Clean Surface Technology*, Vol. 1. Edited by K. L. Mittal. Plenum Press, New York, 1987.

[14]W. Y. Pan, Q. M. Zhang, Q. Y. Jiang, and L. E. Cross, "Electric Field Induced Strain in (Pb,La)(Zr,Ti)O_3 Ferroelectric Ceramics under the Tetragonal–Rhombohedral Morphotropic Phase Boundary," *Ferroelectrics*, **88**, 1–15 (1988).

APPENDIX 15

GRAIN SIZE DEPENDENCE OF ELECTRIC FATIGUE BEHAVIOR OF HOT PRESSED PLZT FERROELECTRIC CERAMICS

Qiyue Jiang, E. C. Subbarao, and L.E. Cross

Materials Research Laboratory
The Pennsylvania State University
University Park PA 16802

ABSTRACT

The decrease in remnant polarization, P_r, and increase in coercive field, E_c, of ferroelectric ceramics subjected to a large a.c. electric field is termed electric fatigue. In transparent hot-pressed lanthanum doped lead zirconate titanate (PLZT) ceramics, electric fatigue was not detected even after 10^9 cycles when grain size is small (~5 μm) but became increasingly severe as the grain size increases to 10 μm and beyond. The electric field causes large strains ($\geq 10^{-3}$) due to the anisotropic piezoelectric and electrostrictive coefficients of the material, which results in intergranular microcracking due to incompatible deformations. The effective field on a grain in a cracked sample is less than the applied field, limiting domain switching and polarization. The microcracking occurs only in the electroded, fatigued region of the sample and is initiated on the high voltage terminal side. The microscopic and acoustic emission data support the proposed mechanism of electric fatigue. An estimate of the critical grain size for microcracking due to electric stress, based on energy criterion, is in good agreement with experiment. The process of crack growth during electric fatigue is also elucidated.

I. INTRODUCTION

One of the chief characteristics of a ferroelectric material is the existence of a hysteresis loop, arising from changes in polarization under the influence of an applied a.c. field. Four decade ago, McQuarrie [1] reported changes in the shape of the hysteresis loop (i.e. in remnant polarization, P_r, maximum polarization, P_m, and coercive field E_c) when the electric field is applied for a long time (i.e. many cycles) and the phenomena is named 'aging' or 'electric fatigue'. This is attributed to the various impediments to the free, easy domain wall motions [1-4]. This effect severely limits the long term reliability of ferroelectric and piezoelectric ceramics in high strain applications such as electromechanical actuators and in thin film non-volatile memory devices.

Fracture behavior is exhibited in single phase ceramics due to elastic anisotropy when they are subjected to cyclic mechanical stress or due to thermal expansion anisotropy under the influence of temperature cycling [5-7]. Various factors influencing fracture behavior of ceramics due to cyclic mechanical and thermal stress have been studied, including the importance of grain size, phase transitions and pores [8-11]. In the case of ferroelectric ceramics of concern here, application of an a.c. electric field over a long period can also lead to electric fatigue. Though some investigations have been carried out on electric fatigue of ferroelectric ceramics [12,13], covering the wave character of the applied field [12], types of electrodes [12,14], ambient conditions [12], restoration of decayed properties though annealing [12] etc., there appear to be some contradictions. Therefore a comprehensive study of electric fatigue of PZT and PLZT ceramics was undertaken [15], which included the effects of surface contamination [16], porosity [17], composition and temperature. The present paper covers the influence of grain size on electric fatigue behavior of hot pressed PLZT ceramics.

Ceramic PLZT was chosen for this study because of its relatively low coercive field, large polarization and square hysteresis loop. Hot pressed PLZT ceramics are transparent, nearly pore free and thereby some of the complications present in conventional ceramics are avoided. The effect of grain size on electric fatigue and the estimation of critical grain size are emphasized here. The process of crack growth during electric fatigue was investigated. A mechanism for electric fatigue based on large anisotropic deformations is suggested.

2. EXPERIMENTAL

2.1. Specimen Preparation

The hot pressed lanthanum doped lead zirconate titanate, PLZT 7/68/32 (mole ratio of La/Zr/Ti) samples were obtained from the Shanghai Institute of Ceramics in China. According to Li et al [18], the preparation procedure consists of the following steps: for the

preparation of powders, the citrate solutions of the different elements (Pb, Zr, Ti and La) were prepared and the elemental concentration in each solution was determined. For the desired oxide composition of the formula $Pb_{0.93}La_{0.07}(Zr_{0.68}Ti_{0.0.32})_{0.9825}O_3$ the required volumes of the different citrate solutions were computed, measured and mixed. The mixed solution was sprayed into alcohol. After coprecipitation, the precipitates were vacuum dried, thermally decomposed and synthesized, resulting in a highly dispersed, homogeneous, active powder. Green bodies of cylindrical shape were formed from these powders by isostatic pressing and finally hot pressed at a temperature of 1200 °C for 20 hours under a pressure of 200 kg/cm^2. Lead loss during hot pressing was compensated by including excess PbO during baking. The hot pressed ceramic specimen was cut into slugs and the slugs were heated at temperature from 1340 °C to 1370 °C for 72 to 288 hours to achieve grain growth. The reheating at temperatures 140–170°C higher than the hot pressing temperature did not lead to changes in porosity, density, grain boundary thickness or crystalline habits. The original hot pressed sample has a grain size of 5 μm, which increased to 10, 18 and 25 μm as a result of the heat treatment.

2.2. Electrical Properties

The surfaces of the ceramic specimen (150–300 μm in thickness) were carefully cleaned using an improved procedure to avoid fatigue induced by surface contamination [16] and finally electroded with sputtered gold.

The properties studied were the remnant polarization (P_r), the maximum polarization (P_m) and the coercive field (E_c), as a sine wave of 100 Hz was applied to switch the polarization. Using a conventional Sawyer–Tower circuit, the P–E hysteresis loops were recorded on a Nicolet 214 digital oscilloscope. The polarization and coercive field were calculated from the measured hysteresis loops. The transverse strain due to the application of an a.c. field, the same as in polarization studies, was measured by a foil type strain gage (Kyowa KRF-02-C1-11) bonded to the sample surface with a suitable gage cement. The resistance of the strain gage changes with the same frequency due to its dimensional change caused by electrostriction of the sample. The resistance changes were converted into corresponding voltages and recorded on a Nicolet 214 digital oscilloscope, simultaneously with the P–E hysteresis loops.

The I–V characteristics of the virgin and fatigued samples were studied using a HP 4140B picoammeter to sweep the voltage and measure the current.

2.3. Microscopy

The surfaces and fractured faces of the fatigued samples were observed by Scanning

Electron Microscope (SEM), while the changes in the bulk of ceramic were studied using an optical microscope, taking advantage of the transmitted light through the transparent PLZT ceramics. The gold electrodes had to be removed by chemical etching or polishing before microscopic examination.

2.4. Acoustic Emission

Acoustic emission (AE) which detects elastic waves generated by sudden deformation in stressed material was employed to study the fatigue behavior of PLZT ceramics. A R15 sensor which has a sensitivity of 0.33 millivolts/μbar at the 100–500 Hz frequency range was bonded to the sample with vacuum grease. The acoustic signals from the sample were converted into electric signals, amplified, filtered and processed through a LOCAN 320 computerized acoustic emission system and finally displayed on a screen or printed on a strip chart recorder. The ringdown counts which is the number of times the AE signal exceeds the threshold are employed to observe the cumulative counts and count rate as a function of time.

3. RESULTS

3.1. Electric Fatigue

The normalized polarization and coercive field of hot pressed 7/68/32 PLZT ceramics of four different grain sizes is shown in Fig.1 as a function of the number of switching cycles. Clearly, PLZT ceramics with the smallest grain size (5 μm) does not show fatigue effect even after nearly 10^9 cycles, while Pr and Ec are affected markedly in ceramics with larger grain sizes. The start of the degradation occurs at lower number of cycles, as the grain size increases. In order to make a quantitative comparison of the fatigue rates, a parameter $C(P_n)$ is defined as the switching cycles when the normalized polarization equals P_n ($0 \leq P_n \leq 1$). Such P_n parameters are listed in Table 1 for three grain sizes and three P_n values, deduced from Fig.1. The fatigue rates vary by 1 to 3 orders of magnitude for different grain sizes.

The strain in the fatigue process was measured in the specimen with a grain size of 18 μm, together with the corresponding polarization (Fig.2a). The strain-field curves for the same sample at the beginning and end of the fatigue experiment as shown in Fig.2b. The strain as well as polarization decrease rapidly with increase in switching cycles.

The fatigued samples were heat treated at 300 °C for 2 hours. However the electrical properties were not fully restored by heat treatment (Table 2), through there was partial recovery. During a repeat fatigue test on the heat treated sample with 10 μm size grains, it showed a faster fatigue rate than in the previous fatigue test.

3.2. Microcracking

The scanning electron micrograph of a fatigued sample with 18 μm gains (Fig.3a) shows that the grains were loosely connected with each other and some pull-outs occur near the surface but no transgranular cracking is evident. On the other hand, the micrograph of the fractured surface of the same sample (Fig.3b) shows mainly transgranular fracture with some intergranular cracking near the surface region. Under transmitted light, the optical micrograph distinguishes the electroded, fatigued area (shaded portion) from the unelectroded, unfatigued area (white portions) in Fig.4. The fatigued portion became only partially transparent since light appears not to go through grain boundaries, perhaps due to grain-grain separations resulting from intergranular microcracking. Further, it was observed that the cracked layer due to intergranular cracking exists near the high voltage terminal side and does not extended through the body, consistent with the scanning electron micrograph (Fig.3b) which shows that intergranular fracture does not go through the thickness direction.

The occurrence of microcracks during the fatigue test on a sample with 18 μm grain size is further corroborated by the extensive acoustic emission activity detected in this sample (Fig.5). The acoustic emission counts observed soon after the application of the a.c. field are due to the macroscopic cracking occurring near the edges of the electrodes.

4. DISCUSSION

The electrical, microscopic and acoustic emission study clearly shows that electric fatigue is absent in PLZT samples with small grain size (~5 μm) and increases in severity as the grain size of PLZT samples increases (≥10 μm). The micrographs and acoustic emission further demonstrate that the enhanced fatigue rate in large grain PLZT ceramics is due to microcracking. Though the relationship between electric fatigue and microcracking in ferroelectric ceramics has not been investigated earlier, the role of electric field on microcracking of these materials has been studied and is summarized below.

4.1. Origin of Microcracks

Microcracking in single phase conventional ceramics can result from internal stress between grains due to incompatible strains produced by phase transformation [19], thermal expansion anisotropy [5-7, 20-28], elastic anisotropy [24, 29], thermal shock etc.[30]. In the case of ferroelectric ceramics, microcracking due to phase transition and thermal expansion anisotropy in $BaTiO_3$ [10] and $PbTiO_3$ [9, 32] has been studied and the role of grain size [9, 11, 31] in this connection has been examined. In addition, stress concentrations during poling of ferroelectric ceramics particularly lead zirconate titanate (PZT) ceramics, $BaTiO_3$ and $PbTiO_3$ by large dc electric fields can also cause microcracking

[8, 11, 13, 33-42]. One of the characteristics of piezoelectric and ferroelectric materials is the large deformation ($\geq 10^{-3}$) under applied electric field, which makes these materials excellent transducer and actuator materials. This strain is near the failure strain ($\sim 10^{-3}$) in conventional ceramics [43]. The piezoelectric and electrostrictive coefficients are anisotropic and therefore electric stress causes non-uniform deformation depending upon different orientations of the grains.

Thus, microcracking in the fatigue process in large grain PLZT ceramics could result from incompatible deformation of grains under large electric field. As can be seen in Fig.2b, a large contraction ($\sim 10^{-3}$) in PLZT sample can be produced by applied field due to direct piezoelectric and electrostrictive effects. Since piezoelectric and electrostrictive coefficients of crystalline solids are anisotropic, the strains produced by these two effects are also anisotropic and can be expressed by

$$x_{ij} = d_{mij} E_m + M_{mnij} E_m E_n \qquad (1)$$

where x, E, d and M are strain, electric field, piezoelectric coefficient and electrostrictive coefficient, respectively.

In the PLZT polycrystalline samples, each grain is surrounded by other grains which have different crystallographic orientations; the orientation mismatch of grains can give rise to incompatible deformation when a large electric field is applied, which in turn generates internal stress between individual grains. When these stresses exceed a certain value, microcracking takes place in brittle solids to relieve the strain energy. The intergranular microcracking observed in the present work often results from changes in the shape of individual grains [8]. In the present study, microcracking was strongly dependent on grain size; it did not occur until a critical size (5~10 μm) was reached and became more severe with increasing grain size.

4.2. Critical Grain Size for Microcracking

The grain size dependence of spontaneous cracking in ceramics due to thermal expansion anisotropy or phase transformation has been studied extensively [8, 9, 20-25, 28]. There are several models to predict the critical grain size above which the spontaneous cracking can occur. Clarke [20] proposed a 2D energy model for combined effects of internal and applied stress on strength; Davidge and Green [44] gave a 3D energy model for cracking around second phase particles; Cleveland and Bradt [23] presented a model based on an energy criterion to calculate the critical grain size for microcracking in pseudobrookite oxides due to thermal expansion anisotropy and the results were in good agreement with the experimental observations. Since microcracking in our experiments is due to the anisotropic changes in the shapes of the individual grains, the energy criterion model is adapted and

modified in our work.

The energy criterion for microcrack formation is based on the necessary, but not always sufficient, condition that when internal microcracks occur, the released elastic strain energy must equal or exceed the energy required for the formation of new fracture surfaces. When microcracks form, the anisotropic strain energy (U_a), which is a volume function, will be converted to fracture surface energy (U_s), which is an areal function. The energy equation can be expressed as:

$$U_t = U_o - U_a + U_s \tag{2}$$

where U_t is the total energy of the system and Uo is the energy of the unmicrocracked body. The total energy of a grain is:

$$U_t = U_o - E_a l^3 + g_b l^2 \tag{3}$$

where E_a is the average anisotropic energy per unit volume, g_b is the average fracture surface energy per unit area, l is the average grain size. Differentiating equation (3) with respect to l and setting it to zero yields the critical grain size; l_c:

$$l_c = \frac{2g_b}{3E_a} . \tag{4}$$

The anisotropic strain energies in PZT and PLZT 7/68/32 ceramic systems are mainly produced by piezoelectric effects, and can be expressed as:

$$E_a = \frac{1}{2} s X^2 = \frac{1}{2} c x^2$$

$$= \frac{1}{2} c ((d_{33} - d_{31})E)^2 \tag{5}$$

where E is the electric field. For PZT and PLZT ceramics with compositions close to phase boundary, $c^D_{11} = c^D_{22} \sim 14 \times 10^{10}$ N/m^2 [45]; $d_{33} \sim 800 \times 10^{-12}$ m/v, and $d_{31} = d_{32} \sim -400_x 10^{-12}$ m/v which were measured at large electric field (E =15 kv/cm). Here we choose $c = c^D_{11}$. Substituting these values in the equation (5) results in :

$$E_a = 2.27 \times 10^5 \text{ N/m}^2.$$

The g_b may be approximated from the fracture surface energy g_{pc} of polycrystalline ceramic by taking $g_b \sim 2/3\ g_{pc}$, because the atomic bounding at grain boundary is imperfect [43]. The g_{pc} in PZT ceramic system is 4 J/m^2 according to Pohanka and Smith [46], resulting in $g_b \sim$ 2.4 J/m^2. Substituting E_a and g_b value into Eq. (4) gives:

$$l_c = \frac{2g_b}{3E_a} = 7.05 \times 10^{-6} \text{ m} = 7.05 \ \mu\text{m} .$$

This value is in good agreement with the experimental result; when the grain size was larger than 5 μm, microcracking occurred. The critical grain size can be used to predict fatigue behavior and is a limiting parameter in designing reliable devices. The reader should be aware that since the calculation of the critical grain size is an approximate estimation, and does not consider the effect of the physical defects, such as pores and microcracks which

may already exist before the field is applied, the critical grain size for microcracking in real situations may be somewhat lower than the calculated value.

4.3. Crack Growth in Fatigue Process

Microcracking due to thermal expansion anisotropy or dielectric stress during DC poling can relieve the strain energy and relax the internal stress. However, in the case of AC field switching, the situation is complicated by cyclic deformation of grains at a certain frequency. The noncracked grains experience the full magnitude of the applied field and are therefore switchable with the field, while grains containing microcracks see a lower effective field because of the voltage drop across the cracks, if the cracks are perpendicular to the applied field. This lower effective field may not be large enough to switch these grains.The enhanced dielectric stress concentration at the crack tips can result in severe incompatible deformation near the tips of the cracks. As can be seen from Fig.4, this dielectric stress concentration greatly promoted the cracks to grow perpendicularly to the field direction until the cracks spread all over the electroded region, similar to the observation on poled PZT ceramics [33]. In the large grain samples (>10μm), it was observed that the cracked grains formed a layer which was almost parallel to the surface; this layer was closer to the high voltage terminal face. The measurement of the current as a function of voltage shown in Fig.6 indicates that the resistance of the fatigued sample did not change even after the fatigued sample was soaked in warm water for 24 hours, which proves that microcracking in large grain samples did not propagate across the sample thickness. This can also explain why electric breakdown was never observed in our fatigue experiments.

The decrease of the polarization and increase of the coercive field with the switching cycles in large grain samples are due to the fact that the applied field is concentrated on the cracks perpendicular to it, resulting in the decrease of the effective field on the grains. This reduction of the effective field may have two consequences: (1) the cracks at the grain boundaries are so wide that most of the applied field acts on the cracks with the effective field over grains reduced to a level less than the coercive field, resulting in non-switching of domains and consequent decrease of the polarization, (2) although the grain boundaries cracked, the grains still have intimate contact with each other (not by atomic bonding), the field only partially acts on the cracks; and the rest of the field acting on these grains is still large enough to switch the domains of these grains. In the latter case, the E_c is increased due to the partial voltage drop at the cracks, thus explaining why the E_c always increases in the fatigue resulting from mechanical cracking. From our experiments it is found that the change of E_c can be used to determine qualitatively the mechanism of the fatigue: when the E_c increases sharply with switching cycles, the fatigue process is dominated by microcracking

mechanism; if the E_c remains nearly constant, the fatigue process is dominated by domain pinning mechanism.

5. CONCLUSIONS

Grain size dependence of fracture in ceramics due to microcracking arising from elastic and thermal expansion anisotropy is well studied. In the present study, transparent, hot pressed ferroelectric ceramics (lanthanum doped lead zirconate titanate, PLZT) was subjected to a large a. c. electric field of 100 Hz frequency, similar to the conditions employed in electromechanical actuators and non-volatile memory devices requiring high reliability. Electric fatigue, defined as a decrease of permanent polarization and increase of coercive field under a. c. field, was not detected for small grain size (~5 μm) samples. but was found at large grain sizes (≥10 μm). The severity of fatigue, indicated by the beginning and magnitude of decay in electrical properties, increased with grain size.This is attributed to intergranular microcracking caused by incompatible large deformations ($\sim 10^{-3}$) brought about by the anisotropic piezoelectric and electrostrictive coefficients. Microscopic and acoustic emission data provide evidence for the microcracking. The electric field in a microcracked sample gets concentrated at the crack tips, resulting in an effective field less than the applied field acting on the grain, which limits the domain switching and consequently polarization. An estimate of the critical grain size for microcracking due to electric stress in PLZT ceramics is made on the basis of energy criterion and is in good agreement with the experiment. The crack growth was found to take place across the sample near the high voltage terminal face and not across the thickness of the sample. This is substantiated by the absence of electrical breakdown or change in electrical resistance in fatigued (microcracked) samples.

Acknowledgements–The authors are grateful to the Office of Naval Research for financial support.

REFERENCES

1. M. McQuarrie, *J. Appl. Phys.*, **24**, 1334 (1953).
2. W. J. Merz and J. R. Anderson, *Bell Lab. Record*, **33**, 335 (1955).
3. J. R. Anderson, G. W. Brady, W. J. Merz and J. P. Remeika, *J. Appl. Phys.*, **26**, 1387 (1955).
4. G. W. Taylor, *J. Appl. Phys.*, **38**, 4697 (1967).
5. W. R. Buessem, in *Mechanical Properties of Engineering Ceramics*, ed. W. W. Kriegel and H. Palmour III, p.127 Interscience, New York (1961).
6. A. G. Evans, *Acta Metall.* **26**, 1845 (1978).
7. V. D. Krstic, *J. Amer. Ceram. Soc.*, **67**, 589 (1984).
8. R. W. Rice and R. C. Pohanka, *ibid* **62**, 559 (1979).
9. T. Matsuo and H. Sasaki, *ibid* **49**, 229 (1966).
10. R. C. Pohanka, R. W. Rice and B. E. Walker, Jr., *ibid* **59**, 71 (1976).
11. B. C. Shin and H. G. Kim, *Ferroelectrics* **100**, 209 (1989).
12. W. C. Stewart and L. S. Cosentino, *ibid* **1**, 149 (1970).
13. K. Carl, *ibid* **9**, 23 (1975).
14. D. B. Fraser and J. R. Maldonado, *J. Appl. Phys.* **41**, 2172 (1970).
15. Q. Y. Jiang, Ph.D. thesis, Pennsylvania State University, (1992).
16. Q. Jiang, W. Cao and L. E. Cross, *J. Amer. Ceram. Soc.* **77**, 211 (1994).
17. Q. Y. Jiang and L. E. Cross, *J. Mater. Sci.* **28**, 4536 (1993).
18. C. E. Li, H. Y. Ni and Z. W. Yin, J. Chinese Silicate Soc. **10**, 9 (1982).
19. V. Srikanth and E. C. Subbarao, *J. Mater. Sci.* (in Press).
20. F. J. P. Clarke, *Acta Metall.* **12**, 139 (1964).
21. H. P. Kirchner and R. M. Gruver, *J. Amer. Ceram. Soc.* **53**, 232 (1970).
22. J. A. Kuszyk, and R. C. Bradt, *ibid*, **56**, 420 (1973).
23. J. J. Cleveland and R. C. Bradt, *ibid*, **61**, 478 (1978).
24. R. W. Rice, S. W. Freiman and P. F. Becher, *ibid* **64**, 345 (1981).
25. R. W. Rice and S. W. Freiman, *ibid* **64**, 350 (1981).
26. V. Srikanth, E. C. Subbarao, D. K. Agrawal, C. Y. Huang, R. Roy and G. V. Rao, *ibid* **74**, 365 (1991).
27. V. Srikanth, E. C. Subbarao and G. V. Rao, *Ceramics International* **18**, 251 (1992).
28. F. J. Parker and R. W. Rice, *J. Amer. Ceram. Soc.*, **72**, 2364 (1989).
29. V. Tvergaard and J. W. Hutchinson, *ibid* **71**, 157 (1988).
30. D. P. H. Hasselman, *ibid* **52**, 600 (1969).
31. Y. Matsuo, M. Fujimura and H. Sasaki, *ibid* **48**, 111 (1965).

32. V. Srikanth and E. C. Subbarao, *Acta Metall. Mater.* **40**, 1091 (1992).
33. K. Nejezchleb, F. Kroupa, M. Boudys and J. Zelenka, *Ferroelectrics* **81**, 339 (1988).
34. H. T. Chung and H. G. Kim, *ibid* **76**, 327 (1987).
35. H. Iwasaki and M. Izumi, *ibid* **37**, 563 (1981).
36. F. Kroupa, K. Nejezchleb and I. Saxl, *ibid* **88**, 123 (1988).
37. F. Kroupa, K. Nejezchleb, J. Rataj and I. Saxl, *ibid* **100**, 281 (1989).
38. C. I. Cheon, S. J. Kim and H. G. Kim, *ibid* **115**, 35 (1991).
39. H. T. Chung, B. C. Shin and H. G. Kim, *J. Am. Ceram. Soc.*, **72**, 327 (1989).
40. B. C. Shin and H. G. Kim, *Ferroelectrics* **76**, 261 (1988).
41. W. Pan and H. Cao, *ibid* **129**, 119 (1992).
42. E. C. Subbarao, V. Srikanth, W. Cao and L. E. Cross, *Ferroelectrics* , **145**, 271 (1993).
43. R. W. Davidge, in *Mechanical Behavior of Ceramics*, p.32, p.80, Cambridge University Press(1979).
44. R. W. Davidge and T. J. Green, *J. Mater. Sci.* **3**, 629 (1968).
45. D. A. Berlincourt, D. R. Curran and H. Jaffe, in *Physical Acoustics*, vol.**1**, part A, p.204, ed. by W. P. Mason, Academic Press, New York (1964).
46. R. C. Pohanka and P. L. Smith, p.58 in *Electronic Ceramics*, ed. by Lionel M. Levinson. Marcel Dekker, Inc. New York (1988).

Table 1. The fatigue rates C(Pn) (cycles) of hot pressed PLZT 7/68/32 with different grain sizes.

Grain size	C(0.8)	C(0.7)	C(0.6)
10 μm	$2*10^6$	$2*10^7$	$>5*10^7$
18 μm	$9*10^4$	$1.5*10^5$	$2*10^5$
25 μm	$3.5*10^4$	$5.5*10^4$	$8*10^4$

Table 2. Changes of the remnant polarization and coercive field for large grain PLZT 7/68/32 ceramics

Grain size	10 μm		18 μm		25 μm	
($\mu c/cm^2$), (kv/cm)	P_r	E_c	P_r	E_c	P_r	E_c
Before fatigue	26.4	7.3	26.6	6.5	27.0	6.6
After fatigue	18.5	8.9	3.2	11.2	2.6	9.3
After 300 °C, 2hrs	23.0	9.1	4.8	11.7	6.0	11.4

Figure Caption:

Fig. 1. The normalized remnant polarization and coercive field as a function of the switching cycles of hot pressed PLZT 7/68/32 ceramics with different grain sizes.

Fig. 2. (a) The transverse strain and the polarization as a function of the switching cycles, and (b) the transverse strain–field curves, for hot pressed PLZT 7/68/32 ceramic with grain size 18 μm.

Fig. 3. Microstructure of the fatigued sample (hot pressed PLZT 7/68/32) observed by SEM. (a) Surface under electrode and (b) fractured surface.

Fig. 4. Microcracks in a hot pressed PLZT 7/68/32 large grain sample observed by optical microscope. (a) 500X, and (b) 1000X.

Fig. 5. Acoustic emissions as a function of time detected from hot pressed PLZT 7/68/32 sample with 18 μm grain size. (a) Emission rate and (b) cumulative emission.

Fig. 6. Current as a function of voltage for hot pressed PLZT 7/68/32 sample with 25 μm grain size.

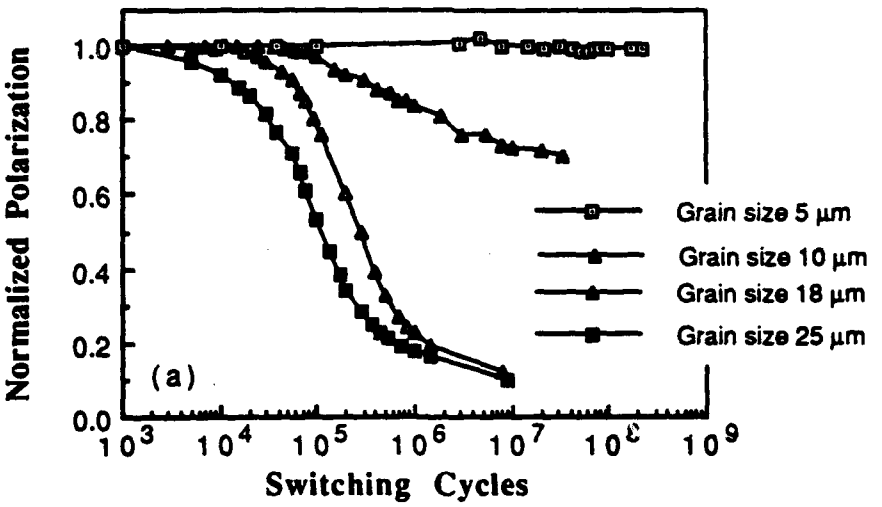
Normalized Polarization
1.0
0.8
0.6
0.4
0.2
0.0
(a)
Grain size 5 μm
Grain size 10 μm
Grain size 18 μm
Grain size 25 μm
10^3 10^4 10^5 10^6 10^7 10^8 10^9
Switching Cycles

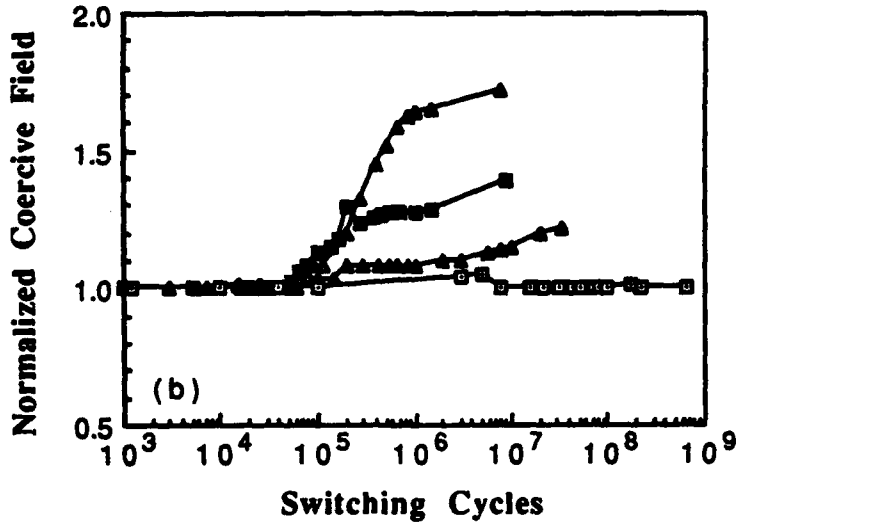
Normalized Coercive Field
2.0
1.5
1.0
0.5
(b)
10^3 10^4 10^5 10^6 10^7 10^8 10^9
Switching Cycles

Fig 1

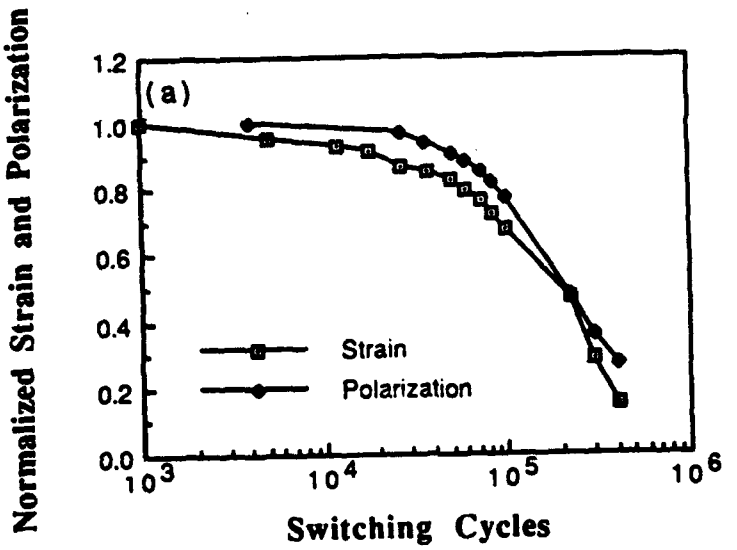

Fig 2(a)

Jiang et al

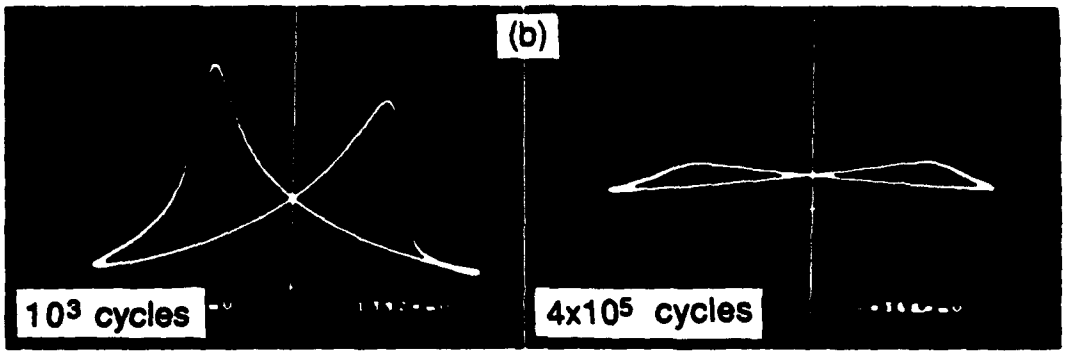

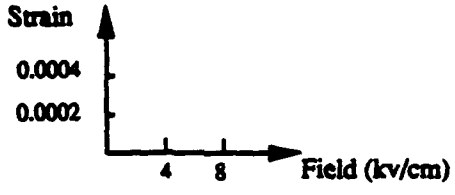

Fig 2: a

..; et al


(a)
12KU 0.49KX 10U 0002 PL313924
(b)
12KU 0.52KX 10U 0001 PL313924

Fig 3.

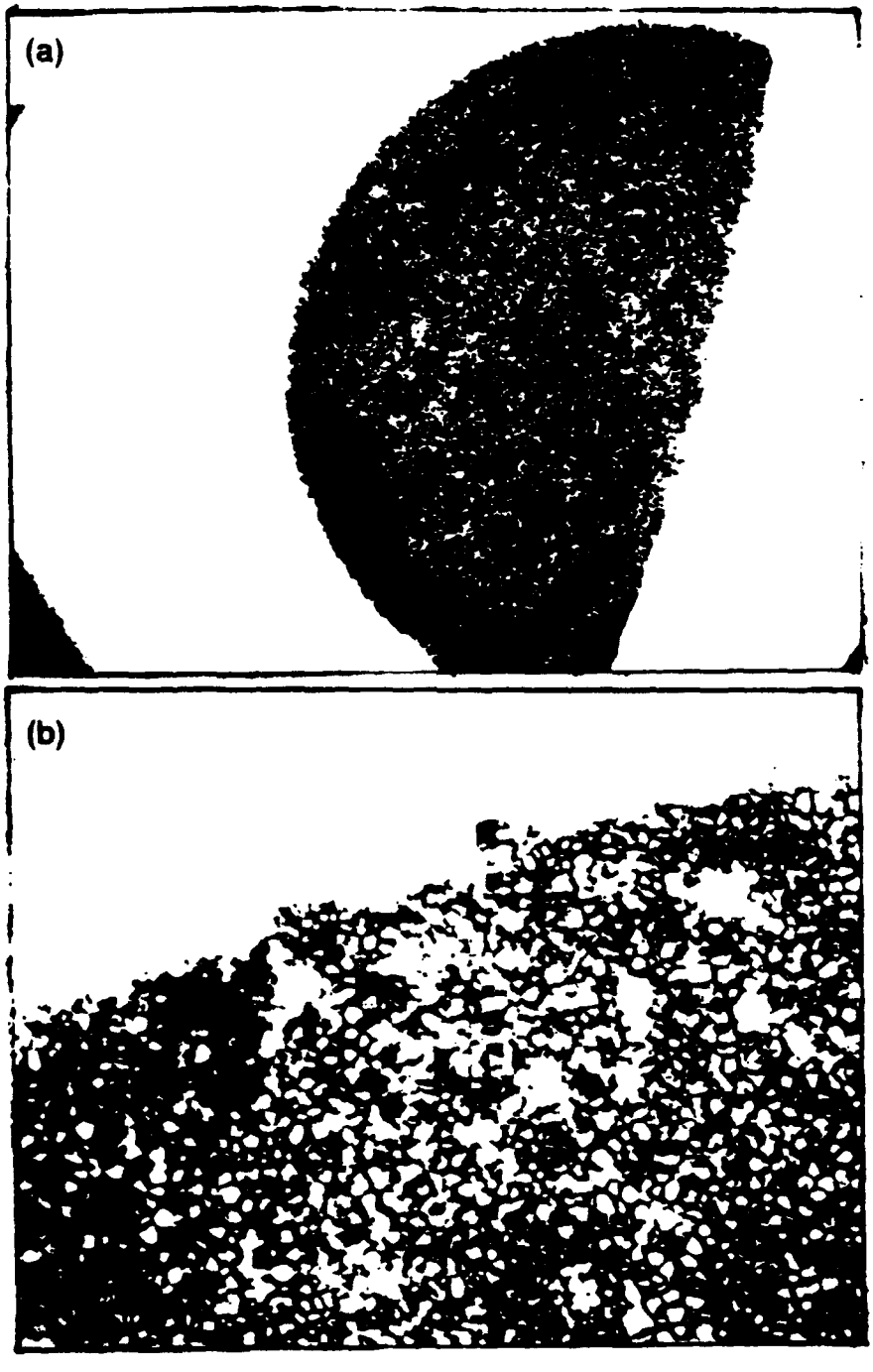

Fig 4

Jiang et al

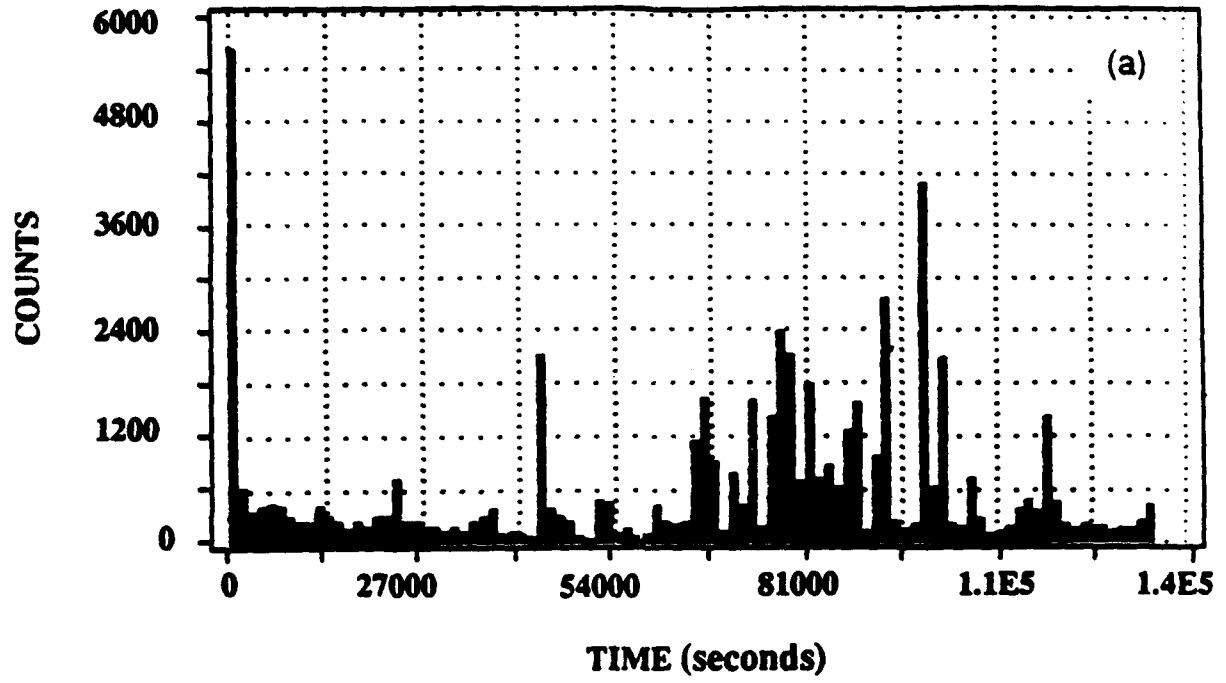
(a)
COUNTS
6000
4800
3600
2400
1200
0
0
27000
54000
81000
1.1E5
1.4E5
TIME (seconds)

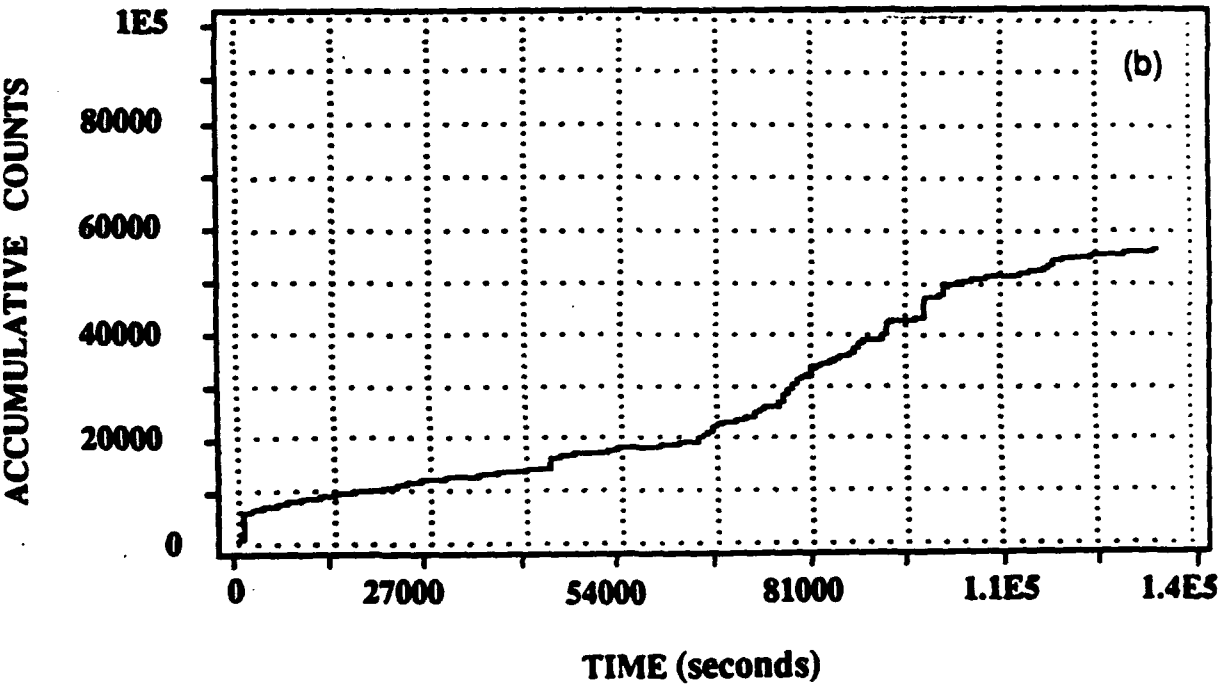
(b)
ACCUMULATIVE COUNTS
1E5
80000
60000
40000
20000
0
0
27000
54000
81000
1.1E5
1.4E5
TIME (seconds)

Fig 5

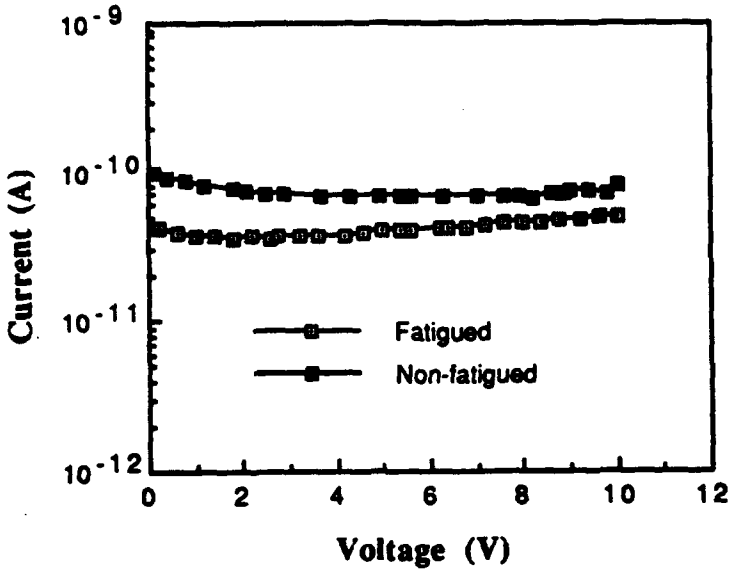

Fig 6

J. Song et al

APPENDIX 16

EFFECT OF COMPOSITION AND TEMPERATURE ON ELECTRIC FATIGUE OF LA-DOPED LEAD ZIRCONATE TITANATE CERAMICS

Q. Y. Jiang, E. C. Subbarao and L. E. Cross
Materials Research Laboratory
The Pennsylvania State University
University Park, PA. 16802

ABSTRACT

Composition and temperature of ferroelectric La-doped lead zirconate titanate (PLZT) ceramics influence its electric fatigue behavior, defined as the degradation of the electrical properties under the action of an a.c. field applied for a long time. Compositions of rhombohedral symmetry exhibit little or no fatigue compared with those of tetragonal and orthorhombic symmetry. At temperatures higher than the dielectric maximum, no fatigue effect was detected. Compositions close to phase boundaries (FE-AFE, FE-FE, or FE-PE) display significant fatigue behavior. Electric fatigue arises from the pinning of domains by space charges or injected carriers or from microcracking. The former (which are charge related) is accompanied by smaller strains and is recoverable by thermal and electrical treatment, while the latter (arising from microcracking) arises from large incompatible stresses between grains and is a permanent damage. The understanding of the mechanism of electric fatigue gained in the present study provides guidelines for enhancing the long term reliability of devices based on ferroic materials.

I. INTRODUCTION

Composition-temperature diagrams play an important role in the understanding of the behavior of materials. In the case of lanthanum-doped lead zirconate titanate ceramics, which constitute an important class of ferroelectric materials with applications spanning from high-strain electromechanical transducers to thin film non-volatile memory devices, such a composition-temperature diagram encompasses: (i) a variety of ferroic phases such as one or more ferroelectric (FE), antiferroelectric (AFE) and paraelectric (PE) phases separated from each other by phase boundaries; spatial composition fluctuations within a given sample, resulting in a ferroelectric relaxor type behavior, are also possible and (ii) a cubic perovskite structure with a range of subtle distortions giving rise to tetragonal (T) and rhombohedral (R) symmetries. Pure lead zirconate has monoclinic symmetry.

These features are displayed in the phase diagram for the PLZT system at room temperature (Fig. 1) in which the hatched region separating the FE-AFE and FE-PE phases denotes a region where a diffuse, metastable ferroelectric phase can be induced by a sufficiently large electric field. The addition of La to the basic lead zirconate titanate (PZT) system confers many beneficial effects such as increased squareness of the (P-E) hysteresis loop, decreased coercive field (E_c), enhanced dielectric and piezoelectric properties and larger electromechanical coupling coefficients, improved mechanical compliance and transparency[1]. A property exhibited by various PLZT compositions, which is of specific significance to the present study, is the variety of hysteresis loops. These include (a) ferroelectric (FE_T) square loop with a large E_c and a linear electro-optic behavior; (b) ferroelectric switchable square loop (FE_R) with high polarization and low E_c; (c) Slim loop with no remanant polarization but high induced polarization when subjected to an electric field, also possessing a bifringence which is a quadratic function of the electric field, and a large electrostrictive effect; and (d) a double hysteresis loop, characteristic of AFE materials, near the AFE-FE phase boundary. Thus, a

wide variety of ferroic behavior is exhibited by these materials, depending upon composition and crystal symmetry.

Another aspect of considerable importance to the present study is the fact that the crystal structure of some of these compositions is very sensitive to the electric field and stress[2], for example, a thermally depoled state which is macroscopically cubic with micropolar regions[3] and electrically poled states with macrodomains having an orthorhombic symmetry at room temperature[2,4,5].

To ensure the long term reliability of a range of important devices based on these materials involving application of an a.c. field for a large number of cycles, a clear understanding of the physics underlying their behavior is necessary and is undertaken as a part of a comprehensive study of the fatigue behavior of PLZT ceramics[6] including the effect of surface treatment[7], porosity[8], grain size[9] etc..The property studied is electric fatigue, which is the change in electrical properties (decrease of remanant polarization, P_r, and increase of coercive field, E_c) under the influence of an a.c. field. A range of compositions in PLZT system were selected to cover ferroelectric, antiferroelectric, paraelectric and relaxor ferroic behavior, spanning cubic, tetragonal, rhombohedral and (induced) orthorhombic symmetries. For a given composition, electric fatigue at various temperatures was examined to elucidate the role of the type of ferroic behavior and crystal structure. For clarification of the arguments presented, two materials not belonging to the PLZT system were included in the study; these are the well known relaxor ferroelectric of lead magnesium niobate (PMN) composition and a single crystal of ferroelectric triglycine sulfate (TGS) which has only 180° domain configuration.

There are three earlier studies of relevance to the present work. Taylor[10] studied the compositional dependence of the fatigue behavior of $Pb_{0.99}[(Zr_xSn_y)_{1-z}\ Ti_z]_{0.98}Nb_{0.02}O_3$ ternary composition and found minimum fatigue at x=0.5, y=0.5 and z=0.14 and maximum fatigue at x=0.8, y=0.2 and z=0.06. These effects were attributed to the magnitude of the field induced strain (due to domain reorientations), the larger strain leading to a greater decay.

However, some of the samples of the present study on hot pressed PLZT (7/68/32 and 7/65/35) with a small grain size has the same magnitude of strain as the most fatigued composition of Taylor, but without exhibiting any electric fatigue, suggesting that factors other than the magnitude of electrically induced strain need also to be considered. Freimen et al[11] found that the critical fracture toughness K_{1C} (stress intensity factor) of PZT ceramics plotted as a function of % $PbTiO_3$ exhibited minima at the phase boundaries (AFE_O-$FE_R^{(LT)}$, $FE_R^{(LT)}$-$FE_R^{(HT)}$ and $FE_R^{(HT)}$-FE_T), especially at the morphotropic boundary between tetragonal and rhombohedral phases (Fig. 2). According to these authors, both domain twinning and microcracking could reduce and redistribute the stress and increase the fracture energy with a trade-off between twinning and microcracking giving rise to the observed minima and maxima in Fig. 2. It must be pointed out that the behavior of these materials under an applied a.c. electric field may not necessarily correspond to the fracture behavior under static mechanical stress.

The only study of the effect of temperature on fatigue behavior of ferroelectrics is that of Stadler[12] who did not find any consistent fatigue behavior in $BaTiO_3$ single crystals in the temperature range of -195 °C and room temperature.

II. EXPERIMENTAL

There are two ferroelectric (rhombohedral and tetragonal), an antiferroelectric and a paraelectric phases present at room temperature in the PLZT system (Fig. 1). The compositions (La/Zr/Ti) for the present study were selected to include the ferroelectric rhombohedral phase (7/68/32, 7/65/35, 7.6/70/30), the vicinity of the rhombohedral-tetragonal phase boundary (8/65/35, 8.4/65/35), the vicinity of the FE-AFE mixed region (7.9/70/30) and the FE-PE mixed region (9.5/65/35), as marked in Fig. 1.

Schulze[13] has shown that there is no difference in the phases obtained by conventional sintering and hot pressing processes. In order to obtain dense, pore-free, transparent ceramics.

all compositions except 7/65/35 were hot pressed at 1200 °C under a pressure of 200 kg/cm^2 for 20 hours (Table I). The average grain size was 5-7 μm in these samples (Table 1). The composition 7/65/35 was prepared both by hot pressing and solid state sintering route at 1300±20 °C. The surfaces of the ceramic sample were ground with 3 μm abrasive and carefully cleaned using an improved procedure[7] to avoid fatigue induced by surface contamination, and finally electroded with sputtered gold.

The properties studied were the remanant polarization (P_r) and coercive field (E_c), calculated from the P-E hysteresis loops obtained using a conventional Sawyer-Tower circuit and recorded on a Nicolet 214 digital oscilloscope. The frequency of the applied a.c. field for fatigue study is also listed in Table 1. The shape of the hysteresis loops provides important data on the nature of the ferroic behavior.

In order to study the effect of crystal structure and ferroic nature on electric fatigue, fatigue studies were carried out at temperatures below and above the temperature corresponding to maximum dielectric constant (T_m, listed in Table 1 for each composition, which decreases with increasing La content). In most cases, room temperature studies are also included.

The surfaces and fractured faces of the fatigued samples were observed by scanning electron microscope (SEM), while changes in the bulk of the sample were studied by using an optical microscope, taking advantage of the transparency of the hot pressed samples. The gold electrodes were removed before optical microscopic examination. The growth of the cracks can be deduced by focussing the optical microscope at different heights of the sample disc.

III. RESULTS

1. Compositional Dependence

A. Fatigue in PLZT x/65/35 compositions

Fatigue tests were carried out on hot pressed PLZT samples with compositions of the same Zr/Ti ratio, x/65/35, for x=7, 8, 8.4, and 9.5. The location of each composition is

marked in the phase diagram (Fig. 1). The composition 7/65/35 is in the rhombohedral phase and has stable square hysteresis loop; 8/65/35 and 8.4/65/35 are near the morphotropic phase boundary region and have unstable square hysteresis loops which are very sensitive to the measuring frequencies at room temperature; 9.5/65/35 is near the mixed ferroelectric-paraelectric phase region and has a slim hysteresis loop at room temperature. The fatigue experiments were carried out at room temperature for all compositions except that the composition 9.5/65/35 was studied at -140 °C because of the absence of the square hysteresis loop at room temperature. Fig. 3 shows that fatigue did not occur for 7/65/35, but occurred in the other three compositions and proceeded significantly for 8/65/35 and 8.4/65/35. The P_r and P_m (which is not shown here) decreased and E_c increased with the increase of the switching cycles in the three fatigued specimens. The variation of E_c is nearly a mirror image of that of P_r. Fig. 4 shows the hysteresis loops for each composition before and after fatigue tests; it is noted that the most fatigued two compositions have initial distorted hysteresis loops.

All the fatigued samples did not recover after thermal treatment at 300 °C for 2 hours; the permanent damage usually indicates the microcracking mechanism[9]. The optical micrographs of the fatigued specimens through transmitted light after the removal of the gold electrodes, are shown in Fig. 5 for the composition 8/65/35. The sample was partially electroded and the center circle was the switched region in Fig. 5(a). A macrocrack was found which started from the edge of the electrode and extended to the unelectroded region (bottom left corner of Fig. 5(a), while macrocracks were not observed inside the switched region. The opaque ring in Fig. 5(a) observed after fatigue test indicates a microstructure change, with the center area still remaining transparent and undamaged. Further observation under higher magnification of part of the opaque ring is shown in Fig. 5(b), (c) and (d) when the picture was focused near the bottom face of the sample (b), in the middle level (half above the bottom) (c), and near the top surface (d). Three features were noticed under the optical microscope: (1) the microcraking was completely inside the switched region; (2) the mode of the microcracking was intergranular;

(3) the microcracks started from the electrode edges near the surface and propagated towards the other face, with the propagation paths of the cracks being a combination of the horizontal and vertical directions. A unique character of the microcracking is noticed in this sample, *i.e., in the* microcracked region, all the grains break up to give a sand-like appearance. Since very few ceramics are transparent, this type of cracking has rarely been observed in such a direct striking way.

Microcracking was more severe for 8.4/65/35, and started both from edges and from surface as observed by SEM (Fig. 6). In Fig. 6(a) macrocracks can be seen on the fractured cross section of the fatigued sample near the surface; after wiping off part of the gold electrode on the surface, it is found that some of the grains were partially pulled out as shown in Fig. 6(b). The fatigued sample became partially opaque; the opaque regions were parallel to the surfaces and close to the high voltage terminal face. After removal of the discolored region (half of the thickness) by grinding, the sample recovered nearly to its original state, and Table II lists the changes of its P_r and E_c.

B. Fatigue in PLZT x/70/30 compositions

PLZT 7.6/70/30 and 7.9/70/30 are close to the phase boundary between ferroelectric rhombohedral phase and antiferroelectric phase (Fig. 1); their T_m and the a.c. frequencies for fatigue tests are listed in Table 1. The results of their fatigue tests together with that of composition 7/68/32 (Fig. 7(a)) show that fatigue occurred in both compositions and more severely in composition 7.6/70/30. Fig. 7(b) shows the hysteresis loops for each composition measured at the beginning and the end of the fatigue tests, where composition 7.9/70/30 showed double hysteresis loops.

It is noticed that the three compositions (8/65/35, 8.4/65/35, and 7.6/70/30) which fatigued most severely have similar hysteresis loops as can be seen in Fig. 4 and Fig. 7(b). The same cracking pattern as occurred in 8.4/65/35 and 8/65/35 samples was also observed by

optical microscope in fatigued 7.6/70/30 samples (not shown here).

Although the grain sizes of those compositions ranged from 5μm to 7 μm, the rates of the fatigue for the severely fatigued compositions (8.4/65/35,7 μm; 8/65/35,5μm; 7.6/70/30,7 μm) were obviously higher than that of 7/68/32 composition with 10 μm grain size[9]. Therefore there is no doubt about the compositional effect on the fatigue behavior, and the mechanism of the composition effect will be discussed later.

C. Fatigue in antiferroelectric ceramics

Lanthanum doped lead zirconate titanate stannate antiferroelectric ceramic system was studied extensively by Berlincourt et al[14], among others. The composition used in our study is $Pb_{.97}La_{.02}(Zr_{.53}Ti_{.12}Sn_{.35})O_3$ which is in the antiferroelectric tetragonal phase close to the phase boundary of antiferroelectric tetragonal and ferroelectric rhombohedral phases, and its coercive field is 25 kv/cm at low frequency. The samples were fabricated by conventional sintering method. The average grain size is 6 μm and the sizes of pores range from 1 μm to 30 μm.

The fatigue study carried out at 600 Hz up to 10^9 switching cycles shows that the polarization decreased slowly with the switching cycles, and the coercive field was stable until 10^8 switching cycles, then increased slowly with continuous switching (Fig. 8(a)). The double hysteresis loops recorded at 10^4 and 10^9 switching cycles (Fig. 8(b)) show no significant changes in the shapes of the loops.

D. Fatigue in TGS single crystal

Tri-glycine sulfate (TGS) single crystal, $(NH_2CH_2COOH)_3 \cdot H_2SO_4$, has monoclinic symmetry; its Curie temperature is 49 °C. Ferroelectricity is found along the direction of the two fold polar axis, monoclinic b axis (Jona and Shirane[15]). TGS is water soluble and undeteriorated surfaces are difficult to obtain during sample preparation. Thus the samples used

in the present experiments were prepared by cleavage of the crystal planes which are perpendicular to the b axis, resulting in very clean and undamaged surfaces. The thicknesses of the samples ranged from 1 to 2 millimeter.

The fatigue experiment was carried out at a frequency of 900 Hz, using silver paint as electrode. The results show that fatigue did not occur even after 10^8 switching cycles (Fig. 9(a)). The hysteresis loops at 10^3 and 10^8 are shown in Fig. 9(b), the coercive field at 900 Hz is 0.35 kv/cm. Stability of the ferroelectricity under AC field switching in TGS single crystal could be due to the fact that only 180° domain configuration exists in the crystal; this will be further discussed in the following section.

2. Temperature Dependence

A. Fatigue behavior of PLZT ceramics

Compositions of PLZT 7/65/35 (T_m=140 °C) made by conventional sintering and hot pressed 9.5/65/35 were studied for temperature effects. Fig. 10(a) shows the results of fatigue tests for sintered PLZT 7/65/35 at 30 °C, 87 °C, 118 °C, 152 °C, and 167 °C temperatures, the maximum field and the frequency for all different temperatures were kept constant (11 kv/cm and 400 Hz). The corresponding hysteresis loops recorded before and after fatigue tests are shown in Fig. 11(a) for each temperature except at 167 °C at which the loops were straight lines and did not change with switching cycles. In Fig. 10(a), the fatigue rates decrease as temperature increases. It was expected that when temperature is higher than T_m, the fatigue should stop since above T_m the majority of the structure is transformed to the paraelectric phase. However, fatigue still occurred at 152 °C (12 °C higher than T_m) with a much slower rate and finally at 167 °C (27 °C higher than T_m), fatigue was no longer observed. The P_m decreases with the increase of temperature (Table III). In Fig. 11(a) the remanant polarization decreases with increasing temperature and did not completely disappear until the temperature was higher

than T_m. Constrictive neck (double) hysteresis loops were not observed as temperature increases which often occur in the compositions near phase boundaries. The mechanism of fatigue in composition of sintered 7/65/35 is mainly due to domain pinning by space charges[8]. How temperature affects the space charge pinning will be discussed later.

The composition 9.5/65/35 was chosen to study the low temperature behavior because it has lower T_m (55 °C) and the square hysteresis loops occurred only at very low temperatures. Fatigue experiments were carried out at three temperatures, –140 °C, 25 °C, and 105 °C with the frequencies of 160 Hz, 50 Hz, and 100 Hz, respectively; the results are shown in Fig. 10(b) and 11(b). It is surprising to find that the fatigue at -140 °C (with large polarization and square loop) proceeded much more slowly than that at 25 °C with slim loop. The P_m and the P_r at -140 °C were 37.5 and 27.7 $\mu c/cm^2$ and higher than the P_m (23 $\mu c/cm^2$) at 25 °C; this is different from the situation in sintered 7/65/35 composition. When temperatures were high enough both the samples did not fatigue any more; though the remanant polarizations approach zero and hysteresis loops become slim, fatigue still occurred (as long as temperature is below T_m). It can be concluded from these results that when ferroelectric ceramics are in paraelectric phase (at a temperature about 30 °C higher than the T_m), fatigue does not occur either in sintered or hot pressed PLZT ceramics.

Fatigued 9.5/65/35 samples did not recover after thermal treatment. Fatigue that occurred in these samples is due to microcracking since its grain size (7 µm) is larger than the critical size[9] and the observations under optical microscope with transmitted light on 9.5/65/35 sample fatigued at 25 °C revealed not only microracking but also macrocracking, which propagated severely as shown in Fig. 12(a). In the 9.5/65/35 sample fatigued at –140 °C only some sandlike grains were observed by optical microscope with transmitted light (Fig. 12b); the cracking at low temperature was much less severe than that of the sample fatigued at 25 °C. The different cracking behaviors will be discussed later.

B.Fatigue behavior of PMN ceramics

PMN ceramic specimens with average grain size 5 μm were made by conventional sintering method and have a low T_m, about –15 °C. Fatigue did not occur at 25 °C up to 10^9 switching cycles, and at –140 °C the P_m and P_r, which had initial values of 32.0 μm/cm^2 and 18.4 μc/cm^2, started decreasing after 10^6 switching cycles, with the E_c almost unchanged. Fig. 13(a) shows the changes of polarization with switching cycles at 25 °C and -140 °C. Fatigue in PMN at low temperature proceeded much more slowly than that in sintered PLZT sample whose hysteresis loop at room temperature had the same shape as that of PMN at –140 °C. After 10^8 switching cycles at –140 °C the polarization only dropped by 10% of the initial value. When the sample temperature returned to room temperature, the P_m measured again was the same as that measured before the fatigue experiment; thus fatigue at low temperature in PMN did not cause permanent damage. Fatigue in this case was caused by domain pinning, and not by microcracking, since it is impossible to heal microcracks at room temperature. In addition, these samples were sintered by conventional method and had low density (97%); their fatigue mechanism should be the same as in sintered PLZT and PZT samples[8].

Fatigue experiments were also carried out on hot pressed PMN doped with 1% lanthanum at room temperature and -140 °C. After 10^9 switching cycles under applied AC field, the P_m and P_r did not decrease and E_c was unchanged. Fig. 13(b) shows the Pr as a function of switching cycles at both 25 °C and -140 °C. The grain size of hot pressed PMN was 2 μm and below critical grain size; like the hot pressed PLZT 7/68/32 and 7/65/35 ceramic with small grain size, fatigue did not occur in hot pressed PMN ceramic with grain size less than 5 μm. It shows once again that high density is a necessary requirement to avoid the onset of fatigue.

IV. DISCUSSION

A. Compositional Effect

The results given in previous sections have clearly revealed that fatigue behavior is

sensitive to the composition and temperature. It is noticed that the compositions of PLZT with pure rhombohedral phase did not fatigue, while the compositions located near phase boundaries fatigued; thus, fatigue behavior could be actually affected by crystal structure and/or domain structure.

Both the compositions 7/65/35 and 7/68/32 which did not fatigue, belong to rhombohedral phase under applied field; no phase changes occurred during AC switching processes as shown in Fig. 4 and 7(b) exhibiting normal ferroelectric loops without any distortion. Switching by electric field takes place more easily in ferroelectric rhombohedral phase (FE_R) than in ferroelectric tetragonal and orthorhombic phases (FE_T, FE_O), since the E_c value of FE_R compositions of PLZT is about half the E_c of FE_T compositions of PLZT [1]. This indicates that for rhombohedral structure internal stresses are smaller during the switching process than those for tetragonal and orthorhombic phases. This can be further proved by $BaTiO_3$ single crystal in which the E_c for orthorhombic phase at $-90_{(+)}$ °C is 1.45 kv/cm while for rhombohedral phase of the same crystal at almost same temperature – $90_{(-)}$ °C the E_c is 0.9 kv/cm (Jona and Shirane[15]). Stadler[12] found that none of $BaTiO_3$ crystals tested at -195 °C (rhombohedral phase) suffered any change in switching charge after $4x10^8$ cycles and the charge switched at room temperature (tetragonal phase) dropped to less than half its original value after $4x10^7$ cycles. The rhombohedral crystal structure is derived from cubic structure by shear deformation. Since the shear elastic modulus is only half of the normal elastic modulus, the energy needed for shear deformation is less than for normal deformation, and the internal stress resulting from the shear deformation should also be smaller than that due to the normal deformation. The internal stresses in PLZT ceramics for several compositions with different crystal structures have been studied quantitatively by Okazaki[16] using microindentation method; he found that the internal stress in FE_R is smaller than that in FE_T, and increases with increasing c/a ratio in tetragonal compositions. From the above discussion it is clear that the ease of switching by electric field and smaller internal stress in FE_R are the main reasons for the

absence of electric fatigue and microcracks in 7/65/35 and 7/68/32 PLZT compositions in our study.

PLZT 8/65/35 and 8.4/65/35 and 7.6/70/30 which are the three compositions exhibiting severe fatigue have similar constricted neck hysteresis loops as can be seen in Fig. 4 and 7(b). All the three compositions are located in the cubic matrix region before poling, and change to orthorhombic after poling[4], indicating field induced phase transformation at room temperature, while the 7/65/35 and 7/68/32 compositions sustain their rhombohedral phase structures after poling. The occurrence of the necks in the hysteresis loops of 8/65/35, 8.4/65/35, and 7.6/70/30 compositions also indicates the transformation of macrodomain states with orthorhombic symmetry to microdomain states in cubic matrix; this transformation can be further proved by the measurement of the electric field dependence of transmittance of the PLZT sample at different temperatures (Yin et al.[17]). Their results showed that when the hysteresis loops have square shapes without necks at low temperature (-10 °C), the maximum transmittance is very low (<6%) in switching process; once the necks occurred (at 7 °C and 13 °C) the maximum transmittance can reach above 80% twice in one switching cycle,which indicates that the cubic matrix state can recur in the switching process. Therefore the structure changes from cubic matrix with microdomains to orthorhombic macrodomain state twice in one cycle in the sample with a constricted neck hysteresis loop. The changes of crystal and domain structure could result in large internal strain fluctuations and internal stresses which cause microcracking and failure. This may explain the occurrence of severe fatigue in these three samples.

The hysteresis loops for the composition 7.9/70/30 are pseudo-antiferroelectric type, with very small remanant polarization and remanant strain (Fig. 7(b)). The field forced phase change returns to the original state before the field drops to zero, and no macrodomains are left to be switched to microdomains by the reversal field; this could greatly reduce the internal stresses, and result in less fatigue in composition 7.9/70/30 than in the other three compositions

discussed above.

In true antiferroelectric materials (AFE) the switching of the polarization has a different mechanism; no spontaneous polarization exists in AFE, and the orientations of the dipoles are alternately aligned in opposite directions. The field forced ferroelectric phase is stable only under high field, and at low fields, FE returns to the AFE state. Fatigue in the antiferroelectric sample (Fig. 8) is much less severe, which is possibly due to the fact that in the switching process of the AFE to FE, the polarization direction changes only by 180 °C with consequent smaller internal stresses than in switching the spontaneous polarization of the ferroelectrics by 90°. The slow fatigue observed in AFE samples may be partially contributed by space charge pinning[8], since the samples were made by conventional sintering method, which gives rise to voids and pores.

It is not surprising that fatigue did not occur in TGS single crystals, because there are only 180° domains in this crystal. In switching process, only some atoms or atom groups of TGS rotate under the applied field, with no change in the crystal structure; therefore, the internal stresses involved in switching process should be quite small. Further, defects in high quality TGS organic crystals are rare; hence domain pinning is difficult to occur.

2. Temperature Effect.

Since the main mechanism of fatigue in sintered PLZT 7/65/35 is domain and defect pinning by space charges, the explanation of the temperature dependence of fatigue should consider both domain states and space charge mobility at different temperatures. As temperature increases, the maximum polarization decreases (Table III) and the remanant polarization decreases faster (Fig. 11(a)), since less domain walls are available for pinning. At higher temperatures near T_m, the samples are highly polarizable under the applied field, and the domains or defects which have been pinned by space charges could be depinned by AC field: Stewart and Cosentino[18] found that fatigued soft PZT sample could be restored to nearly its

original condition by heating the sample to 150 °C and then applying 60 Hz excitation. The change in the mobility of the space charge with temperature may have much less effect on fatigue compared with the changes of the polarization. So it can be concluded that the lower fatigue rates at higher temperatures could primarily be contributed by the decrease of the polarization in PLZT 7/65/35 sintered ceramics.

The disappearance of fatigue at 167 °C (Fig. 10(a)) can be easily explained; the sample was almost completely in paraelectric phase (27 °C higher than T_m), the spontaneous polarization disappeared and domains no longer existed. A slow fatigue observed at 152 °C could be due to the fact that relaxor materials have diffuse phase transformations because of the coexistence of ferroelectric and paraelectric phases arising from the inhomogeneous compositional fluctuations, and the polar regions can exist at temperatures somewhat above T_m (Cross[3]); in addition, the applied field can force some of the nonpolar regions into the polar region; under long time continuous AC switching some of the polar regions could be stabilized by space charge or injected carriers, with a slow decrease of the switchable polarization.

The decrease of the polarization can not explain the temperature dependence of fatigue in hot pressed 9.5/65/35 samples (Fig. 10(b)), which showed greater fatigue at 25 °C than at -140 °C, since the main fatigue mechanism of hot pressed high density (>99%) PLZT ceramics is microcracking and differs from that of sintered low density (92-97%) PLZT samples[8]. The phase relations in x/65/35 PLZT at different temperatures deduced from X-Ray, dielectric and piezoelectric measurements by O'Bryan[5] show that the PLZT 9.5/65/35 at 25 °C has a pseudocubic structure and is placed in the AFE (pseudocubic region), based on the existence of a double hysteresis loop. However, a double hysteresis loop can also be due to the field induced ferroelectric phase at temperatures near T_c or T_m as in the case of $BaTiO_3$ crystal, or the field forced transformation of microdomains to macrodomains[19]; in addition, the superlattice crystal structure associated with AFE phase in $PbZrO_3$ was not observed in this phase region[5]. Fatigue due to microcracking at 25 °C could be caused by the nonuniform deformation of mismatched

grains and concentration of stresses near the electrode edges. Although at this temperature the remanant polarization is small and the piezoelectric contribution can be neglected, the electrostriction is quite large in this composition (relaxor ceramic) at room temperature. The electrostrictive coefficients Q_{11} and Q_{12} measured by Meng et al.[20] for PLZT 9.5/65/35 are 21.0×10^{-3} m^4/C^2 and -9.1×10^{-3} m^4/C^2, respectively. The initial polarization of the sample used in the fatigue experiment at 25 °C was 23.0 $\mu C/cm^2$ under an applied field of 22 kv/cm, and the longitudinal strain calculated from Q_{11} and P_m is 11×10^{-4} which is of the same order as the piezoelectric strains. This high strain and the large grain size (7 μm) resulted in microcracking.

At 105 °C, a temperature 50 °C higher than T_m of 9.5/65/35 composition, the sample is in paraelectric phase. As the polarization is only half of the value at 25 °C, so the strain is only one fourth of that at 25 °C; in addition, the local microstructure stresses which exist below T_c due to the phase transformation from cubic to ferroelectric phase are released. Hence, the microcracking (fatigue) did not occur at this high temperature.

The occurrence of fatigue at low temperature (-140 °C) is more complicated (Fig. 10(b)): both the P_m and P_r are quite high and the field induced strain could be larger than that at room temperature. The different structures at 25 °C and -140 °C may explain this fatigue behavior. At -140 °C, the sample should be in the ferroelectric rhombohedral phase which has smaller internal stresses than other ferroelectric phases. The square hysteresis loops without necks (Fig. 11(b)) indicate that the crystal structure was stable at low temperature under an applied field. Therefore the field applied to the sample at low temperature mainly caused the switching of the spontaneous polarization and did not cause a change of the crystal structure, while it is known[3] that at room temperature the applied field could induce the transformation of nonpolar regions to polar states and produce unstable lattice distortions, resulting in microstructure stresses which enhance microcracking and increase the rate of fatigue. The slow fatigue at low temperature may also be related to the change in the mechanical strength of the sample; since the lattices contract with the decrease of temperature, producing compressive internal stresses in the sample, the

fracture strength could be higher at low temperatures. The occurrence of slow fatigue could be attributed to the large grain size which results in microcracking.

Fatigue behavior in PMN ceramic system is similar to that in PLZT ceramics. The conventionally sintered samples with a grain size of 5 μm showed fatigue at low temperature (-140 °C) with a rather slow rate. The cause of the fatigue is believed to be domain and defect pinning since after the sample was reheated to room temperature (40 °C higher than T_m), the initial state was recovered without permanent damage. The slower fatigue rate in PMN sample than in sintered PLZT 7/65/35 could arise from three reasons: (1) the density of the sintered PMN ceramic is higher than that of sintered PLZT 7/65/35 ceramic; less pores and defects are available to provide space charges[8], (2) PMN is a stoichiometric compound, and has fewer intrinsic defects (which can be pinned by space charge or injected carriers) and cleaner grain boundaries, (3) the mobility of the space charge may be less at low temperature.

Hot pressed PMN (1% La) did not fatigue at low temperature, which is attributed to its high density and small grain size. At room temperature, fatigue did not occur in both the PMN samples because both were in paraelectric phase.

V. CONCLUSIONS

Evidence has been presented to establish the relationship between fatigue behavior and composition in the PLZT system. In the x/65/35 compositions, fatigue increased from nil at x=7 through x=9.5, 8 to most severe for x=8.4. The two compositions (x=8.4 and 8) with severe fatigue rates had exhibited constricted hysteresis loops before the fatigue experiment. The fatigue rate of 7.6/70/30 PLZT composition was greater than that of 7.9/70/30. On the other hand, antiferroelectric (modified PLZT) composition as well as single crystal triglycine sulfate (TGS) did not show any significant fatigue effect, which is attributed to the fact that polarization changes under applied a.c. field involve only 180° domain switching in these cases. Temperature was also found to influence the fatigue rates of these materials. At temperatures

higher than T_c or T_m (by 30 to 50 °C), no fatigue effects were observed and this was attributed to the absence of domains and spontaneous polarization in the paraelectric state. At other temperatures, fatigue rate depends upon the ease of domain switches, and associated strains.

Both the compositional and temperature dependence of fatigue behavior translate into the influence of the crystal symmetry and ferroic state of the material under the action of applied a.c. field for long periods. Among the ferroelectric phases, the rhombohedral symmetry, with its small internal stress associated with the shear distortion of the cubic lattice, has the least fatigue rate compared to that of the ferroelectrics with tetragonal and orthorhombic symmetries. Antiferroelectric materials and ferroelectric TGS crystal exhibit little or no fatigue effect, since polarization changes only by 180° in these materials with no accompanying strain. On the other hand, the samples close to the phase boundaries (due to composition, temperature or electric field) undergo most severe fatigue behavior and this is attributed to easy polarization changes and consequent large lattice distortions. Electric fatigue can be due to either domain pinning by space charges or injected charge carriers or intergranular microcracking resulting from incompatible stresses between grains. The former is recoverable by thermal and electrical treatment, while the latter (microcracking) is a permanent damage.

The conclusions drawn from the present study provide guidelines for enhancing the long term reliability of devices based on ferroic ceramics.

ACKNOWLEDGMENTS

The authors are grateful to the Office of Naval Research for financial support.

REFERENCES

1. G. H. Haertling, *Ferroelectrics.*, **75**, 25 (1987).
2. E. T. Keve and K. L. Bye, *J. Appl. Phys.*, **46**, 810 (1975).
3. L. E. Cross, *Ferroelectrics*, **76**, 241 (1987).
4. E. T. Keve, ibid, **10**, 169 (1976).
5. H. M. O'Bryan, Jr., *J. Amer. Ceram. Soc.* **56**, 385 (1973).
6. Q. Y. Jiang, Ph.D. thesis, Pennsylvania State University, (1992).
7. Q. Y. Jiang, W. Cao and L. E. Cross, *J. Amer. Ceram. Soc.*, (in press).
8. Q. Y. Jiang and L. E. Cross, *J. Mater. Sci.* **28**, (in press).
9. Q. Y. Jiang, E. C. Subbarao and L. E. Cross (submitted).
10. G. W. Taylor, *J. Appl. Phys.*, **38**, 4697 (1967).
11. S. W. Freiman, L. Chuck, J. J. Mecholsky, J. J., D. L. Shellman, and L. J. Storz, in *Fracture Mechanics of Ceramics*, edited by R. C. Bradt, D. P. H. Hasselman, and F. Lange (Plenum Press New York-London, 1986) p. 175.
12. H. L. Stadler, *J. Appl. Phys.*, **29**, 743 (1958).
13. W. A. Schulze, J. V. Biggers, and L. E. Cross, *J. Amer. Ceram. Soc.*, **61**, 46 (1978).
14. D. Berlincourt, H. H. A. Krueger, and B. Jaffe, *J. Phys. Chem. Solids*, **25**, 659 (1964).
15. F. Jona, and G. Shirane, *Ferroelectric Crystals*, (Macmillan Company New York, 1962). p. 28 and p. 119.
16. K. Okazaki, *J. Amer. Ceram. Soc.*, **63**, 1150 (1983).
17. Z. W. Yin, X. M. He, C. Li, Z. Wei, H. Ni, *J. Chinese Silicate Soc.*, **11**, 410 (1983).
18. W. C. Stewart, and L. S. Cosentino, *Ferroelectrics*, **1**, 149 (1970).
19. X. Yao, Z. Chen, and L. E. Cross, *J. Appl. Phys.* **54**, 3399 (1983).
20. Z. Y. Meng, U. Kumar, and L. E. Cross, *J. Amer. Ceram. Soc.*, **68**, 459 (1985).

TABLE I. The grain size, temperature of maximum dielectric constant and a.c. frequency for fatigue study of PLZT ceramic with different compositions.

Composition	Grain Size μm	T_m(°C)	f (Hz)
7/65/35	1*, 5	140	100
8/65/35	5	100	100
8.4/65/35	7	92	40
9.5/65/35	7	55	160
7/68/32	5	130	200
7.6/70/30	7	90	60
7.9/70/30	7	82	100

* Sintered; rest are hot pressed.

TABLE II. The changes of the polarization and coercive field of the PLZT 8.4/65/35 sample due to fatigue and its recovery.

	P_r ($\mu c/cm^2$)	E_c (kv/cm)
After 10 switching cycles	27.9	3.1
After 10^6 switching cycles	10.7	4.7
After removal of discolored region	24.7	3.4

TABLE III. The maximum polarization of sintered PLZT 7/65/35 ceramic at different temperatures

T (°C)	37	87	118	152	167
P_m ($\mu c/cm^2$)	28.0	26.0	21.5	15.0	12.6

Figure caption:

Fig. 1. Room temperature phase diagram of PLZT ceramics with selected compositions (Ref. 1).

Fig. 2. Critical fracture toughness K_{1C} as a function of composition in PZT ceramic system. Vertical line indicates the position of the phase boundaries at 25 °C. (Ref. 11)

Fig. 3. The normalized remanant polarizations and coercive fields as a function of the switching cycles for hot pressed PLZT ceramics with compositions x/65/35.

Fig. 4. Hysteresis loop curves recorded during fatigue tests for Hot pressed PLZT ceramics with compositions x/65/35.

Fig. 5. Microstructure of the fatigued PLZT 8/65/35 sample observed by optical microscope with transmitted light. (a) shows the total fatigued area (within circle); (b), (c) and (d) show further observation under higher magnification for part of the opaque ring in (a), when the picture was focused near the bottom face of the sample (b), in the middle level (half above the bottom) (c), and near the top surface (d).

Fig. 6. Fractured cross section of a fatigued PLZT 8.4/65/35 sample observed by SEM. (a) Fractured cross section and (b) microstructure changes of the surface beneath the electrode.

Fig. 7. (a) The normalized remanant polarization as a function of the switching cycles, (b) hysteresis loop curves recorded during fatigue tests for hot pressed PLZT ceramic of three compositions.

Fig. 8. (a) The normalized polarization and coercive field as a function of switching cycles. (b) hysteresis loop curves recorded during fatigue experiment for antiferroelectric $Pb_{.97}La_{.02}(Zr_{.53}Ti_{.12}Sn_{.35})O_3$ ceramic.

Fig. 9. (a) The normalized remanant polarization and coercive field as function of the switching cycles for TGS single crystal, (b) its hysteresis loop curves recorded during fatigue test (P_r= 2.5 μc/cm^2, E_c= 0.35 kv/cm).

Fig. 10. The normalized polarization as a function of the switching cycles for (a) sintered PLZT 7/65/35 ceramic and (b) hot pressed PLZT 9.5/65/35, at different temperatures.

Fig. 11. Hysteresis loop curves recorded during fatigue tests (a) at four temperatures for sintered PLZT 7/65/35 ceramic and (b) at three temperatures for hot pressed 9.5/65/35 PLZT ceramic.

Fig. 12. Cracks observed in fatigued hot pressed 9.5/65/35 ceramics by optical microscope with transmitted light. (a) Fatigued at room temperature and (b) fatigued at – 140 °C.

Fig. 13. Polarization as a function of the switching cycles for (a) sintered PMN and (b) hot pressed 1% La doped PMN.

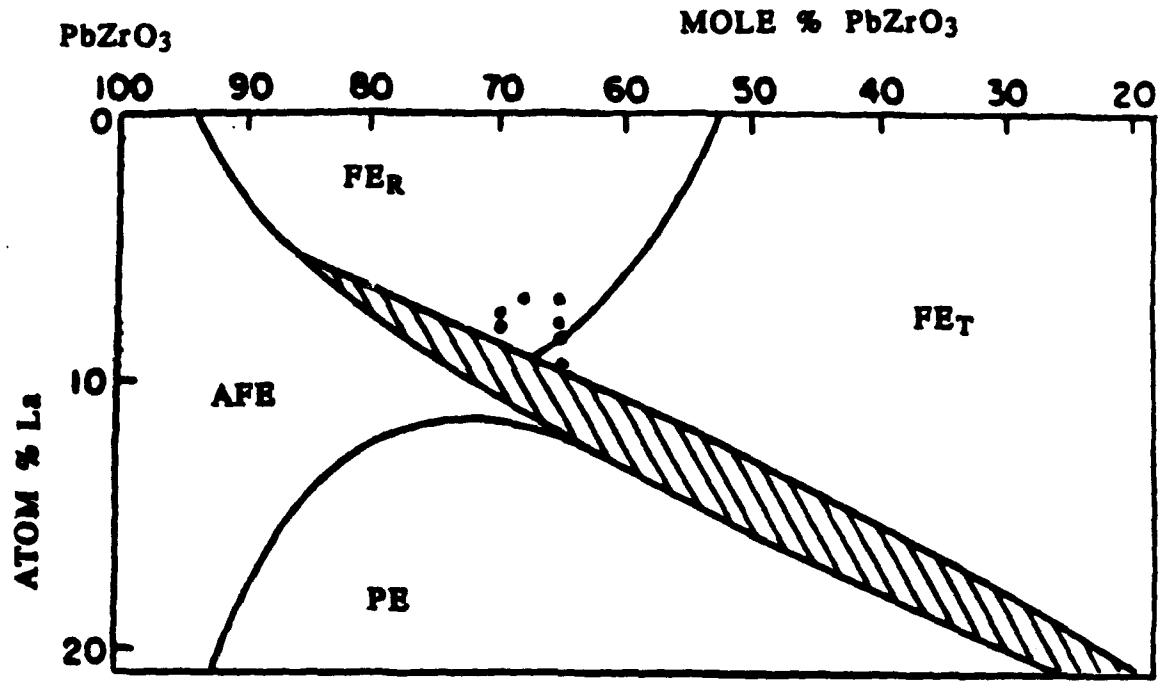
PbZrO3
MOLE % PbZrO3
100
90
80
70
60
50
40
30
20
0
10
20
ATOM % La
FER
FET
AFE
PE

Fig

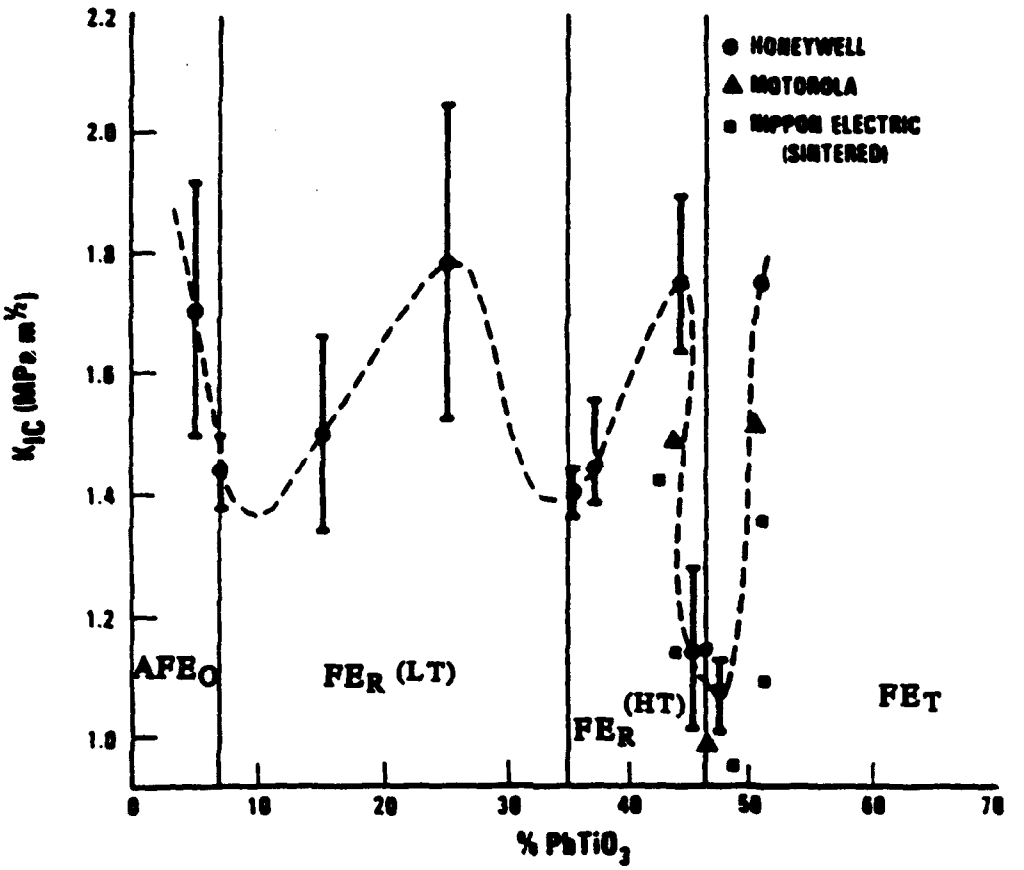
2.2
2.0
1.8
1.6
1.4
1.2
1.0
K_{IC} (MPa $m^{1/2}$)
HONEYWELL
MOTOROLA
NIPPON ELECTRIC (SINTERED)
AFE_O
FE_R (LT)
FE_R (HT)
FE_T
0
10
20
30
40
50
60
70
% $PbTiO_3$

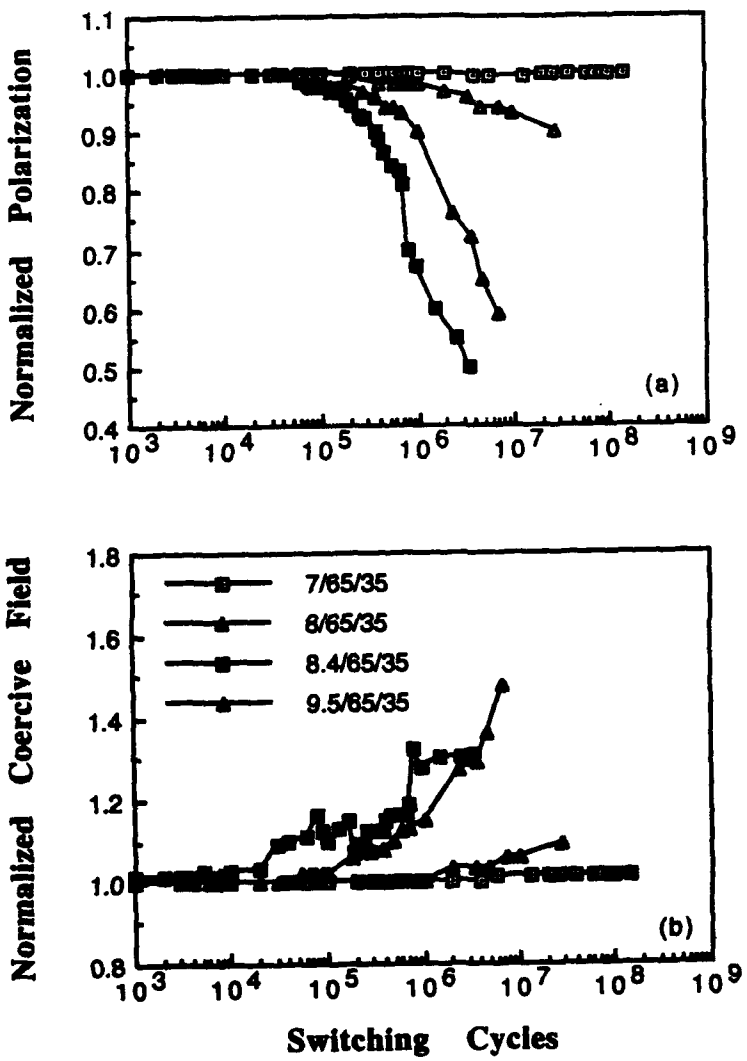
Normalized Polarization
1.1
1.0
0.9
0.8
0.7
0.6
0.5
0.4
10^3 10^4 10^5 10^6 10^7 10^8 10^9
(a)
Normalized Coercive Field
1.8
1.6
1.4
1.2
1.0
0.8
7/65/35
6/65/35
8.4/65/35
9.5/65/35
(b)
Switching Cycles

Fig. 3.

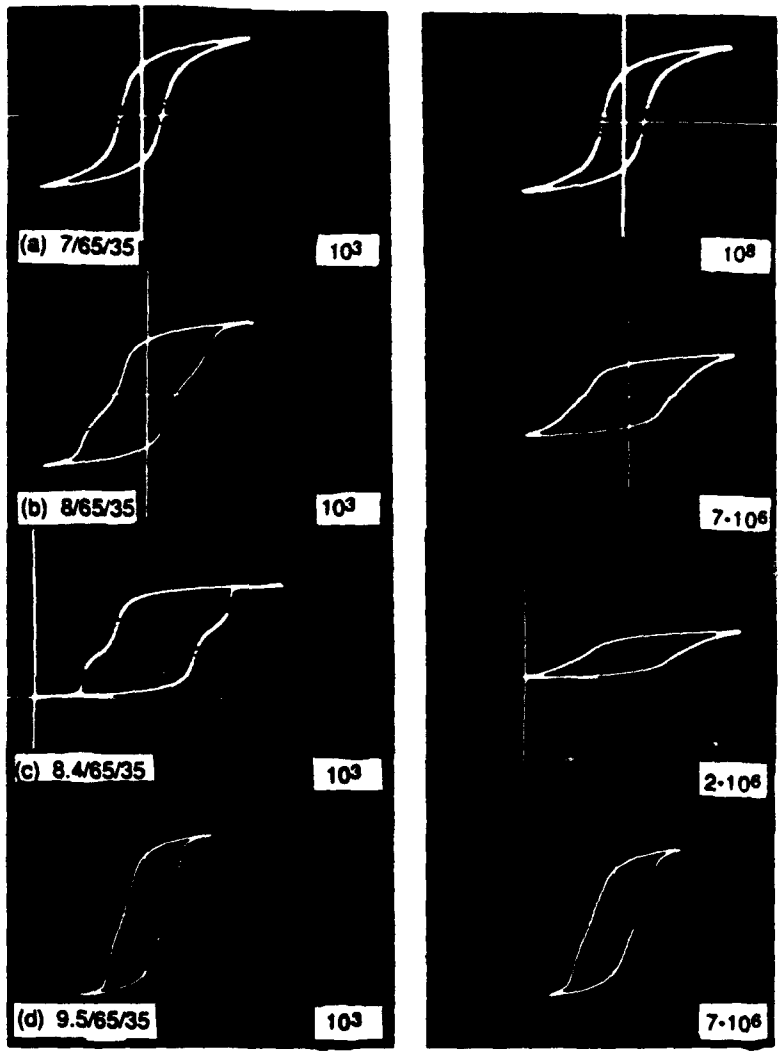
(a) 7/65/35
10³
10⁸
(b) 8/65/35
10³
7·10⁶
(c) 8.4/65/35
10³
2·10⁶
(d) 9.5/65/35
10³
7·10⁶

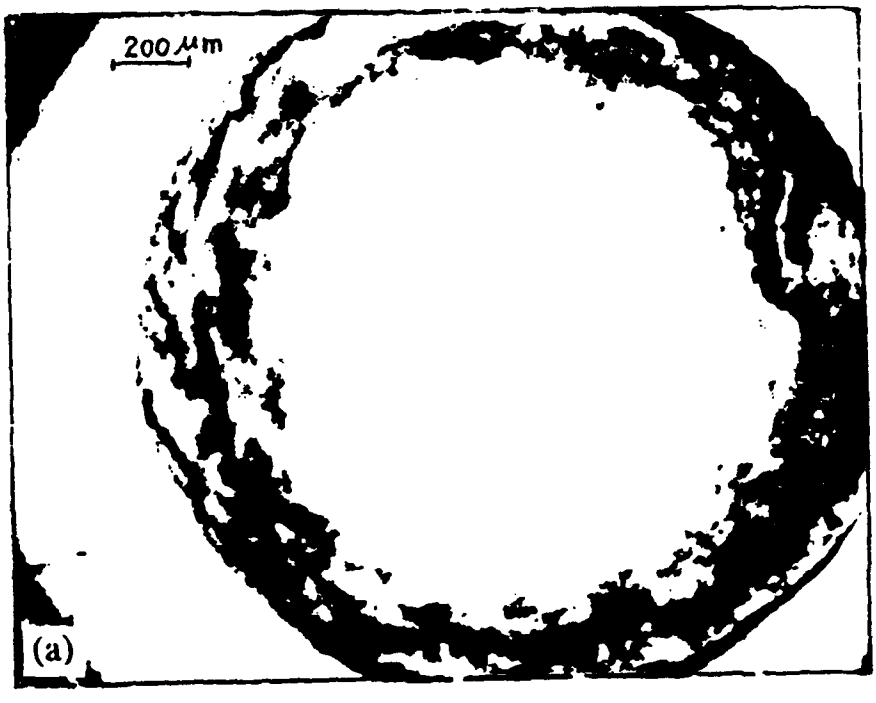

Fig 5(a)

(b)

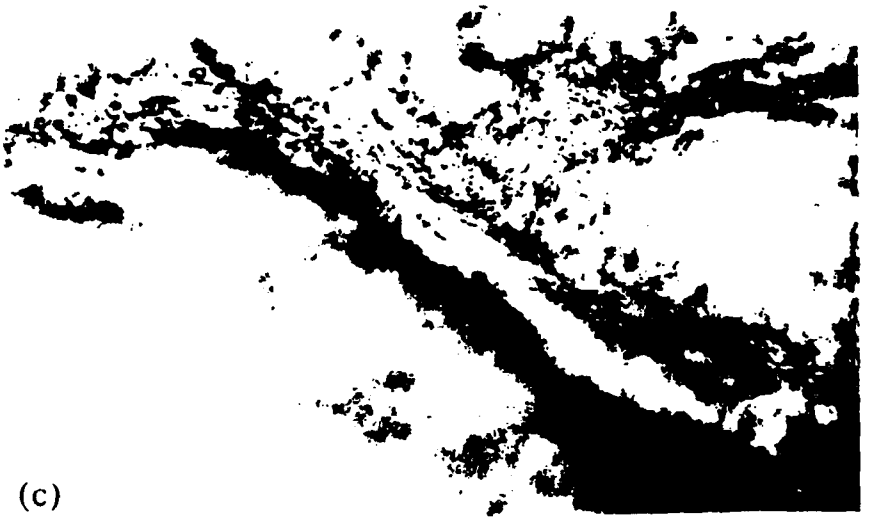

(c)

(d)

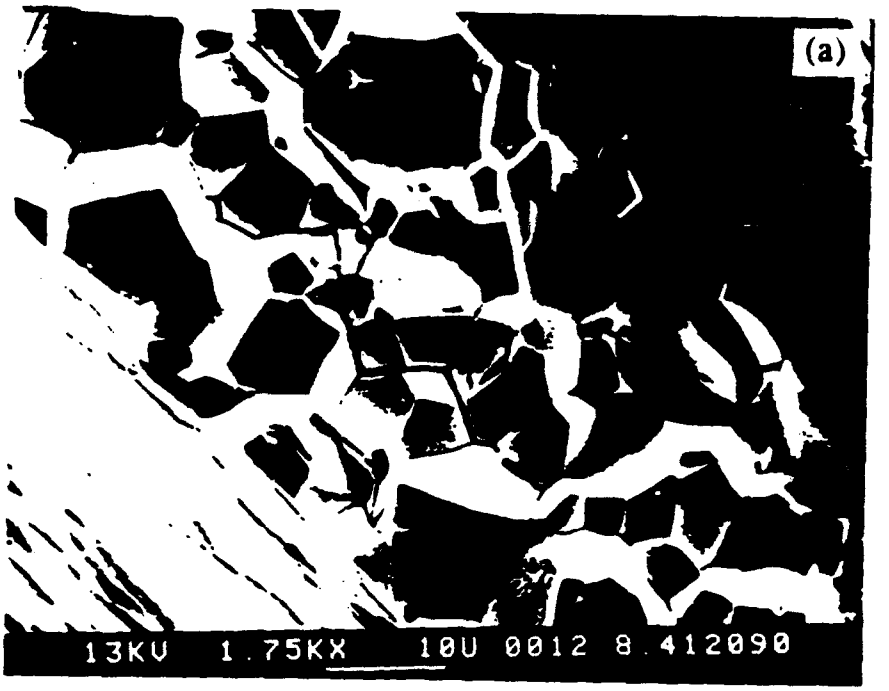

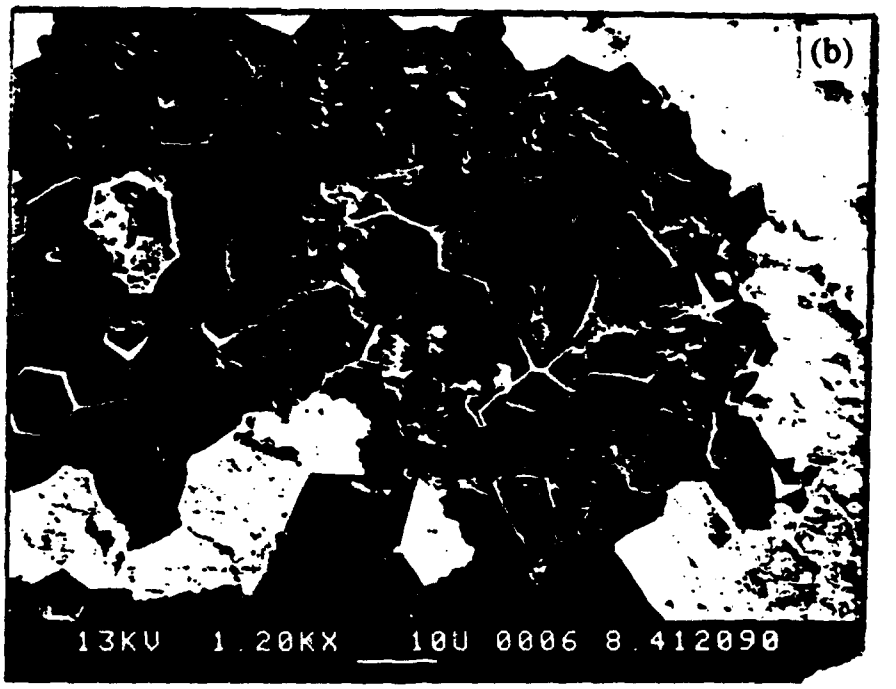

Fig. 6 (a) (b)

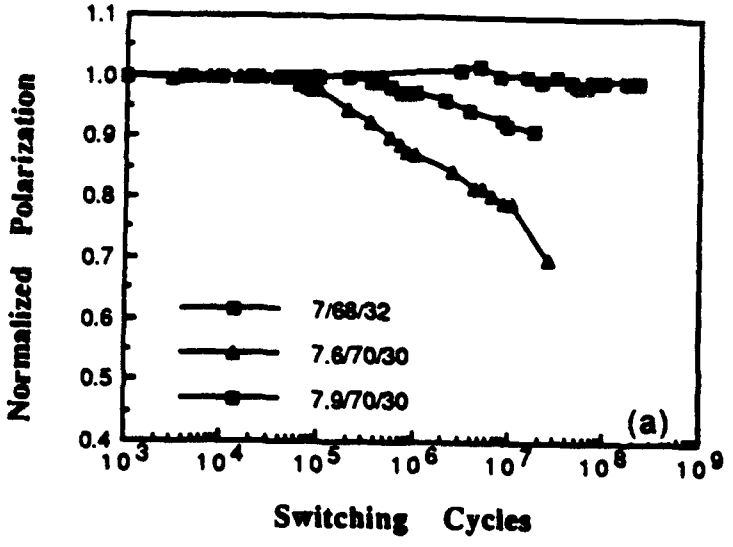
Normalized Polarization
1.1
1.0
0.9
0.8
0.7
0.6
0.5
0.4
7/68/32
7.6/70/30
7.9/70/30
(a)
10^3
10^4
10^5
10^6
10^7
10^8
10^9
Switching Cycles

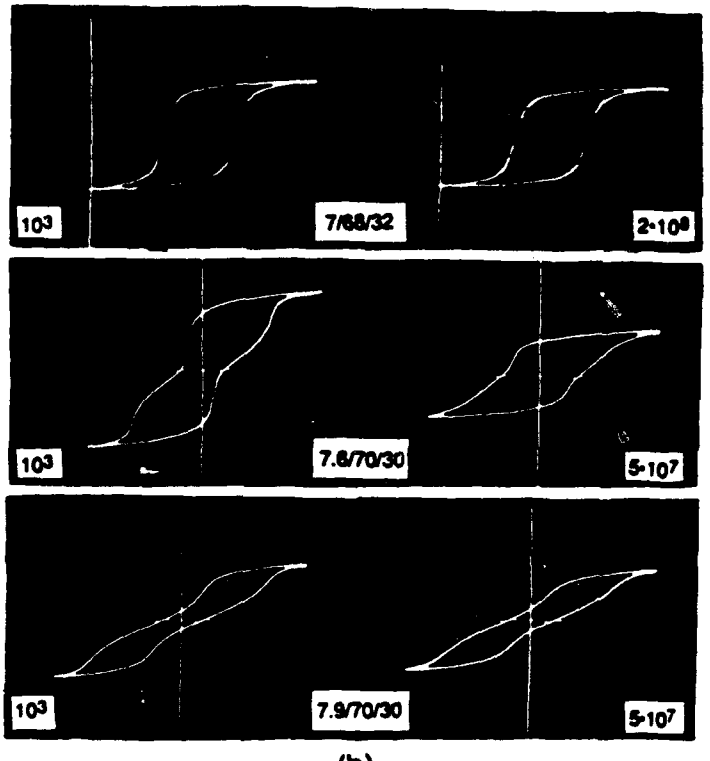
10^3
7/68/32
2·10^8
10^3
7.6/70/30
5·10^7
10^3
7.9/70/30
5·10^7

(b)

F

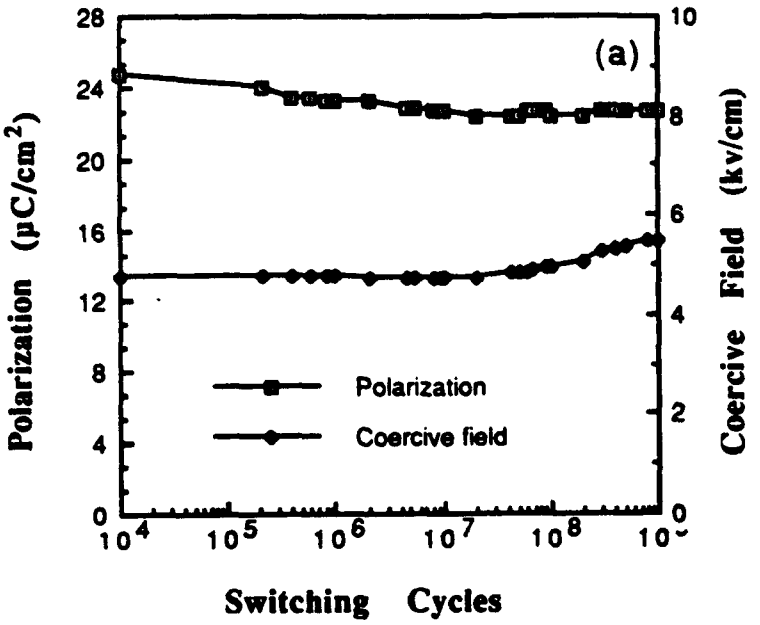
(a)
Polarization (μC/cm²)
Coercive Field (kv/cm)
Polarization
Coercive field
Switching Cycles


(b)
10⁴ cycles
10⁹ cycles

Fig.

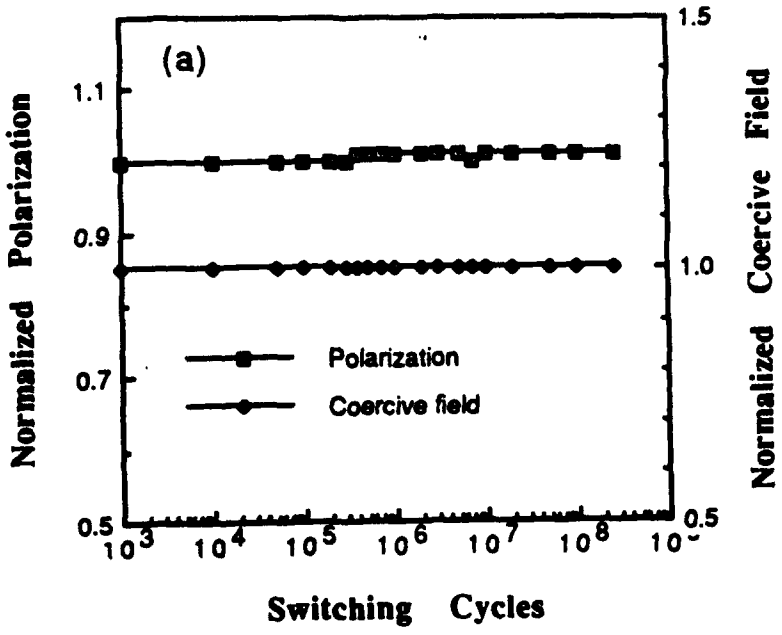
(a)
Normalized Polarization
Normalized Coercive Field
1.5
1.1
0.9
1.0
0.7
0.5
0.5
Polarization
Coercive field
10^3 10^4 10^5 10^6 10^7 10^8
Switching Cycles

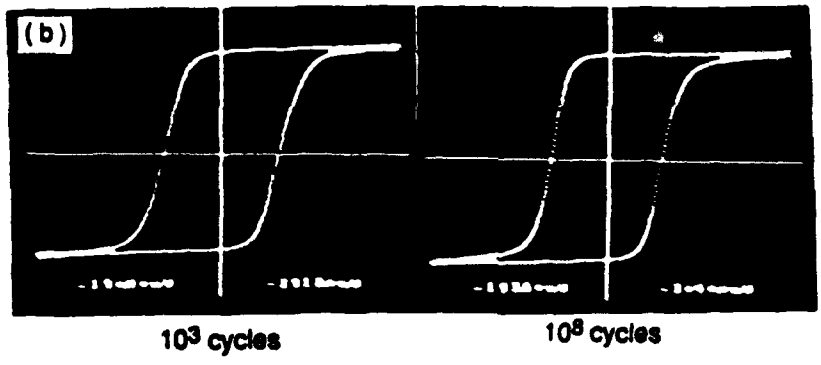
(b)
10^3 cycles
10^8 cycles

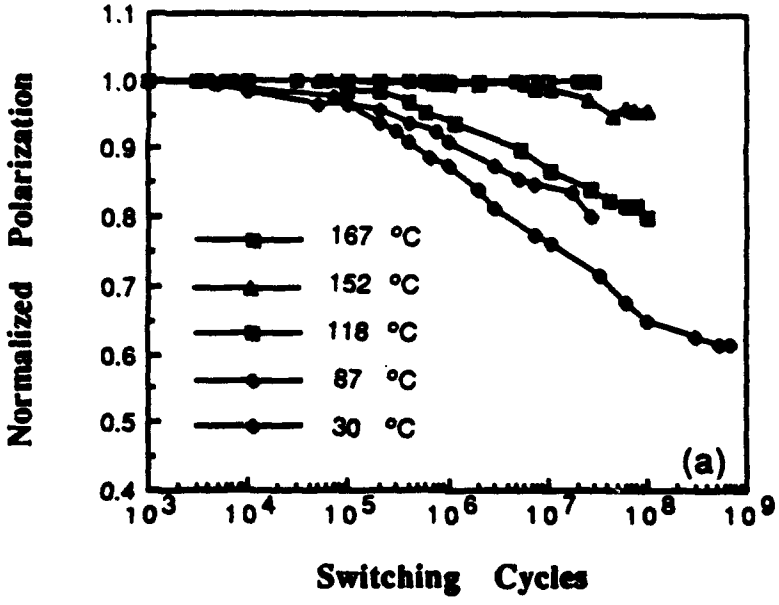
Normalized Polarization
1.1
1.0
0.9
0.8
0.7
0.6
0.5
0.4
167 °C
152 °C
118 °C
87 °C
30 °C
(a)
10^3
10^4
10^5
10^6
10^7
10^8
10^9
Switching Cycles

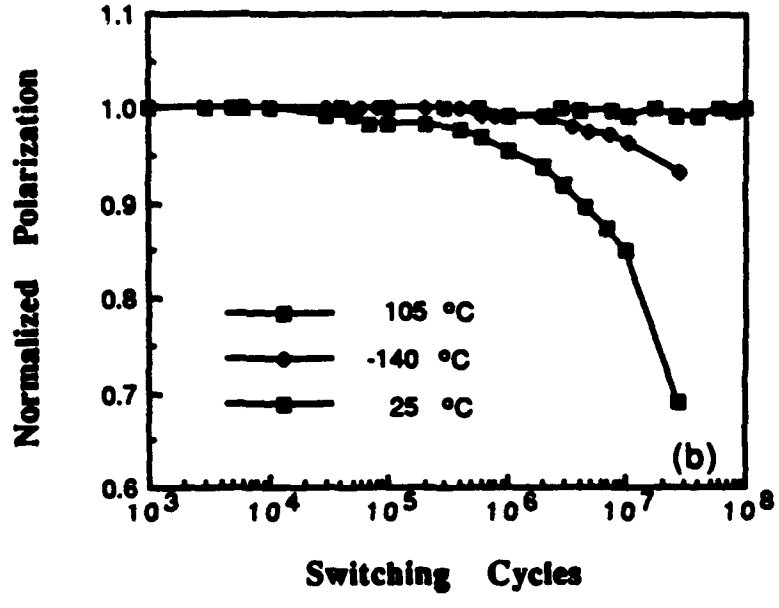
Normalized Polarization
1.1
1.0
0.9
0.8
0.7
0.6
105 °C
-140 °C
25 °C
(b)
10^3
10^4
10^5
10^6
10^7
10^8
Switching Cycles

Fig. 10

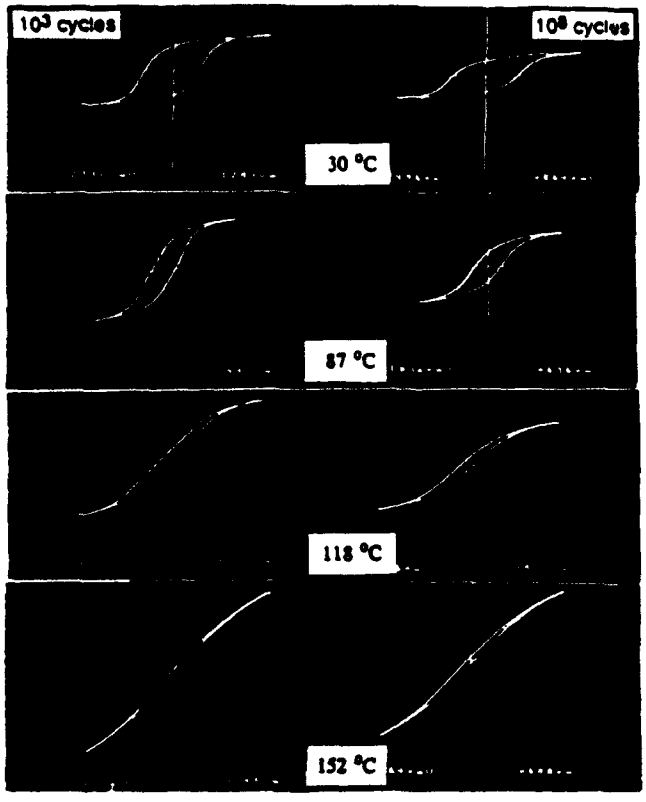
10^3 cycles
10^8 cycles
30 °C
87 °C
118 °C
152 °C

(a)

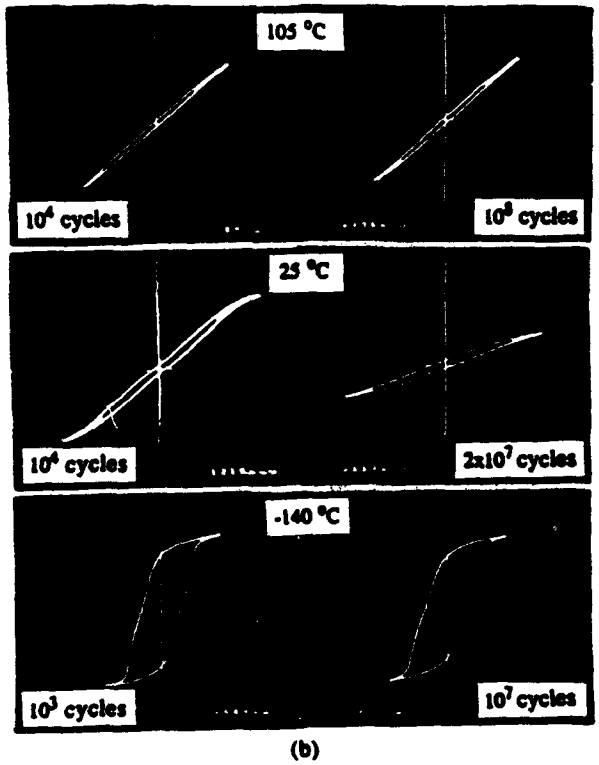
105 °C
10^4 cycles
10^8 cycles
25 °C
10^4 cycles
$2x10^7$ cycles
-140 °C
10^3 cycles
10^7 cycles

(b)

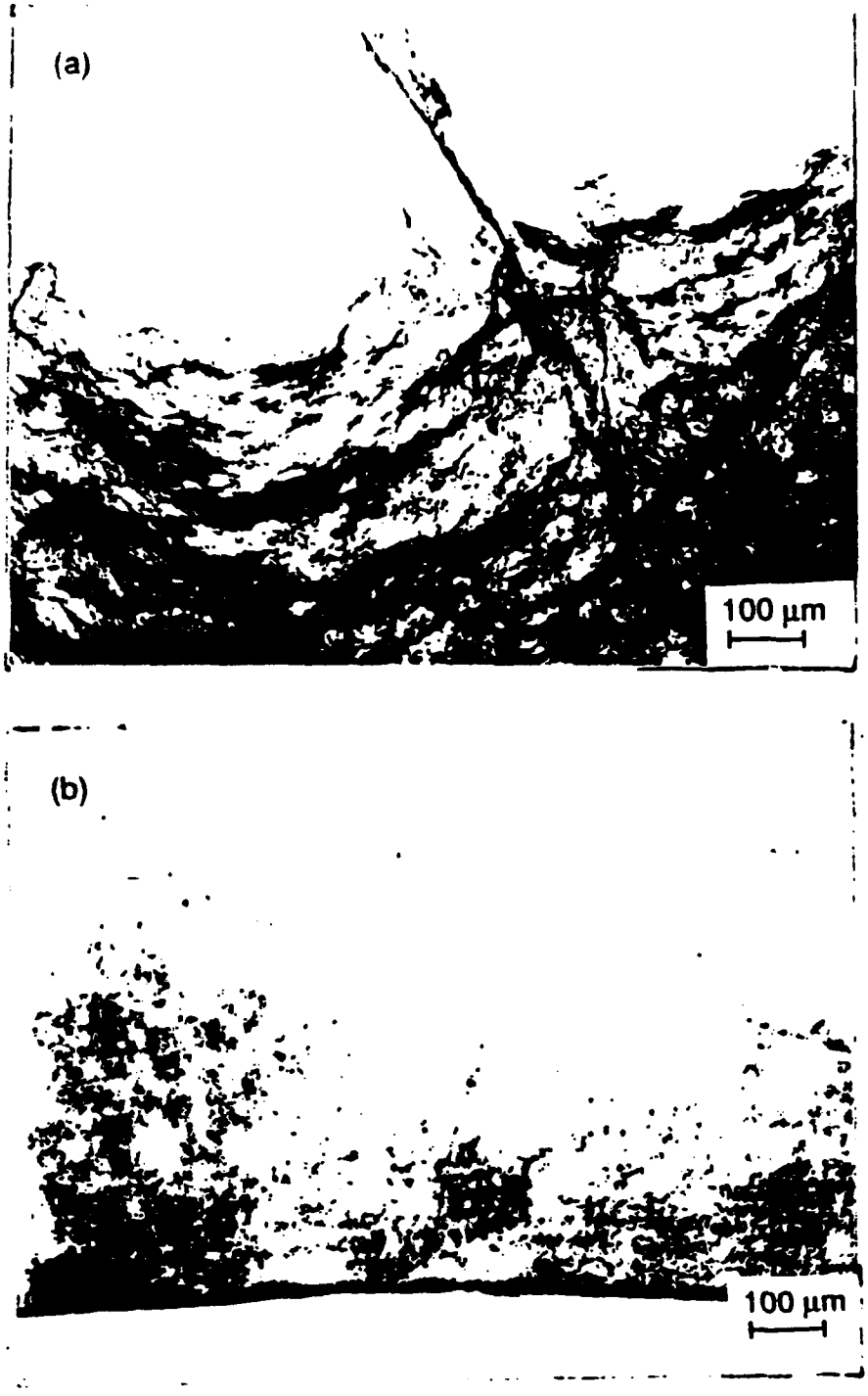

Fig. 12

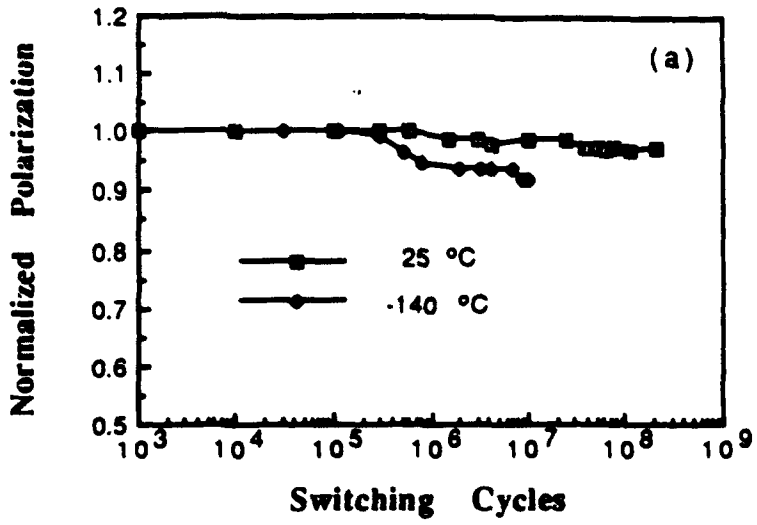
(a)
Normalized Polarization
1.2
1.1
1.0
0.9
0.8
0.7
0.6
0.5
25 °C
-140 °C
10^3 10^4 10^5 10^6 10^7 10^8 10^9
Switching Cycles

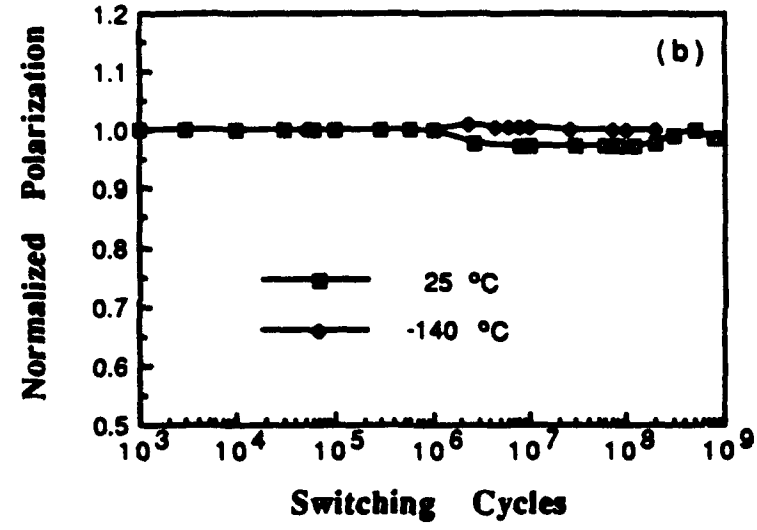
(b)
Normalized Polarization
1.2
1.1
1.0
0.9
0.8
0.7
0.6
0.5
25 °C
-140 °C
10^3 10^4 10^5 10^6 10^7 10^8 10^9
Switching Cycles

Fig. 13.

APPENDIX 17

Effects of porosity on electric fatigue behaviour in PLZT and PZT ferroelectric ceramics

Q. Y. JIANG, L. E. CROSS
Materials Research Laboratory, The Pennsylvania State University, University Park PA 16802 USA

Electric fatigue, namely the decay of the polarization and the consequent elastic strain with increased number of switching cycles under high a.c. field, severely limits the applications of ferroelectric and piezoelectric materials in high-strain electro-mechanical actuators and in thin films used in non-volatile memory devices. Electric fatigue tests have been conducted on lead zirconate titanate (PZT) and lanthanum-doped lead zirconate titanate (PLZT) ferroelectric ceramics. It was found that electric fatigue can be initiated by various factors, the porosity being one of them. Electric fatigue occurred in low-density(93%–97%) PLZT 7/65/35 ceramics after 10^4 switching cycles, while the high-density (>99%)PLZT specimens of the same composition did not fatigue after 10^9 switching cycles. It was also observed that for PZT ceramics, fatigue proceeded much more slowly in the samples with higher density (~98%) than those with lower densities (92%–96%). A tentative explanation for the origin of the fatigue mechanism associated with porosity is proposed.

1. Introduction

It is well known that under many circumstances when a ferroelectric crystal or ceramic is switched under high a.c. field, the switched charge (polarization) and the consequent elastic strain decay with increased number of cycles [1–4], which is the so-called electroactive or electric fatigue. This effect severely limits the applications of ferroelectric and piezoelectric materials in high-strain electro-mechanical actuators and in thin films used in non-volatile memory devices.

Our systematic study [5] has revealed that electric fatigue in ferroelectric ceramics is much more complicated than was originally expected. Fatigue could be initiated by various factors; surface conditions, ceramic microstructure, electroding methods, compositions, and temperature, can all make contributions to fatigue behaviour. In a previous paper [6], we reported that fatigue which occurred after only thousands of switching cycles in hot-pressed fine-grain lanthanum-doped lead zirconate titanate PLZT 7/68/32 was initiated by surface contamination. Fatigue of this type could be avoided by an improved cleaning procedure before electroding [6]. The present investigation is concerned with the effects of ceramic microstructure, i.e. densities and pores, on fatigue behaviour. The grain size, composition, temperature, and electrode effects will be discussed in following papers.

Study of the influence of porosity on dielectric failure strength (breakdown) in PLZT ceramic system by Furman [7] indicated that hot-pressed high-density (>99%) PLZT ceramics have a dielectric strength almost twice the value in conventionally sintered samples of the same composition (density 92%–96%). The existence of pores in sintered samples caused the reduction of the dielectric strength because of the enhanced field concentration and discharge in the voids. Another electric failure mode in ferroelectric ceramics is d.c. degradation [8, 9], which is also affected by porosity defects. Herbert [10] reported that the rate of d.c. degradation was greatly increased by voids and flaws in ferroelectric ceramics. It is rational to expect that the porosity or voids could also influence dynamic fatigue under high a.c. field because the field concentrations and space-charge accumulation in the pores also exist when ceramic samples are experiencing a.c. fields. However, no published work has been found on this subject. Because pores or voids are common in ceramic materials, it is necessary to know how these defects are related to fatigue behaviour. The study of the density (pore) effects was carried out on conventionally prepared PLZT, lead zirconate titanate (PZT), and hot-pressed PLZT ceramics; the results showed that the porosity could initiate and accelerate the fatigue process. The mechanism of fatigue of this type is discussed.

2. Experimental procedure

Lanthanum-doped lead zirconate titanate 7/65/35 (mole ratio of La/Zr/Ti) ceramic specimens were fabricated by both conventional-sintering and hot-pressing techniques. In the conventional-sintering procedure, the starting oxides powders of reagent grade were PbO, La_2O_3, ZrO_2, and TiO_2. The mixed oxides were milled in a rotary mill for 24 h. After milling, the slurry was dried in an oven. The dried powder was calcined at 780 °C for 6 h, and then ground and recalcined at 780 °C. Then the powders which were mixed with polyvinyl alcohol (PVA) binder and dried were pre-

0022–2461

ssed into pellets using a 0.9 cm diameter die, and pressure up to 40 000 p.s.i. (10^3 p.s.i. = 6.89 N mm^{-2}). The thicknesses of the pellets ranged from 1–2 mm. After the binder was burned out, the pellets and a mixture of PbO and ZrO_2, which was used to control the lead atmosphere, were placed on platinum sheets in alumina crucibles which were then sealed with cement and sintered in an automatic temperature-controlled furnace with a heating rate of 200 °C h^{-1}. The sintering temperature was chosen as 1280, 1300 or 1320 °C. It was found that all three temperatures fall into the sintering-temperature range. However, the samples sintered at 1300 °C showed better dielectric properties. The average grain size was 2 μm. The hot-pressed PLZT samples with average grain size 5 mm were obtained from Honeywell Inc. Soft PZT samples were commercial PZT 5 made by both conventional-sintering and tape-casting techniques. Hard PZT samples were commercial PZT 8.

All samples had ground surfaces and their thicknesses ranged 150–300 μm. The improved cleaning procedure [5, 6] was applied to clean all specimens before electroding to avoid fatigue induced by surface contamination. Sputtered gold was used for the electrode.

The properties studied here were the remnant polarization, P_r, the maximum polarization, P_m, and the coercive field, E_c. Sinewave a.c. field was applied to switch the polarization. The hysteresis loops were measured through a conventional Sawyer–Tower circuit and recorded at intervals on a Nicolet 214 digital oscilloscope. The polarization and coercive field were calculated from the measured hysteresis loops.

3. Results

3.1. Fatigue in conventionally sintered 7/65/35 PLZT ceramics

The sintered PLZT 7/65/35 specimens have an average grain size of 2 μm, and their density is in the range of 93%–96% theoretical. The microstructure is shown in Fig. 1a, observed on the fractured surface by SEM. A large number of pores was found, and the sizes of the pores ranged from less than 1 μm to several tens of micrometres.

Fatigue experiments were carried out on several sintered samples which were cut from selected batches to obtain different densities. The normalized polarization and normalized coercive field which represent the percentages of the polarization and coercive field with respect to their initial values obtained at 10^2 or 10^3 switching cycles, are used in this paper in order to compare the results from different specimens and emphasize the changes of the measured properties. Fig. 2a and b show typical hysteresis loops measured before and after fatigue tests in a specimen with a density of 93%. The normalized remnant polarization and coercive field as functions of the switching cycles, for three samples at a frequency of 300 Hz are shown in Fig. 3. The remnant polarizations decrease with increasing switching cycles for all samples, while the rates of fatigue are different. After 10^8 switching cycles, only 30% of the polarization of the original value in Sample 3 (density 93%) was left, but for Sample 1 (density 96%) 60% of the polarization was still switchable, and for Sample 2 (density near 95%) the fatigue rate lay between the other two samples. The maximum polarizations which are not shown here fatigued in a similar manner to the P_r. For a quantitative comparison, we define a parameter $C(P_n)$ which is the number of the switching cycles when the normalized polarization equals P_n ($0 \leq P_n \leq 1$) to characterize the fatigue rate. For instance, in Fig. 3a the number of the switching cycles for $P_n = 70\%(0.7)$ is 4×10^7 for Sample 1, it is designated $C(0.7) = 4 \times 10^7$. The $C(P_n)$ data of the samples with three P_n values and the sample densities are listed in Table I. The rates of fatigue for the samples of the same composition but different densities can differ by two orders of magnitude. Unlike the polarization, the coercive fields do not change significantly (Fig. 3b). E_c either increases to some extent, or decreases slightly, or remains constant, depending on the individual sample. The fatigue rate does not significantly depend on the frequency in the range 1–600 Hz in our study.

Thermal treatments were applied to the fatigued samples at 300 °C for 2 h. Sample 3, which fatigued most severely, only had a slight change, as seen in Fig. 2c, but for the fatigued Sample 2, the polarization

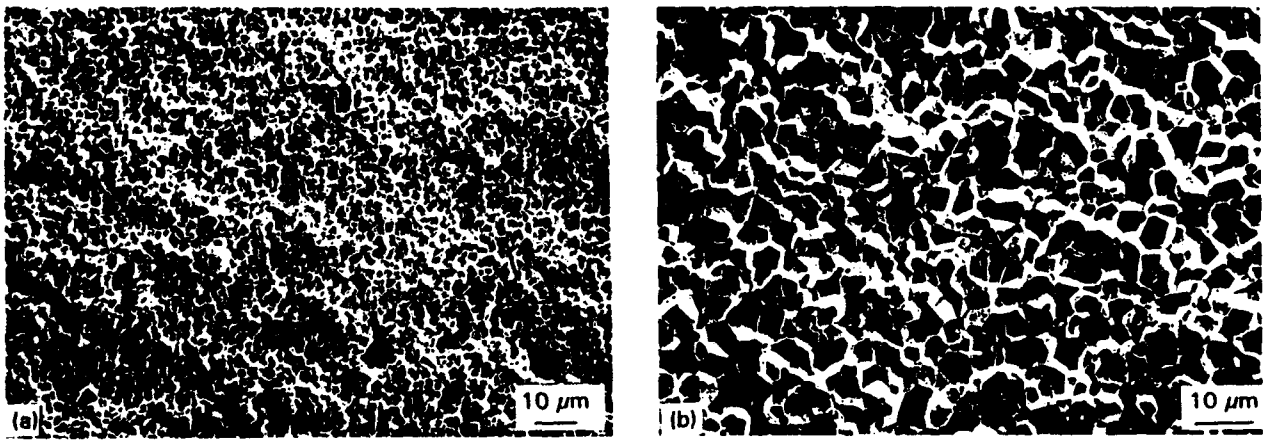

Figure 1 Microstructures of (a) conventionally sintered and (b) hot-pressed PLZT 7/65/35 ceramics observed by SEM on the fractured surfaces.

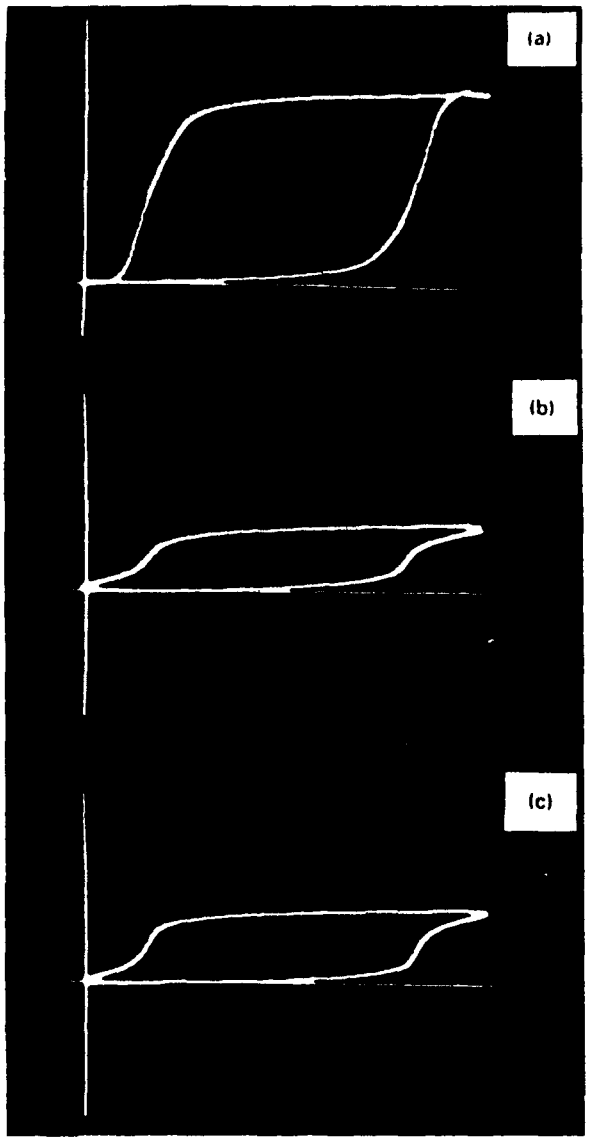

Figure 2 Hysteresis loop curves for a sintered PLZT 7/65/35 sample, recorded at (a) 10^3 cycles; (b) 10^8 cycles; and (c) heated at 300 °C for 2 h after the fatigue test.

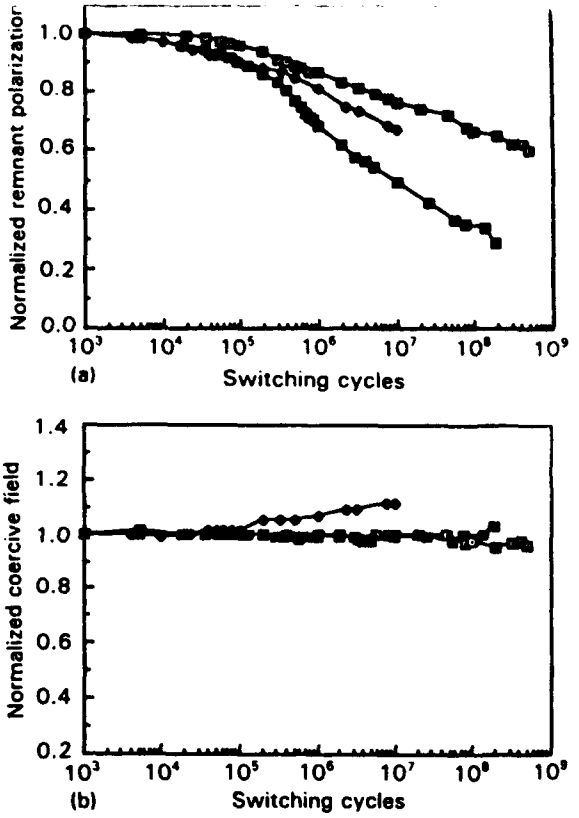

Figure 3 (a) Normalized remnant polarizations and (b) normalized coercive field as functions of the switching cycles for the three sintered PLZT 7/65/35 samples. (□) Sample 1, (◆) Sample 2, (■) Sample 3.

and coercive field almost recovered to their original values after thermal treatment (Fig. 4). The changes of P_r and E_c for Sample 2 after fatigue test and heating at different frequencies are listed in Table II. The origin of the fatigue, the cause of the difference of fatigue rates, and the thermal treatment effects will be discussed in Section 4.

3.2. Fatigue in hot-pressed 7/65/35 PLZT ceramics

Hot-pressed 7/65/35 PLZT ceramics with average grain size 5 μm had high density (> 99%) and no pores were found by SEM. The microstructure is shown in Fig. 1b. Fatigue tests were conducted on several specimens; the results showed a good consistency for all samples. The hot-pressed 7/65/35 samples showed good resistance to fatigue, as can be seen from Fig. 5 which shows the normalized remnant polarization and coercive field as functions of the switching cycles and the hysteresis loops recorded before and after the fatigue test. After the samples were switched up to 10^9 cycles under a.c. field at a frequency of 300 Hz, the polarizations and coercive fields did not change significantly. Similar results were also obtained for hot-pressed 7/68/32 PLZT samples, as discussed in our previous paper [6]. Comparing these

TABLE I Fatigue rates $C(P_n)$ (cycles) for PLZT and PZT ceramics

	$C(0.8)$	$C(0.7)$	$C(0.6)$	Density(%)
Sample 1 (7/65/35)	3×10^6	4×10^7	3×10^8	96
Sample 2 (7/65/35)	1.5×10^6	7×10^6	-	95
Sample 3 (7/65/35)	3×10^5	8×10^5	1.4×10^6	93
Commercial soft PZT	1×10^4	1.5×10^4	2.4×10^4	92
Tape-cast soft PZT	5×10^7	5×10^8	$> 10^9$	98
Commercial hard PZT	2×10^7	2×10^8	-	97

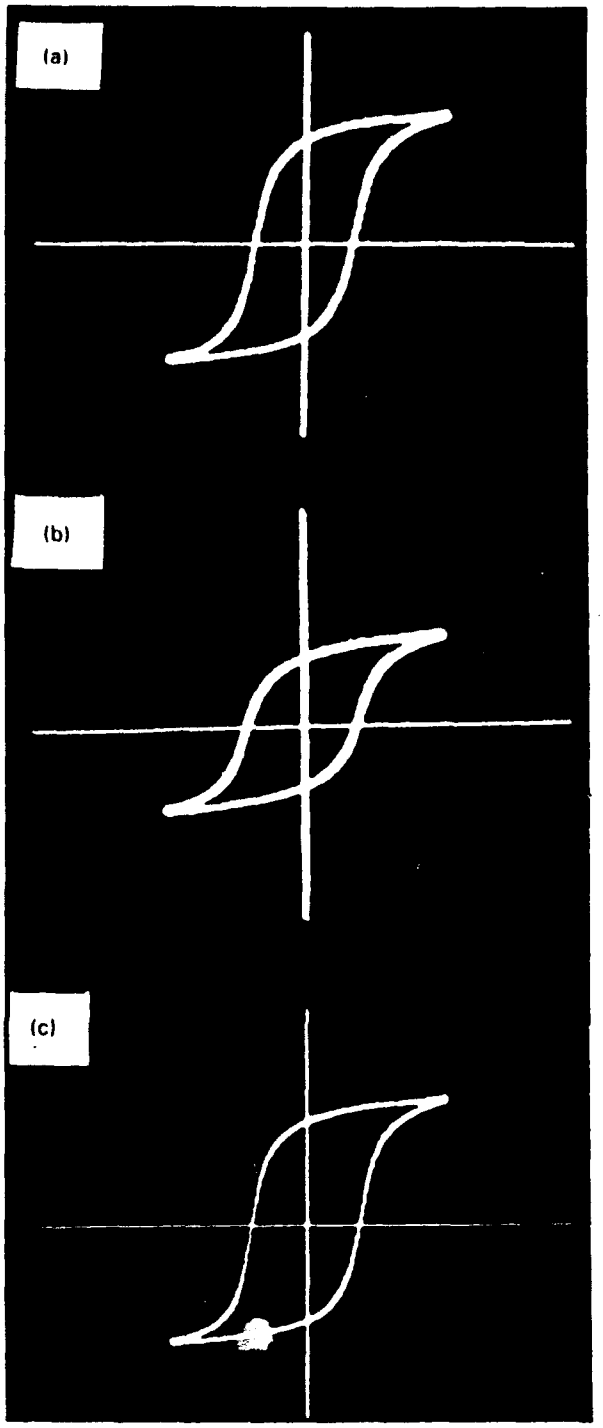

Figure 4 Hysteresis loop curves for a sintered PLZT 7/65/35 sample, recorded at (a) 10^3 cycles, (b) 10^7 cycles, and (c) heated at 300 °C for 2 h after the fatigue test.

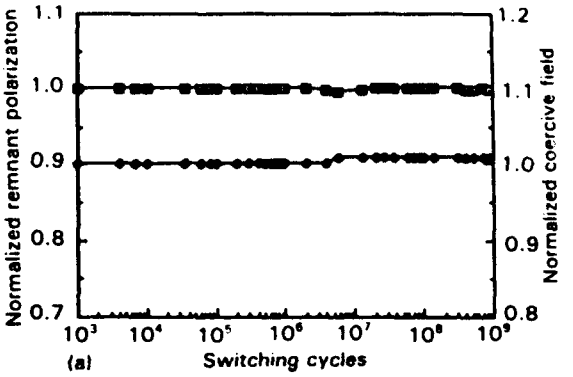

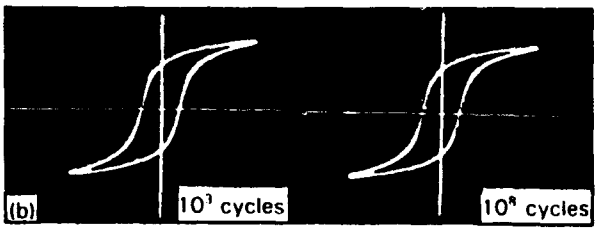

Figure 5 (a) The (▪) normalized polarization and (◆) coercive field as functions of the switching cycles, and (b) hysteresis loop curves for hot-pressed PLZT 7/65/35 ceramics.

results with the fatigue behaviour of the sintered samples, it is clear that the density (porosity) and ceramic-processing methods play an important role in determining the fatigue process. The improvement of fatigue behaviour in hot-pressed ceramics could be mainly due to the high density and the absence of defect pores, which will be discussed in detail in Section 4.

3.3. Fatigue in soft PZT ceramics

The remnant polarization and coercive field at a frequency of 1 Hz for commercial PZT 5 sintered samples with average grain size 3 μm are 36.5 $\mu C\,cm^2$ and 10 $kV\,cm^{-1}$, respectively, which fell into the reasonable ranges; the squareness of the hysteresis loops is excellent. The density is only about 92%. A large number of pores was found in the specimens as shown in Fig. 6a. Fatigue tests were conducted at frequencies of 1 and 100 Hz; similar fatigue behaviour was observed for the two frequencies. The results at 100 Hz

TABLE II The remnant polarization, P_r, and coercive field, E_c, for conventionally sintered PLZT 7/65/35 at the three frequencies

	1 Hz		10 Hz		100 Hz	
	$P_r(\mu C\,cm^{-2})$	$E_c(kV\,cm^{-1})$	$P_r(\mu C\,cm^{-2})$	$E_c(kV\,cm^{-1})$	$P_r(\mu C\,cm^{-2})$	$E_c(kV\,cm^{-1})$
Before fatigue test	26.0	6.2	26.9	6.5	22.4	4.7
After fatigue test	15.6	5.9	15.6	6.7	15.2	5.5
Heated at 300 °C for 2 h	24.5	6.4	24.8	6.5	22.4	5.3

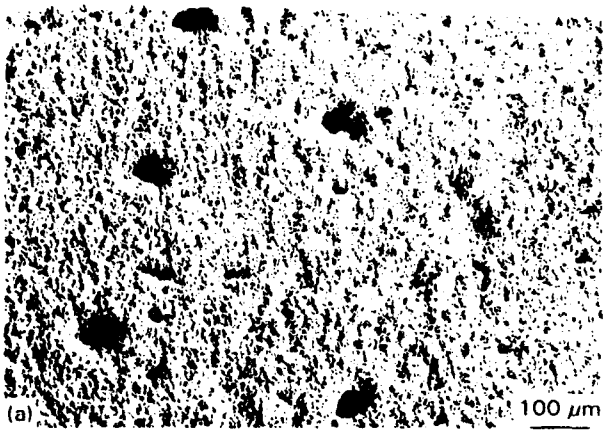

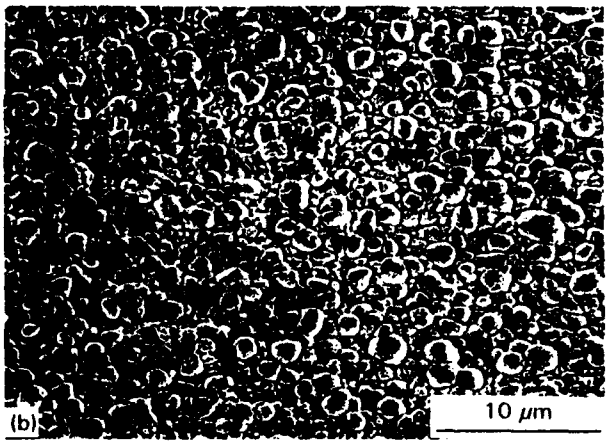

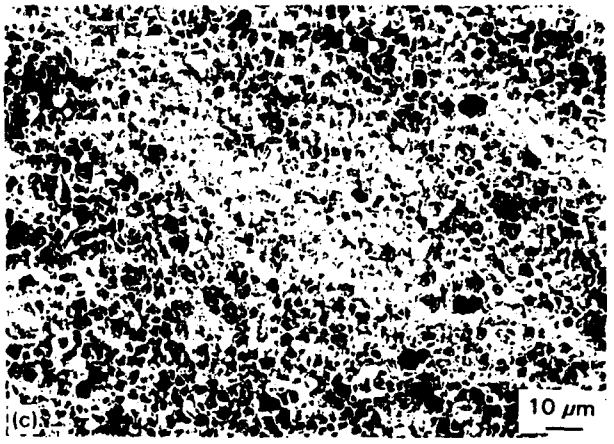

Figure 6 Microstructures of PZT ceramics observed by SEM. (a) Commercial soft PZT 5, (b) tape-cast soft PZT, and (c) commercial hard PZT.

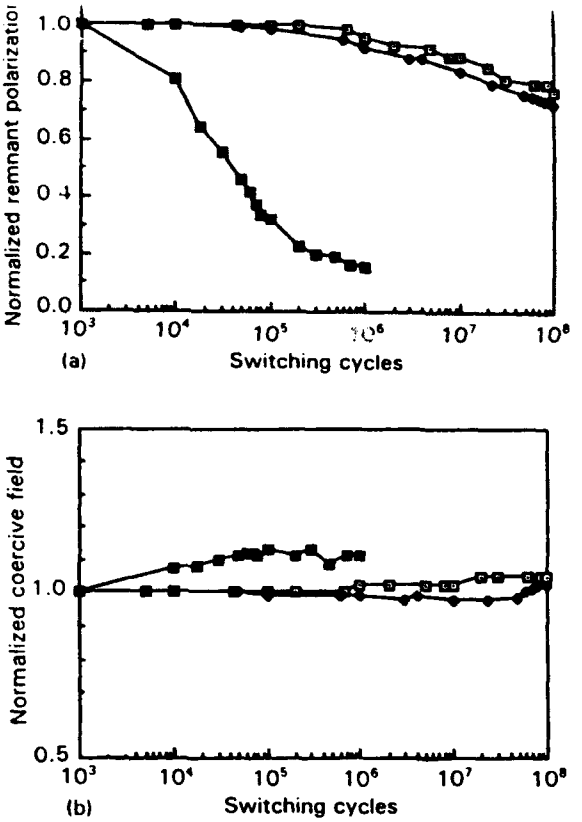

Figure 7 (a) Normalized polarizations and (b) coercive fields as functions of the switching cycles for (■) commercial soft PZT 5, (□) tape-cast soft PZT 5, and (◆) commercial hard PZT 8 ceramics.

are shown in Fig. 7, curve (a); the polarization decreased very quickly and dropped below 20% of the original value within 10^6 switching cycles, but the coercive field increased only slightly. Thermal treatment on the fatigued sample brought P_r back to 15 $\mu C\,cm^{-2}$ from 5.3 $\mu C\,cm^{-2}$ (the initial value was 33.1 $\mu C\,cm^{-2}$). The changes in the shapes of the hysteresis loops are shown in Fig. 8.

Fatigue tests were also conducted on soft PZT specimens made by tape-casting which had much fewer pores than those made by conventional sintering. Fig. 6b shows the microstructure observed under the SEM. The average grain size is about 1 μm, and the density is near 98%. Fatigue results shown in Fig. 7 indicate that the tape-cast sample fatigued much more slowly than the sintered samples; the fatigue rates of the polarizations are four to five orders smaller (Table I). Of the original remnant polarization, 66% was still switchable after 10^9 switching cycles, and the change of the coercive field was very small (Fig. 7). The hysteresis loops recorded during the fatigue process are shown in Fig. 9. After thermal treatment at 350 °C for 2 h the polarization and coercive field recovered almost completely.

3.4. Fatigue in hard PZT ceramics

Commercial PZT 8 samples which were conventionally sintered with a density near 97% have a coercive field twice the value of that in soft-PZT. The fatigue results are shown in Fig. 7. Like all other sintered PZT samples, hard PZT also fatigued under a.c. field switching. After 10^8 switching cycles, 73% of the original P_r was still switchable. The fatigue in hard PZT samples proceeded at a slower rate than that of the sintered soft PZT samples, close to the rate of the tape-cast soft PZT sample. $C(P_n)$ parameters of hard PZT 8 are listed in Table I. The E_c of hard PZT in Fig. 7 was stable without obvious change during the fatigue process. The ceramic microstructure is shown in Fig. 6c; the number of pores is less than that of the commercial soft PZT samples, but more than that of tape-cast soft PZT samples, and the average grain size for hard PZT

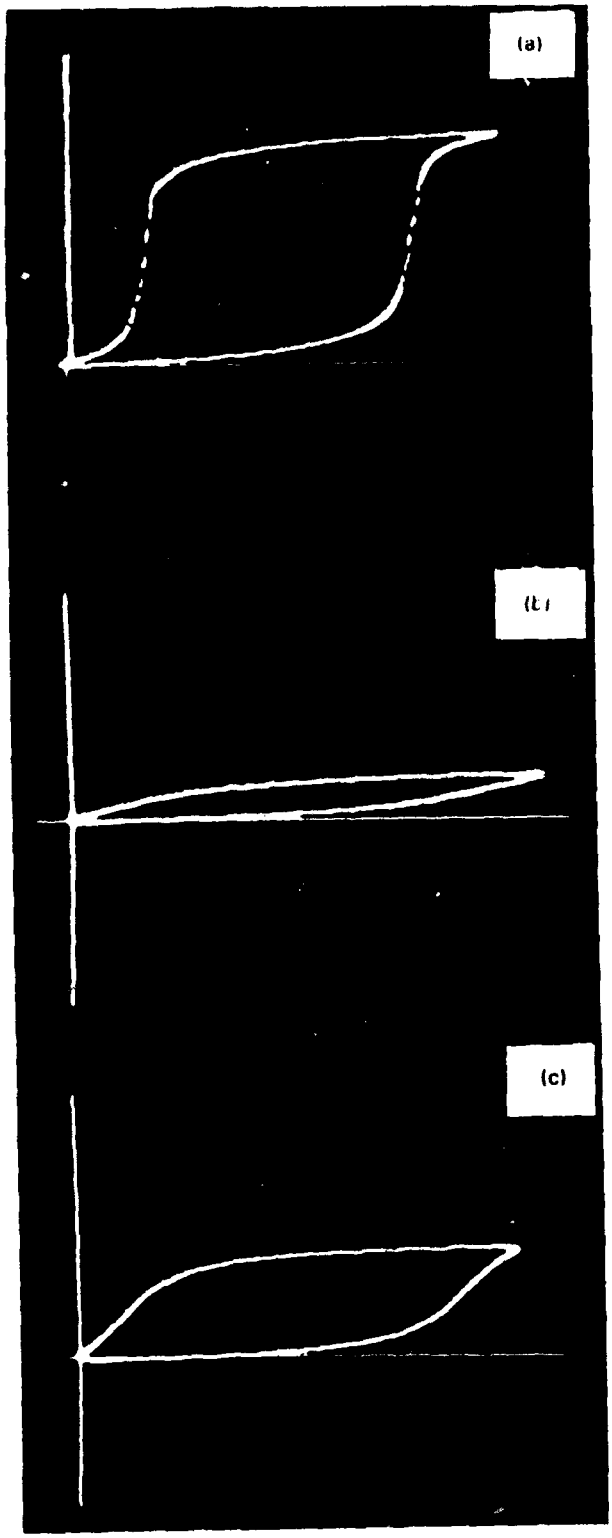

Figure 8 Hysteresis loop curves for commercial soft PZT 5 ceramic, recorded at (a) 10^3 cycles, (b) 10^6 cycles, and (c) heated at 350 °C for 1 h after the fatigue test.

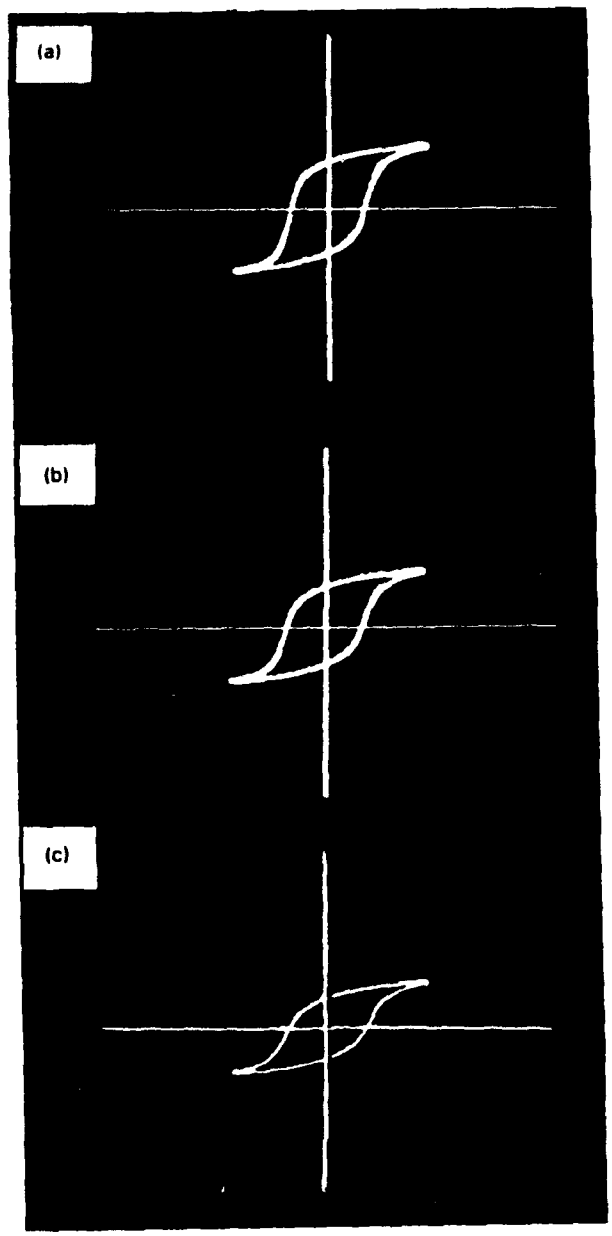

Figure 9 Hysteresis loop curves recorded during the fatigue process for tape-cast soft PZT ceramic, recorded at (a) 10^3 cycles, (b) 10^7 cycles, and (c) 10^9 cycles.

is 4 μm. The mechanism of fatigue in PZT ceramics will also be discussed in the following section.

4. Discussion

The fact that the hot-pressed 7/65/35 and 7/68/32 PLZT ceramics did not fatigue at least up to 10^9 switching cycles indicates that fatigue occurred in conventionally sintered PLZT and PZT low-density ceramics is not concerned with the intrinsic behaviour. One of the possible mechanisms of the fatigue in specimens with pores and low densities is domain pinning caused by space charge [11–13]. The direct evidence is that the fatigued properties in some of the samples can be recovered by heating the samples to a temperature higher than the dielectric maximum temperature (to the paraelectric phase). When the fatigued samples were heated to their paraelectric phase, both pinned and switchable domains disappeared due to the elimination of the spontaneous polarization. With the temperature cooled down, the paraelectric phase transferred to ferroelectric phase and domains were formed again without pinning. Thus the samples were restored from their fatigued states. In Table II, after experiencing 10^7 switching cycles, not more than 30% of the initial P_r and P_m (which is not shown in

Table II) could be switched, on heating at 500 °C for 2 h, P_r and P_m at 100 Hz completely recovered to the initial values, and for other frequencies, P_r and P_m recovered more than 95%. The most likely other possible mechanism of fatigue is microcracking [5, 6], but it is not possible to heal the cracks or microcracks at such low temperatures. Furthermore when acoustic emission tests were conducted on the recoverable samples during fatigue experiments, cracking signals were not detected.

Two questions must be addressed. Why does domain pinning happen in 7/65/35 PLZT and PZT ceramic samples with low density and pores, but not in high density 7/65/35 PLZT samples? Where does the space charge needed to pin domain come from? In the process of ceramic fabrication, when the temperature cools down, ferroelectric ceramics experience a phase transformation, from paraelectric to ferroelectric phase accompanied by the occurrence of the spontaneous polarization which forms domain structures to minimize electric energy, so that the macroscopic polarization is zero. On the surfaces the polarization is neutralized by the development of space charges, this is well proven by pyroelectric measurements. Pores inside the ceramics can produce a large area of internal free surface and the space charges must be accumulated on these internal surfaces to neutralize the spontaneous polarization. Therefore, the pores can be served as reservoirs of space charge. The grain boundaries are also polarization discontinuity regions and can trap charges. Under a high a.c. field the space charges can be pumped into the grains and grain boundaries, and react with domain walls and the defects in domains, and reorient domains into a more stable state, i.e. minimum energy configuration which can no longer be switched by the applied field, resulting in a decrease of polarization (fatigue). Campbell [14] studied the domain patterns of the fatigued $BaTiO_3$ single crystal; he found that the fresh crystals which were poled revealed a domain pattern which extended from one surface to another. In fatigued crystals, however, there was no correlation between the patterns of the two opposite surfaces. Many of the domains do not go through the crystal but end somewhere in the bulk. This indicates the presence of domain pinning by space charges in the crystal. Using the pinning model, the more pores and thicker grain boundaries that exist, the more easily fatigue occurs. This explains well the different fatigue rates listed in Table I for samples with different densities. The soft PZT obtained by tape casting and the hard PZT fatigued much less severely than other samples because they have fewer pores than the others; the commercial soft PZT is most porous, and fatigued most severely. In addition to trapped space charges, large pores and voids can also cause fatigue by local breakdown mechanism due to electric field concentration.

For some of the most severely fatigued PLZT 7/65/35 and commercial soft PZT samples, the fatigued properties cannot be recovered, even to half of their initial values, by heating and annealing in the paraelectric phases (Figs 2 and 8). In these samples, fatigue was not solely caused by the stabilization of pinned domains. Observation by optical microscopy and the naked eye showed that the surfaces of these samples changed in colour from yellowish to dark blue or pale white and that parts of the surface layer were peeled off from the electrode edges in 7/65/35 samples or the whole electroded surfaces expanded (loosen) in PZT samples, as shown in Fig. 10 in which the area inside the circles is the electroded area, i.e. fatigued area, and the area outside the circles is non-fatigued regions (the electrodes were removed by polishing the surfaces after fatigue tests). In Fig. 10a, damage occurred along the electrode edge (some silver paint which was used to stick the silver contact wire is left in the centre region). The fatigued properties cannot be restored in these samples because of the permanent damage of the surfaces. The surface deterioration could be the result of electrochemical reactions which change the colour of the samples [15]. The discharge in the pores near the surfaces can cause both discoloration and mechanical damage. The increase of

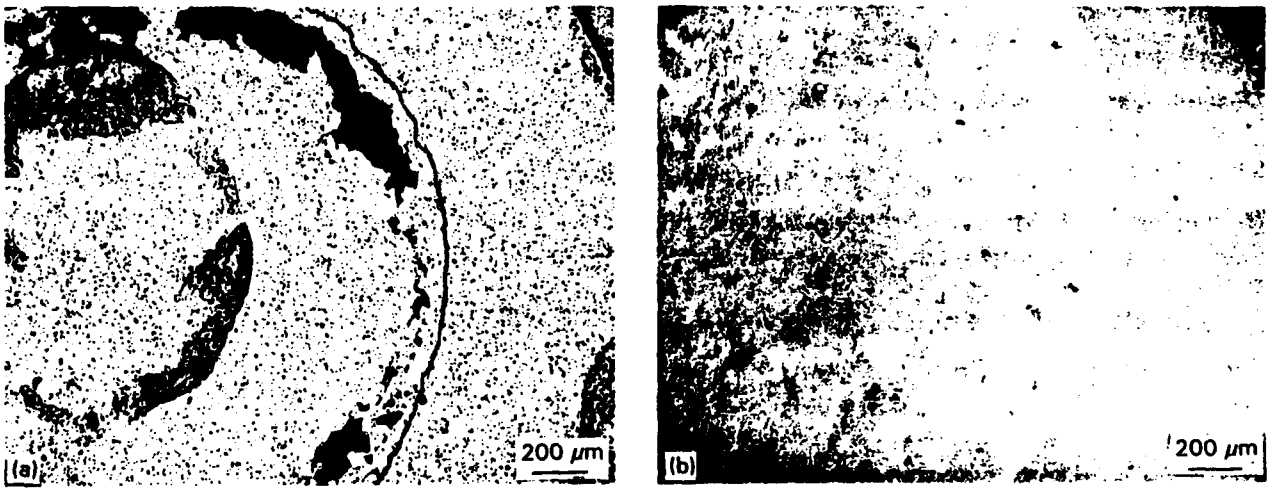

Figure 10 Damaged surfaces of the fatigued samples observed by the optical microscope after removal of the electrodes by polishing the surface. (a) Sintered PLZT 7/65/35, and (b) commercial soft PZT 5.

the applied field can enhance these effects, which is in good agreement with the experimental results. The applied field for the soft PZT sample was twice the field applied to PLZT 7/65/35 samples, and more severe damage was observed on the surfaces of the commercial soft PZT than on those of sintered PLZT 7/65/35.

5. Conclusion

Electric fatigue occurring under high a.c. field in conventionally sintered PLZT and PZT ceramics is mainly caused by low densities (92%–98%) and the existence of pores. The rate of fatigue depends on the porosity of the specimens. Fatigue proceeds faster in specimens with high porosity than in those with low porosity. Within 10^9 switching cycles, the fatigue rate could differ by two to four orders of magnitude. It is found that the hot-pressed PLZT 7/65/35 and 7/68/32 with high density (>99%) and average grain size 5 μm did not fatigue after 10^9 switching cycles. This is an encouraging finding for the application of PLZT and PZT ferroelectric and piezoelectric ceramics in actuators and memory devices. Two mechanisms for fatigue occurring in low-density PLZT and PZT ceramics are proposed: the gradual domain stabilization (pinning) by space charges and the surface deterioration caused by the large a.c. field.

Acknowledgement

The support of the Office of Naval Research for this investigation is greatly appreciated.

Received 5 January
and accepted 3 February 1993

References

1. M McQUARRIE, *J. Appl. Phys.* **24** (1953) 1334.
2. W. J. MERZ and J. R ANDERSON, *Bell Lab. Record* **33** (1955) 335.
3. J. R. ANDERSON, G. W BRADY, W. J. MERZ and J. P. REMEIKA, *J. Appl. Phys.* **26** (1955) 1387.
4. G. W TAYLOR, *ibid.* **38** (1967) 4697.
5. Q. Y. JIANG, PhD thesis, Pennsylvania State University (1992).
6. Q. Y. JIANG, WENWU CAO and L. E. CROSS, *J. Am. Ceram. Soc.*, in press.
7. E. FURMAN, PhD thesis, Pennsylvania State University (1987).
8. R. WASER, TUDOR BAIATU and KARL-HEINZ HARDTL, *J. Am. Ceram. Soc.* **73** (1990) 1645.
9. M. P. HARMER, Y. H. HU, M. LAL and D. M. SMYTH, *Ferroelectrics* **49** (1983) 71.
10. J. M. HERBERT, "Ceramic Dielectrics and Capacitors" (Gordon and Breach, New York, 1985) p. 58.
11. E. FATUZZIO and W. J. MERZ, "Ferroelectricity" (North-Holland, New York, 1967) pp. 102, 104.
12. R. WILLIAMS, *J. Phys. Chem. Solids* **26** (1965) 399.
13. A. YU. KUDZIN and T. V. PANCHENKO, *Sov. Phys. Solid State* **14** (1972) 1599.
14. D. S. CAMPBELL, *Philos. Mag.* **79** (1962) 1157.
15. K. LEHOVEC and G. A. SHIRN, *J. Appl. Phys.* **33** (1962) 2036.

APPENDIX 18

EFFECTS OF ELECTRODES AND ELECTRODING METHODS ON FATIGUE BEHAVIOR IN FERROELECTRIC MATERIALS

QIYUE JIANG, E. C. SUBBARAO, AND L. E. CROSS
Materials Research Laboratory, The Pennsylvania State University
University Park, PA. 16802

Abstract Electric fatigue behavior, measured by the change in remnant polarization with the switching cycles under high AC field, in ferroelectrics (PLZT ceramics and TGS crystal) has been found to be related to electrode materials and electroding methods. Sputtering gold and rubbed In-Ga were superior to many commonly used electrodes, such as air-dry and co-fire silver pastes. Sputtering is better than evaporating to give a good sample-electrode contact, which has been found to be the key factor in achieving the intrinsic fatigue rate of the material.

INTRODUCTION

Many fatigue studies on ferroelectric ceramics (e.g. PLZT [1-3], $Pb(Zr, Sn, Ti)O_3$ [4] and single crystals (e.g. $Bi_4Ti_3O_{12}$ [5]) employing a variety of electrode materials (Au, Cr-Au, Sn O_2-Au, In, In-Ga, Al, Ag, Au-Mg, Pb, Sn-Ag, SnO_2-In, etc.) produced a set of conflicting results, which remain unexplained. In the present work, hot pressed PLZT 7/65/35 and 7/68/32 ceramics and TGS crystal were electroded with a variety of materials by several techniques to elucidate the factors affecting the electric fatigue behavior.

RESULTS AND DISCUSSION

A. Electroding Method

Hot pressed PLZT 7/65/35 samples with 5 μm grain size were electroded with gold by vacuum evaporation and sputtering. Fatigue tests showed no decrease of remnant

polarization, P_r, even after 10^8 switching cycles in the case of sputtering gold electrode and a decrease of P_r by 20% in 10^7 cycles for evaporated gold electrode (Figure 1). In the case of evaporated gold the contact is purely physical and weak, so that under high AC field, it could degrade and debond. On the other hand, sputtering involves ion bombardment and high temperature both of which help to clean the sample surface (itself a desirable feature) and the bombardment results in an intimate contact.

Interestingly, the same sputtered gold electrode, which is good in the case of PLZT ceramic, when applied to TGS crystal results in severe fatigue, though air dry silver electrode was excellent for TGS crystal (Figure 2(a)). The specimen with sputtered gold electrode showed a decrease of P_r by 57% and an increase of E_c by 50% after it is fatigue tested for 10^8 switching cycles (Figure 2(b)).Sputtering caused decomposition of the organic crystal (TGS), which is unstable above 80 °C. The damage caused by ion

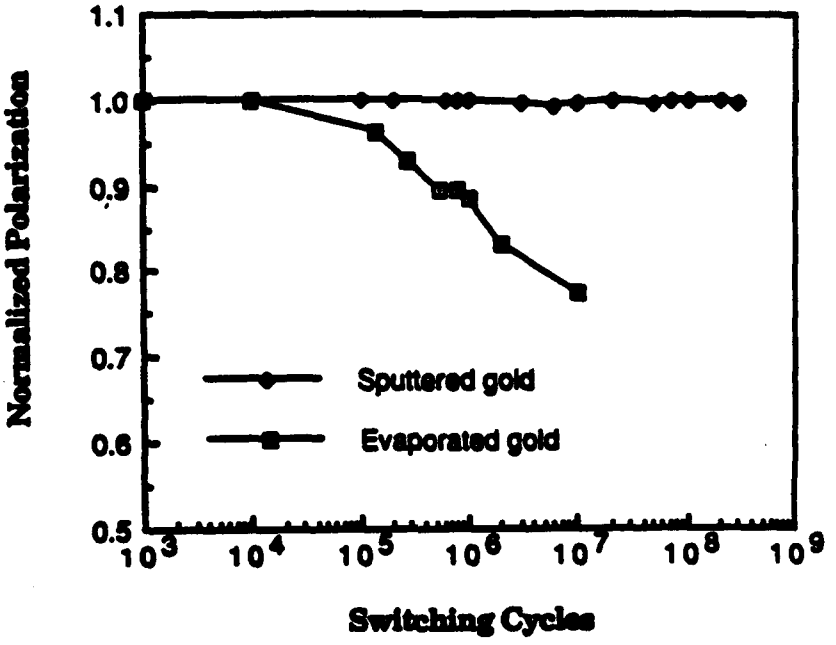

Figure 1 The normalized remnant polarization as a function of the switching cycles for hot pressed PLZT 7/65/35 ceramics with (a) sputtered gold electrode and (b)evaporated gold electrode.

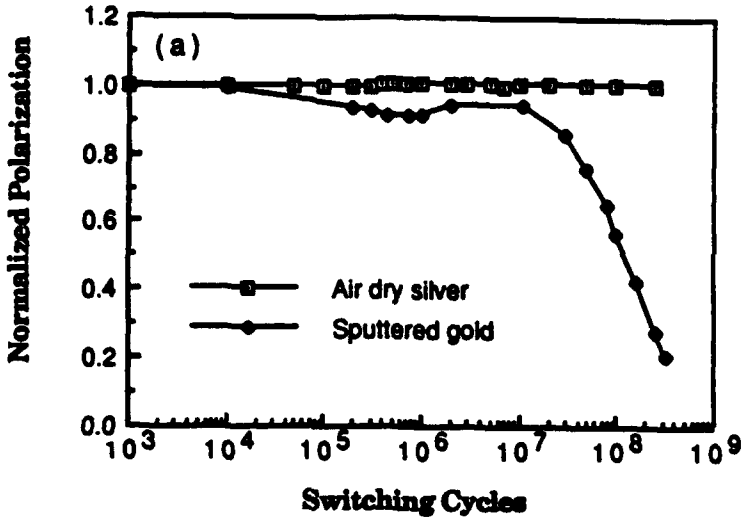

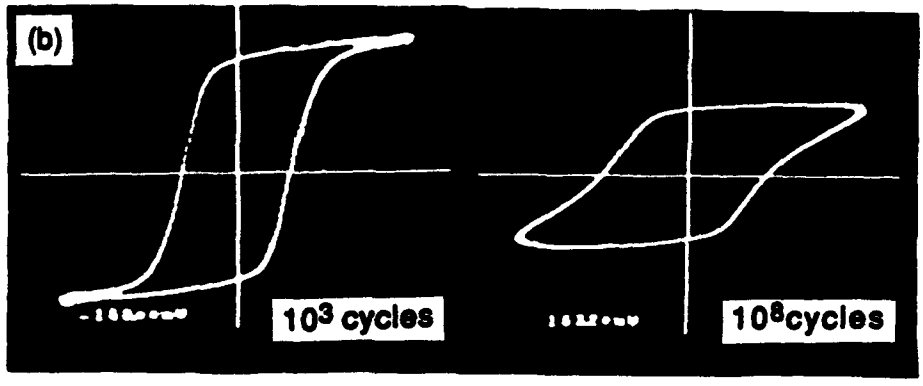

Figure 2 (a) The normalized remnant polarization as a function of the switching cycles for TGS crystals with different electrodes. (b) Hysteresis loops of TGS crystal with sputtered gold electrode.

bombardment and temperature rise is accentuated by AC field switching, resulting in the transparent crystal turning black during the fatigue test (the darkening increasing with switching cycles). On the other hand, air dry silver has an organic liquid as a carrier, which helps to make an excellent contact with an organic crystal such as TGS but not with inorganic ceramics.

B. Electrode Materials

Evaporated Indium was found to be comparable to evaporated gold electrode but not as good as sputtered gold. However, when In or In-Ga mixture was rubbed over the evaporated electrode, contact improved and no fatigue was detected up to 10^9 cycles. Co-fire silver paste, one of the most common electrodes, gave poor results (compared to sputtered gold) (Figure 3), which was traced to a darkening of the ceramic-electrode interface, caused possibly due to the discharge resulting from the high voltage drop across the poor contact. The importance of the quality of contact is further illustrated by the increase in P_r accompanied by decrease in E_c between 10^6 and 10^8 cycles in the case of a hot pressed PLZT 7/68/32 (grain size 5 μm) with rubbed In-Ga electrode (Figure 4). This unusual behavior is attributed to better contact caused by improved diffusion of the low melting (In, 156 °C; Ga, 30 °C) electrode materials, promoted by self heating of the sample subjected to high AC field switching.

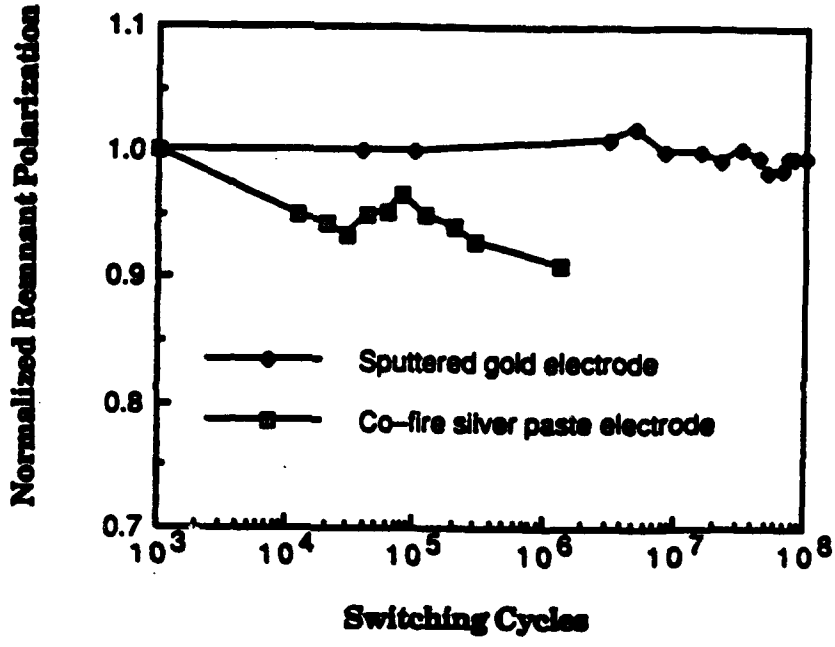

Figure 3. The normalized remnant polarization as a function of the switching cycle for hot pressed PLZT 7/68/32 ceramics with different electrodes.

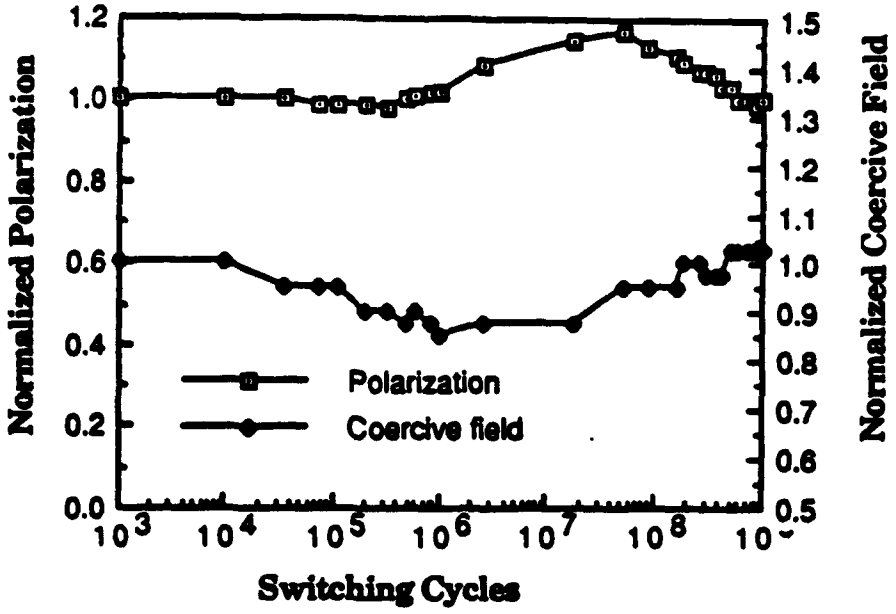

Figure 4. The normalized remnant polarization and coercive field as a function of the switching cycles for hot pressed PLZT 7/68/32 ceramics with In-Ga electrode.

CONCLUSIONS

(1) The adherence of electrode to the ceramics is the key factor. Thus, sputtering gold and In-Ga electrodes are better than many commonly used materials, such as air dry or co-fire silver pastes.

(2) Sputtering results in a stronger contact than the evaporation method, and hence is preferable for ceramics used under high AC field for long periods of time. However, ion bombardment and high temperature rise of the substrate involved in the sputtering process can lead to decomposition of an organic crystal such as TGS.

(3) Appropriate electrode materials applied by a suitable technique can enable the electric fatigue rates to approach the intrinsic rates of the ferroelectric material.

Acknowledgements–The authors are grateful to the Office of Naval Research for financial support.

REFERENCES

1. W. C. Stewart and L. S. Cosentino, Ferroelectrics 1, 149 (1970).
2. W. R. Salanek, ibid, 4, 97 (1972).
3. D. B. Fraser and J. R. Maldonado, J. Appl. Phys. 41, 2172 (1970).
4. G. W. Taylor, ibid, 38, 4697 (1968).
5. C. E. Palvari and J. R. Srour, IEEE Trans. on Electron Devices, ED-16, 532 (1969).

APPENDIX 19

FATIGUE IN PLZT: ACOUSTIC EMISSION AS A DISCRIMINATOR BETWEEN MICROCRACKING AND DOMAIN SWITCHING

Q. Y. JIANG, E. C. SUBBARAO, AND L. E. CROSS
Materials Research Laboratory , The Pennsylvania State University
University Park, PA. 16802

Abstract Acoustic emission study of electric fatigue in hot pressed PLZT ceramics during DC field poling and AC field switching shows that the count rate for domain switching is nearly two order of magnitude smaller than that for microcracking. The amplifier gain setting can be used to discriminate the two processes.

INTRODUCTION

The application of DC field during poling or an AC field in electromechanical applications results in domain reorientations or microcracks in a ferroelectric material, such as PLZT ceramics. A nondestructive method to distinguish between the two processes and to signal the onset of microcracking, which causes a permanent deterioration of the electrical properties, will be valuable. The mechanical deformations accompanying those two processes give rise to acoustic emissions (AE). The AE techniques were exploited for this purpose, as part of a comprehensive study of electric fatigue of hot pressed PLZT ceramics[1]. The parameters studied here are effects of grain size, magnitude and frequency of AC field, DC poling, instrumental parameters (amplifier gain and threshold).

EXPERIMENT

Hot pressed PLZT (La/Zr/Ti = 7/68/32) of 5 μm grain size in all cases was used, except for one sample of 18 μm grains to study grain size effect. The experiment setup employed for acoustic emission study of electric fatigue is shown in Figure 1. The acoustic emission count rate is plotted as a function of time for various experimental conditions and instrument settings.

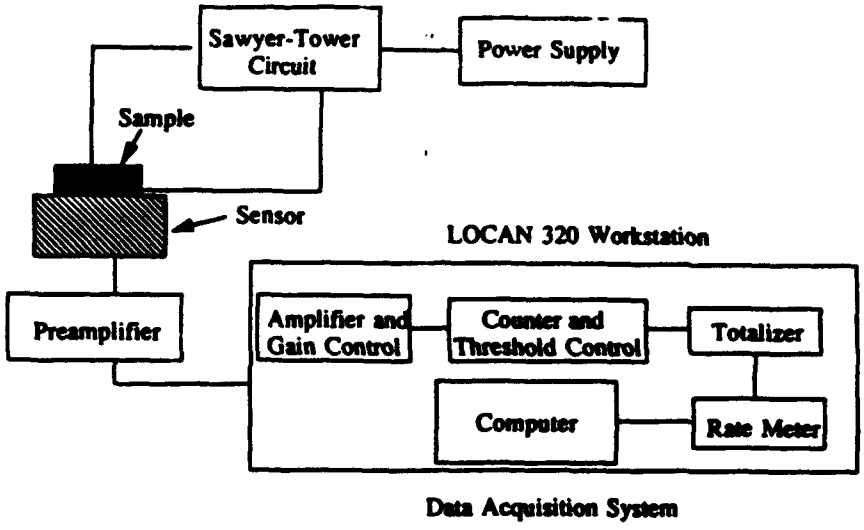

Figure 1 Experimental set-up for acoustic emission study of electric fatigue.

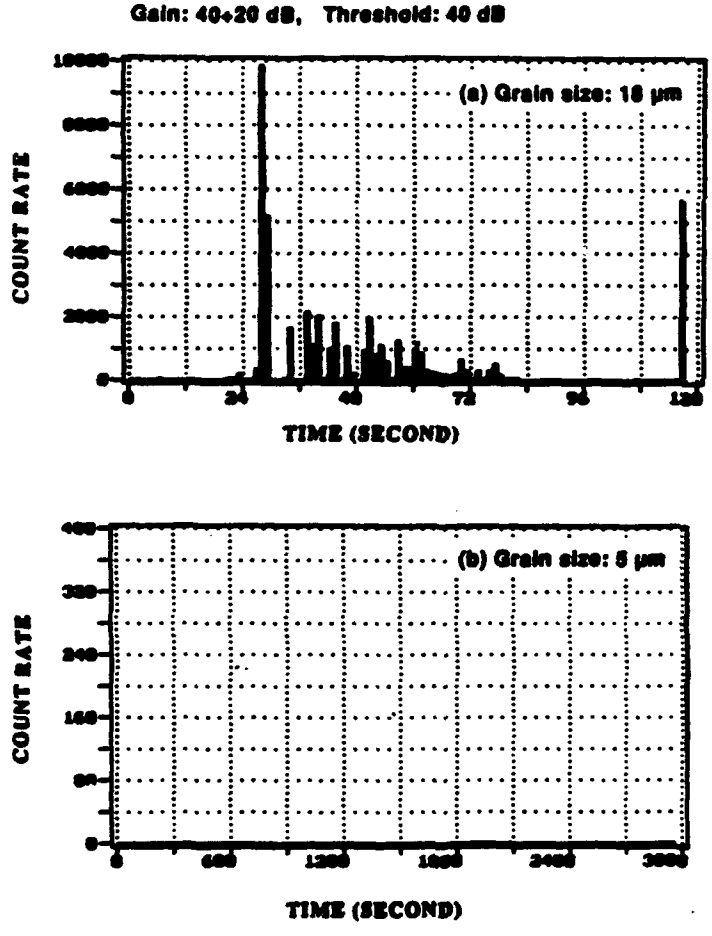

Figure 2 Effect of grain size on acoustic emission from a hot pressed PLZT 7/68/32 ceramic sample under high AC field.

RESULTS AND DISCUSSION

(1) Grain Size: The results for 5 μm and 18 μm grain size hot pressed PLZT ceramics (Figure 2) show absence of any AE activity in the fine grain material whereas a large AE count rate (~10^4) in the 18 μm material is detected under high AC field, signifying the occurrence of microracking due to large deformations in the large grain sample.

(2) Magnitude of AC Field: A significant increase in the AE count rate was detected when the AC field was increased from 35 to 55 v/cm in a prepoled sample (Figure 3) and was attributed to more extensive domain flipping.

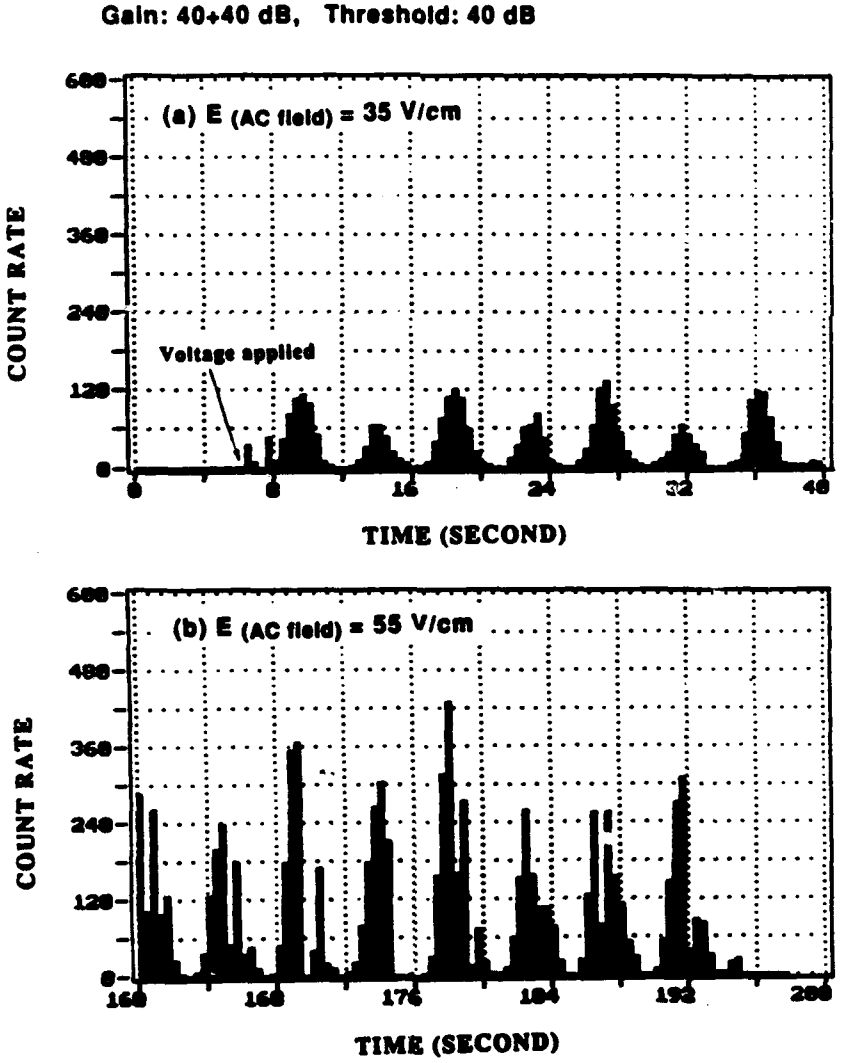

Figure 3 Acoustic emission from a prepoled PLZT 7/68/32 ceramics with 5 μm grain size under small (35 and 55 v/cm) AC signal at 0.1 Hz.

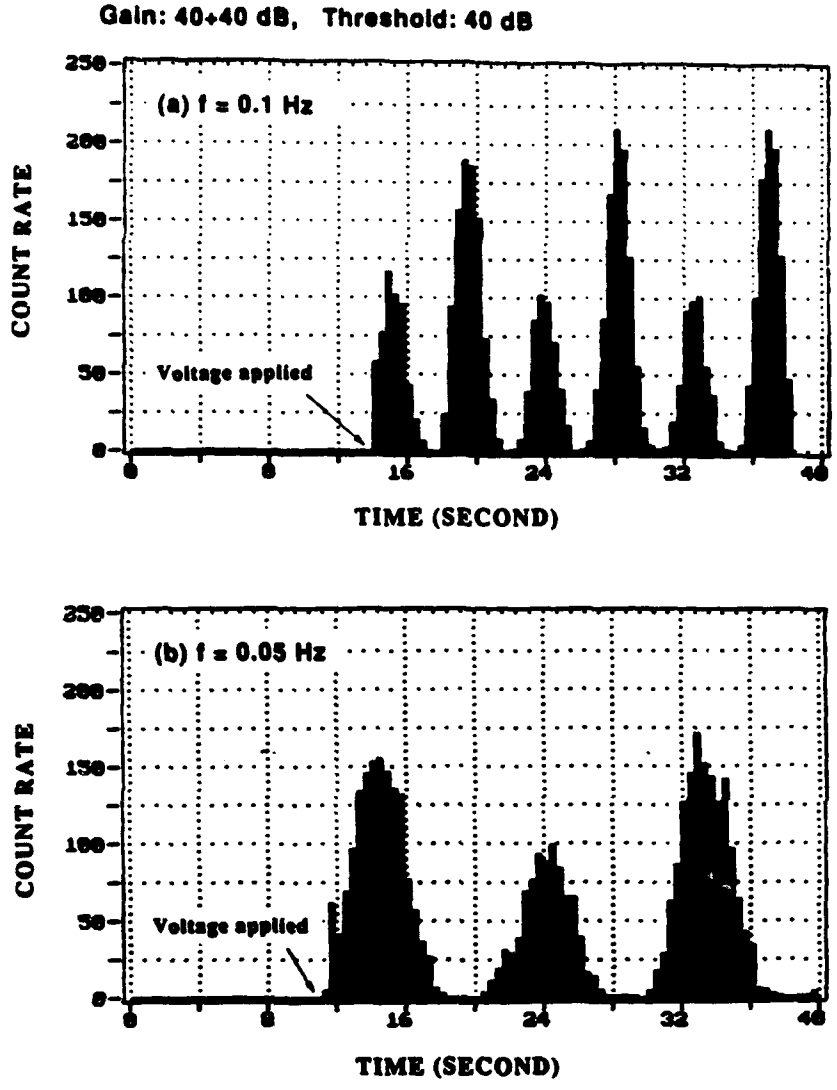

Figure 4 Acoustic emission from a prepoled PLZT 7/68/32 ceramics with 5 μm grain size under small AC signal at two frequencies.

(3) Frequency of AC Field: When the frequency of AC field was increased from 0.05 to 0.1 Hz, the maximum count rate remained nearly same, but the total count per cycle decreased(Figure 4). The count rate is periodic, same as the frequency of the AC field.

(4) Amplifier Gain: Acoustic emission signals due to domain reorientations, which could not be detected at an amplifier gain of 60 dB, could be clearly observed at a gain of 75 dB (Figure 5). On the other hand, AE signals arising from microcracking can be detected even with an amplifier gain of 60 dB.

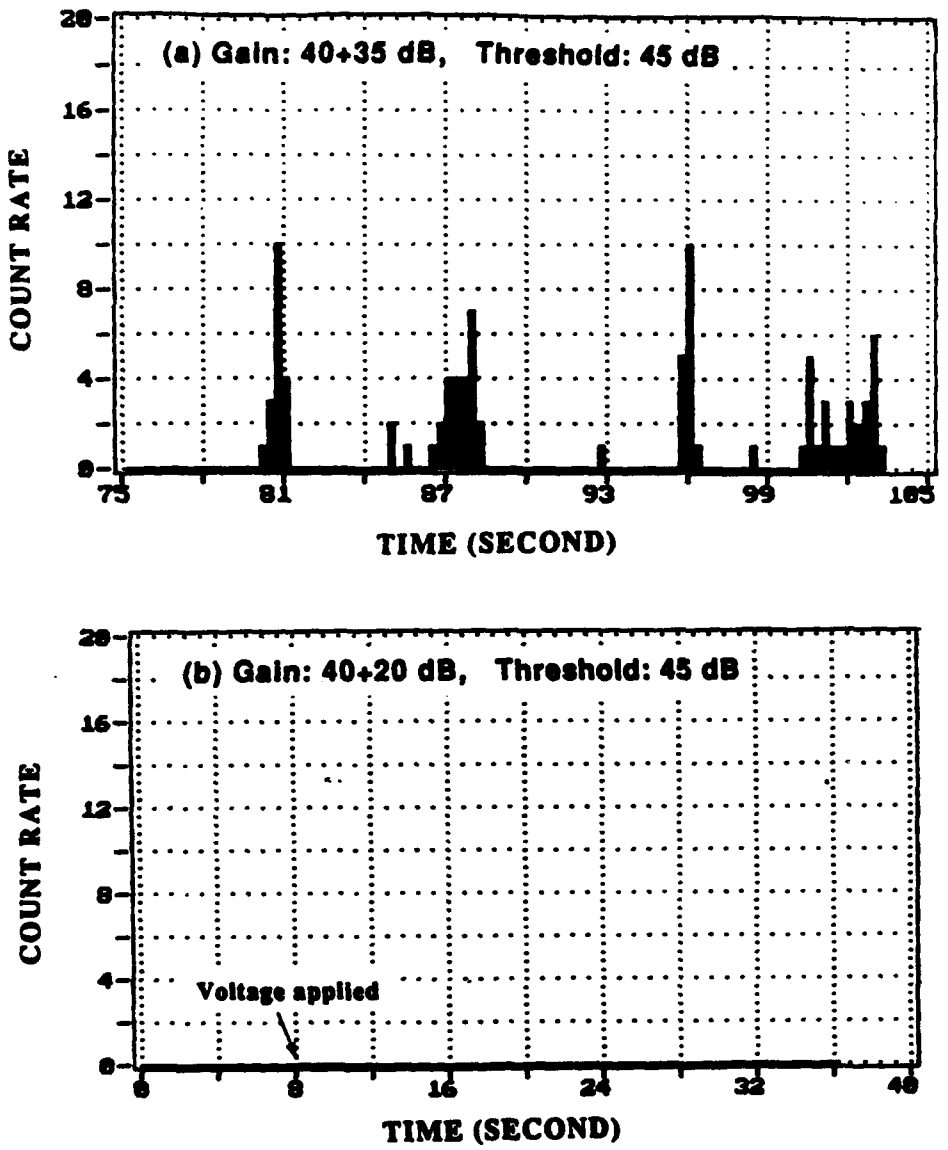

Figure 5 Effect of amplifier gain setting on the acoustic emission count rate detected in PLZT 7/68/32 ceramics with small grain size under high AC field at 0.07 Hz.

(5) DC Poling: Intense AE activity due to domain reorientations was detected as soon as the poling field was applied and persisted for 7-8 seconds till all the domains which were in a favorable position to undergo reorientation became oriented in the field direction[2] (Figure 6). The discontinuous nature of the domain switches during poling may be contrasted with the essentially continuous, periodic variation of count rate when the frequency or magnitude of the AC field was varied.

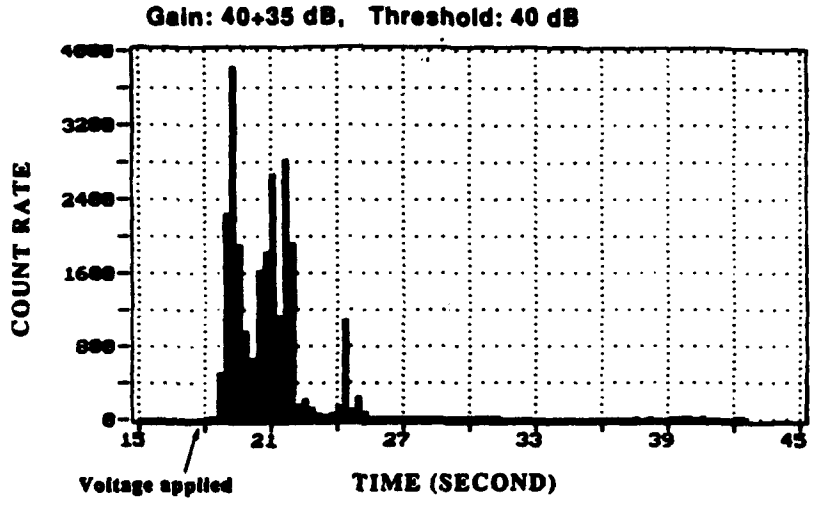

Figure 6 Acoustic emission detected as a function of time from a PLZT 7/68/32 ceramics during DC poling (15 kv/cm) process.

CONCLUSIONS

(1) AE signals generated during domain switching can only be detected by a high amplifier gain setting (70 -100 dB) and their intensity, which is a function of the applied AC or DC field, is about two order of magnitude smaller than the AE counts produced by microcracking during electric fatigue.

(2) PLZT (7/68/32) ceramics with grain size larger than 10 μm fatigued after 10^4 switching cycles, generating AE signals due to microcracking. In samples with 5 μm grain size, electric fatigue did not occur even after 10^8 switching cycles, and AE signals were not detected.

(3) AE technique can be fruitfully employed as a nondestructive tool in the development of reliable electromechanical transducers, actuators and non-volatile memory devices.

Acknowledgements: The authors are grateful to the Office of Naval Research for financial support.

REFERENCES

1. Q. Y. Jiang, Ph.D. thesis, Pennsylvania State University, (1992).
2. E. C. Subbarao, V. Srikanth, W. Cao and L. E. Cross, Ferroelectrics, (submitted).

APPENDIX 20

FIELD INDUCED STRESS CONCENTRATIONS AND ELECTRIC FATIGUE IN FERROELECTRIC CERAMICS

Q. Y. Jiang, E. C. Subbarao, Member IEEE and L. E. Cross*, Fellow IEEE

ABSTRACT

Experimental study of permanent degradation of electrical properties (polarization and coercive field) of ferroelectric ceramics subjected to AC field revealed that microcracks responsible for this electric fatigue get initiated inside the electrode edge near the high voltage terminal side and form a circular ring which moves towards the center with continued switching cycles. The microcracks arise due to incompatible intergranular stresses created by the large strains generated by the AC field in these materials which possess large anisotropic piezoelectric and electrostrictive coefficients. A finite element analysis of this case was carried out in three directions (r, ϕ, and z) which established the maximum tensile stress to exist on the top surface inside the electrode edge and propagate in the ϕ direction. The pattern of distribution of tensile stress thus fully confirms proposed mechanism for the initiation and growth of microcracks responsible for electric fatigue of ferroelectric ceramics.

* The authors are with the Materials Research Laboratory, The Pennsylvania State University, University Park, PA 16802.

I. INTRODUCTION

Some of the more demanding applications of ferroelectric ceramics include piezoelectric and electrostrictive actuators and non-volatile memory devices. For example, ceramic actuators have excellent ability to control precise positioning (± 0.01 μm), are small in size and simple in configuration. Their general characteristics include [1] a large range of displacements (10^{-2} to tens of micron), high response speed (~10 μs), high generative force (~400 kg/cm^2) and smaller (by an order of magnitude) driving power compared to electromagnetic motors. A number of practical devices, such as active structure acoustic control [2], deformable mirrors [3,4], cutting error correction[5], impact dot-matrix printers [1], and ultrasonic motors [6,7], are under development based on these materials. The ferroelectric memory devices are based on the bistable polarization characteristic of these materials. The memory is non-volatile and does not require a hold voltage. Information can be recorded by reversing or reorienting the polarization by an electric field greater than the coercive field (E > Ec) and can be erased by returning the polarization to the initial state by an applied field of opposite polarity. The information can be read electrically by using a ferroelectric field effect device or optically by means of the photorefractive effect. The large coupling between optical and electrical properties allows efficient non-destructive read-out of the stored information.

These various devices involve high strain or large polarization and can become practical realities only when they can perform reliably for 10^5 to 10^{11} cycles in the case of actuators and for more than 10^{12} switching cycles for memory devices. In this case, one is concerned with fatigue which refers to degradation of the properties of materials or the performance of devices with time under applied cyclic (electrical or mechanical) forces and not so much with aging which covers degradation when no external forces are involved. The reliability of materials is affected by such intrinsic factors as domain wall pinning, micro and macrodefects, anisotropy, limit of dynamic mechanical strength etc., as well as extrinsic factors of electrical origin such as electrode-ceramic interface degradation, electric field concentration near electrode edge, large amplitude of AC field or of mechanical or compositional origin like induced internal stress through phase transformation, stress concentration due to inhomogeneities in the component, applied external stresses, heat and load effects etc.. While aging studies on ferroelectric capacitors [8-10] and piezoelectric transducers [11] have been carried out, which established the importance of domain wall pinning to stabilize domain structures, no serious examination of electric fatigue under cyclic high AC field has been reported.

Three types of devices operate under high AC field: (1) electrostrictive actuators, (2) piezoelectric high power transducers and (3) ferroelectric memory devices. While cyclic

reorientation of spontaneous or induced polarization takes place at the frequency of the applied AC field in the case of electrostrictive actuators and ferroelectric memory devices, the relationship between stress and strain, electric field and electric displacement, and strain and electric field is linear only for limited range of input stress or electric field in high power piezoelectric transducers. The linear regime varies widely for different piezoelectric ceramics, being roughly related to the coercive field. At large input electric field, the relationship becomes non-linear. Non-linearity of the strain-field relationship produces distortion of the mechanical output; non-linearity of the electric displacement-field relation causes increase in dielectric loss, which may generate heat leading to depolarization [12]. In low field applications of a transducer, the reliability is mainly limited by electric field because of depoling either by direct field or generated heat. In the high frequency applications, eg. impact printer head, transducer is usually working near the resonant frequency and the dynamic mechanical strength becomes the limiting factor.

The reliability of the electrostrictive actuators is severely affected by the dynamic strength because the large strain generated can be larger than the general limit of the fracture strain (10^{-3}) for structural ceramics. The reliability of the ferroelectric memory devices is most difficult to control among the three types. It is complicated by the cyclic reorientation of large spontaneous polarization and domain switching. The dynamic strength is the dominant limiting factor, while domain pinning and continuous defect entrapment for some materials such as ferroelectric thin films can make a major contribution to the gradual failure of the devices.

In the light of the above, a comprehensive study of electric fatigue in hot pressed lanthanum doped lead zirconate titanate (PLZT) ceramics was undertaken [13] to elucidate the intrinsic (eg. pores [14], grain size [15], composition and temperature [16]) and extrinsic (eg. surface contamination [17], electrodes and electroding methods [18]) factors responsible for this behavior. The underlying mechanism consists of domain wall pinning due to a variety of micro and macro defects or intergranular microcracking due to inhomogeneous stresses set up under high AC fields. Microscopic examination revealed the cracks to be initiated near the high voltage side and extend nearly parallel to the electrode in a zagged fashion and not so much in the field direction, to cause mechanical failure or electrical breakdown. While the microscopic and electrical data support the proposed mechanism for electric fatigue, it would be worthwhile to estimate the pattern of stress distribution, including regions of stress concentration, in these materials when they are subjected to large AC fields. This is carried out in the present paper using finite element analysis and the results are compared with experimental observations.

II. EXPERIMENTAL

Various compositions of lanthanum doped lead zirconate titanate (PLZT) ferroelectric ceramics, which are excellent candidates for electromechanical actuators and non-volatile memories, were prepared by hot pressing. The surfaces were thoroughly cleaned and electroded by sputtering gold. From the P-E hysteresis loops, remanant polarization (P_r) and coercive field (E_c) were estimated and plotted as a function of time (switching cycles). The fatigued samples were examined by a scanning electron microscope but observation under an optical microscope with transmitted light through the transparent ceramics was more informative.

Stress distribution in a ferroelectric PLZT ceramics subjected to a large AC field was analyzed, using finite element analysis methods, to locate regions of stress concentration, initiating microcracks and the pattern of stress variation, to deduce the geometry of microcrack growth.

III. RESULTS AND DISCUSSION

A. Microcracking

Application of an AC field to PLZT ceramics resulted in electric fatigue, displayed as a decrease of the polarization and increase of the coercive field. Typical results for a range of x/65/35 compositions are shown in Fig. 1. The electric fatigue arises from the pinning of domain walls by space charge or injected carriers, or from microcracking. The former is due to smaller strains and is recoverable by thermal and electrical treatment. The latter arises from large incompatible stresses between grains and is a permanent damage. The optical micrographs of fatigued PLZT (8/65/35) ceramics under transmitted light are shown in Fig. 2. The sample was partially electroded and the circular region in the center shows the switched region (Fig. 2(a)), with the unswitched, unelectroded region outside the circle. The opaque ring in Fig. 2(a) is due to microcracking which starts from the electrode edges near the surface and propagates in a zagged fashion towards the other surface, as shown more clearly in Fig. 2(b), (c) and (d) which were obtained by focussing the microscope near the bottom face, at middle level and near the top surface, respectively.

In order to obtain the details of the miocrocracking process, a sample of PLZT 8.4/65/35 which exhibits most severe fatigue was chosen. The scanning electron micrographs of this sample (Fig. 3) shows that the regions which became opaque due to microcracking were parallel to the surface and close to the high voltage terminal face and extended only half way through the thickness after 10^6 switching cycles. To confirm that the electrode edge is a region of stress concentration during an electric fatigue experiment, two samples of PLZT 8.4/65/35 were electroded, one only in the center as a circle and the other to the edges of the sample (Fig. 4(a)) using identical conditions. The fatigue results of these samples clearly show that fatigue in partially electroded sample starts by 10^3 switching cycles, much earlier than the fully electroded samples

(10^5 cycles) (Fig. 4(b)). In partially electroded sample, the edges were constrained by the unelectroded ceramic body, and the stress concentrations were highly enhanced around the edges. The results clearly show that the initiation of microcracking and the growth of microcracks are closely related to the discontinuity of the electric field, which inevitably results in the inhomogeneous deformation of ceramics.

The stress concentrating effect of cracks is fundamental to fracture mechanics [19]. Fatigue phenomena in the present study is primarily caused by mechanical failure i.e. microcracking (fracture) which is controlled by stress concentrations. The factors either intrinsic or extrinsic which can generate stress concentration under high AC field have been shown to contribute to fatigue. The fact that electric fatigue due to microcracking always started from the electrode edges suggests that the stress concentrations in field discontinuity regions control initiation and growth of cracks. Therefore, it is necessary to know the magnitude and distribution of the stresses induced by AC electric field.

B. Finite Element Analysis

Finite element analysis (FEA), which is a very useful tool to solve the complex mechanical stress problems [20], was used to calculate the stress distribution in the present study. In this method, the sample is divided into small discrete elements, the so-called finite elements. The mechanical displacements and stress as well as electrical potential and charge can be determined at the joints of these elements. The values of these mechanical and electrical quantities at an arbitrary position on the element are given by a linear combination of polynomial interpolation functions with the values of these quantities at the joints as coefficients.

The diameters of the disc and the electroded circle area of a disc sample (PLZT 8/65/35) which was chosen for FEA calculation, are 5 mm and 3 mm, respectively, and the thickness of the sample is 0.5 mm, as illustrated in Fig. 5. Due to the symmetric distribution of the stress along thickness direction (z axis), it is only needed to consider half body of the sample divided along z axis. The half body then was divided into 5 layers along z axis, and each layer was further divided into 20 elements; together there were 100 ring elements with quadrilateral cross sections, as well as 126 joints as shown in Fig. 6. The stress and displacement are generated by electromechanical coupling effect, mainly piezoelectric effect. Therefore, the necessary parameters for FEA calculation of PLZT 8/65/35 were: applied electric field = 15 kv/cm, piezoelectric coefficients d_{33} = 682 and $d_{31} = d_{32}$ = -320 pC/N, density = 7.8×10^3 kg/m^3, elastic constant = 8.0×10^{10} N/m^2, and Poisson ratio = 0.33.

The calculated results by FEA method are shown in Figs. 7 and 8 where only one quarter of the whole cross section was plotted. In Fig. 7 the broken lines represent the original shape, and the

solid lines represent the deformed shape under applied electric field; it can be seen that the sample expanded along z direction and contracted along r direction under applied field; at the electrode edge the deformation is not uniform. The stress distributions are clearly shown in Fig. 8 for three directions (r, ϕ, and z); the positive sign of stress represents the tensile stress, and the negative sign represents the compressive stress. Stresses in all three directions have their maximum values of tensile stresses at the circumference with a diameter slightly smaller than the electrode edge, and their maximum value of compressive stresses at the circumference with a diameter slightly larger than the electrode edge; all these maximum stresses are close to the surfaces of the sample. Since the maximum tensile stress (36.1MPa) is larger than that of the compressive stress (32.4 MPa) and for brittle materials the tensile strength is usually about one to two orders of magnitude lower than the compressive strength[19], only the effects of tensile stress need to be considered in this case.

The maximum tensile stresses in r, ϕ, and z directions are 36.1, 25.9 and 11.6 MPa, all of which are near the electrode edge and are much larger than the stresses in the sample body which are 12, 12, and 0 MPa for r, ϕ and z direction, respectively, as shown in Fig. 8. Since the tensile strength data for PLZT ceramics are not available, the average of hoop tensile strengths of Navy standard rings for PZT ceramics measured by Pohanka and Smith[21] are employed for purpose of comparison. These values are 41, 43, 47 MPa for unpoled, axially poled and radially poled samples, respectively. Since the dynamic strength is always lower than the static strength,the maximum tensile stresses (36.1 MPa) in our experiments are large enough to initiate a crack as observed in real situations. The cracking patterns and character of crack growth can also be understood from the calculated stress distributions in Fig. 8. The tensile stress in r direction should cause the cracks to start near the electrode edges and grow along the ϕ direction (circle); the tensile stress in the ϕ direction can cause cracks to start near the electrode edges and grow in the r direction; and the tensile stress in the z direction can also cause crack to start near edges and grow parallel to the surfaces. Since the largest stress is in r direction, it is expected that the crack gets initiated near the electrode edges and grows mainly in the ϕ direction. Fig. 2 shows that the cracks in fact started inside edges of the electrode and propagated in ϕ direction. Microcracks in Fig. 2 growing circularly towards the center can be also be explained by the stress distribution; after microcracks occurred inside the electrode edges these microcracks soon became new edges and replaced old ones; the stresses could redistribute and the stress concentrations moved to new inside edges and caused further microcracking which then became new edges. With the continuous switching this process repeated again and again, causing microcracks to move closer and closer to the center.

IV. CONCLUSIONS

The decrease of polarization and increase of coercive field of ferroelectric ceramics subjected to AC field is termed electric fatigue. It is caused by domain pinning or microcracking. The former is recoverable by electrical or thermal treatments and the latter is permanent. Microcracking occurs due to stress concentrations created by incompatible large strains between grains under large AC field. The anisotropic piezoelectric and electrostrictive coefficients of these materials are responsible for these strains. The microcracking was observed to get initiated inside the electrode edge on the high voltage terminal side and propagate as a circular ring which moves towards the center. Finite element analysis of the stress distribution in three directions (r, ϕ and z) shows that the maximum tensile stress is observed near the surface slightly inside the electroded portion and that the stress contours extended in a circular pattern, with the circles moving towards the center. Since ceramics are weaker in tension than in compression, the finite element analysis thus confirms the proposed mechanism for the initiation and growth of microcracks responsible for electric fatigue in PLZT ferroelectric ceramics.

Acknowledgements–The authors are grateful to the Office of Naval Research for financial support.

REFERENCES

[1] K. Uchino, "Electrostrictive Actuators: Materials and Applications," *Amer. Cerm. Soc. Bull.*, vol. 65, pp. 647-652, 1986.

[2] J. W. Hardy, "Active Optics: A New Technology for the Control of Light," *Proc. IEEE*, vol. 66, pp. 651-660, 1978.

[3] R. J. Silcox, S. Lefebvre, T. B. Beyer, and V. L. Metcalf, "Active Control of Interior Noise Using Piezoceramic Actuators," *J. Acoust. Soc. Am.*, vol. 90, pp. 2269-2269, 1991.

[4] T. Sc[illegible], H. Ishikawa, O. Ikeda, S. Nomura and K. Uchino, "Deformable 2-D Mirror Using Mu[illegible]ered Electrostrictors," *Applied Optics*, vol. 21, pp. 3669-3672, 1982.

[5] S. J. Jang, "Electrostrictive Ceramics for Transducer Applications," Ph.D. thesis, The Pennsylvania State University, University Park, PA. 1980.

[6] A. Kudama, "A Piezoelectric Ultrasonic Motor," *Jpn. J. Appl. Phys.*, vol. 24 (suppl. 24-2), pp. 739-741, 1985.

[7].Y. Tomikawa, T. Nishitsuka, T. Ogasawara, and T. Takano, *Sensors and Materials*, vol. 1-6, pp. 359-379, 1989.

[8] M. C. McQuarrie, "Time Effects in Hysteresis Loop of Polycrystalline Barium Titanate," *J. Appl. Phys.*, vol. 24, pp.1334-1335, (1953.

[9] M. C. McQuarrie and W. R. Buessem, "Aging Effect in Barium Titanate," *Am. Ceram. Soc. Bull.*, vol. 34, pp. 402-406, 1955.

[10] M. Kahn, D. P. Burks, I. Burn, and W. A. Schulze, "Ceramic Capacitor Technology," in *Electronic Ceramics*, ed. L. M. Levinson, Marcel Dekker, New York ,1988, p. 191.

[11] W. P. Mason, "Aging of the Properties of Barium Titanate and Related Ferroelectric Ceramics," *J. Acoust. Soc. Am.*, vol. 27, pp. 73-79, 1955.

[12] D. Berlincourt, H. H. A. Krueger, and B. Jaffe, "Stability of Phases in Modified Lead Zirconate with Variation in Pressure, Electric Field, Temperature and Composition," *J. Phys. Chem. Solids*, vol. 25,pp. 659-674, 1964.

[13] Q. Y. Jiang, " Electrically Induced Fatigue Effects and Reliability in Piezoelectric and Electrostrictive Ceramics," Ph.D. thesis, The Pennsylvania State University, University Park, PA.,1992.

[14] Q. Y. Jiang and L. E. Cross, " Effects of Porosity on Electric Fatigue behavior in PLZT and PZT Ferroelectric Ceramics," *J. Mater. Sci.*, vol. 28, pp. 4536-4543, 1993.

[15] Q. Y. Jiang, E. C. Subbarao and L. E. Cross, "Grain Size Dependence of Electric Fatigue of Hot Pressed PLZT Ferroelectric Ceramics," (submitted to *Acta. Metall. Mater.*).

[16] Q. Y. Jiang, E. C. Subbarao and L. E. Cross, "Effects of Composition and Temperature on Electric Fatigue of Ferroelectric La-doped Lead Zirconate Titanate Ceramics," (submitted to *J.*

Apply. Phys.)

[17] Q. Y. Jiang, W. Cao and L. E. Cross, "The influence of Surface Contamination on Electric Fatigue in Ferroelectric Ceramics," *J. Amer. Ceram. Soc.*, vol. 76, (in press).

[18] Q. Y. Jiang, E. C. Subbarao and L. E. Cross, "Effects of Electrode Material and Electroding method on Fatigue behavior of Ferroelectric Materials," (*Ferroelectrics*, in press).

[19] R. W. Davidge, "Mechanical Behavior of Ceramics," Cambridge University Press, 1979, p. 32, p. 80.

[20] Zienkiewicz, O. C., "The Finite Element Method in Engineering Science," McGraw–Hill New York, 1971.

[21] R. C. Pohanka and P. L. Smith, "Recent Advances in Piezoelectric Ceramics," in "Electronic Ceramics," Ed. by Lionel M. Levinson, Marcel Dekker, Inc. New York,1988, p. 62.

Figure Caption:

Fig. 1. The normalized remanant polarization and coercive field as a function of the switching cycles for hot pressed PLZT ceramics with compositions x/65/35.

Fig. 2. Microstructure of the fatigued PLZT 8/65/35 sample observed by optical microscope with transmitted light. (a) shows the total fatigued area (within circle); (b), (c) and (d) show further observation under higher magnification for part of the opaque ring in (a), when the picture was focused near the bottom face of the sample (b), in the middle level (half above the bottom) (c), and near the top surface (d).

Fig. 3. Fractured cross section of a fatigued PLZT 8.4/65/35 sample observed by SEM.

Fig. 4 (a). Electrode configurations: fully electroded (A) and partially electroded (B). (b) The normalized remnant polarization as a function of the switching cycles of hot pressed PLZT 8.4/65/35, (A) fully electroded sample, and (B) partially electroded sample.

Fig. 5. Sample configuration used for FEA calculation.

Fig. 6. Joint identification of one quarter of cross sectional area.

Fig. 7. Deformed shape (solid line) and undeformed shape (dash line) of a one quart of cross sectional area.

Fig. 8. Stress distribution in (a) r, (b) ϕ, and (c) z directions.

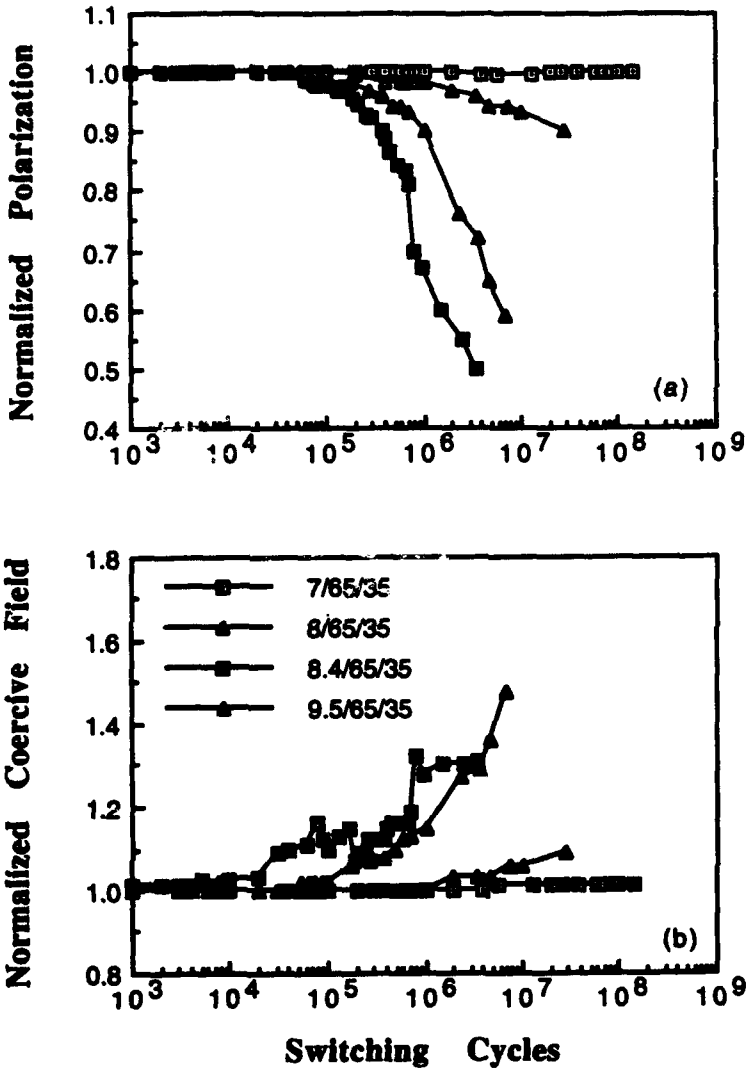
Normalized Polarization
1.1
1.0
0.9
0.8
0.7
0.6
0.5
0.4
(a)
Normalized Coercive Field
1.8
1.6
1.4
1.2
1.0
0.8
7/65/35
8/65/35
8.4/65/35
9.5/65/35
(b)
10^3 10^4 10^5 10^6 10^7 10^8 10^9
Switching Cycles

Fig. 1.

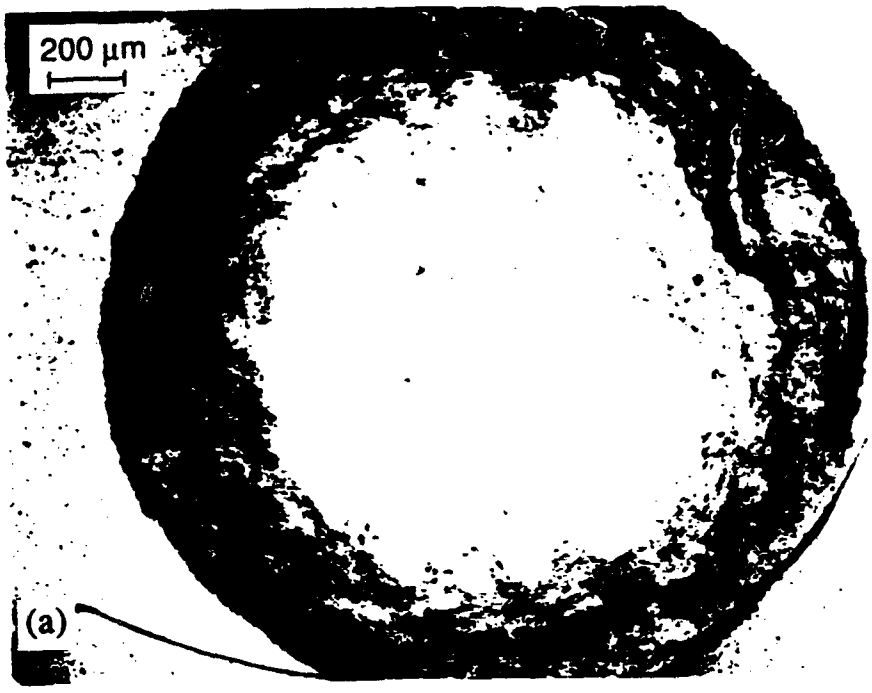

Fig 2 (a) (b)

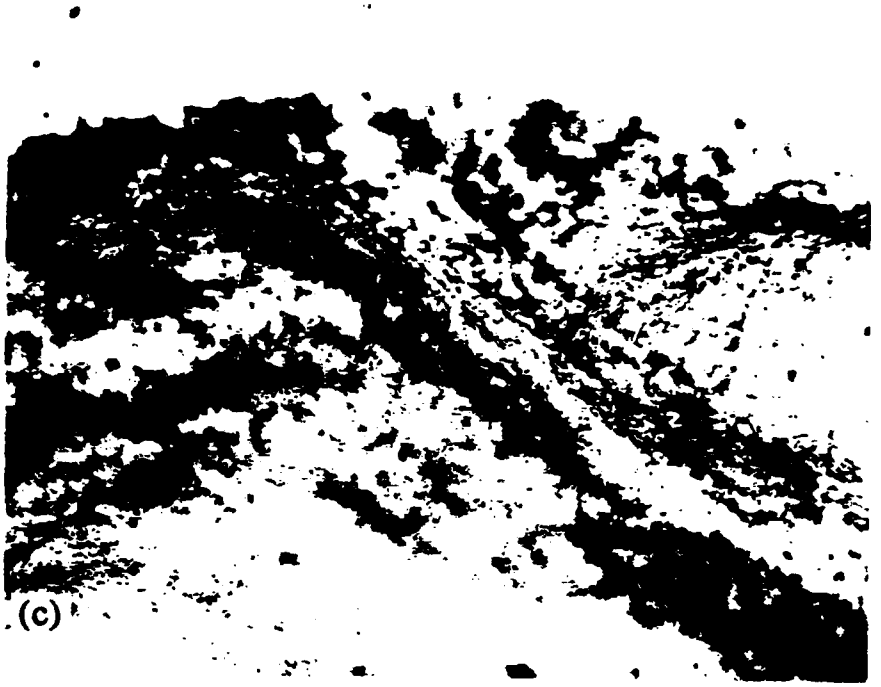

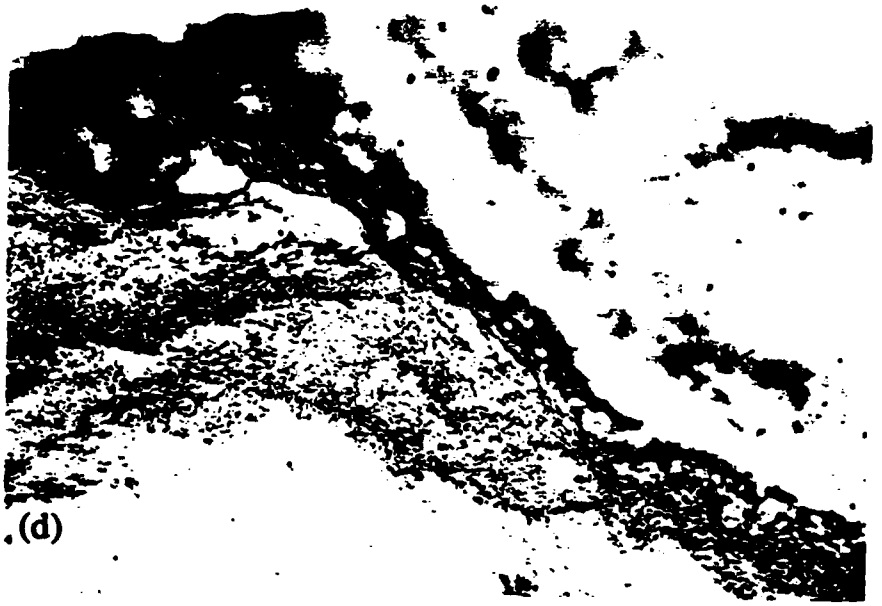

Fig 2(c). (d)

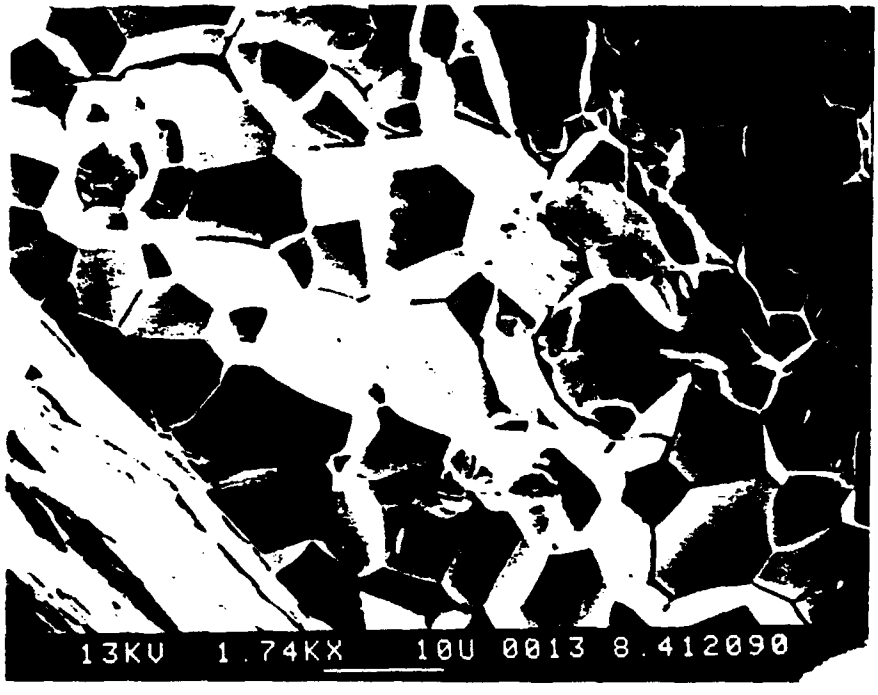

Fig. 3

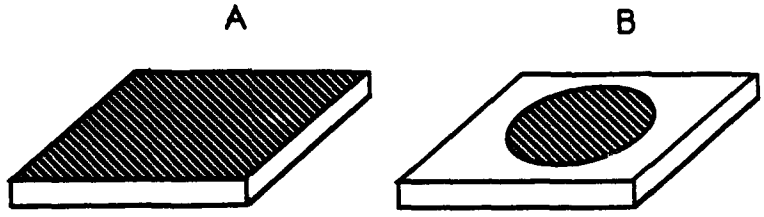
A
B

(a)

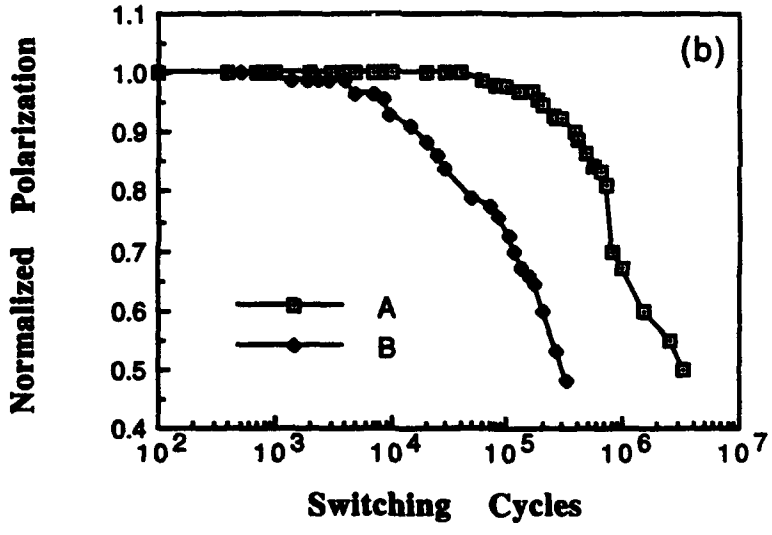
(b)
Normalized Polarization
1.1
1.0
0.9
0.8
0.7
0.6
0.5
0.4
A
B
10^2
10^3
10^4
10^5
10^6
10^7
Switching Cycles

Fig. 4

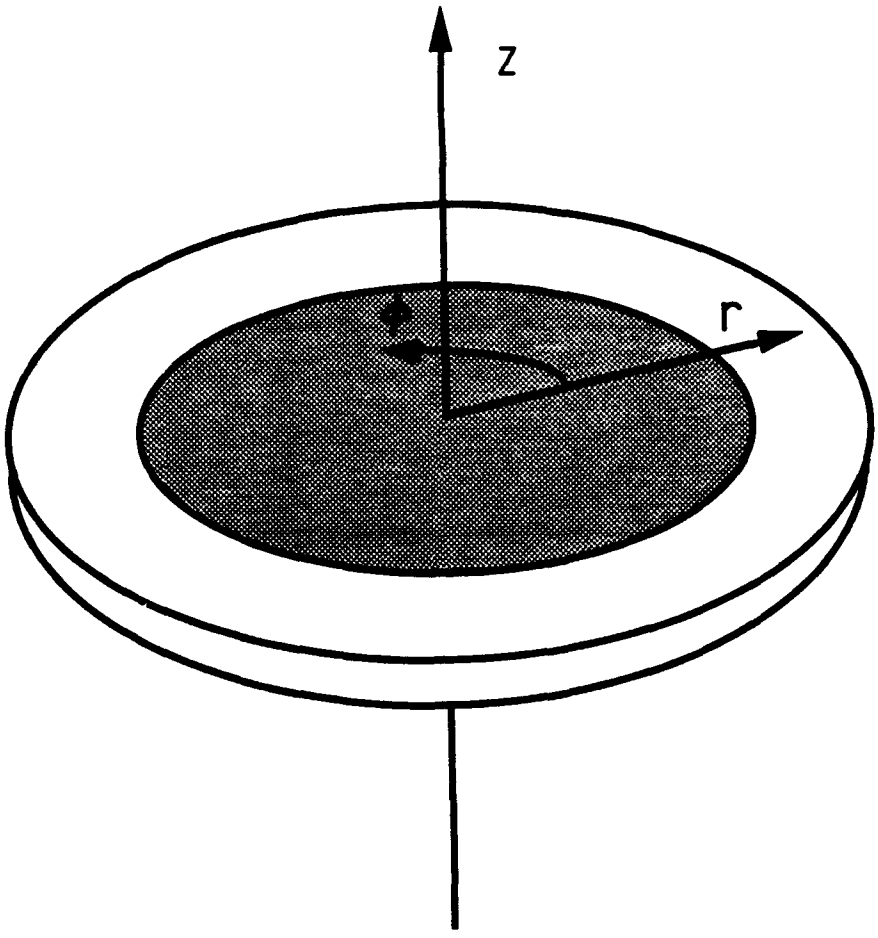

Fig. 5

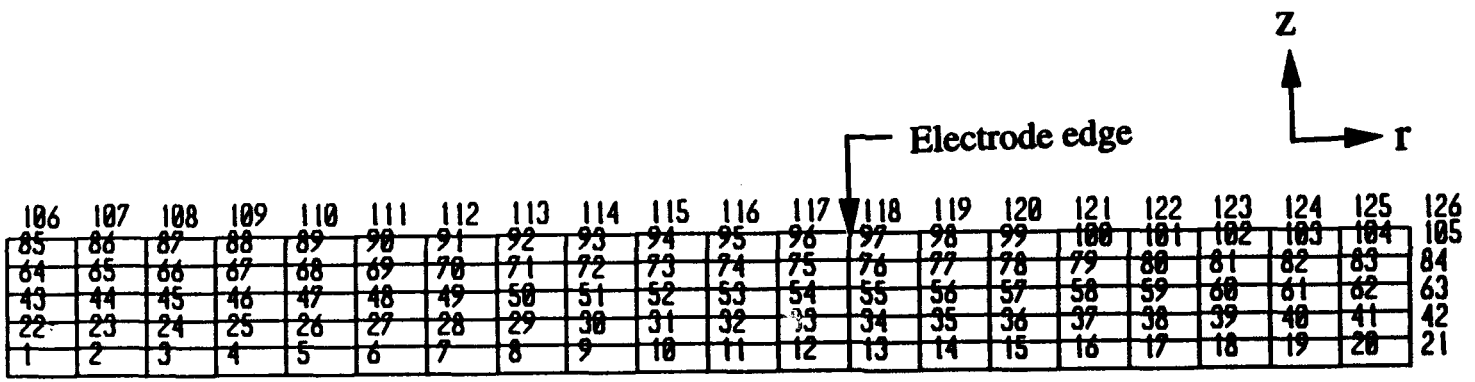
z
r
Electrode edge
106 107 108 109 110 111 112 113 114 115 116 117 118 119 120 121 122 123 124 125 126
85 86 87 88 89 90 91 92 93 94 95 96 97 98 99 100 101 102 103 104 105
64 65 66 67 68 69 70 71 72 73 74 75 76 77 78 79 80 81 82 83 84
43 44 45 46 47 48 49 50 51 52 53 54 55 56 57 58 59 60 61 62 63
22 23 24 25 26 27 28 29 30 31 32 33 34 35 36 37 38 39 40 41 42
1 2 3 4 5 6 7 8 9 10 11 12 13 14 15 16 17 18 19 20 21

Fig. 6.

Fig. 7.

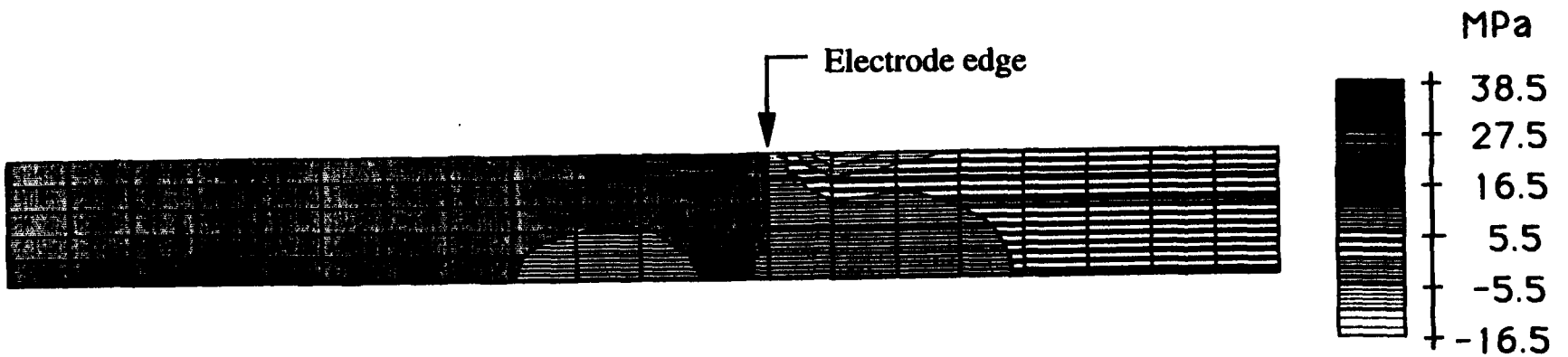

(a) Maximum compressive stress is -12.9 MPa at joint 119 (see Fig. 6), and maximum tensile stress is 36.1 MPa at joint 117. The stress in the body is about 12.0 MPa.

Fig 8(a)

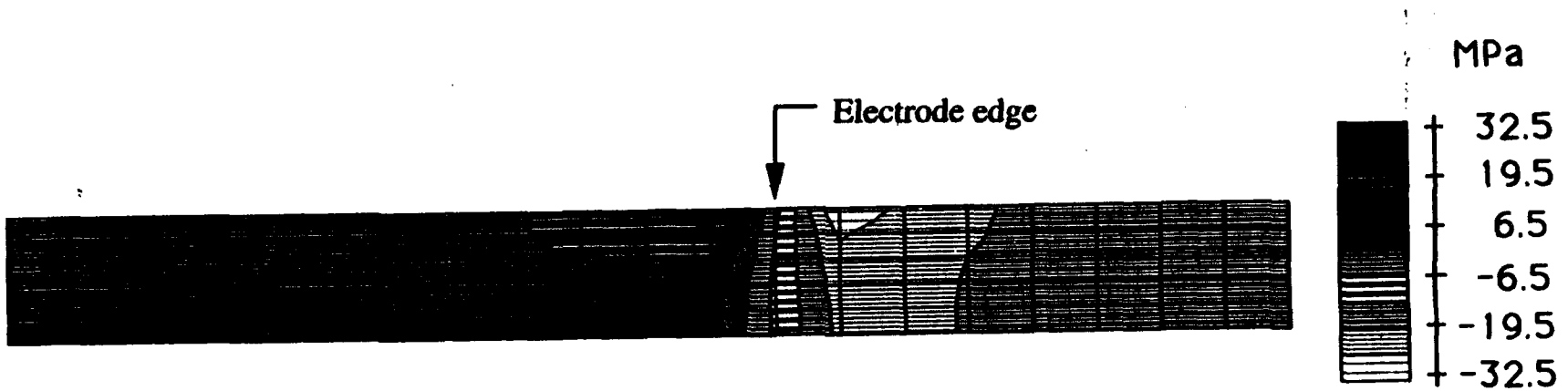

(b) Maximum compressive stress is -32.4 MPa at joint 119 (see Fig. 6), and maximum tensile stress is 25.9 MPa at joint 117. The stress in the body is about 12.0 MPa.

Fig 8(b)

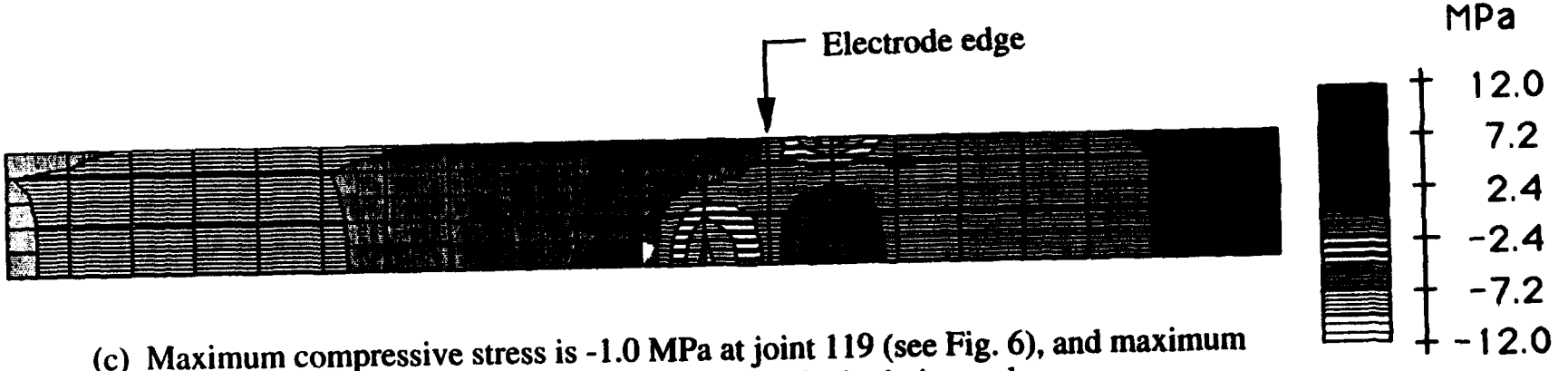

(c) Maximum compressive stress is -1.0 MPa at joint 119 (see Fig. 6), and maximum tensile stress is 11.6 MPa at joint 117. The stress in the body is nearly zero.

Fig 8(c)

APPENDIX 21

DIELECTRIC PROPERTIES OF SINGLE GRAIN IN PLZT FERROELECTRIC CERAMICS

Q. Y. JIANG, E. C. SUBBARAO, L. E. CROSS
Materials Research Laboratory, The Pennsylvania State University
University Park, PA. 16802

Abstract. The hot pressed and grain-grown transparent ceramics with maximum grain size 80~100 μm provides the possibility of investigating the dielectric properties of single grain from ceramic specimens. The ion milling technique was employed to separate the grains. The dielectric permittivities of single grain of PLZT have been measured. It is found that the range of dielectric constant of single grains in unpoled state is larger than that of the bulk ceramic. Poling in both single grains and bulk ceramics reduces the dielectric constant in the poling direction, and increases it in the direction perpendicular to the poling field. The anisotropy of dielectric permittivity for PLZT 8/65/35 is calculated from the single grain data.

Lanthanum doped lead zirconate titanate (PLZT) ceramic system has been the subject of much interest due to their high optical transparency, excellent electro-optical characteristics, unusually high dielectric constant and piezoelectric constants, and square ferroelectric hysteresis loop with low coercive field.[1,2] PLZT ceramic is one of the best candidate materials for electro-optical devices and the non-volatile memory devices which have been developed rapidly in recent years.

Unfortunately, single crystal growth of PLZT is so difficult that it can only be made as a polycrystalline ceramic. Thus, there are no single crystal data available. However, the transparent PLZT polycrystalline ceramic with maximum grain size 30 to 100 μm can be obtained from the hot pressed specimens by the grain-growth technique, which provides the possibility of investigation of the physical properties of the single grain from ceramic samples. In the present work, the dielectric constants of the PLZT single grain in unpoled and poled states and the temperature dependence of dielectric constant of single grain thick specimens were measured. The results are compared with the thick PLZT ceramic samples.

The composition of the PLZT is 8/65/35 (La/Zr/Ti, mole ratio) and this composition is located near the rhombohedral, tetragonal, and cubic phase boundary. PLZT 8/65/35 exhibits typical ferroelectric relaxor behavior.[3,4] Small discs with diameters ranging from 6 μm to 100 μm were obtained by the ion milling technique as follows. First the sample was polished, cleaned, and annealed at 600 °C for 1 hour, then one face of the samole was metallized with aluminium. After bonding to a thin glass

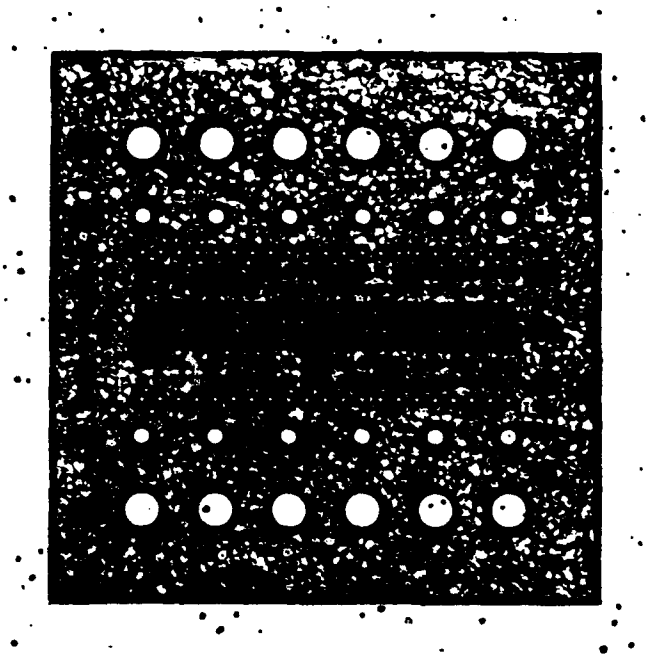

FIGURE 1. The top view of the ion milled PLZT sample (area 1).\Figures on the left side are diameters of the dots (ranged from 6 μm to 100 μm), and figures on the right side are the number of dots for each diameter.

slip, the sample was lapped to 8.9 μm thickness. Then the top surface was also metallized with gold. After reticulation masking was applied to the top of the surface of the two regions, the edges of the dots were defined by ion milling. The milling depth was 2 μm for one region (called area 1) and 7 μm for another region (called area 2). The view of the well defined discs with diameters of 100 μm, 50 μm, 20 μm, 15μm, 12μm, 10μm, 8μm, and 6 μm for area 1 is shown in Figure 1. Area 2 which was ion milled to a depth of 7 μm is not shown here.

The dielectric permittivity (constant) for each disc of different diameters was measured with General Radio 1621 Precision Capacitance Measurement System at 1 KHz. The contact between disc and measurement device was made possible by probes through the optical microscope.

The dielectric constant measured from the discs of all sizes in area 1 and area 2 at room temperature without prepoling are shown in Figure 2(a) and (b), respectively. For each diameter the measurements were carried out on at least five discs, and for some diameters on more than 30 discs. The dielectric constants of discs with different size ranged from 3800 to 8000 for area 1,and 4200 to 9000 for area 2. A dispersion of the dielectric constants of the discs with same diameter was observed (Fig. 2), and the effect was larger as the diameter of the disc decreased. The change of the dielectric constant ranged from 12% for 100 μm diameter to 47% for 6 μm diameter (Fig. 2(a)). From Figure 2 one can see that the average dielectric constant of area 2 is larger than that of area 1. This can be more clearly seen in Figure 3, in which the temperature dependence of dielectric constant of 100 μm and 50 μm discs in area 1 and area 2 are shown. The different mechanical boundary conditions between two areas due to the different milling depth (2 μm and 7 μm for area 1 and 2, respectively) are responsible for this difference. 78% of the disc edge in area 2 was free and 22% of the edge was clamped, compared with 22% free and 78% clamped in area 1.

The grain boundaries in area 1 are clearly visible under the optical microscope, and the discs with only single grains in them (including 8, 10, 12 , and 15 μm diameters)

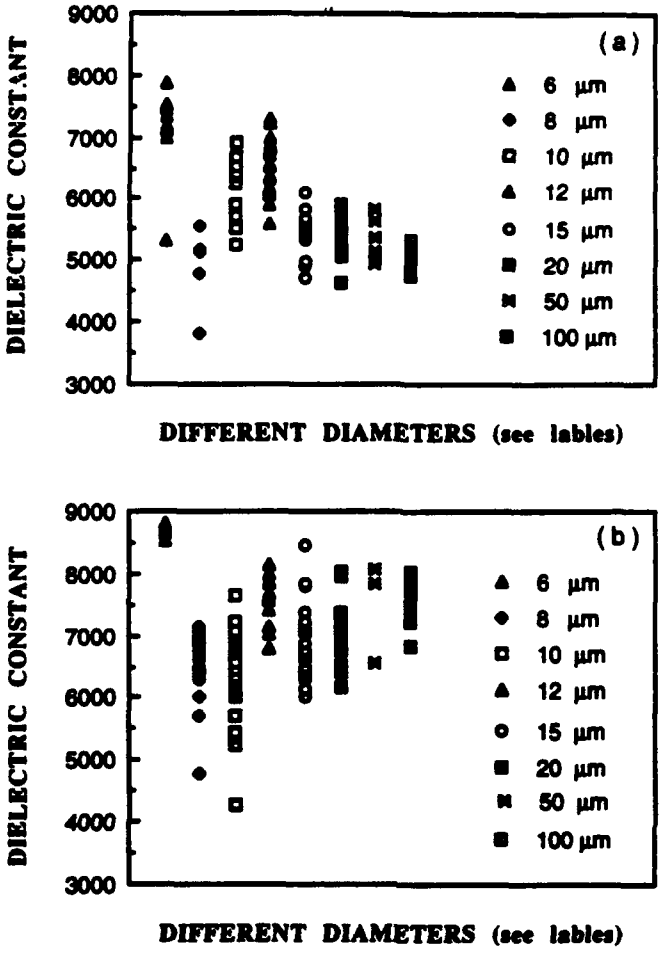

FIGURE 2. The dispersion of the dielectric constant of different diameters for discs of all sizes in (a) area 1 and (b) area 2 at 1 kHz without prepoling.

could be distinguished from those with multigrains (contained 1 to 3 grain boundaries). The dielectric constants of these single grains in unpoled states are shown in Figure 4(a) together with those of multigrains of same diameters (Figure 4(b)).There are no dramatic changes of the dielectric constants in single grains and multigrains. This can be understood by the fact that the polarization in an unpoled single grain is not aligned along one direction, and many microdomains existed within a grain. Therefore, both the multigrain discs and the single grain discs are assemblies of multidomains, except that the multigrain discs contained grain boundaries also. The results in Figure 4 also indicate that the grain boundaries connected parallel to grains do not significantly affect dielectric permittivity.

Anisotropy of the dielectric permittivity in PLZT single grains could be studied by poling the single grain discs under DC field (20 Kv/cm) larger than the coercive field (5 Kv/cm). The dielectric constants measured before and after poling are shown in Figure 5 and Table 1. The poled dielectric constants are smaller than the unpoled ones, which is in agreement with the dielectric data obtained from bulk PLZT ceramics by us. This can be explained by the formation of macrodomains from microdomains under high DC field [5]. The contribution to the weak field properties by microdomains is greatly reduced. The extent of the decrease of the dielectric constant was not always same for all singe grain

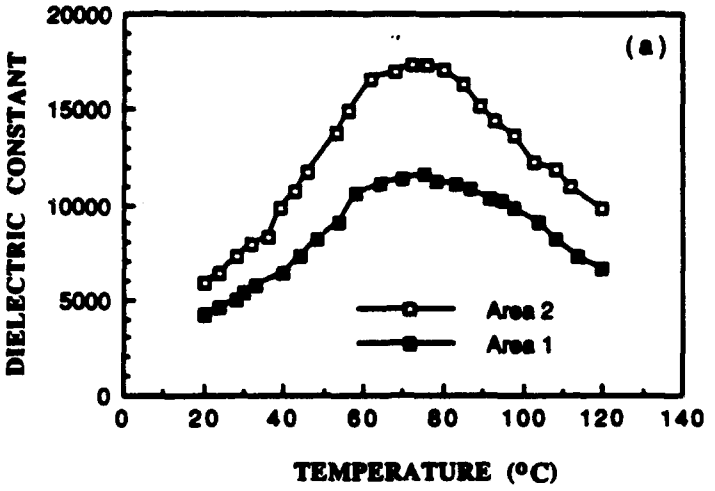

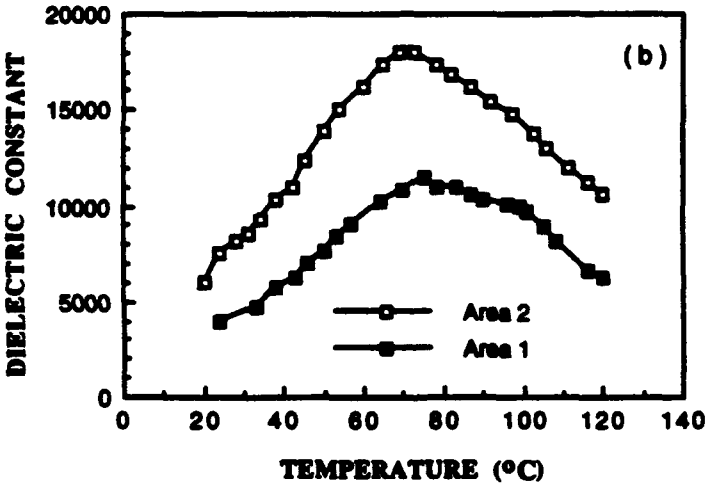

FIGURE 3. Temperature dependence of the dielectric constant of ion milled PLZT sample with disc diameter (a) 50 μm and (b) 100 μm.

TABLE 1 The Measureed Dielectric Constant for Both Single Grains and bulk Ceramic of PLZT 8/65/35.

	Dielectric Constant	
	Single grains	Bulk ceramic
Unpoled	5000 ~ 7000	4500 ~ 5000
Prepoled	3000 ~ 6000	4100 (K_{33}) 5900 (K_{11})

discs both with different diameters and same diameter, and the decrease ranged from 8% to 30%. Since the crystallographic axes of the single grains are not always aligned in the same direction, the angle between the measured direction and crystallographic axis after poling is a function of individual grains, ranging from 0° to ±30° for orthorhombic phase, 0° to ±35.5° for rhombohedral phase, or 0 to ±45° for tetragonal phase, provided that the poling is complete. The poled phase of PLZT 8/65/35 is orthorhombic.[6, 7] If we take the

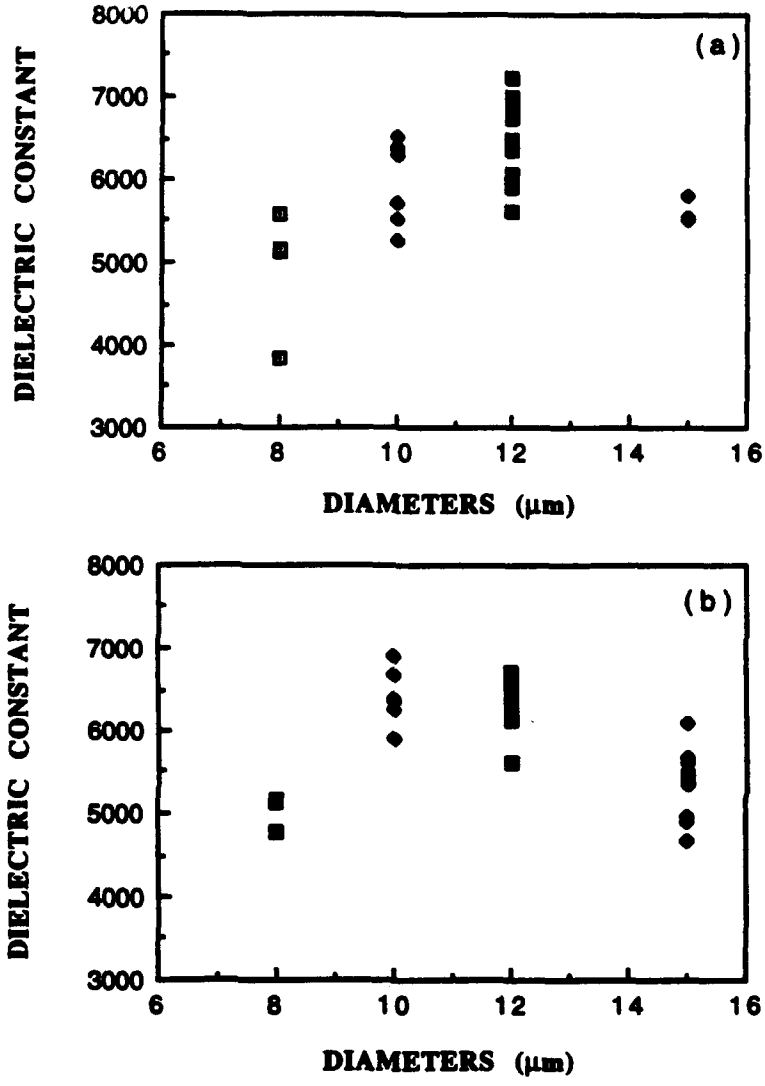

FIGURE 4. The dispersion of the dielectric constant of (a) single grains and (b) multigrains for four diameters at 1 kHz without prepoling.

minimum of the measured single grain dielectric constant as the K^T_{33} which is 3000, and the maximum 6000 as K^T along the direction of 30° away from the c axis (Table 1). The relationship among K^T_{11}, K^T_{33}, and K^T for single grain is

$$K^T = (1 - (\cos 30^o)^2)K^T_{11} + (\cos 30^o)^2 K^T_{33}, \qquad (1)$$

where it is assumed that $K^T_{22} \sim K^T_{11}$, since the lattice parameters a (5.777A) and b (5.794A) are very close in 8/65/35 composition.[6] After replacing K^T_{33} and K^T by 3000 and 6000 in equation (1), we have

$$K^T_{11} = 15000.$$

The calculated K^T_{11} is larger than K^T_{pole} (3000 ~ 6000) and K^T_{unpole} (5000 ~ 7000) in single grains, which is consistent with the results of the bulk PLZT 8/65/35 samples in which the measured K^T_{11} (perpendicular to the poling direction) is 5900, and K^T_{33} (parallel to the poling direction) is 4100, and K^T_{unpole} is 5000 (Table 1).

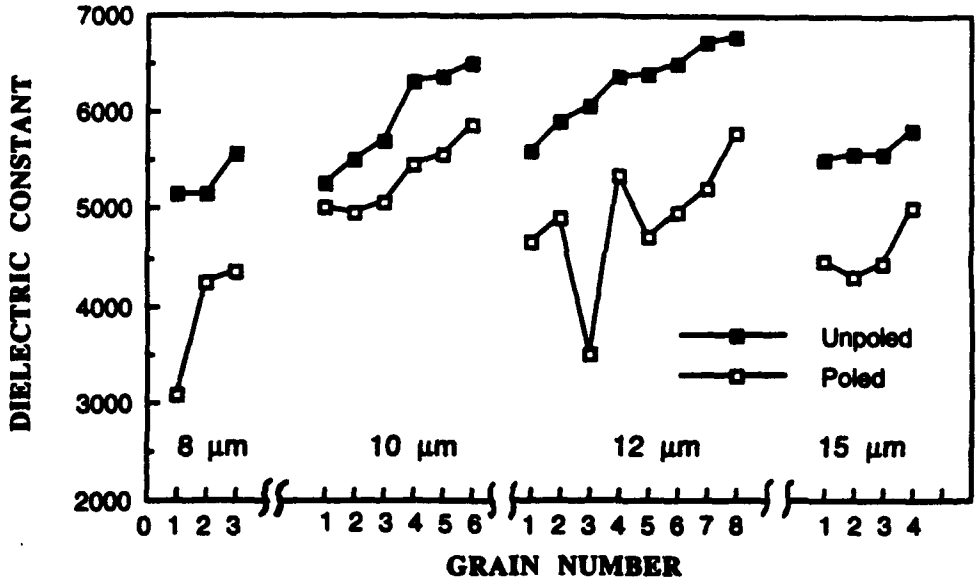

FIGURE 5. The dielectric constant of single grains measured before and after poling for four diameters.

In conclusion, the anisotropy of dielectric permittivity for PLZT 8/65/35 has been derived from the data measured from the single grains. The dielectric constant in c direction is ≤ 3000, and in a or b direction ≥ 15000. The range of dielectric constant (5000 ~ 7000) of single grains in unpoled state is larger than that of the unpoled bulk ceramic (4500 ~ 5000). The parallel grain boundaries do not severely affect the dielectric property of PLZT, but the mechanical boundary condition can influence the dielectric measurement. It is found that both in single grains and bulk ceramics poling process reduces the dielectric constant along the direction parallel to the poling field, and increases it along the direction perpendicular to the poling field, which is different from the PZT normal ferroelectric ceramics.

ACKNOWLEDGEMENT: The authors wish to thank Shanghai Institute of Ceramics in China for providing PLZT samples, and D. J. Pedder and R. A. C. Bache in Plessey Company for helping preparing samples by ion milling.

REFERENCES:

1. G. H. Heartling and C. E. Land, J. Am. Cer. Soc. 54, 1 (1971).
2. C. E. Land, P. D. Thacher, and G. H. Heartling, Appl. Solid State, 4, 137 (1974).
3. M. Yokosuka and M. Marutake, Jap. J. Appl. Phy., 25, 981 (1986).
4. Fan Shemin, He Jiawen, and Xi Yao, Ferroelectrics, 77, 181 (1988)
5. Yao Xi, Chen Zhili, and L. E. Cross, J. Appl. Phys., 54, 3399 (1983).
6. E. T. Keve and K. L. Bye, J. Appl. Phys., 46, 810 (1975).
7. E. T. Keve, Ferroelectrics, 10, 169 (1976).

APPENDIX 22

Materials Letters 17 (1993) 21–26
North-Holland

MATERIALS LETTERS

Quantitative evaluation of extrinsic contribution to piezoelectric coefficient d_{33} in ferroelectric PZT ceramics

Shaoping Li [1], A.S. Bhalla, R.E. Newnham and L.E. Cross
Materials Research Laboratory, Pennsylvania State University, University Park, PA 16802, USA

Received 19 March 1993

The contribution of 90° domain wall motion to the piezoelectric coefficient d_{33} in ferroelectric PZT ceramics has been evaluated quantitatively by a simple model. The microstructures of PZT ceramics have also been considered through the evaluation process. In order to avoid some formidable and somewhat ambiguous calculations involved and also in order to offer a clear physical picture of the domain contribution to the piezoelectric coefficient d_{33} in ferroelectric ceramics, we have introduced a new concept of the effective number of domain walls in the quantitative evaluation process which reflects the magnitude of domain wall density in ceramics. The obtained calculation result, $\Delta d_{33} \approx 219.4 \times 10^{-12}$ m/V, supports the measured data and also is inherently plausible in terms of the contribution of domain wall motion to the electromechanical properties of ferroelectric ceramics.

1. Introduction

In principle, one of the challenges facing materials scientists is how to develop a scientific foundation for understanding and rational designing the sophisticated materials systems with novel microstructures as well as multiple functional characteristics. One of the key issues for this development is to gain a better understanding of the basic physics in complex systems and to provide more complete physical pictures and underlying theoretical bases for these complex systems in great detail. With the development of modern microelectronics, it is becoming more and more important to quantitatively investigate the physical properties of electronic polycrystalline materials by considering their microstructures in detail.

The basic quantities in ferroelectric polycrystalline materials are the spontaneous macroscopic polarization and displacement, which result, e.g., upon application of an electric field, and persist at null field in two enantiomorphous metastable states of the ceramic system. These quantities are related to the dielectric and piezoelectric coefficients of the ceramic and are different from those in crystals, even in a multidomain single crystal system. The contributions of 90° domain wall motion to the dielectric, piezoelectric, and elastic properties of ferroelectric ceramics have been discussed extensively in the past [1–11]. The strong increase in the piezoelectric coefficient and dielectric coefficients could be understood by shifts and oscillations of 90°-type domain walls. However, the quantitative evaluation of extrinsic contribution to the physical properties in ferroelectric polycrystalline materials is still in its infancy. Arlt et al. [1,2] employed a dynamic equation of domain wall motion to evaluate the dielectric, piezoelectric, and elastic coefficients through averaging the domain wall motion contributions with respect to every individual grain for a ceramic sample. A similar work was also done by some Russian scientists [9,10]. Bondarenko et al. [11] have proposed a method which takes into account an elastic interaction between a multidomain grain and the surrounding ceramic matrix. Although several models have been postulated over the years, the study of quantitative correlation between the domain boundary's displacement and the induced piezoelectric coefficients in polycrystalline materials is still very desirable and demanded in practice.

In the present work, we give an estimate of the pie-

[1] Present address: 115 Sachem Village, West Lebanon, NH 03784, USA.

zoelectric coefficient Δd_{33} in ferroelectric polycrystalline materials based on a very simple model [1,2,4,8], which provides some insight, at the microscopic level, into the basic physics of ferroelectric ceramics. The way of evaluating the piezoelectric constant Δd_{33} presented here is slightly different from those in previous studies [1,2,9–11] in order to provide more comprehensive data and avoid some cumbersome and formidable as well as somewhat ambiguous calculations involved and also in order to offer a clear physical picture of the domain contribution to the piezoelectric coefficient d_{33} in ferroelectric ceramics. Meanwhile, t e microstructures of ceramic samples, i.e. both the width of the domain and the orientational distribution of spontaneous polarization in domains as well as the density of the domain walls, have also been considered explicitly. The results of quantitative calculations are given for a tetragonal PZT ceramic which is one of the most studied and the most useful perovskite ceramics. The obtained results of the quantitative evaluation seem to be pretty much reasonable and accurate in comparison to the experimental data.

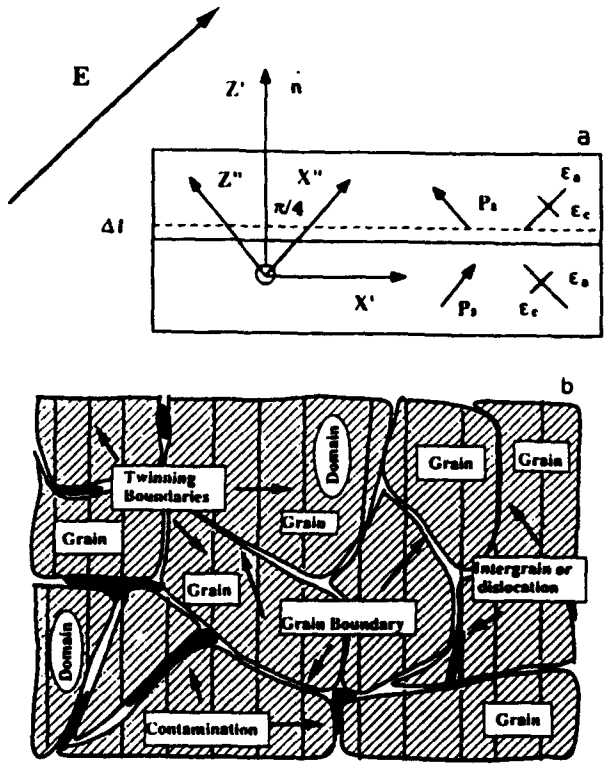

Fig. 1. (a) A basic unit of a crystallite with a displaceable 90°-domain wall, and (b) a schematic illustration of the grain interaction effect in polycrystalline ceramics.

2. Evaluating extrinsic contribution to piezoelectric coefficient Δd_{33}

Fig. 1 shows the domain boundaries (DB) in a ferroelectric ceramic matrix. From Arlt's model [1,2], when the frequency ω of the domain oscillation approaches to zero, the displacement Δl of a domain boundary under a small electric field can be written as

$$\Delta l = F(\theta) P_0 E / f_{90} , \quad (1)$$

where $F(\theta)$ is a factor related to an angular distribution between the direction of spontaneous polarization in a specific domain and the direction of the applied electric field, P_0 is the spontaneous polarization, E is the applied electric field, and f_{90} represents the force constant for the 90° domain wall motion process which can be determined by the experimental measurement. $F(\theta)$ is around 1.4–0.5 in a well poled ceramic since the orientational distribution of domain boundaries is conical. For simplicity, here, we take $F(\theta)$ as 1, which stands for a special case in which the direction of the applied electric field is parallel to the direction of spontaneous polarization in one of the domains near the boundary as shown in fig. 1a. At the resonance frequency of domain wall motions, the equation of domain wall motion becomes [1,2,4,12]

$$m_{D90} \Delta \ddot{l} + f_{90} \Delta l = -P_s E , \quad (2)$$

where m_{D90} is the effective mass of the 90° domain wall. Setting $\Delta l = \Delta l_0 \exp(i\omega t)$, from eqs. (2) and (1), we have

$$\Delta l_{90} = P_s E / (f_{90} - m_{D90} \omega^2) , \quad (3)$$

where Δl_{90} represents the displacements for the 90° domain wall motion. On the other hand, when the wall boundary is displaced by a distance Δl, the induced polarization should be written as

$$\Delta P_{90} = P_s \Delta l_{90} / L , \quad (4)$$

where ΔP_{90} is the induced polarization for the 90°

domain wall motion process, and L is the width of 90^0 domain walls. It should be noticed here that we use the symbol Δ to indicate all quantities with the symbol Δ arising from the 90^0-domain wall vibration only. Combining eqs. (3) and (4), the force constant f_{90} can be expressed as

$$f_{90} = P_s^2 / L \Delta\chi_{90} , \quad (5)$$

where $\Delta\chi_{90}$ is the value of ultra low frequency susceptibility which is assumed to arise exclusively from the 90^0 domain wall motion process because all domains should be almost 90^0 domains [13] in the distorted tetragonal and well poled ceramics. Meanwhile, it is important to note that here the force constant f_{90}, the susceptibility $\Delta\chi_{90}$ and the displacement Δl_{90} of the 90^0 domain boundary are all varied with temperature because these quantities are caused by the 90^0 domain boundary movement. At low temperatures, ΔP_{90} and the consequent piezoelectric effect will disappear as long as the 90^0 domain wall motion is frozen out. Obviously, if $\Delta\chi_{90}$ is becoming zero, i.e. there is no 90^0 domain wall motion contribution to the piezoelectric properties of ferroelectric ceramics, the induced displacement Δl_{90} of the domain wall motion should be also equal to zero at the same time according to eqs. (1) and (5). In the present analysis, we only discuss the situation at room temperature. For $Pb(Zr_{0.50}Ti_{0.50})O_3$ samples, using the values $P_s = 0.6$ C/m^2, $L = 3\times10^{-7}$ m, and $\Delta\epsilon_{33} = 1167$, one has

$$f_{90} = 1.158\times10^{14} \text{ kg/s}^2\,\text{m}^2 , \quad (6)$$

where $\Delta\epsilon_{33}$ is the value of the dielectric constant only arising from 90^0 domain wall motion. As we know, it is believed that the electromechanical properties in ferroelectric polycrystalline materials are caused not only by the ionic displacement (the intrinsic effect) in connection with the change of the polarization magnitude, but also by the movements of domain walls (the extrinsic contribution). Experimental studies on materials such as $BaTiO_3$ and PZT have shown that as much as 45–70% of dielectric constant and piezoelectric moduli values may originate from the extrinsic contributions at room temperature [13–16]. Here, we approximately estimate $\Delta\epsilon_{33}$ as the two third of the measured value ($\epsilon_{33} = 1760$) for the extrinsic dielectric constant $\Delta\epsilon_{33}$ in a $Pb(Zr_{0.50}Ti_{0.50})O_3$ ceramic. The average width of domains can be determined experimentally [16,17]. The relationship between the displacement $\Delta\delta$ of the entire ceramic sample and the displacement Δl of an individual domain boundary can be approximately expressed as

$$\Delta\delta = \Delta l [(c-a)/c] n_{\text{eff}} , \quad (7)$$

where $\Delta\delta$ is the domain-induced displacement of the entire sample under an applied electric field, Δl_{90} is the displacement of an individual domain boundary, and n_{eff} is the effective number of domain walls cross a specific direction for the ceramic sample. Here we have introduced a new concept of the effective number of domain walls in a ceramic sample which reflects the magnitude of domain wall density in ceramics. It should be emphasized that the domain width L and the effective number n_{eff} of domain boundaries are correlated to each other because the thickness of the sample is fixed as shown in fig. 2. In an ideal case, the thickness, D, of a ceramic sample is equal to the sum of the width, L, of domains within the sample as illustrated in fig. 2a. Taking $D = 2$ mm and $L = 0.3$ μm, the number of domain boundaries having 45^0 angle with the direction of the applied field is about 6600 in this ideal case (see fig. 2a). In reality, there always exists a conical distribution of remnant polarization in grains with respect to a poled ceramic (see fig. 2b), the number of domain boundaries possessing 45^0 angle with the direction of the applied field (or the poling direction) should be much less than that in the ideal case. Meanwhile, it should also be realized that only some types of oriented domain walls can contribute to the piezoelectric coefficient d_{33}. In other words, for instance, if the direction of the domain wall boundary is perpendicular to the direction of the applied field, the movement of this type 90^0 domain wall does not have any contribution to the piezoelectric effect as shown in fig. 3a. Therefore, in order to consider and deal with the real situation, we should introduce and utilize the effective number of domain boundaries for quantitative evaluation of the piezoelectric coefficient d_{33}. In addition, from eqs. (4)–(7) it can be clearly found that the domain width L (or n_{eff}, effective number of domain walls) is an important factor for the dynamic behavior of domain wall motions. We will discuss this in detail later. Following, we define the effective number of domain boundaries as 55% of the total number of domain bound-

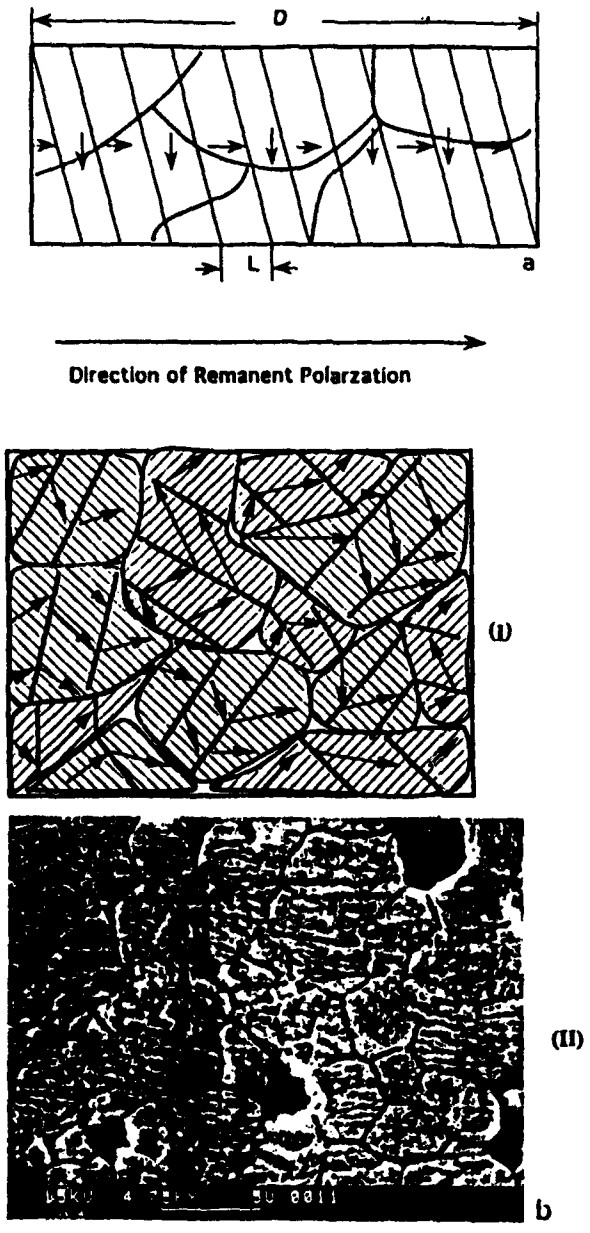

Fig. 2. (a) Illustration of the simple relationship between the thickness D of a sample and the width L of the domain in an ideal case, and (b) illustration of the simple relationship between the thickness of a sample and the width of the domain in a real poled ceramic.

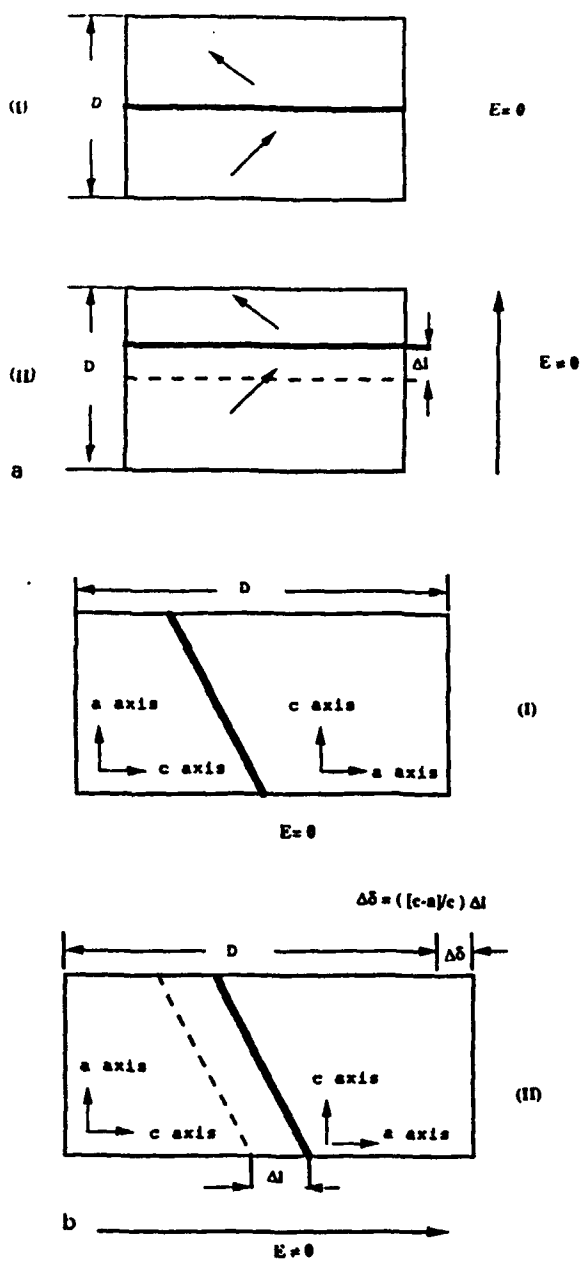

Fig. 3. The displaceable 90° domain wall boundaries with the different directions related to the direction of the applied electric field. (a) When the angle between the direction of the domain wall boundary and the direction of the applied field is 90°, the movement of the 90° domain wall does not cause any contribution to the piezoelectric effect. (b) When the angle between the direction of the domain wall boundary and the direction of the applied field is 45°, the movement of the 90° domain wall has a maximum contribution to the piezoelectric effect of the ceramic.

aries in an ideal case with respect to a well poled ceramic sample ($P_r=0.856\times P_0$). Using $P_0=0.6$ C/m^2, $L=0.3$ μm, $\Delta\epsilon_{33}=1166$, $n_{eff}=3600$, and the thick-

ness of the sample $D=2$ mm, we can quantitatively evaluate both Δl_{90} and Δd_{33} from eq. (1). The calculated value of the displacement Δl of a single domain boundary, and the calculated value of the displacement $\Delta\delta$ for the entire sample as well as both calculated and measured piezoelectric constants, Δd_{33} and Δd^*_{33}, are listed in table 1. All quantities marked with an asterisk are experimentally measured values. Table 2 lists the relevant experimental measurement data. The total displacement δl^* of the ceramic sample under a field was measured by an optical interferometer [15,16] as shown in fig. 4. In table 2, we also take the two third value of the displacement δl^* of the entire sample as the extrinsic contribution of $\Delta\delta^*$ in both calculating domain contribution to piezoelectric effect Δd^*_{33} and calculating the displacement Δl^* of a single domain boundary in order to compare those quantities which are calculated theoretically from eqs. (1)–(7) because of the influence of intrinsic contribution.

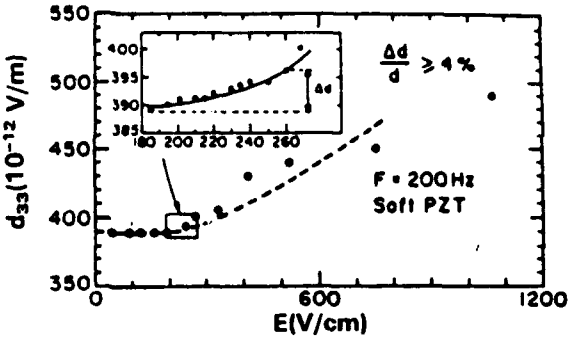

Fig. 4. Piezoelectric coefficients d_{33} as a function of the applied ac electric field.

3. Results and discussion

From tables 1 and 2, it can be found that under a moderate field the calculated value Δl (0.254×10^{-10} m) of the displacement of a single domain boundary is very close to the experimental value Δl^* (0.297×10^{-10} m).

In table 1, the measured value of Δd^*_{33} is taken as the two third value of the real measured value of d^*_{33} ($\frac{2}{3}\times385\times10^{-12}$ m/V) because the intrinsic contribution should also be considered in the evaluation process as mentioned before.

In table 2, δl^* is a real measured displacement of the sample under an ac field. It is worth mentioning here that the domain width L or n_{eff} (effective number of domain walls) are strongly affected by the grain size. It was reported that some ferroelectric ceramics with fine grain size possess very large piezoelectric constants [5–7]. The reason for this situation could be explained from the fact that the domain width in this case is small so that the density of domain walls becomes very large (or saying n_{eff} is very large). Clearly, regardless of the mobility of domain wall motion, from eq. (7), the larger the n_{eff}, the larger

Table 1
Calculated values of the piezoelectric constant Δd_{33} and related displacements in both the sample and an individual domain boundary

Calculated displacement of sample $\Delta\delta$ (m)	Calculated displacement of DB Δl (m)	Calculated piezoelectric coefficient Δd_{33} (m/V)	Measured piezoelectric coefficient Δd^*_{33} (m/V)
21.94×10^{-10}	0.254×10^{-10}	219.4×10^{-12}	256.8×10^{-12}

Table 2
Measured values of d^*_{33} from a vibrational piezoelectric plate as well as the measured displacements in both the sample and an individual domain boundary

Electric field E (V/cm)	Piezoelectric coefficient d^*_{33} ($\frac{2}{3}\Delta d^*_{33}$) (m/V)	Displacement of sample δl^* ($\frac{2}{3}\Delta\delta^*$) (m)	Displacement of DB Δl^* (m)
50	385×10^{-12}	38.5×10^{-10}	0.297×10^{-10}
210	392×10^{-12}	164.7×10^{-10}	1.27×10^{-10}
305	407×10^{-12}	248.3×10^{-10}	1.915×10^{-10}

the contribution to Δd_{33}. In reality, due to the stress constraint in ceramic samples, usually the domain width (or n_{eff}) may change as the grain size changes. This is one of the reasons that ferroelectric polycrystalline materials with different grain size exhibit different features in the dielectric (or piezoelectric) dispersions and possess different dielectric and piezoelectric properties.

Lastly, a special comment should be made here on the measured piezoelectric effect of table 2. Interestingly, from table 2, it can be found that when the displacements of the domain boundary approach or exceed the order of 10^{-8} cm, an appreciable nonlinear effect occurs. In the light of the simple models [1,2,8,18] of domain wall motion, these data seem to implicitly suggest that the onset of nonlinear vibration of the domain wall should be related to the nature of the anharmonic motion of ions in the wall boundary with respect to their double well potentials, which yields a very consistent picture for domain wall motion contributing to the electromechanical properties in ferroelectric ceramics. In summary, the piezoelectric constant d_{33} in a PZT ceramic has been evaluated based on the simple model of domain wall motions. The obtained results of the quantitative evaluation are in very reasonable agreement with the experimental data.

Acknowledgement

This research was supported by the Office of Naval Research.

References

[1] G. Arlt and H. Dederichs, Ferroelectrics 29 (1980) 47.
[2] G. Arlt, H. Dederichs and R. Herbiet, Ferroelectrics 74 (1987) 37.
[3] K.W. Plessner, Proc. Phys. Soc. (London) 69 (1956) 1261.
[4] J. Fousek and B. Brezina, J. Phys. Soc. Japan 19 (1964) 830; Bull. Acad. Sci. USSR 28 (1964) 624.
[5] G. Arlt and H. Peusens, Ferroelectrics 48 (1983) 213.
[6] G. Arlt and N.A. Pertsev, J. Appl. Phys. 70 (1991) 2283.
[7] G. Arlt, Ferroelectrics 91 (1989) 3; IEEE Ultrasonics Symposium (1990) pp. 733; J. Mater. Sci. 25 (1990) 2655.
[8] C. Kittel, Phys. Rev. 83 (1951) 458.
[9] A.V. Turik and E.I. Bondarenko, Ferroelectrics 7 (1973) 303.
[10] A.V. Turik and A.I. Chernobabov, Soviet. Phys. Tech. Phys. 22 (1977) 1127.
[11] E.I. Bondarenko, V.Tu. Topolov and A.V. Turik, Ferroelectrics 110 (1990) 53; Ferroelectrics Letters 13 (1991) 13.
[12] S. Li and L.E. Cross, Solid State Stat. (b), to be published.
[13] B. Jaffe, W.R. Cook and H. Jaffe, Piezoelectric ceramics (Academic Press, New York, 1971).
[14] A.G. Luchaninov, A.V. Shil'nikov, L.A. Shuvalov and I.J.U. Shipkova, Ferroelectrics 98 (1989) 123.
[15] S. Li, W. Cao and L.E. Cross, J. Appl. Phys. 60(10) (1991) 7219.
[16] S. Li, Ph.D. Thesis, Pennsylvania State University (1992).
[17] M.D. Dennis and R.C. Bradt, J. Appl. Phys. 45 (1974) 1931.
[18] J.A. Krumhansl and J.R. Schrieffer, Phys. Rev. B 11 (1975) 3535.

APPENDIX 23

Jpn. J. Appl. Phys. Vol. 32 (1993) pp. L 1281–L 1283
Part 2, No. 9A, 1 September 1993

A High Sensitivity, Phase Sensitive d_{33} Meter for Complex Piezoelectric Constant Measurement

Hong WANG, Qiming ZHANG and Leslie Eric CROSS
Materials Research Laboratory, The Pennsylvania State University, University Park, PA 16802, U.S.A.

(Received April 6, 1993; accepted for publication July 28, 1993)

Based on the direct piezoelectric effect and signal comparison method, a quasi-static, high sensitivity, phase sensitive d_{33} meter has been developed. The system is capable of measuring the complex piezoelectric d_{33} constant down to about 1 pC/N and has a phase resolution of $\pm 0.05°$. The advantage of this apparatus is that its operation is almost as easy as that of the commercial Berlincourt d_{33} meter, hence, it is suitable for everyday routine usage.

KEYWORDS: piezoelectricity, instrumentation, complex materials

Reflecting the imperfect energy conversion between mechanical form and electrical form, piezoelectric coefficients of most ferroelectric materials contain noticeable loss part. That is, similar to dielectric constant and elastic compliance piezoelectric coefficients are complex quantities.[1] In designing piezoelectric devices and understanding the basic mechanism of the material response towards external fields, the knowledge of the imaginary part of piezoelectric constants is often required. In the past several decades, a great deal of efforts has been devoted to the development of techniques to measure the complex piezoelectric constants of a material either directly or indirectly.

For a piezoelectric material, the constitutive equations are:[2]

$$D_m = d_{mj} T_j + \varepsilon_{mn} E_n \tag{1a}$$

$$S_i = s_{ij} T_j + d_{ni} E_n \tag{1b}$$

where stress T_j and electric field E_n are taken as the independent variables, ε_{mn} and s_{ij} are dielectric permittivity and elastic compliance of the material. The piezoelectric strain coefficient d_{mj} of the material, therefore, can be acquired through the direct piezoelectric effect (eq. (1a)), as well as the converse piezoelectric effect (eq. (1b)). In the direct effect, induced charges which is proportional to the electric displacement D_m are measured when a stress is applied on a sample,[2] while in the converse piezoelectric effect, the strain S_i induced in the sample by an external electric field E_n is measured. Piezoelectric d coefficient can also be obtained by the resonance technique which involves both the direct and converse piezoelectric effects.[3] Although each apparatus or technique developed has their merit of characterizing complex piezoelectric constants, there exist limitations such as the stiffness and the mechanical loss of the material to be measured. For instance, some apparatus can only be used to measure polymeric specimens since a large strain of the material is required.[4] For samples with high loss, the resonance method may not be able to provide accurate measurement and in principle, it is not suitable for the high loss materials due to the restriction of irreversible thermodynamic process. Above all, these techniques and apparatus developed are not very handy. Their operations are complicated and usually, special preparation of samples and sample mounting are needed.

When piezoelectric coefficients of a material are complex, the response process of the material is not a thermodynamically reversible process. In this case, there will be a question as to whether the thermodynamic relations of eqs. (1a) and (1b) derived from the reversible process are still held, specifically, whether the complex piezoelectric constants measured through the direct piezoelectric effect and through the converse piezoelectric effect will be equal. When the loss is high, it is expected that the relationships derived from the reversible thermodynamics will no longer be valid. However, when the loss is low, it has been shown, through the irreversible thermodynamics, that the relations in eqs. (1a) and (1b) are still valid for a single phase material.[5] For materials consisting of multi-phases, such as piezoelectric composite materials and polymeric piezoelectric materials, the situation is more complicated and there seems no universal answer to the question raised above.

In this paper, we will report an instrument developed recently of characterizing complex piezoelectric d_{33} constant of a piezoelectric material through the direct piezoelectric effect. The system can measure piezoelectric materials with d_{33} value of 1 pC/N, and the phase angle of $0.05°$. The operation of the system is easy and no special requirement is needed for sample geometry compared with the other techniques. Several piezoelectric materials such as PZT ceramics and PVDF copolymer were tested by the system. The results are compared with those measured through the converse effect by using an ultra-dilatometer also developed in this laboratory in the past.[6] The two systems, therefore, provide a comlete characterization of the piezoelectric response in complex materials and the constitutive relations in these materials.

The complex piezoelectric strain coefficient is defined as

$$d^* = |d| e^{-j\theta} = d' - jd'' \tag{2}$$

Where $j = \sqrt{-1}$, d and θ $(=\tan^{-1}|d''/d'|)$ are the amplitude and the phase angle of the d^* coefficient, respectively. Hence, in order to characterize the complex piezoelectric d^* coefficient, both amplitude and phase angle need to be determined. Figure 1 is the schematic drawing of the apparatus. The system consists of a

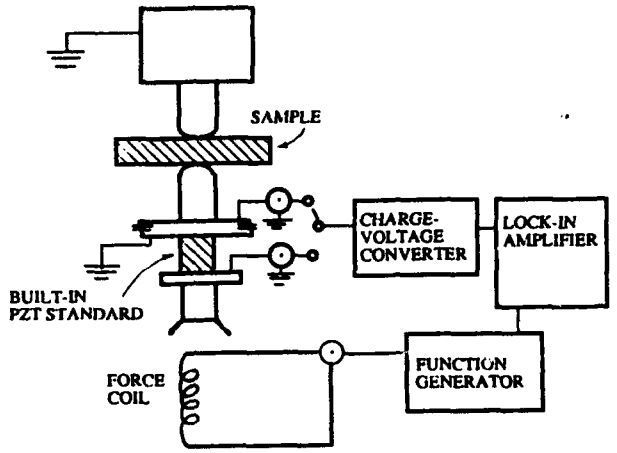

Fig. 1. Schematic drawing of the high sensitivity, phase sensitive d_{33} meter.

force generator, a charge to voltage converter (EG&G PARC Model 181 current sensitive preamplifier), and a phase sensitive detector (EG&G PARC 5208 lock-in amplifier). The force generator is that from a commercial Berlincourt piezo d_{33} meter (Channel Products, Model CPDT 3300), which has a force level of about 0.5 Newton. However, it is not difficult to build a force generator for the application here. A function generator is used to drive the coil of the force generator and this driving signal is also fed to the lock-in amplifier for the reference signal. The charge to voltage converter has a sensitivity in the range from 10^{-9} A/V to 10^{-4} A/V. For the sample tested, the sensitivity used was from 10^{-7} A/V to 10^{-6} A/V, which yielded a output voltage from mV to hundreds of mV for the samples characterized. The basic operation principle of this apparatus is similar to that of the original Berlincourt d_{33} meter. The charge output from a sample to be measured is compared to that of a standard and through the ratio, the piezoelectric constant of the sample is determined. To measure complex d_{33} coefficient, both phase angle and amplitude of the standard should be known. In our experiment, the piezoelectric constant d_{11} of a x-cut quartz crystal was chosen as the standard. Because quartz crystal has very high mechanical Q value, the piezoelectric loss of quartz crystal is negligibly small and within the phase resolution of this apparatus (0.05° in phase angle resolution for the lock-in amplifier used), the phase angle of quartz can be practically taken as zero.

A typical measurement procedure is as the following. The quartz crystal was inserted into the probe head of the force generator and induced charges were measured with respect to that of the built-in standard PZT (in the original Berlincourt d_{33} meter), and both the amplitudes and phase angles were recorded by the lock-in amplifier for the quartz (V_q and θ_q) and the built-in standard PZT (V_{b1} and θ_{b1}). Then by replacing the quartz with a sample to be measured, the charges induced on the sample and the built-in PZT were measured, and the amplitudes and the phase angles were recorded (V_T and θ_T for the sample, and V_{b2} and θ_{b2} for the built-in PZT). Combining two sets of data from the two measurements, both the phase θ and amplitude d^*_{33} of the sample can be determined

$$d_{33}=\frac{V_T V_{b1}}{V_{b2} V_q} d^q_{11}$$

and

$$\theta=\theta_T-\theta_{b2}+\theta_{b1}-\theta_q \tag{3}$$

As is clear from the above description, a commercial Berlincourt d_{33} meter can be readily converted to a phase sensitive d_{33} meter and the apparatus is quite convenient for routine operation.

To determine the sign of the d_{33} constant of a specimen, the poling direction of the sample needs to be known. In addition, the orientation of the x-cut quartz also needs to be determined. By comparing the phase angles of the sample and the quartz, the sign of d_{33} of the specimen can be easily determined.

In the testing process of this apparatus, no systematic change in both the amplitude and phase was found when a sample in the test port was reversed (the original up-face now is down) except a 180° phase angle change which was expected. The variation in the phase angle and amplitude when a sample was reversed was within the range of data scattering which would also occur when the measurement was repeated. The typical data scattering for the phase angle is ±0.05° and for the amplitude, is less than 2%. Similarly, when the quartz crystal was reversed in the test port, within the data scattering, the results did not change except 180° phase change. These are clear indications that there is no systematically spurious signal in the measurement. To further confirm this, we also tested samples having no piezoelectricity and found that the reading in the lock-in amplifier did not change for these samples with and without stress within the noise level. This noise level is much smaller than the signal from the x-cut quartz crystal. The quartz crystal used in the test has a d_{11} constant of 2.35 pC/N, which was determined using the ultra-dilatometer.[7] Therefore, we can conclude that this apparatus is capable of measuring piezoelectric d_{33} constant at least down to 1 pC/N.

Listed in Table I are the results from the measurement of several doped lead zirconia-titanate (PZT) ceramic samples and PVDF-TrFE copolymer samples. All the samples were purchased from commercial sources. PZT samples were from the Piezo-Kinetics

Table I. Complex piezoelectric d_{33} constant of some typical piezoelectric materials.

Specimen	d_{33} (pC/N)	θ	θ'[b]
PZT 5H[a]	590	0.9	1.1
Hard PZT[a] (PZT-400)	253	0.3	0.4
PVDF-TrFE	−30.7	1.15	1.2

a. PZT-5H is the trade mark of Morgon Matroc Inc., Vernitron Div. for its PZT and PZT-400 is that of Piezo-kinetics Inc.

b. θ' is the phase angle measured from the converse piezoelectric effect using a laser dilatometer.[7]

Inc. and Morgon Matroc Inc. Vernitro Div. and the PVDF-TrFE (75–25) samples were from the Atochem North America Inc. The typical dimensions for the samples tested were 1 or 2 mm in thickness and 5×5 mm^2 in area. Both surfaces of the PZT ceramic samples and quartz crystals were electroded by gold-sputtering. For PVDF-TrFE samples, the electrodes were silver paint and they were made from the manufacturer. Samples with different dimensions were also tested and it is found that the sample size is not very critical to the measurement as long as a sample is not very thin (no flexure mode will be excited) and sample area is not small compared with that of the probe head of the test port which applies force on the sample. The operation frequency range of this instrument is from 50 Hz to 200 Hz. The frequency limitation is due to the existence of mechanical resonances in the force generator and apparently, the influence of the mechanical resonance on the phase measurement is more severe than on the amplitude. In this frequency range, the complex d_{33} coefficients for the samples measured shows no changes within the data scatters in both the amplitude and phase angle.

For the comparison, the phase angles of these same specimens were also measured by the ultra-dilatometer, which also possesses a phase resolution of $\pm 0.05°$ but is far more complicated in operation. The results are also presented in Table I. Although the phase angle measured from the two piezoelectric effects are almost equal (within the data scattering), there is a systematic trend in the difference between the two sets of data and the phase angles measured from the converse piezoelectric effect seem to be a little bit larger than those from the direct piezoelectric effect. The implication of the result is beyond the scope of this paper and they will be addressed in the future.

In summary, based on the direct piezoelectric effect and signal comparison method, a high sensitivity, phase sensitive d_{33} meter has been developed which is capable of measuring complex piezoelectric d_{33} constant down to about 1 pC/N and has a phase resolution of $\pm 0.05°$. The great advantage of this apparatus is that the operation of this apparatus is almost as easy as that of the commercial Berlincourt d_{33} meter, hence, it is quite suitable for everyday routine usage. Since the set-up is modified from a commercial Berlincourt d_{33} meter, it is needed to measure the signals from the standard (quartz) and from the test sample separately. In principle, the built-in PZT in the Berlincourt d_{33} meter can be replaced by the quartz standard and the measurement procedure can be further simplified. To further facilitate the measurement, the quartz standard can also be replaced by another single domain ferroelectric crystal as the standard, which has a higher piezoelectric constant while negligible piezoelectric loss. For example, $LiNbO_3$ single crystal has a d_{33} constant about two and a half times larger than that of x-cut quartz and its piezoelectric loss is also very low.

The authors wish to thank Mr. P. Moses for many helps and suggestions concerning this project. This work was supported by the Office of Naval Research.

1) R. Holland: IEEE Trans. Sonics & Ultrasonics SU-14 (1967) 18.
2) *IEEE Standard on Piezoelectricity, 1987* (ANSI/IEEE Std. 176-1987).
3) J. G. Smiths: *IEEE SU-23 (1976) 393.*
4) T. Furukawa, M. Data and E. Fukada: Rep. Progr. Polym. Phys. Jpn. **13** (1970) 375.
5) R. Haase: *Thermodynamics of Irreversible Processes* (Dover, NY, 1990).
6) W. Y. Pan, H. Wang and L. E. Cross: Jpn. J. Appl. Phys. **29** (1990) 1570.

COMPOSITE SENSORS

APPENDIX 24

US005276657A

United States Patent [19]

Newnham et al.

[11] Patent Number: 5,276,657

[45] Date of Patent: * Jan. 4, 1994

[54] METAL-ELECTROACTIVE CERAMIC COMPOSITE ACTUATORS

[75] Inventors: Robert E. Newnham; Qichang C. Xu, both of State College; Shoko Yoshikawa, Bellefonte, all of Pa.

[73] Assignee: The Pennsylvania Research Corporation, University Park, Pa.

[*] Notice: The portion of the term of this patent subsequent to Mar. 12, 2008 has been disclaimed.

[21] Appl. No.: 835,245

[22] Filed: Feb. 12, 1992

[51] Int. Cl.[5] H04R 17/00

[52] U.S. Cl. 367/157; 367/159; 367/163; 310/334; 310/337

[58] Field of Search 310/334, 337; 367/157, 367/158, 159, 161, 163, 165, 174

[56] References Cited

U.S. PATENT DOCUMENTS

2,912,605	11/1959	Tibbetts	367/163
3,166,730	1/1965	Brown, Jr. et al.	367/163
3,277,433	10/1966	Toulis	367/155
4,845,688	7/1989	Butler	367/174
4,862,429	8/1989	Rolt	367/165
4,922,470	5/1990	McMahon et al.	367/163
4,999,819	3/1991	Newnham et al.	367/157

Primary Examiner—J. Woodrow Eldred

Attorney, Agent, or Firm—Thomas J. Monahan

[57] ABSTRACT

The metal-ceramic actuator includes an electroactive substrate having at least a pair of opposed planar surfaces and a determined thickness, with the ceramic substrate being poled in its thickness dimension. Conductive electrodes sandwich the ceramic substrate and are bonded to its planar surfaces. Metal caps, each having a concave cavity bounded by a rim, are bonded to both planar surfaces of the ceramic substrate. A potential is applied to the conductive electrodes to cause an expansion of the ceramic substrate in its thickness dimension and a concomitant contraction in its planar dimensions. The contraction creates a flexure of the metal caps, which flexures are used to actuate another instrumentality.

7 Claims, 4 Drawing Sheets

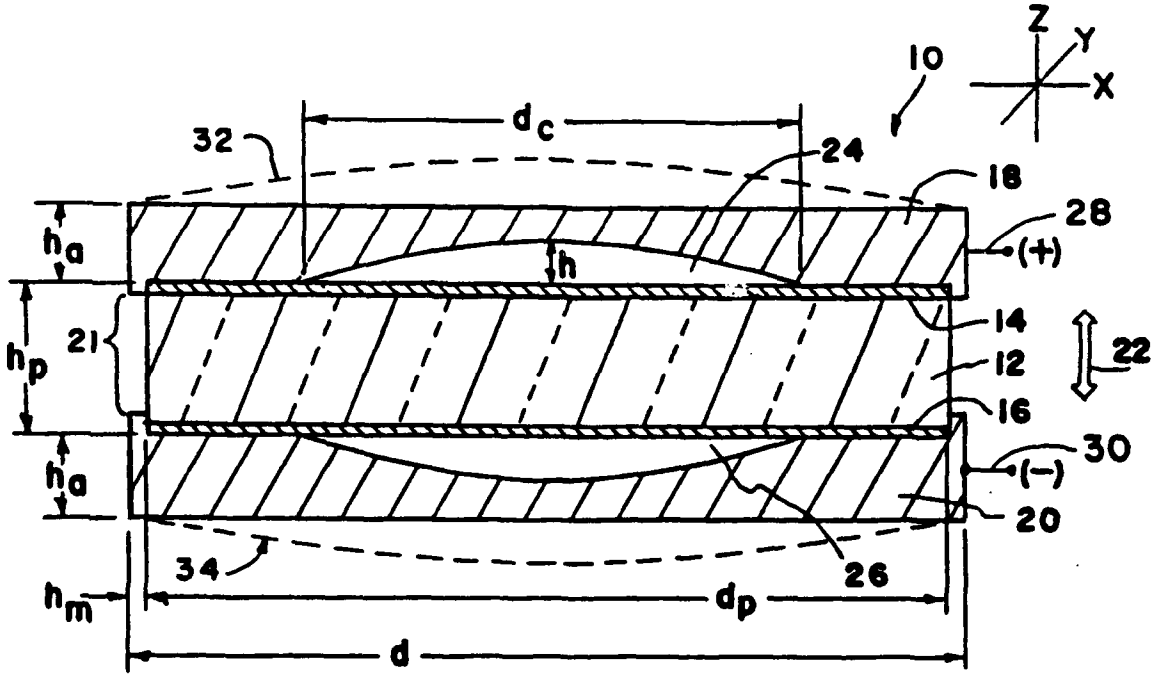

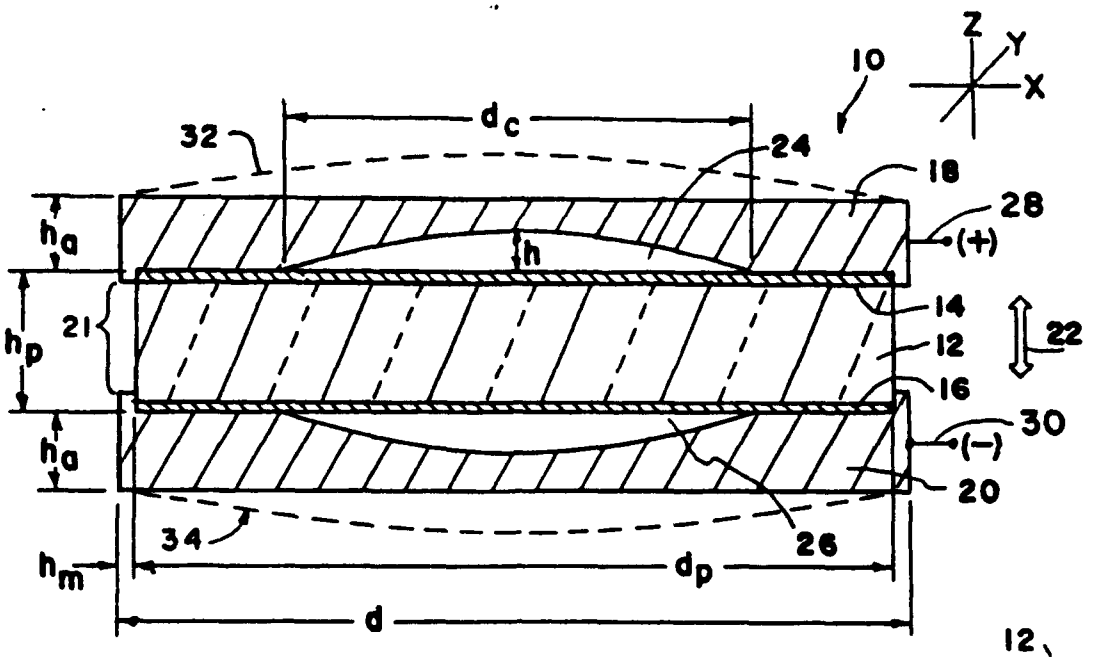

FIG. 1

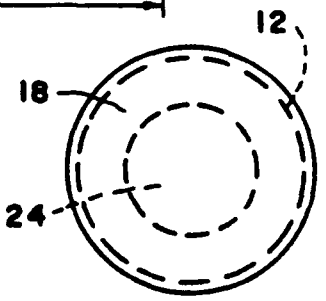

FIG. 2

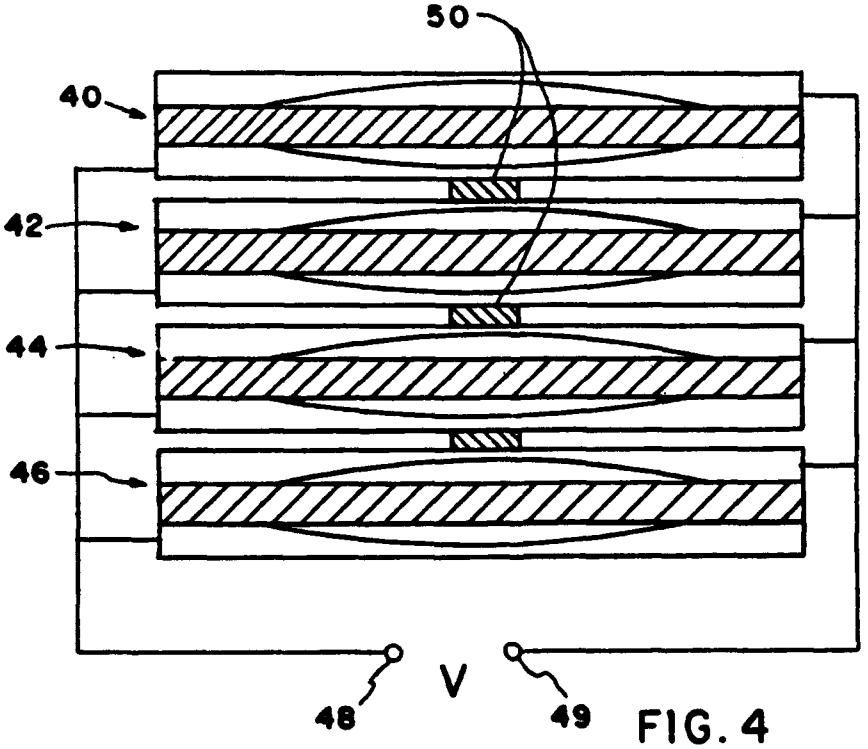

FIG. 4

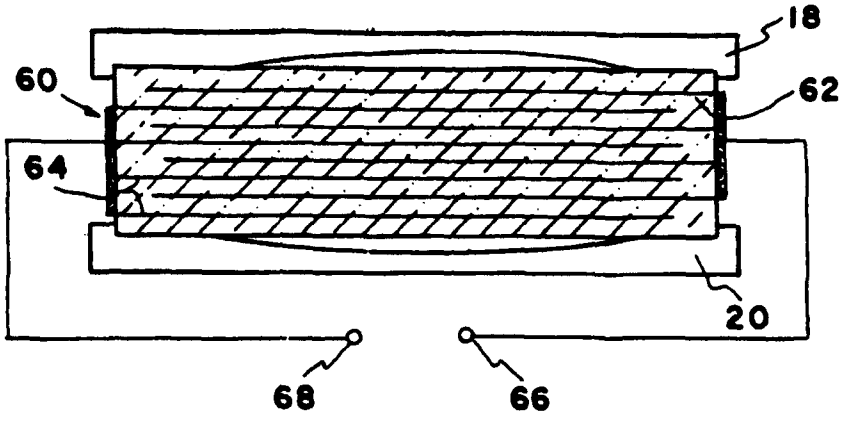

FIG. 5

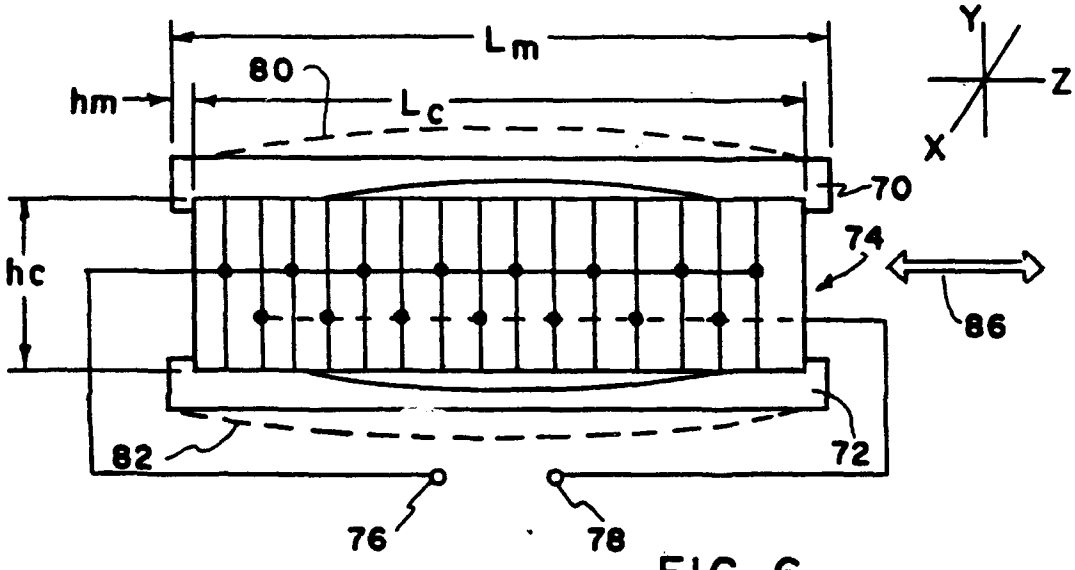

FIG. 6

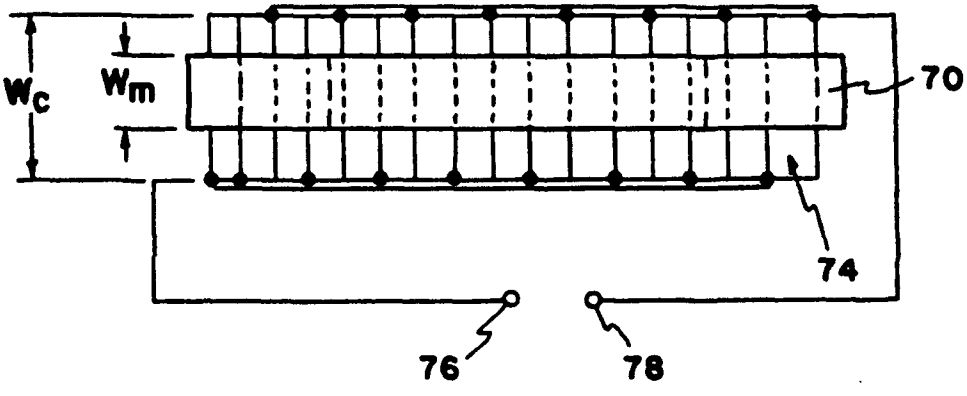

FIG. 7

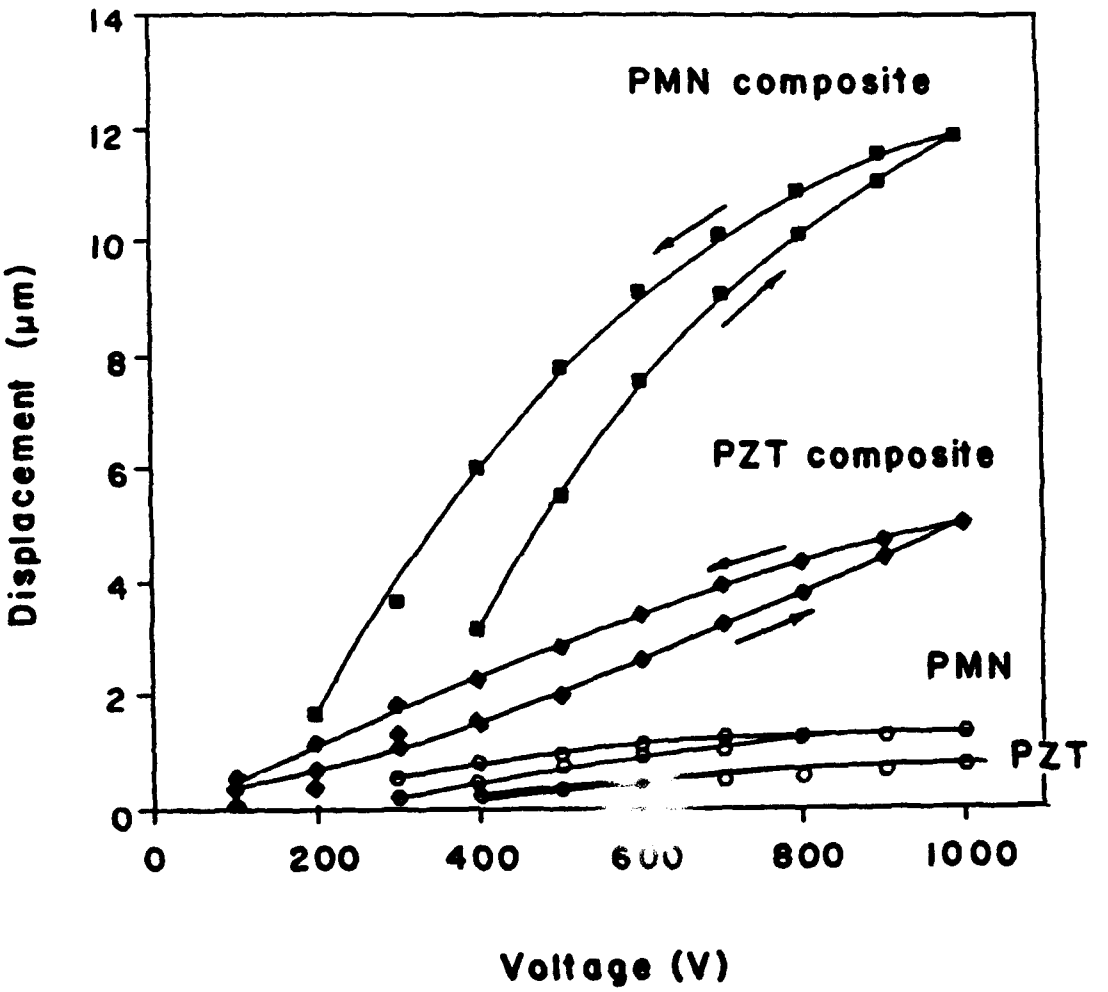
14
12
10
8
6
4
2
0
Displacement (μm)
PMN composite
PZT composite
PMN
PZT
0
200
400
600
800
1000
Voltage (V)

FIG. 3

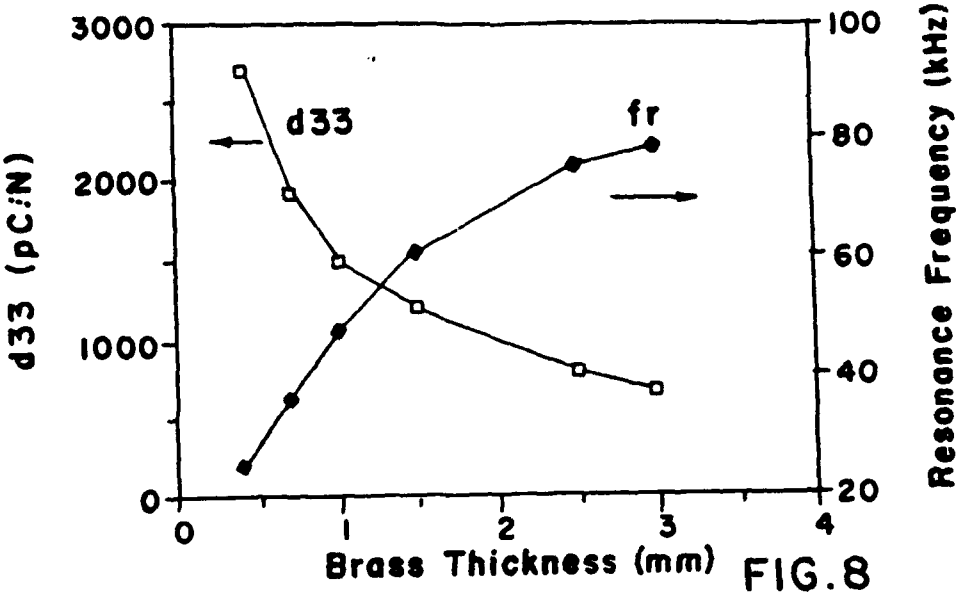

FIG.8

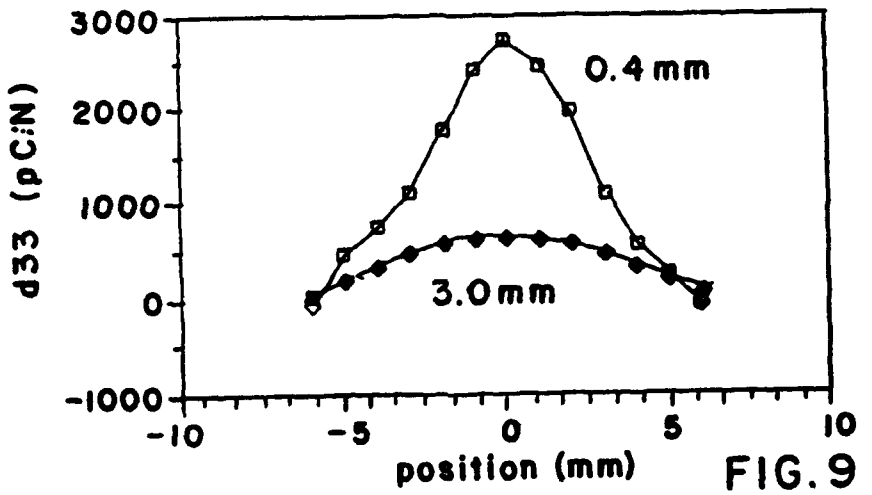

FIG.9

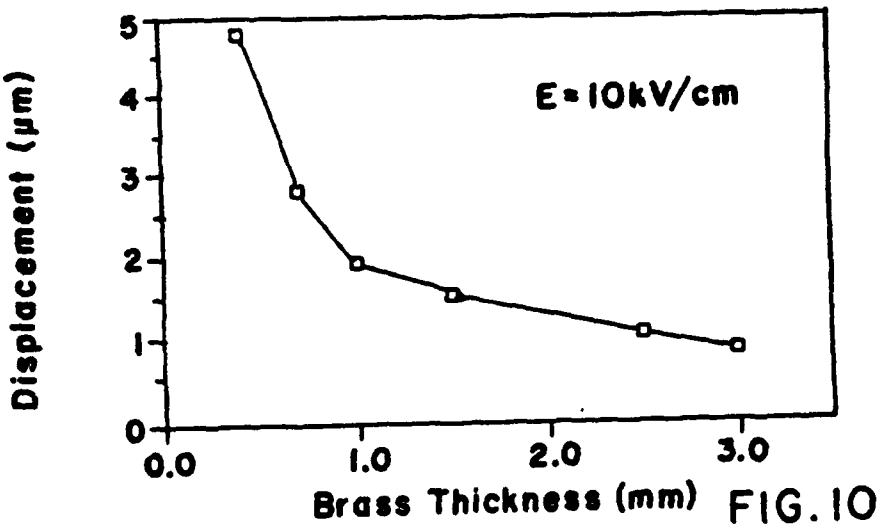

FIG.10

METAL-ELECTROACTIVE CERAMIC COMPOSITE ACTUATORS

GOVERNMENT SUPPORT

This invention was made with Government support under Grant N00014-89-J-1689 and Contract N00014-86-K-0767 awarded by the U. S. Department of the Navy. The Government has certain rights in the invention.

FIELD OF THE INVENTION

This invention relates to electroactive ceramic devices (piezoelectric, electrostrictive, etc.) and, more particularly, to a metal-ceramic electroactive actuator exhibiting large positional displacements.

BACKGROUND OF THE INVENTION

In recent years, piezoelectric, and electrostrictive ceramics have been used as displacement transducers, precision micropositioners, and for other actuator applications. An important drawback to such devices, however, is the fact that the magnitude of strain in such ceramics is limited to approximately 0.1%. Magnification mechanisms have, therefore, been developed to produce sizeable displacements at low voltages. The two most common types of electroactive ceramic actuators are the multi-layer ceramic actuator with internal electrodes, and the cantilevered bimorph actuator.

A bimorph-type actuator will execute a large bending or "wagging" motion with the application of an AC or DC field. Although such actuators exhibit large displacements (generally on the order of several hundred microns), their generative force and response speeds are not high. Multilayer-actuators exhibit significantly larger generative forces, although their displacement values are limited. For instance, a fifteen millimeter multilayer stack provides a displacement of approximately 10 microns. Such a stack characteristically comprises a lead titanate-lead zirconate (PZT) ceramic or a lead titanate-doped lead magnesium niobate (PMN-PT) type ceramic, having a hundred volts of DC applied. There is a need for an electroactive ceramic actuator to provide sizeable displacements with sufficient force to carry out actuator applications.

In U.S. Pat. No. 4,999,819 the inventors hereof previously described an acoustic transducer, of sandwich construction, that was particularly useful for the transformation of hydrostatic pressures to electrical signals. A pair of metal plates were positioned to sandwich a piezoelectric element, with each plate having a cavity formed adjacent to the piezoelectric element. The plates were bonded to the piezoelectric element to provide a unitary structure. The cavities provided a stress-transforming capability which amplified an incoming compressive stress and converted it to a radial extensional stress in the ceramic. The ceramic was generally poled in the thickness dimension and exhibited d_{33}, d_{31} and d_{32} piezoelectric coefficients.

As is known to those skilled in the art, the d_{33} coefficient lies in the plane of a ceramic's poling, whereas the d_{31} and d_{32} coefficients describe the action of the ceramic in a plane that is orthogonal to the direction of poling. In the transducer shown in the '819 patent, the cavities transform most of an incoming stress in the d_{33} direction to the d_{31} and d_{32} directions in the piezoelectric slab. By monitoring the voltage generated across the slab, the resulting pressure wave was sensed. There is no indication in U.S. Pat. No. 4,999,819 of the application or use of the aforedescribed structure for actuation purposes.

Accordingly, it is an object of this invention to provide an improved electroactive, metal-ceramic actuator.

It is another object of this invention to provide a metal-ceramic actuator which exhibits substantially improved actuation distances.

It is another object of this invention to provide a metal-ceramic electroactive actuator of inexpensive design.

SUMMARY OF THE INVENTION

The metal-ceramic actuator includes an electroactive substrate having at least a pair of opposed planar surfaces and a determined thickness, with the ceramic substrate being poled in its thickness dimension. Conductive electrodes sandwich the ceramic substrate and are bonded to its planar surfaces. Metal caps, each having a concave cavity bounded by a rim, are bonded to both planar surfaces of the ceramic substrate. A potential is applied to the conductive electrodes to cause an expansion of the ceramic substrate in its thickness dimension and a concomitant contraction in its planar dimensions. The contraction creates a flexure of the metal caps, which flexures are used to actuate another instrumentality.

DESCRIPTION OF THE DRAWINGS

FIG. 1 is a side sectional view of an actuator embodying the invention;

FIG. 2 is a plan view of the actuator of FIG. 1;

FIG. 3 is a chart showing plots of displacement versus voltage for ceramic actuators constructed in accordance with prior art and actuators constructed in accordance with the invention;

FIG. 4 is an actuator that employs a plurality of the actuators shown in FIG. 1;

FIG. 5 is a sectional view of an actuator embodying the invention, which actuator employs segmented ceramic electroactive slabs with interspersed electrodes;

FIG. 6 is another actuator embodiment constructed in accordance with the invention.

FIG. 7 is a plan view of the actuator of FIG. 6.

FIG. 8 shows the d_{33} coefficient and resonant frequency plotted as a function of cap thickness.

FIG. 9 shows the positional dependance of the d_{33} coefficient for two actuators with cap thicknesses of 0 4 mm and 0.3 mm.

FIG. 10 shows a plot of maximum displacement as a function of cap thickness.

DETAILED DESCRIPTION OF THE INVENTION

Referring to FIGS. 1 and 2, actuator 10 includes a piezoelectric or electrostrictive ceramic disk 12, having conductive electrodes 14 and 16 bonded to its major surfaces. A pair of conductive metal end caps 18 and 20 are bonded to conductive electrodes 14 and 16, respectively. Each end cap is provided with a small lip 21 that extends over the ends of disk 12. In FIG. 2, a plan view is shown of the actuator structure.

If ceramic disk 12 is a piezoelectric material, it is poled, during manufacture, in the directions indicated by arrows 22. If ceramic disk 12 exhibits electrostrictive effects, then it need not be poled.

End caps 18 and 20 are provided with cavities 24 and 26 respectively, so that only the rims that surround the cavities are bonded to ceramic disk 12 and make connection to conductors 14 and 16. A pair of terminals 28 and 30 are connected to end caps 18 and 20, respectively, and provide input conductors for enabling operation of actuator 10.

When a potential is applied across terminals 28 and 30, ceramic disk 12 expands in the z dimension (d_{33}). At the same time, it contracts in the x and y dimensions and (d_{32} and d_{31}), causing end caps 18 and 20 to bow outwardly, as shown by dotted lines 32 and 34, respectively. The bowing action amplifies the actuation distances created by the contraction of ceramic disk 12, and enables the use of the structure as an actuator.

The stress transformation created by the configuration shown in FIG. 1 substantially magnifies the motion of ceramic disk 12's z direction motion. The displacement of each end cap is 10 times larger than that of the ceramic disk alone and exerts a large generative force. The specific values of the displacement and generative force depend on the actuator's design, the diameters of cavities 24 and 26, the depth of the cavities, the thickness and material of end caps 18 and 20, and the thickness of ceramic disk 12.

Piezoelectric actuator materials that are used with the structures shown and described herein are based primarily on the lead zirconate titanate (PZT) family including PLZT($(PbLa)(Zr,Ti)O_3$). Electrostrictive ceramic disks utilize lead magnesium niobate (PMN)-based ceramics. Lead titanate-modified PMN (PMN-PT) is preferred.

Various compositional modifications may also be made in the aforesaid materials.

Metal end caps 18 and 20 may be any metallic material with high conductivity and high modulus. Brass, copper and aluminum are representative materials that are suitable. Requirements of the bonding material which connect end caps 18 and 20 to ceramic disk 12 are strong mechanical bonding between metal and ceramic as well as good electrical conductivity. Examples of such materials are a glass flux containing silver paste, metal mesh with epoxy, very thin layer epoxy solder or active metal brazing alloys.

Referring now to the chart shown in FIG. 3, displacements measured for composite actuators driven by PZT and PMN ceramics are plotted versus voltage. Displacements for uncapped PZT and PMN ceramics are shown for comparison. As shown, displacements larger than 10 microns were obtained with a PMN actuator having brass end caps. A corresponding curve for a composite actuator containing PZT shows a five micron displacement. Ceramic displacements without end caps were on the order of one micron.

As above indicated, one actuator whose performance is plotted in FIG. 3 was a PMN-PT disk, end capped with brass disks. Dimensions of this sample were as follows (using the dimensions shown in FIG. 1).

d = 13 mm; dc = 6 mm; h = 150microns; dp = 11 mm; hp = 1 mm; and hm = 0.4 mm.

The applied electric field was 1 kilovolt per millimeter, and produced a 10 micron displacement. It is to be noted that each of the plots in FIG. 3 shows some hysteresis which should be taken into account in the design of the actuator.

A PZT 501 disk, end capped with brass disks produced a 9.6 micron displacement at one kilovolt per millimeter applied voltage. The dimensions of that sample were as follows: d = 11 mm; dp = 11 mm, dc = 7 mm, hp = 1 mm; h = 50 microns; and hm = 0.5 mm

Referring now to FIG. 4, a stacked actuator arrangement is shown comprising a plurality of individual actuators 40, 42, 44 and 46, all of which are activated in parallel by a voltage supply applied to terminals 48 and 49. Separators 50 enable the displacement of one actuator to be transmitted to an adjacent actuator. Thus, the respective displacements are additive and provide a total displacement that is a multiple of a single transducer.

Turning to FIG. 5, the structure shown in FIG. 1 has been modified to employ a multilayer ceramic part 60. Ceramic part 60 comprises a plurality of ceramic layers having interdigitated electrodes 62 and 64. Electrodes 62 are connected to terminal 66 whereas electrodes 64 are connected to terminal 68. By utilizing this arrangement, the voltage applied across electrodes 66 and 68 can be reduced in value while still achieving a desired voltage per millimeter value. The operation of the actuator of FIG. 5 is in other respects, identical to that shown in FIG. 1.

Turning now to FIGS. 6 and 7, a further preferred arrangement of the invention is shown. In this case, end caps 70 and 72 sandwich ceramic actuator 74, which actuator is oriented so that its d_{33} poled direction is parallel to the planar dimensions of end caps 70 and 72. Ceramic actuator 74 is multilayered, as shown in FIG. 5. Similarly, it comprises a plurality of interdigitated conductive layers with interspersed ceramic layers.

When the actuator of FIG. 6 and 7 is initially constructed, end caps 70 and 72 are constructed so that their overall length is longer than ceramic part 74. Then, when end caps 70 and 72 are bonded to ceramic part 74, they are bonded in a bowed fashion as shown by dotted lines 80 and 82. When, a potential is applied across terminals 76 and 78, multilayer ceramic 74 expands in the direction hown by arrow 86 and causes end caps 70 and 72 to become unbowed.

Using the structure shown in FIGS. 6 and 7, a greater than 15 micron displacement was obtained using an applied voltage of 150 volts. The result was obtained with only one metal end cap in place. If end caps are applied to both sides of multilayer ceramic part 74, a greater than 30 micron displacement can be obtained for same applied voltage. Dimensions of the actuator shown in FIG. 6 & 7 were as follows: Lm = 21.5 mm; Wm = 6.8 mm; hm = 0.5 mm; Lc = 20.5 mm; Wc = 9.6 mm; hc = 9.6 mm; and h = 0.3 mm.

EXPERIMENTAL RESULTS

Composite actuators were made from electroded PZT5A disks (11 mms in diameter and 1 mm thick) and brass end caps (13 mm in diameter with thicknesses ranging from 0.4 to 3 mm). Shallow cavities 6 mm in diameter and 150 micron center depth were machined into the inner surface of each brass cap. The PZT disk and the end caps were bonded around the circumference taking care not to fill the cavity or short circuit the ceramic electrodes. Silver foil (25 micron thickness) and silver paste were used as bonding materials. The composite was heated to 600° C. under stress to solidify the bond. After cooling, the actuator was encapsulated using Spurrs epoxy resin, followed by curing at 70° C. for 12 hours. Electrodes were attached to the brass end caps and the ceramic was poled at 2.5 Mv/m for 15 minutes in an oil bath held at 120° C.

The direct piezoelectric coefficient was measured at a frequency of 100 Hz using a Berlincourt d_{33} meter. The converse piezoelectric coefficient of the ceramic was determined with a laser interferometer. Displacements of the composite actuator were measured with a linear voltage differential transducer having a resolution of approximately 0.05 microns. The effective d_{33} coefficient of a composite was obtained by dividing the strain by the applied electric field. In comparing the resulting d_{33} with that of a ceramic, the total thickness of the composite was employed in calculating the field-induced strain. Resonant frequencies were obtained with a Hewlett Packard L. F. Impedance Analyzer Number 4192A.

FIG. 8 shows the d_{33} coefficient and resonant frequency plotted as a function of brass cap thickness. As expected, thinner end caps flexed easier, resulting in larger piezoelectric coefficients. The d_{33} values were measured at the center of the brass end caps using a Berlincourt d_{33} meter. Values as high as 2500 pC/N were obtained, approximately five times that of PZT 5A alone. The fundamental flextensional resonant frequency decreased rapidly with decreasing brass thickness, dropping to less than 20kHz for a thickness of 0.4 mm.

Piezoelectric effects were largest near the center of the transducer, where the flexural motion was largest. The d_{33} values as a function of position are shown in FIG. 9. Plots are shown for two brass thicknesses of 0.4 and 3.0 mm respectively. Ample working area of several square millimeters was obtained with the actuators.

Maximum displacements obtained with a single brass end cap on an actuator are shown in FIG. 10. The values were recorded with the LVDT system in a field of 1 MV/m which is well below the breakdown field of PZT. The largest displacements were obtained with actuators having thin end caps. It was determined that even thin end caps are capable of exerting forces in excess of 2 kgf. Experiments were also carried out with actuators incorporating PMN ceramics. As mentioned above, PMN does not need to be poled because it utilizes the electrostrictive effect rather than piezoelectric electricity. The PMN composite actuator results are plotted in FIG. 3.

It should be understood that the foregoing description is only illustrative of the invention. Various alternatives and modifications can be devised by those skilled in the art without departing from the invention. Accordingly, the present invention is intended to embrace all such alternatives, modifications and variances which fall within the scope of the appended claims.

We claim:

1. An actuator comprising:

circular electroactive ceramic substrate means having a pair of opposed planar surfaces and a thickness aspect, said substrate means having a d_{33} direction parallel to said thickness aspect and d_{31} and d_{32} directions parallel to said planar surfaces;

conductive electrodes sandwiching said ceramic substrate means and covering said opposed planar surfaces;

a first metal cap having a concave cavity formed therein and exhibiting a continuous rim bounding said cavity, said rim bonded about its entire surface to said conductive electrode on a first said planar surface of said ceramic substrate means;

a second metal cap having a concave cavity formed therein and exhibiting a continuous rim bounding said cavity, said rim bonded about its entire surface to said conductive electrode on a second planar surface of said ceramic substrate means, said second planar surface opposed to said first planar surface; and

means for applying a potential across said conductive electrodes to enable a field in the d_{33} direction that causes a contraction of said ceramic substrate means in the d_{31} and d_{32} directions, and through said bonded rims, a flexure of said metal caps.

2. The actuator of claim 1 wherein said electroactive ceramic substrate is poled along with d_{33} direction and exhibits a piezoelectric characteristic.

3. The actuator of claim 2 wherein said potential is applied to said metal caps.

4. The actuator of claim 1 wherein said electroactive ceramic substrate means exhibits an electrostrictive characteristic.

5. The actuator of claim 1 wherein said electroactive ceramic substrate means comprises a stack of ceramic substrates, with conductive electrodes positioned therebetween, said means for applying a potential connecting one potential to every other conductive electrode and connecting another potential to conductive electrodes not connected to said one potential.

6. The actuator of claim 5 wherein said ceramic substrates and conductive electrodes lie in planes that are parallel to said conductive electrodes.

7. An actuator comprising a plurality of actuators, each actuator structured as recited in claim 1, said actuators stacked one upon the other, with insulating means interspaced therebetween, said means for applying a potential connected in parallel to said plurality of actuators.

* * * * *

APPENDIX 25

METAL-CERAMIC COMPOSITE TRANSDUCER, THE "MOONIE"

Katsuhiko Onitsuka, Aydin Dogan, James F. Tressler
Qichang Xu, Shoko Yoshikawa and Robert E. Newnham

Materials Research Laboratory
The Pennsylvania State University
University Park, PA 16802

Abstract

A new type of metal-ceramic composite transducer, the "Moonie," has been developed by sandwiching a poled lead zirconate titanate (PZT) ceramic between two specially designed metal end caps. Piezoelectric coefficients an order of magnitude larger than PZT were obtained. The metal-ceramic composites are being developed as fish finders, hydrophones, actuators, and transducers with integrated sensing and actuating functions. This paper describes the moonie principle, optimization of the moonie design using finite element analysis, and the performance of the device for several different applications.

KEY WORDS : composite, PZT, transducer, fish finder, hydrophone, actuator

INTRODUCTION

A new type of metal-ceramic composite transducer, the moonie, has been developed by sandwiching a poled lead zirconate titanate (PZT) ceramic between two specially designed metal end caps. Piezoelectric coefficients an order of magnitude larger than PZT were obtained. The metal-ceramic composites are being developed as fish finders, hydrophones, actuators and transducers with integrated sensing and actuating functions. This paper describes the moonie principle, optimization of the moonie design using finite element analysis, and the performance of the device for several different applications.

The moonie consists of a piezoelectric or electrostrictive ceramic disk sandwiched between two metal end caps, each having a crescent-shaped cavity on its inner surface (hence the name "moonie"). These metal end plates serve as mechanical transformers for converting and amplifying the lateral displacement of the ceramic into an axial motion normal to the plates. Both the d_{33} and d_{31} coefficients of the piezoceramic contribute to the axial displacement of the composite. The cavities are used as a mechanical transformer for transforming the high acoustic impedance of the ceramic to the low acoustic impedance of the surrounding medium.[1]-[6]

Figure 1 shows the basic configuration of the moonie transducer. The ceramic element can be a piezoelectric ceramic or an electrostrictive ceramic either in single layer or multilayer form. Electrostrictive ceramics generally show less hysteresis than PZT but are highly nonlinear. Multilayer elements consist of a number of thin ceramic layers with internal electrodes thus have lower drive voltages.

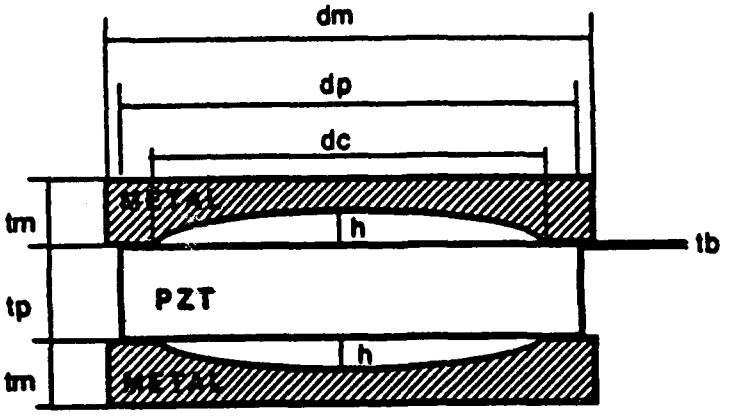

d_m : Metal cap diameter, d_p : PZT diameter, d_c : Cavity diameter, h : Cavity depth
t_m : Metal cap thickness, t_p : PZT thickness, t_b : Bonding layer thickness

Figure 1 The cross sectional view of the moonie transducer

APPLICATIONS OF THE MOONIE

Table 1 shows three applications of the moonie transducer: hydrophones, actuators, and fish finders. The materials and dimensions listed in Table 1 were chosen after considering the properties required for each application. Bonding materials and dimensions are the key factors in designing the properties. Finite Element Analysis (FEA) was used to optimize the geometry of the moonie transducer.

Table 1 Applications of the moonie transducer

	Hydrophone	Actuator	Fish Finder
Function	Pressure sensor	Mechanical actuator	Transceiver
Metal	Brass	Brass	Aluminum
Ceramic	PZT-5	PZT-5, PMN-PT	PZT-4
Bonding	Ag paste	Ag paste, Epoxy	Epoxy
Diameter (mm)	11	11	27-45
Thickness (mm)	5	2-5	10-20
d_{33} (pC/N)	2500	4500	1500
Feature	high sensitivity	high displacement	low side lobes

Imanaka et al. utilized the multilayer moonie actuator to control the scanning angle for a micro-optical scanner. Figure 2 shows the schematic diagram of the optical scanner unit containing the multilayer moonie actuator. By replacing the usual multilayer actuator with a multilayer moonie, reduction of the operating voltage and miniaturization of the optical scanner unit size were achieved.[7]-[9]

FINITE ELEMENT ANALYSIS (FEA)

A theoretical analysis of the PZT-metal composite was performed using the finite element analysis program, SAP90. A quarter-section axially symmetric model is shown in Figure 3. The mesh contained 270 quadrilateral shaped elements with 350 nodal points. The material properties used in this analysis are listed in Table 2.

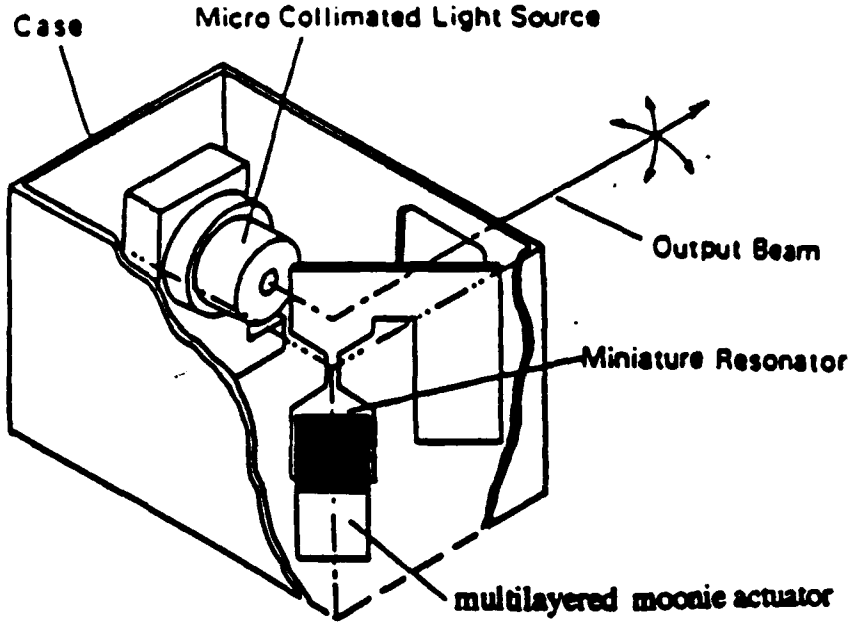

Figure 2 Schematic illustration of the optical scanner unit incorporated with the multilayer moonie actuator [7]-[9]

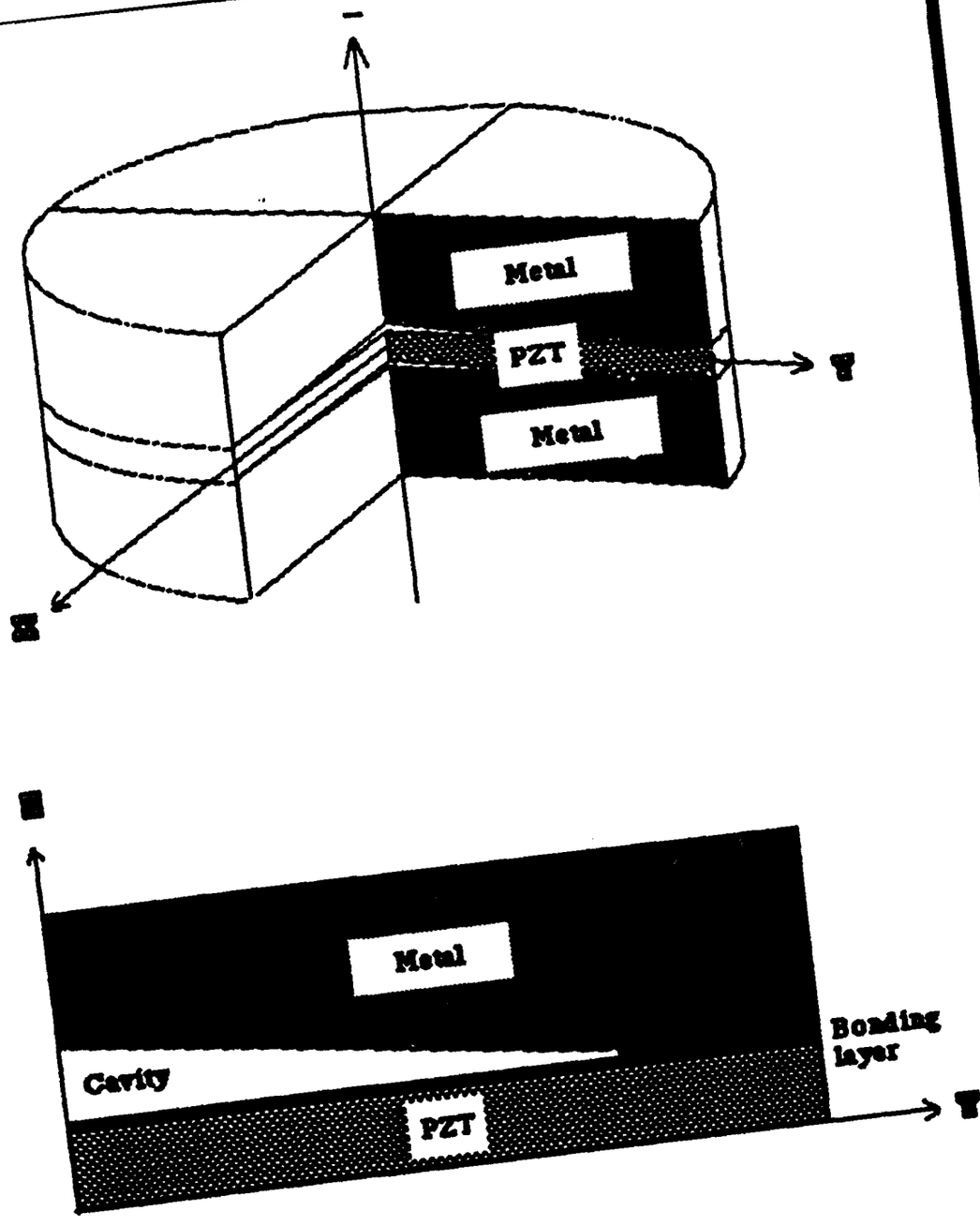

Figure 3 Cross sectional view of the moonie (top) and one quarter of the axisymmetric model for FEA (bottom)

Table 2. Materials properties for the FEA

Material	Density (g/cm^3)	Young's modulus (N/m^2)	Poisson's ratio
PZT-4	7.6	$7.0x10^{10}$	0.33
PZT-5	7.6	$7.0x10^{10}$	0.33
Brass	8.4	$10.5x10^{10}$	0.35
Aluminum	2.7	$6.9x10^{10}$	0.33
Epoxy	1.2	$2.5x10^{9}$	0.40

CALCULATED AND EXPERIMENTAL RESULTS

(1) Moonie fish finder

A fish finder is an underwater transducer which converts a high voltage electrical pulse to mechanical motion. The mechanical motion creates a sound wave that is transmitted efficiently through the water in the desired direction. The sound wave reflects off targets, such as fish or the bottom of the water, and travels back to the transducer. The reflected sound wave "echo" mechanically deflects the transducer and a very low voltage pulse is created. The distance to the target is determined by measuring the time difference between the transmitted pulse and received echo.[10] In some fish finder applications, transducers having a wide main lobe without side lobes are used in searching for fish over a wide area.

Using FEA dynamic analysis, the lowest three vibration modes were calculated and are illustrated in Figure 4. In the first vibration mode, the center of the transducer has maximum displacement. The first vibration mode is found to be useful as a fish finder because it has a wider main lobe than the conventional fish finder design.[6]

The resonant frequencies of the moonie are dependent upon such dimensions as the metal cap diameter, PZT diameter, cavity diameter, metal thickness, PZT thickness and

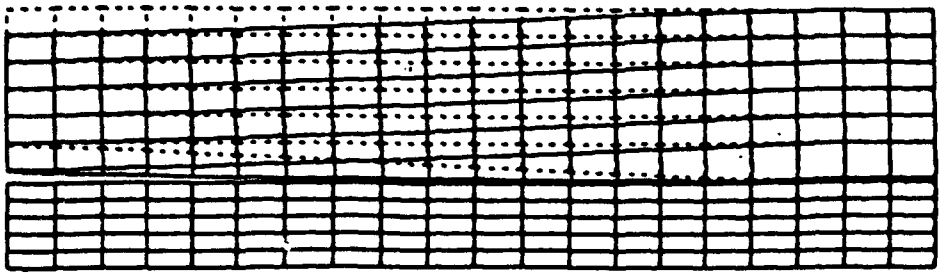

1st. vibration mode

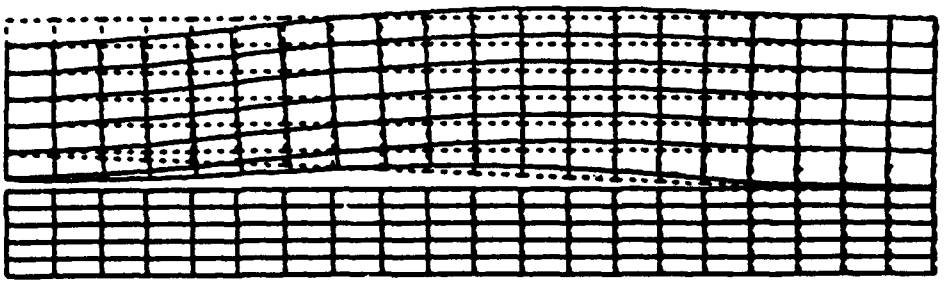

2nd. vibration mode

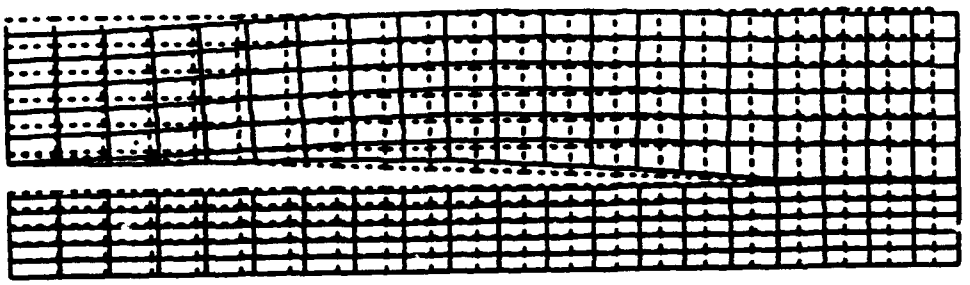

3rd. vibration mode

Figure 4 Quarter section views of the three vibration modes calculated by FEA

cavity depth. By using FEA, the appropriate shape and dimensions can be designed for fish finders with selected resonant frequencies. Figure 5 shows good agreement between experimental and calculated frequencies for the first resonant mode. In Figure 6, the first resonant frequencies measured in actuators with different brass end cap thicknesses are also in good accordance with those calculated.

(2) Moonie hydrophone

One important sensor application is the hydrophone, a device used to detect weak pressure waves in fluids. In many hydrophone applications, there is a great demand for piezoelectric transducers with high pressure tolerance, high dielectric constant (K), high hydrostatic piezoelectric charge coefficient (d_h), high hydrostatic voltage coefficient (g_h), and consequently a high figure of merit ($d_h.g_h$). PZT ceramics have high d_{33} and d_{31}, but their d_h ($= d_{33} + 2\,d_{31}$) values are very low because d_{31} and d_{33} have opposite signs.[10]

In the last decade, several piezoceramic ceramic-polymer composites with different connectivity patterns have been developed for hydrophone and medical transducer applications [11]-[14]. The advantages of these composites over ceramics include higher figure of merit ($d_h.g_h$) to enhance the sensitivity, increased mechanical compliance, smaller acoustic impedance for matching to water or tissue, and lower transverse electromechanical coupling coefficient. Disadvantages of these ceramic-polymer composite transducers however, are lower dielectric constant and lower pressure tolerance than their ceramic counterparts.

PZT-brass composite moonies with dimensions: $d_m = d_p = 11.0$, $d_c = 7.6$, $t_p = 1.1$, $t_m = 1.2$ and $h = 0.15$ (all in mm) were fabricated for the experiment. The brass end caps were bonded to a PZT-5 disk with capacitor electrode silver paste and fired at 600 °C for 10 min. Brass was chosen for its lower thermal expansion coefficient (approximately 15 ppm / °C).

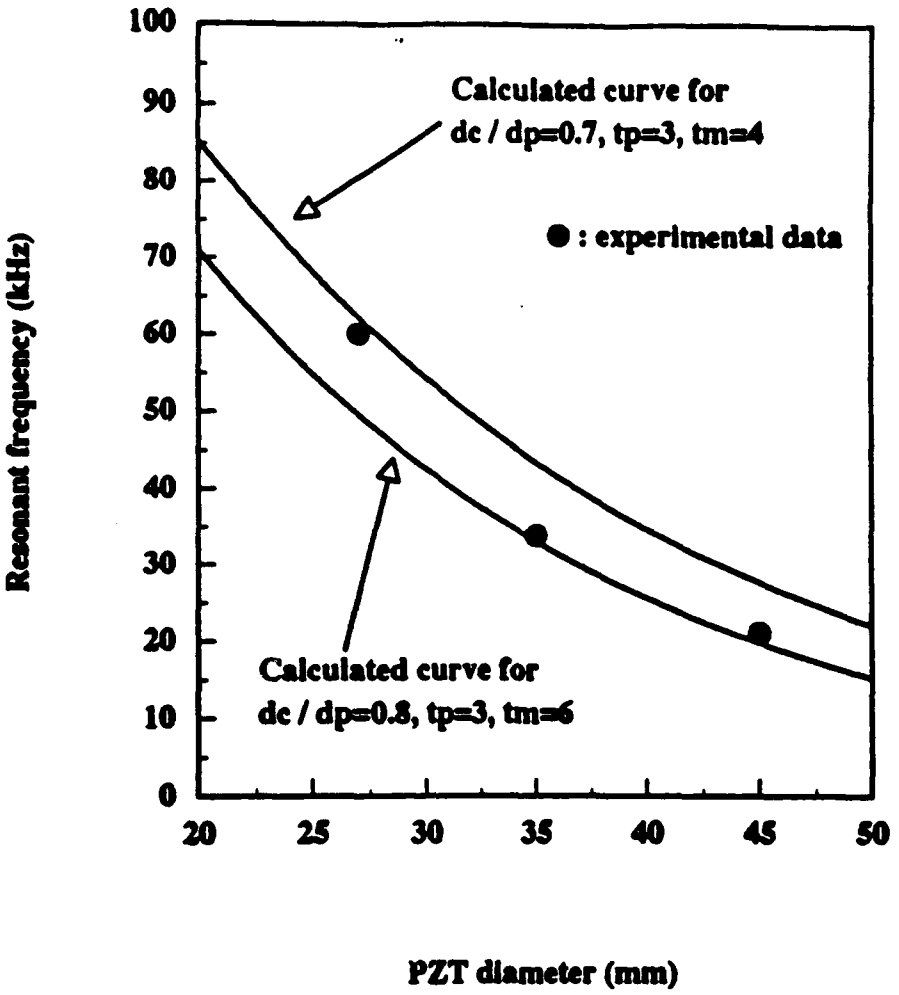

Figure 5 Comparison in the first resonant frequencies calculated by FEA with experimental values plotted as a function of the PZT diameter

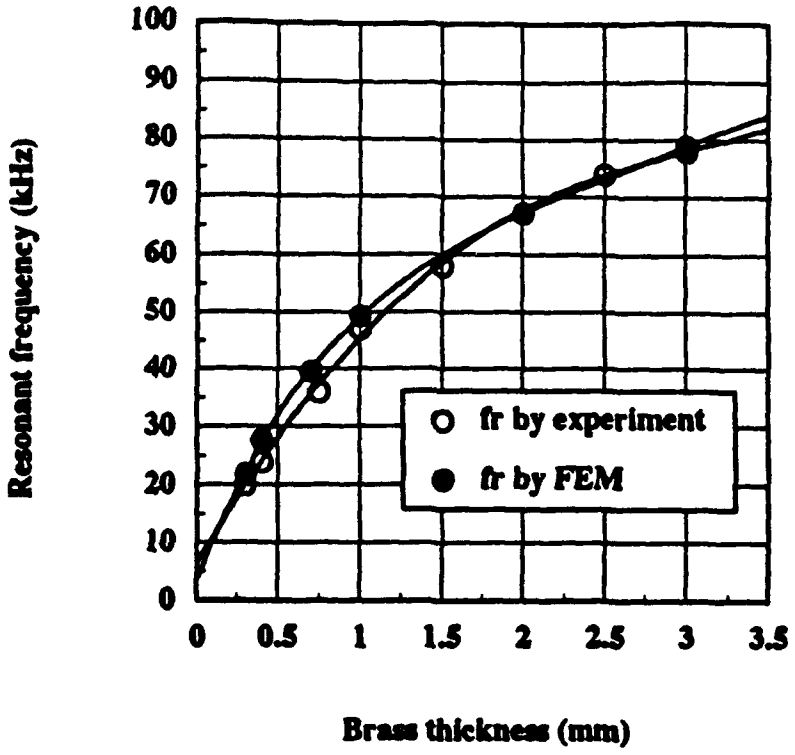

Figure 6 Comparison in the first resonant frequencies calculated by FEA with experimental values plotted as a function of the brass cap thickness

Dimensions : dp=10.8, dm=11.2, dc=8.5, tp=1, tb=0.02, h=0.2 (all in mm)

The moonie composite enhances d_h by converting a portion of the z-directional stress into large radial stresses of opposite sign, thereby causing the d_{33} and d_{31} contributions to d_h to add rather than subtract, leading to a high d_h thus a high figure of merit. Figure 7 shows a comparison of figure of merit of different materials and composites. The moonie exceeds 50,000 x 10^{-15} m^2/N in the figure of merit, which is 500 times larger than the PZT ceramic.[3]

Figure 8 shows the experimental results for d_h and g_h plotted as a function of hydrostatic pressure up to 1000 psi (7.0 MPa). The moonie hydrophone transducer exhibits a high figure of merit as well as a high pressure tolerance with very little aging under static hydrostatic pressures of 350 psi (2.5 MPa).[3]

Figures 9 show the results of the stress analysis when unit hydrostatic pressure was applied to the surface of the transducer. In the longitudinal z-direction (Figure 9a), the stress distribution in the PZT is rather complex. There are 13-15 units of compressive stress concentration at the inner edge of the bonding. On the other hand, at the outer edge of the PZT, 4-6 units of extensive stress concentration is induced. Since ceramics are usually weakest under tensile stresses, the outer edge of the PZT must be reinforced. In the radial direction (Figure 9b), mainly extensive stresses, shown as the ++ region in Figure 9b, are induced in the PZT ceramics, except near the bonded region. A similar stress distribution was obtained in the tangential direction. The extensive forces in the radial and tangential direction in the PZT, coupled to the moonie structure, make the moonie a highly sensitive hydrophone.[5]

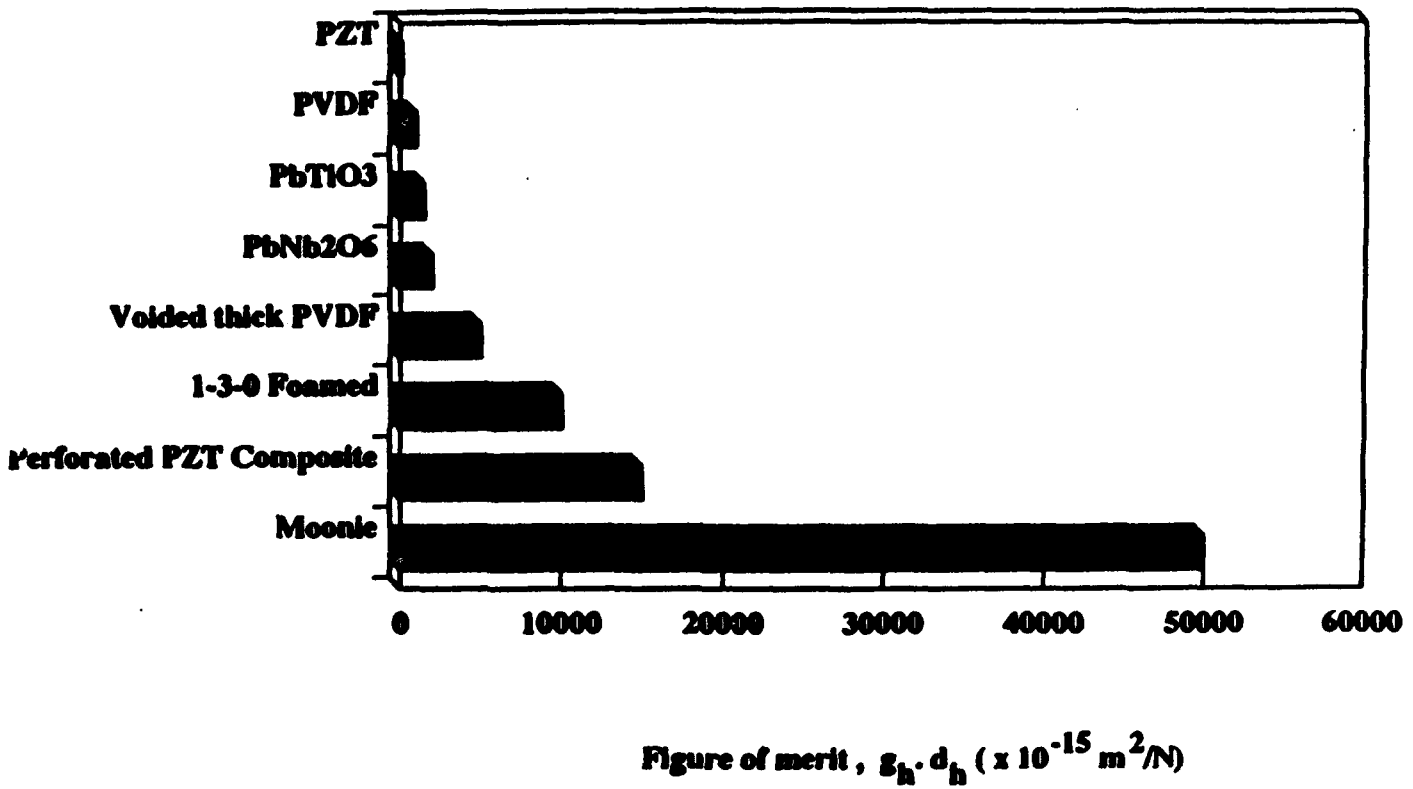

Figure 7 Comparison of figure of merit of different materials and composites for hydrophone application [3] and [11] - [14]

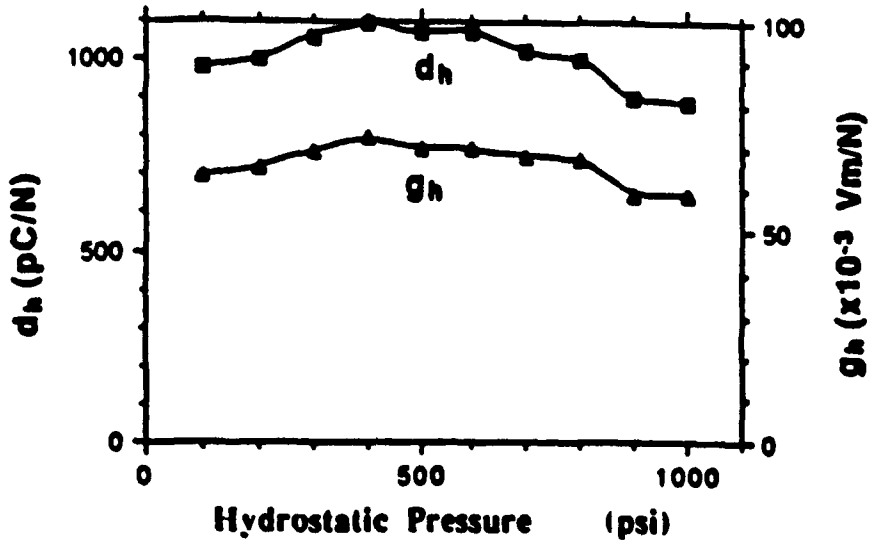

Figure 8 d_h and g_h of the moonie hydrophone as a function of hydrostatic pressure

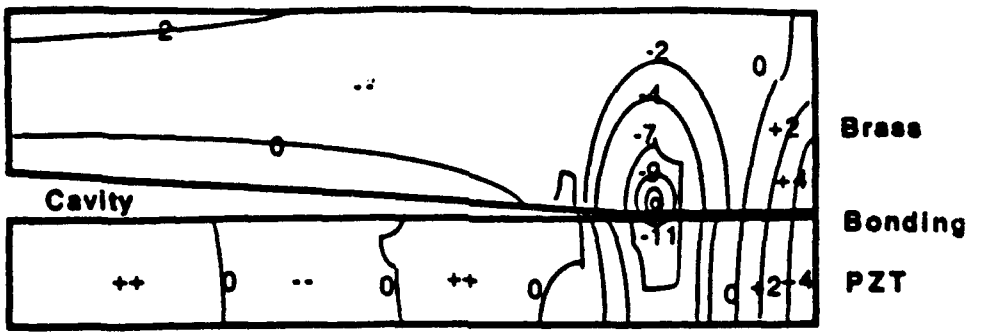

Figure 9a Londitudinal z-directional stress distribution under unit hydrostatic pressure

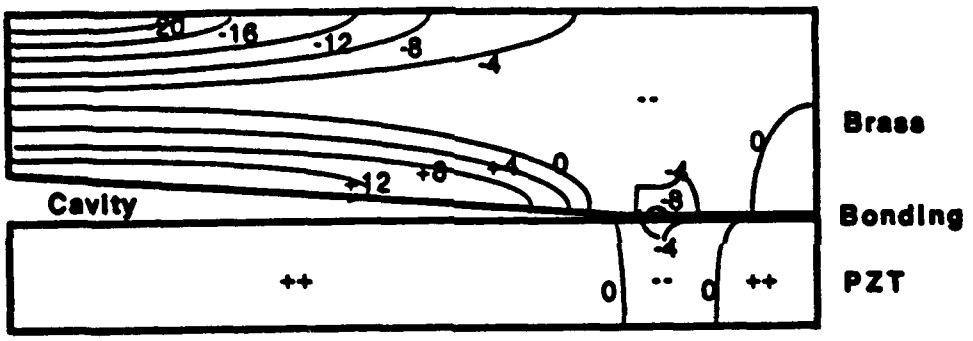

Figure 9b Radial r-directional stress distribution under unit hydrostatic pressure

(3) Moonie actuator

Actuators are electromechanical transducers which develop useful strains by controlling an electric field applied. Figure 10 illustrates the two common types of piezoelectric actuator, the multilayer ceramic actuator with internal electrodes, and the cantilevered bimorph actuator, together with a new type of multistacked multilayered moonie (multi-multi moonie). Multi-multi moonies with large displacements are made by inserting multilayered ceramic actuators between moonie end caps and stacking several moonies together. Normal multilayer actuators produce a large force, but only small displacements. Conversely, bimorphs produce large displacements but the forces are very small. The moonie actuator combines the advantages of both by providing both large displacements and reasonably large generative force.[15]

The desirable properties of actuators are:

1) Large displacement (Large strain)

2) Small hysteresis (Position reproducibility)

3) Small size and weight

4) High power

5) Quick response time

6) Low driving voltage

7) Wide working temperature range

8) No aging

The dependence of the d_{33} coefficient and the first resonant frequency on the brass thickness is shown in Figure 11 . The dimensions of the PZT moonies were d_m = 11.2, d_p =10.8, d_c = 8.5, t_p = 1.0, t_m = 0.3 to 2.5, t_b = 0.02, and h = 0.2 (all in mm). Silver filled epoxy was used as the bonding agent. By reducing the thickness of the end caps, the d_{33} values increase dramatically. Piezoelectric effective d_{33} coefficient of about 13,000 pC/N was obtained for brass thicknesses of 0.3 mm.

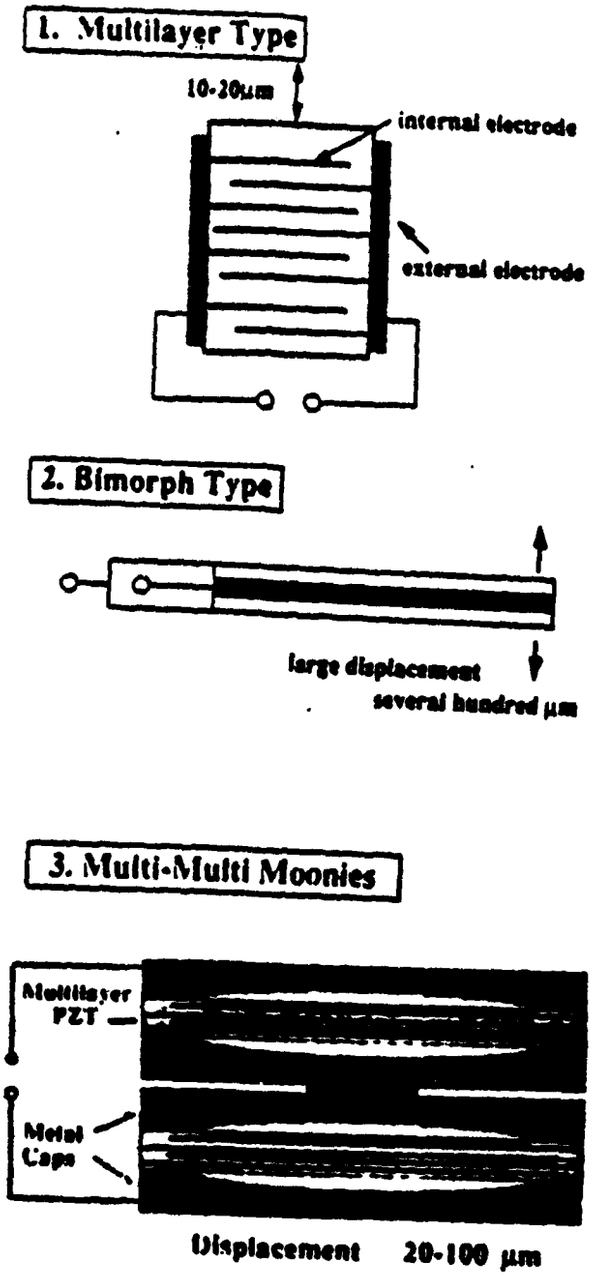

Figure 10 Two common type of actuators and multi-multi moonie actuator

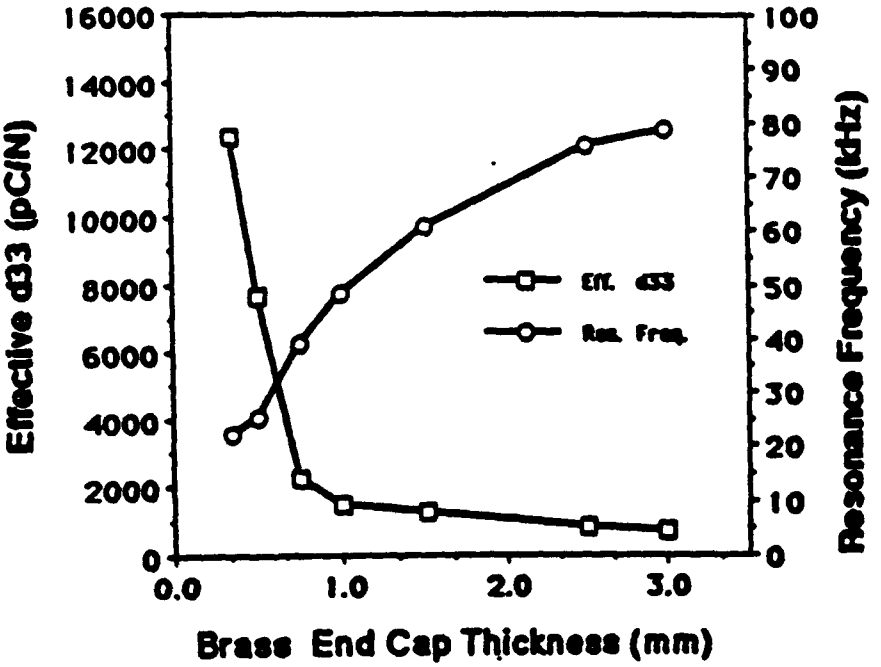

Figure 11 Brass thickness dependence of the d33 and the first resonant frequency

Figure 12 shows the relationship between displacement and brass thickness for a single layer moonie actuator. By decreasing the brass thickness, the displacement increases in the same manner as the effective d_{33} coefficient. A single moonie actuator with brass cap thickness of 0.3 mm can produce a 22 μm displacement under applied electric field of 1 kV/mm.

Figure 13 describes the relationship between displacement and applied force for a moonie actuator having 0.3 mm thick brass caps. Even though the displacements are very high at the center of the brass end caps, the generative force at the center is low. Generative force increases when the location of the measuring point is moved from the center to the edge, while displacement decreases. The moonie can carry 300 grams force by sacrificing one third of its displacement, reducing the value from 22 to 13 μm.

Figure 14 shows the displacement versus electric field curves for a doubly-stacked actuator driven by PZT-5A disk. A displacement of about 40 μm can be obtained under a field of 1 kV/mm, which is twice the single moonie displacement and nearly 20 times that of the uncapped ceramic.

(4) Integrated Sensors & Actuators

The elimination of mechanical vibration or acoustic noise has achieved considerable attention in recent years, both on the macroscopic (smart shock absorbers) and microscopic (active optic systems) scale. The fundamental parameters that must be considered for a vibration control device are its response time, as well as the force and vibration displacement amplitude that has to be cancel. Once these criteria have been met for a particular application, it then becomes desirable to reduce costs by miniaturizing and/or reducing the power delivered to the device.

Using this information, it became our objective to fabricate a vibration control device based on the moonie actuator. In order to produce the most efficient device, the sensing and actuating functions were integrated into a single composite. The prototype

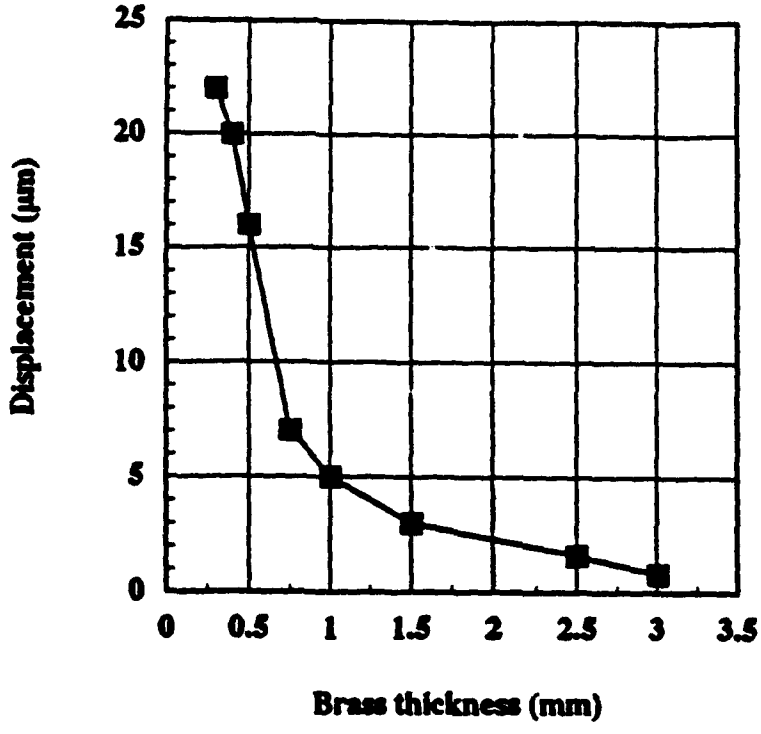

Figure 12 Brass thickness dependence of the maximum displacement at the center of the epoxy bondedmoonie actuator under an applied electric field of 1 kV/mm

Dimensions : dp=10.8, dm=11.2, dc=8.5, tp=1, tb=0.02, h=0.2 (all in mm)

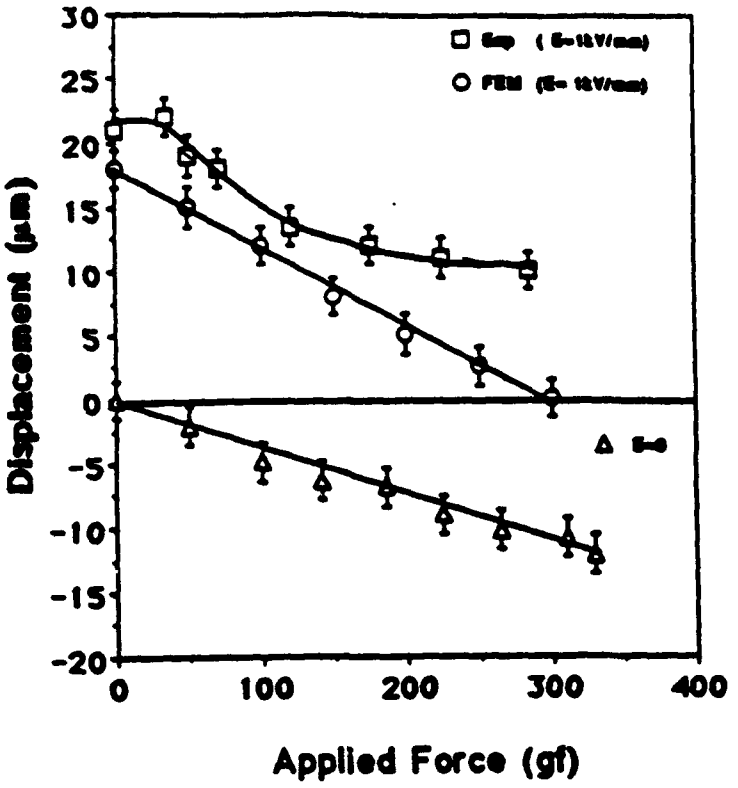

Figure 13 Displacement vs. load curve under an applied 1 kV/mm electric field for the moonie actuator

Dimensions : dp=10.8 dm=11.2, dc=9.0, tm=0.4, tp=1.0, tb=0.02, h=0.2 (all in mm)

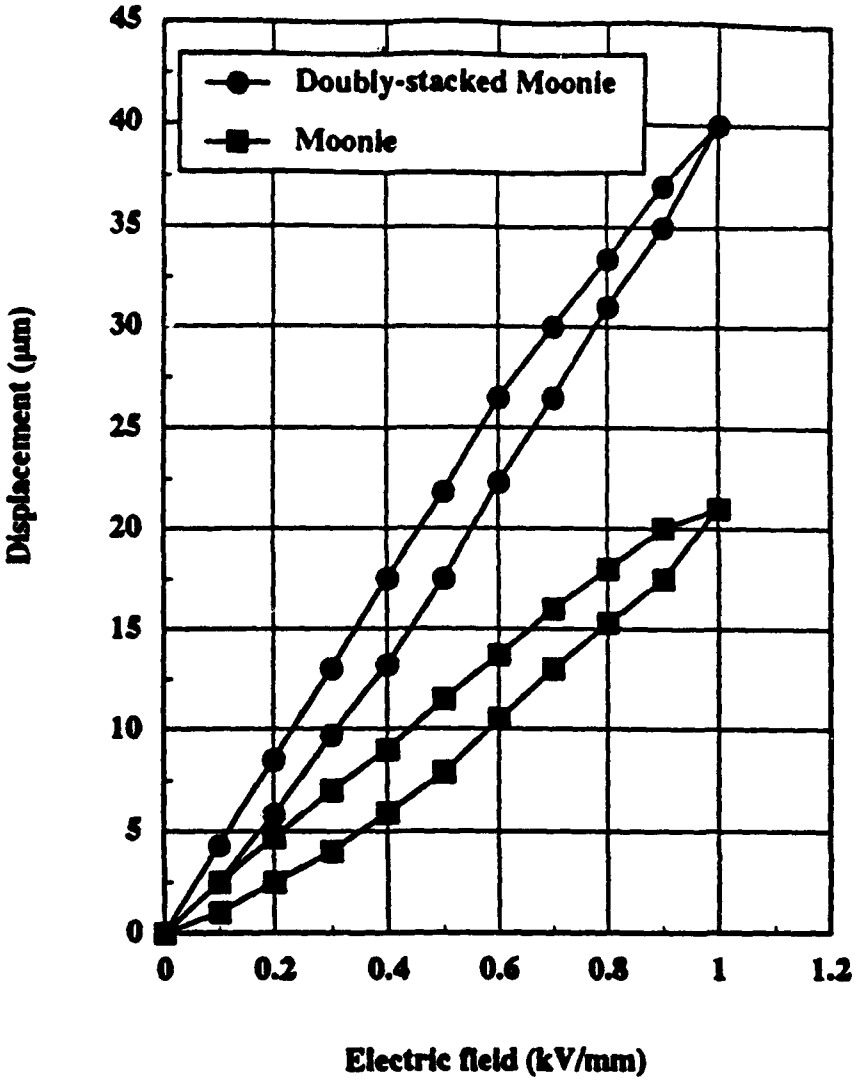

Figure 14 The displacement vs. electric field curves for the moonie actuator and doubly-stacked moonie actuator

Dimensions : dp=10.8, dm=11.2, dc=8.5, tp=1, tm=0.3, tb=0.02, h=0.2 (all in mm)

design is shown in Figure 15. The actuator portion of the device consists of the standard moonie, 11 mm in diameter and 3 mm thick. The sensor is a separate piece of piezoceramic (PZT), 0.1 mm thick, which was imbedded within the upper end cap. The sensor detects sinusoidal vibrations normal to the actuator surface, as shown in the Figure 15, then via a feedback loop, sends a signal of appropriate amplitude and phase back to the actuator so that the latter effectively cancels the external vibration.

The ability of the moonie actuator to actively control external vibrations was determined by placing the device atop a vibrating multilayer actuator of known frequency and displacement amplitude. The dynamic frequency range of the sensor was found by applying a sinusoidal AC field to the moonie actuator and observing the resulting vibration signal on an oscilloscope. The response remained relatively flat between 100 and 6000 Hz.

The data in Figure 16 show that the integrated sensor/actuator device can indeed be used to cancel external vibrations. The horizontal axis shows the 1 kHz electric field applied to the moonie actuator when the field applied (at 1 kHz) to the multilayer vibration source was either 75 V/mm, 125 V/mm, or 250 V/mm. The vertical axis shows the corresponding net vibration signal amplitude, which comes from the sum of the multilayer and moonie vibrations. The results show that whenever the applied fields and phase shift into the moonie are adjusted to the appropriate magnitude, the net vibration signal goes to zero, indicating that the integrated sensor/actuator device has effectively canceled the external vibration. The reason the phase shift is 1° rather than the expected 180° was due to the polarization direction of the sensor being opposite that of the actuator.

Figure 17 shows how the net vibration signal amplitude changes with phase shift when the applied field into the multilayer is 125 V/mm and the field applied to the moonie is 7.05 V/mm. These data show that when the phase shift between the two field is slightly greater than 0°, the moonie and multilayer vibrations have the same displacement amplitude and are exactly 180° out-of-phase, resulting in no net vibration signal.

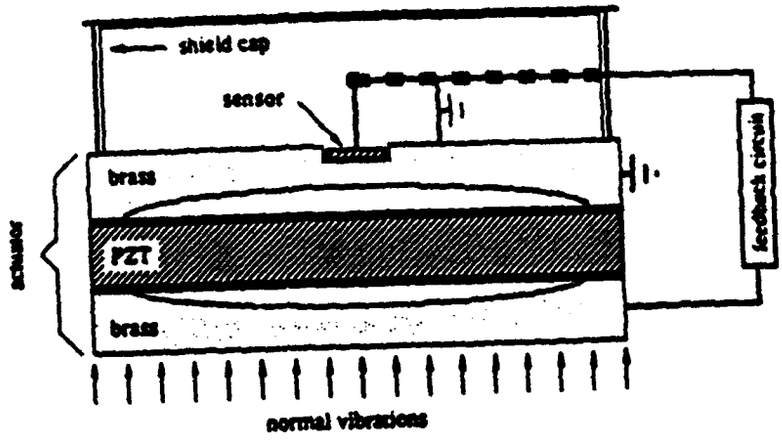

Figure 15 Schematic illustration of the integrated sensor and actuator

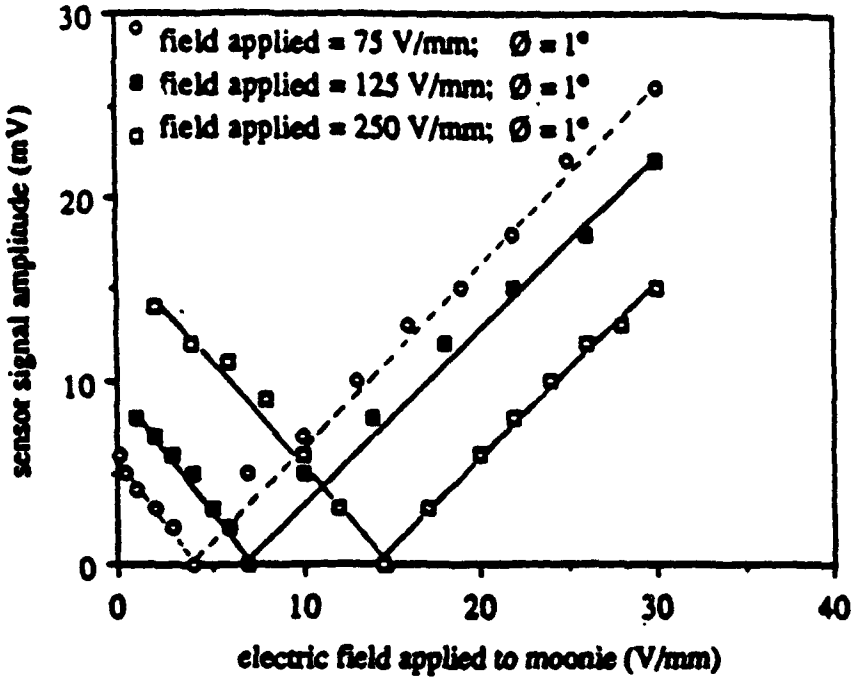

Figure 16 Net sensor signal response for three different field applied to the multilayer vibration source as a function of electric field applied to the moonie at a frequency of 1 kHz

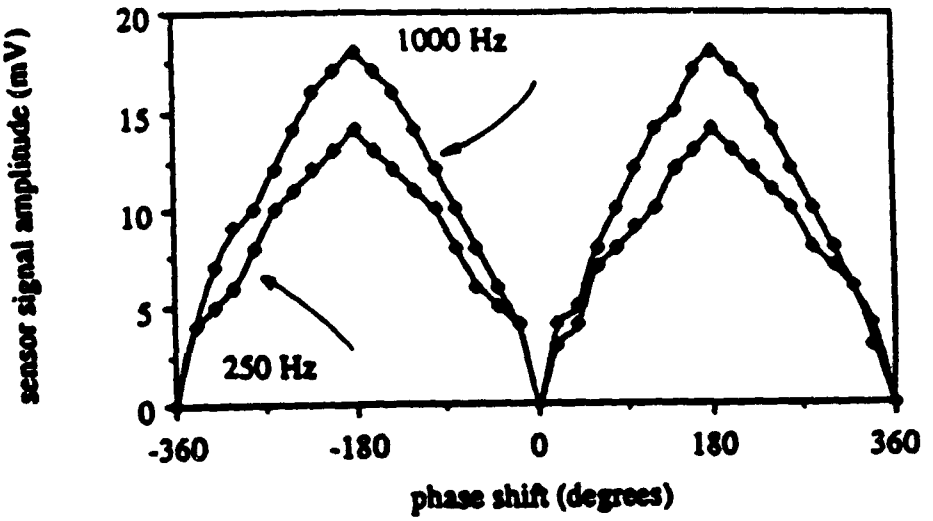

Figure 17 Sensor signal response as a function of phase shift of the electric field applied to the moonie

Figure 18 shows the applied electric field and phase shift (feed back signal) needed to be supplied to the moonie actuator in order to cancel the external vibration over the shown frequency range when the field applied to the multilayer was 75 V/mm.

Figure 19 superimposes the subsequent sensor signal amplitude detected from the multilayer vibration source both with and without the feedback signal activated. These data show that when the feedback field given in Figure 18 is activated, the multilayer vibration signal can be completely suppressed over this frequency range. The reason 2500 Hz was chosen as the cut-off frequency was the inability to prevent "ultrasonic floating" (which arose from incomplete coupling) by the moonie atop the multilayer at higher frequencies.

The minimum and maximum electric fields into the moonie actuator for which the sensor signal remained sinusoidal were 200 V/mm and 370 V/mm, respectively, and were independent of frequency. These fields thus define the dynamic displacement range that the sensor is capable of detecting as being between 0.35 nm and 0.65 μm (as calculated by finite element analysis). [6]

Lastly, the response time of the device, 20 μsec, was estimated from the resonant frequency of the actuator, 50 kHz.

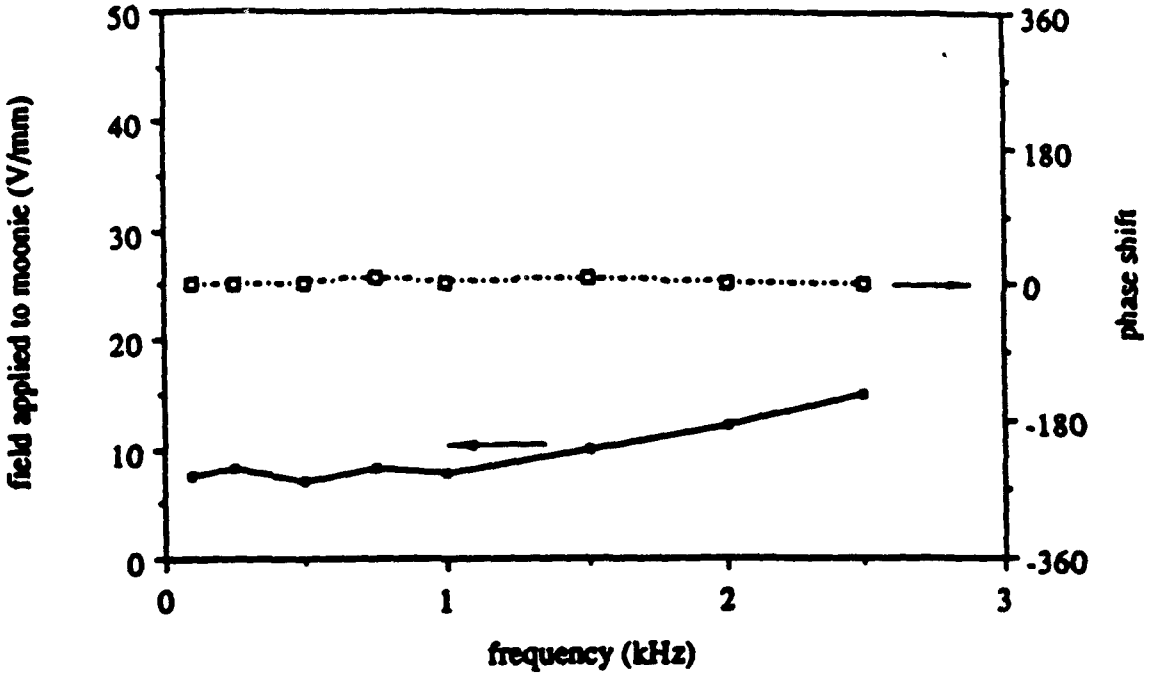

Figure 18 Field and phase shift applied to the moonie actuator needed to cancel the external vibration when the field applied to the multilayer vibration source is 75 V/mm

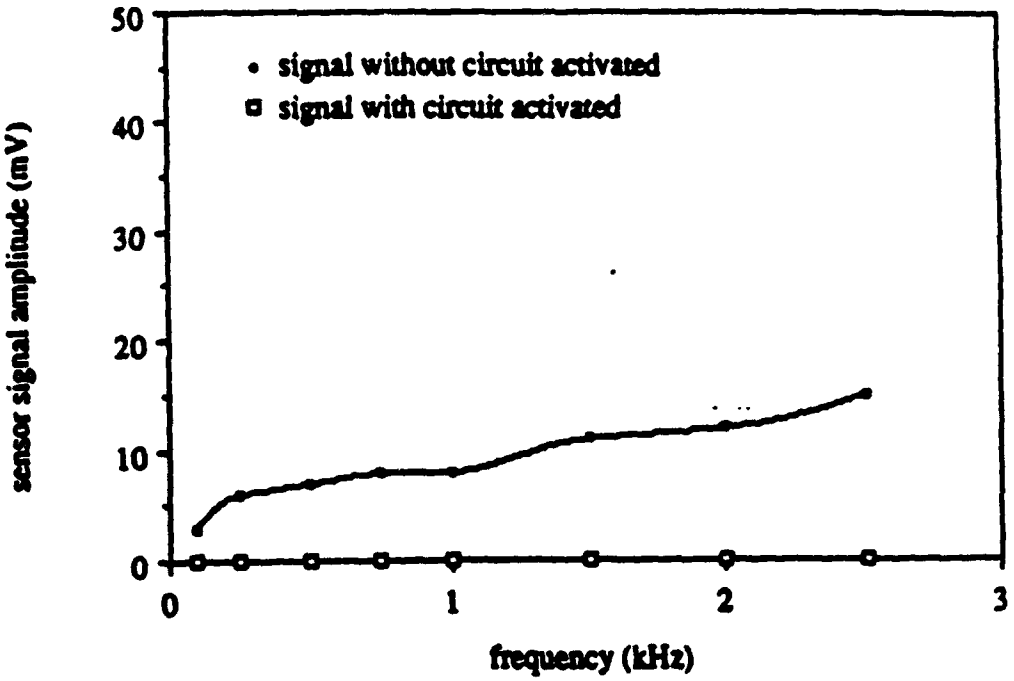

Figure 19 Sensor signal response both with and without the feedback circuit activated

SUMMARY

1. The moonie design has been shown to work well for both sensing and actuating functions.
2. Three specific applications for the moonie have been developed: hydrophone sensors, transceivers for fish finders, and actuators.
3. Finite Element Analysis has been shown to be an effective design method for optimizing the properties required for each application.
4. PZT-brass moonie hydrophones with redistributed stresses show a very high figure of merit as well as high withstanding hydrostatic pressure.
5. A single moonie actuator with brass caps 0.3 mm thick has effective d_{33} coefficients of about 13,000 pC/N, and can produce a 22 μm displacement under applied electric field of 1 kV/mm. By decreasing the brass thickness, the displacement increases in the same manner as the d_{33} coefficient.
6. A doubly-stacked actuator produced 40 μm displacement under a field of 1 kV/mm, which was twice the single moonie displacement and nearly 20 times that of the uncapped ceramic.
7. The newly designed integrated sensor/actuator device has effectively canceled the external vibration.

REFERENCES

(1) R. E. Newnham, G. R. Ruschau , " Smart Electroceramics," J. Am. Ceram. Soc., 74 [3] pp. 463-480 (1991).

(2) Y. Sugawara, K. Onitsuka, S. Yoshikawa, Q. C. Xu, R. E. Newnham and K. Uchino, "Metal Ceramic Composite Actuators", J. of Am. Ceram. Soc. 74, No 4, pp. 996 (1992).

(3) Q.C. Xu, S. Yoshikawa, J. R. Belsick and R. E. Newnham, "Piezoelectric Composites with High Sensitivity and High Capacitance for Use at High Pressure", IEEE Trans. on UFFC Vol. 38, Nov., pp. 634-639 (1991).

(4) Q.C. Xu, A.Dogan, J. Tressler, S. Yoshikawa and R. E. Newnham, "Ceramic-Metal Composite Actuator", Ultrasonic Symposium Proceedings (1991).

(5) R. E. Newnham, Q.C. Xu, K. Onitsuka, S. Yoshikawa, "A New Type of Flextensional Transducer", Proc. of Third International Workshop on Transducers for Sonics and Ultrasonics, pp. 123, May 6-8, Orlande Florida (1992).

(6) K. Onitsuka, Ph.D. thesis, "Effect of Bonding and Geometry on the Flextensional Transducer, "Moonie", The Pennsylvania State University (1993).

(7) H. Goto and K. Imanaka, "Super compact dual axis optical scanning unit applying a torsional spring resonator driven by a piezoelectric actuator", Proc. of SPIE, Vol. 1544, pp. 272-281 (1991).

(8) K. Imanaka, "Micro hybrid integrated devices and components; Micro Photonic Devices", Proc. of SPIE, Vol. 1751 (1992).

(9) K. Imanaka, "Compact Optoelectronics Instrumentation", Business Japan, pp. 72-73, June (1991).

(10) AIRMAR TECHNOLOGY CORP., Application Notes, pp. 8-10a (1989).

(11) R. E. Newnham, "Composite electroceramics", Ann. Rev. Mat. Sci., pp.47-68, Annual Reviews, Inc. (1986).

(12) T. R. Gururaja, A. Safari, R. E. Newnham, and L. E. Cross, "Piezoelectric ceramic polymer composites for transducer application", Electroceramics, L. Levinson, Ed. New York: Marcel Dekker, pp. 92-128 (1987).

(13) H. Banno, "Recent developments of piezoelectric ceramic products and composites of synthetic rubber and piezoceramic particles", Ferroelectrics, Vol. 50, No1-4, pp.329-338 (1983).

(14) Y. Q. Zhuang, Y. G. Hew, and Q. C. Xu, "Sandwich PZT/polymer composite transducer", Ferroelectrics, Vol. 49, pp. 241-249 (1983).

(15) K. Uchino, "Recent Topics of Ceramic Actuators", Ferroelectrics, Vol.91, pp.281-292 (1989).